Design, Development and Pharmacokinetic Studies of Nanoparticulate Drug Delivery Systems of Imatinib Mesylate

THESIS

Submitted in partial fulfilment
of the requirements for the degree of
DOCTOR OF PHILOSOPHY

By
BENDE GIRISH SHAMRAO

Under the supervision of
PROF. RANENDRA N. SAHA

BIRLA INSTITUTE OF TECHNOLOGY & SCIENCE
PILANI (RAJASTHAN) INDIA
2008

Design, Development and Pharmacokinetic Studies of Nanoparticulate Drug Delivery Systems of Imatinib Mesylate

THESIS

Submitted in partial fulfilment
of the requirements for the degree of
DOCTOR OF PHILOSOPHY

By
BENDE GIRISH SHAMRAO

Under the supervision of
PROF. RANENDRA N. SAHA

BIRLA INSTITUTE OF TECHNOLOGY & SCIENCE
PILANI (RAJASTHAN) INDIA
2008

BIRLA INSTITUTE OF TECHNOLOGY & SCIENCE

PILANI (RAJASTHAN) INDIA

CERTIFICATE

This is to certify that the thesis entitled "**Design, Development and Pharmacokinetic Studies of Nanoparticulate Drug Delivery Systems of Imatinib Mesylate**" and submitted by **Bende Girish Shamrao**, ID. No. 2002PHXF032 for award of Ph.D. Degree of the Institute, embodies original work done by him under my supervision.

Date:

(Prof. Ranendra N. Saha)
Professor of Pharmacy
Dean, Faculty Division III &
Education Development Division
B.I.T.S., Pilani

Acknowledgements

It is a moment of great pleasure and immense satisfaction for me to express my deep gratitude and gratefulness towards my research supervisor Prof. Ranendra N. Saha, Dean, Faculty Division III and Educational Development Division, Birla Institute of Technology and Science, Pilani. I sincerely acknowledge his proficient guidance, suggestions, support and time he offered to me throughout the course of this research. The pleasant experience of working under him and the counsel he provided will be remembered and appreciated for a long time to come. It goes without saying that mere acknowledgement in words is simply inadequate to express my deep gratitude to him.

I am sincerely thankful to Prof. L. K. Maheshwari, Vice Chancellor and Director, BITS, Pilani and Prof. S. Venkateswaran, Advisor, BITS, Pilani for providing me the opportunity to pursue my doctoral research work in the Institute. I would like to thank Prof K. E. Raman, Deputy Director, Administration and Prof. G. Raghurama, Deputy Director, Academic for extending support during my research work. I express sincere gratitude to Prof. Ravi Prakash, Dean, Research and Consultancy Division for his constant support and encouragement.

I take this opportunity to specially thank members of the Doctoral Advisory Committee Prof. R. Mahesh, Dr. S. Chandran, Dr. D. Sriram for their continuous support, motivation and constructive advice. I gratefully acknowledge all the faculty members of Pharmacy Group - Dr. P. Yogeeswari, Prof. A. N. Nagappa, Prof. S. M. Ray, Dr. H. R. Jadhav, Dr. P. L. Kole, Mr. M. Raman, Mr. S. C. Charde, Dr. A. Roy, Mrs. Nagasree, Mr. Punna Rao and Mr. M. Pandey for their co-operation in my academic responsibilities. I would like to thank Dr. S. P. Regalla, Dr. S. S. Deshmukh, Dr. S. D. Pohekar, Mrs. M. Sharma and other office staff of Research and Consultancy Division, BITS, Pilani. Thanks are also due to the faculty members of BITS, Pilani - Dr. A. K. Das, Dr. S. K. Saha, Dr. S. Banerjee, who have contributed to my doctoral research.

I must thank all the non-teaching staff members of Pharmacy and Biology Group, Soniji, Rampratapji Mathuramji, Gokulji, Hariramji, Moolji, Sharmaji, Yasinji, Sitaramji, Vishal, Puran, Naveen and Mukesh, who have always been helpful during my research work. Staff members of the Research and Consultancy division, Raghuvirji, Mahipalji and Soniji deserve a special mention for their kind and timely help.

I am especially thankful to Dr. R. C. Gupta, former Deputy Director and Head, Drug Metabolism and Pharmacokinetics Laboratory, Central Drug Research Institute, Lucknow, for providing me special training program. I am also thankful to

Dr. L. Jawahar, Dr. M. Nitin, Dr. G. Vipul, Dr. S. Satyendra, Dr. S. Sabarinath, Dr. S. Rajendra for extending friendship and accepting me as one among them.

I am grateful to Dr. K. C. Jindal, President, Panacea Biotech, Lalru and Mr. M. Talwar, General Manager, Formulations, Panacea Biotech for extending the particle size analyzer facility. I am also thankful to Dr. R. P. Gupta, Central Electronics Engineering Research Institute, for providing access to Atomic Force Microscopy facility at CEERI, Pilani. Sophisticated Analytical and Instrument Facility at All India Institute of Medical Sciences, New Delhi, is acknowledged for the Electron Microscopic analysis.

I am especially thankful to Mr. Mahesh Banekar, Regional Manager, Cipla Limited, Mumbai and Dr. Mergu Raju, General Manager, Research and Development, Medreich Pharmaceuticals, Bangalore, for supplying drugs and excipients needed for formulation and analytical development. I appreciate the help and support provided by Dr. D. Sriram, Mr. M. Dinakaran and Dr. Ashok Akuthota for synthesis of Imatinib metabolite.

Very special thanks to Mr. Sivacharan Kollipara for his active participation and invaluable contribution in this research work. I am especially thankful to Dr. Pravin Jadhav, Dr. Hemant Jadhav, Mr. Shrikant Charde and Dr. Prashant Kole for their friendly advice and valuable suggestions in this research work.

My research work gradually emerged amidst the friendship that animated my BITS life and provided me the most valuable lessons of life. My sincere appreciation goes to all my friends Praveen, Sneha, Shrikant, Venu, Punna, Subrato, Vasant, Laila, Prakash, Sachin, Ganesh, Haritha, Thirumurgan, Venkatesh, Pandi, Kumaran, Shalini, Raghvendran, Meenakshi, Dinakaran, Senthil, Rajkumar, Sunil, Debjani, Arvind, Thimappa, Devdoss, Dilip, Pritesh, Ashok, Buchi, Mallari, Maruthi, Ramchandran, Shashwat, Pradeep, Narayan, Deepak, Ashwin and Manav, who made my stay memorable at Pilani.

I am grateful to the supreme power for blessing me with family and friends, whose love and unconditional support is admirable. I am indebted to my grandparents whose foresight and values paved the way for a privileged education and to my parents and in-laws, who gently offered counsel and support at every turn of the way. I express my deepest admiration to my father-in-law, whose encouragement, support and advice will always be felt, keeping me motivated to achieve the best in my endeavors. Last but not least, I thank my wife Tanushree for being my best friend and offering me unwavering support throughout this work. Without her love, encouragement, understanding and sacrifice, this work would have been a difficult task.

Girish Bende

List of Tables

.

List of Figures

List of Abbreviations and Symbols

λ_{max}	Wavelength of Maximum for UV-Absorbance
°C	Degree centigrade
ABC	ATP Binding Cassette
ADP	Adenosine diphosphate
AFM	Atomic Force Microscopy
AIC	Akaike Information Criterion
ALL	Acute Lymphoid Leukemia
AML	Acute Myelogenous Leukemia
ANOVA	Analysis of Variance
AT	Accelerated Temperature (40 ± 2 °C / 75 ± 5 % RH)
ATC	Anatomical Therapeutic Chemical Classification System
ATF	Activating Transcription Factor
ATP	Adenosine triphosphate
AUC	Area Under the concentration versus time Curve
AUC_∞	Area Under the concentration versus time Curve for time zero to infinity
AUC_t	Area Under the concentration versus time Curve for time zero to time t
AUMC	Area Under first Moments Curve of concentration versus time profile
BAN	British Approved Names
BBB	Blood Brain Barrier
BIC	Bayesian Information Criterion or Schwarz Criterion
CD	Cluster Differentiation Factor
CDDS	Conventional Drug Delivery Systems
CFR	Code of Federal Regulations
CI	Confidence Intervals
c-KIT	C-terminal Receptor Tyrosine Kinase Encoded by the stem cell Oncogene
Cl	Clearance
Cl/F	Clearance scaled by bioavailability
C_{max}	Maximum Concentration of Drug in Serum or Tissue
CML	Chronic Myeloid Leukemia
CNS	Central Nervous System
CPCSEA	Committee for the Purpose of Control and Supervision of Experiments on Animals
CRT	Controlled Room Temperature (25 ± 2°C / 60 ± 5% RH)
CSF	Colony-Stimulating Factor
CYP	Cytochrome P450 enzyme system (with isoenzymes e.g. - 3A4, 2C9 etc)
DDS	Drug Delivery System

DLS	Dynamic Light Scattering
DNA	Deoxyribonucleic Acid
DSC	Differential Scanning Calorimetry
ED_{50}	The dose effective for 50% of the population
EE	The drug Entrapment Efficiency
EGF	Epidermal Growth Factor
EGFR	Epidermal Growth Factor Receptor
EPR	Enhanced Permeation and Retention
ERK	Extracellular Regulated Kinase
F	Absolute Bioavailability
FDA MA	FDA Modernization Act
FDA	Food and Drug Administration
FT	Refrigerated Temperature (5 ± 2°C)
FTIR	Fourier Transform Infra-red Absorption Spectroscopy
g	Gram
GALT	Gut-associated Lymphoid Tissues
GCK	Glucokinase
GIST	Gastrointestinal Stromal Tumors
GIT	Gastrointestinal Tract
GPC	Gel Permeation Chromatography
GRB	Growth Factor Receptor-Bound Protein
HETP	Height Equivalent to Theoretical Plates
HIV	Human Immunodeficiency Virus
HL	Half-Life
HPLC	High Performance Liquid Chromatography
HQC	Quality Control Standards set at Higher Concentration Level
IAEC	Institutional Animal Ethics Committee
IC_{50}	The concentration producing 50% of the maximum inhibitory response
ICH	International Conference on Harmonization
IM	Imatinib Mesylate
INN	International Non-proprietary Names
INR	Indian Rupees
IRIS	International Randomized Interferon versus STI-571 (Gleevec®) Study
ITK	Interleukin-2 Tyrosine Kinase
IUPAC	International Union of Pure and Applied Chemistry
J	Joules
JNK	Jun N-terminal Kinase (Janus Kinase)
k	Degradation Rate Constant
K	Release Rate Constant

KIT	Stem Cell Factor Receptor
L	Liter
LCMS	Liquid Chromatography Coupled with Mass Spectrophotometer
LE	The drug Loading Efficiency
LOD	Limit of Detection
Log P	Log of oil water partition coefficient
Log D	Log of oil water distribution coefficient at a particular pH
LOQ	Limit of Quantitation
LQC	Quality Control Standards set at Lower Concentration Level
M	Molar
MAPK	Mitogen-activated Protein Kinase
MAT	Mean Absorption Time
M-cells	Microfold Cells
MDR	Multi-drug Resistance Protein
MDT	Mean Dissolution Time
MEC	Minimal Effective Concentration
MEK	Mitogen ERK
mg	Milligram
min	Minutes
mL	Milli liter
mm	Millimeter
MQC	Quality Control Standards set at Middle Concentration Level
MRT	Mean Residence Time
MRT	Mean Residence Time
MSSR	Mean Sum of Square Residuals
Myc	Avian Myelocytomatosis Viral Oncogene Homologue
n	Nano
N	Newton
Nano-DDS	Nanoparticulate Drug delivery System
NCI	National Cancer Institute, USA
NDDS	Novel Drug Delivery Systems
NF	National Formulary
NIR	Near Infra-red
NNI	National Nanotechnology Initiative
NSTC	National Science & Technology Council
PAK	p21 Activated Kinase
PCL	Poly caprolactone polymer
PCS	Photon Correlation Spectroscopy
PD	Pharmacodynamics
PDGFR	Platelet Derived Growth Factor Receptor

PECA	Poly (ethyl cyanoacrylate) polymer
PEG	Polyethylene Glycol
PEO	Polyethylene Oxide
PF-68	Poloxamer 188 (copolymer of polyethylene and polypropylene)
P-gp	Permeability Glycoproteins
pH	Negative Log to the base 10 of hydrogen ion concentration
Ph+	Philadelphia Chromosome Positive
PI	Polydispersity Index
PI3K	Phosphatidyl Inositol 3-Kinase
PK	Pharmacokinetics
PK/PD	Pharmacokinetics and Pharmacodynamics Correlation
PKB	Protein Kinase B
PKC	Protein Kinase C
PKI	Protein Kinase Inhibitors
PLA	Poly Lactic acid
PLCγ	Phospholipase C γ
PLGA	Poly (lactide-co-glycolic acid) copolymer
$P_{o/w}$	Apparent oil-water Partition Coefficient
PS	Particle Size
PSTK	Protein Serine Threonine Kinases
PTB	Phospho-tyrosine Binding Domains
PTK	Protein Tyrosine Kinases
PVA	Polyvinyl Alcohol
p-value	Significance Level in Statistical Tests (probability of a type I error)
PVP	Polyvinyl Pyrrolidone
QC	Quality Control Standards
QELS	Quasi-elastic Light Scattering
R	Correlation Coefficient
R^2	Regression Coefficient
RAF	Murine Leukemia Viral Oncogene Homologue
RAS	Rat Sarcoma Viral Oncogene Homologue
RBC	Red Blood Cells
RES	Reticulo-endothelial System
R_f	Retention Factor
RH	Relative Humidity
RNA	Ribonucleic Acid
rpm	Revolutions per Minute
RPTK	Receptor Protein Tyrosine Kinase
RSD	Relative Standard Deviation / Coefficient of Variation

Rt	Retention Time
RT	Room Temperature (25 ± 2 °C / 60 ± 5 % RH)
s	Seconds
S	Slope of the Least Square Regression Line
S6K	S6-Kinase
SD	Standard Deviation
SEM	Scanning Electron Microscopy
SGF	Simulated Gastric Fluid
SH	Src Homology Domain
SIF	Simulated Intestinal Fluid
STAT	Signal Transducer and Activator of Transcription
STEM	Scanning Tunneling Electron Microscopy
STI	Serine Threonine Kinases
$T_{1/2}$	Half Life
$T_{50\%}$	Time taken for 50% of drug release
$T_{90\%}$	Time taken for drug amount to attain 90% of initial amount
TDW	Triple Distilled Water
TEM	Transmission Electron Microscopy
T_f	Tailing Factor
TGF	Transforming Growth Factor
TLC	Thin Layer Chromatography
T_{max}	Time to reach Maximum Concentration of Drug
TPI2	Thiol Proteinase Inhibitor 2
USAN	United States Adopted Names
USP	United States Pharmacopoeia
UV	Ultraviolet
V_d	Apparent Volume of Distribution
VIS	Visible Light
V_{ss}	Apparent Volume of Distribution at Steady-state
WBC	White Blood Cells
σ	Standard Deviation of Y-intercept of Regression Equation

Abstract

The principle objective of the present research work was to design and develop nanoparticulate drug delivery system using biodegradable and biocompatible polymers to improve therapeutic efficacy of Imatinib mesylate by controlling its release characteristics and biodistribution to brain. To achieve this broad objective, following specific studies were carried out in the present work.

Suitable analytical and bioanalytical methods based on spectrophotometric and liquid chromatography were developed and validated for the determination of drug in formulation and biological matrices. Prior to the formulation development, preformulation studies were performed to establish necessary physicochemical data of the drug. Studies were performed to address the product specific questions related to drug solubility, stability, drug-excipient compatibility, etc.

Formulation development was carried out by identifying and optimizing the critical formulation and process parameters. The prepared nanoparticles were characterized for surface morphology and shape, particle size and size distribution, drug content (loading and entrapment efficiency) and in vitro drug release. The optimized formulations were also studied for the drug product stability and reproducibility.

In situ rat intestinal absorption studies were carried out to identify the importance of the efflux transport processes and effect of efflux protein inhibitors on the absorption behavior of the pure drug. The model was also employed to study the relative absorption behavior of the pure drug and drug loaded nanoparticles. Pharmacokinetic studies and biodistribution studies were performed to investigate the overall systemic and tissue (brain and lungs) specific bioavailability of the pure drug and optimized nanoparticulate formulations.

Results indicated that the developed spectroscopic and liquid chromatographic methods were selective and sensitive in the determination of drug. These validated analytical and bioanalytical methods were successfully used for various preformulation, formulation development, pharmacokinetic and biodistribution studies. Preformulation studies indicated that the drug demonstrates a charge dependent solubility profile with increasing solubility towards acidic pH. The pH partition studies showed that ionization of the drug molecules controls the fraction distributed to oil phase. Although the drug was found to be stable under various storage conditions, it was susceptible for oxidative stress condition. Results of the drug-excipient compatibility studies demonstrated no significant interaction with various excipients used in the formulations.

Emulsion solvent evaporation and interfacial polymerization techniques were found to be suitable for the preparation of polymeric nanoparticles using the preformed polymers - Poly (lactic-*co*-glycolic acid) [PLGA] and Poly (ε-caprolactone) [PCL] and monomers - ethyl cyanoacrylate [ECA] respectively. Nanoparticle characteristics such as average particle size and size distribution, particle morphology, drug entrapment and loading efficiency were found to be influenced by various formulation parameters such as proportion of polymer, drug and stabilizer. The various processing parameters such as phase volume ratio, phase pH, energy of emulsification were also found to have impact on the characteristics of the prepared formulations. PLGA and PCL formulations prepared using Poloxamer 188 and Polyvinyl alcohol were found to have small particle size with narrow size distribution. Similarly, interfacial in situ polymerization method has shown to provide small PECA nanoparticles with uniform size distribution.

The particle size analysis and microscopic imaging confirmed that the optimized nanoparticulate formulations were of the small and uniform particle size with good spherical shape. In vitro drug release from the prepared nanoparticles was controlled over 48-72 h, which could be explained by the first order release kinetics. The optimized formulations have shown high drug entrapment within the polymeric matrix with excellent particle morphology. All optimized formulations of PLGA, PCL and PECA nanoparticles demonstrated good stability and re-dispersibility in freeze-dried state. Thus, the developed experimental conditions provided good quality nanoparticles with reproducible characteristics.

In situ absorption studies confirmed that the drug is a good substrate for efflux transport proteins. The stabilizers such as poloxamer 188 and polysorbate 80 used in the preparation of nanoparticles were found to increase intestinal permeability. The biodistribution profile of the drug was found to be altered, when delivered in nanoparticles. A multi fold increase was observed in the area under the drug concentration curve in serum with the drug loaded PLGA and PECA nanoparticles. Similarly, an increase in the elimination half life indicated increase in the drug residence time in systemic circulation. Brain biodistribution studies revealed increased drug availability and residence time in the rat brain. Thus, in vivo pharmacokinetic and biodistribution studies in rat indicated that the PLGA and PECA nanoparticles are effectively enhanced permeability to brain with sustained drug exposure.

Collectively, these results indicate that the prepared nanoparticles have great potential as a targeted delivery system for cancer treatment. The drug delivery using nanoparticles would be advantageous over the currently available commercial formulations.

Table of Contents

1. Introduction

1.1 Cancer and cancer therapeutics

The most significant characteristic of the living matter is its high degree of structural and functional orderliness along with the ability to maintain its organization for survival and growth. This structured organization within a cell is attained through well controlled propagation, survival and death events (1). As the normal cells grow, differentiation is coordinated and regulated through the complex cellular mechanisms and contribute to the genetic stability. Similarly, several other cellular mechanisms maintain the sensitivity of cells towards the programmed cell death for the genetic stability of organism (2, 3).

Carcinogenesis or neoplasia represents the singular phenomenon of uncontrolled differentiation and disorganization leading to increased number of cells. It is distinct from other tumor progression events with its ability to invade surrounding tissues through metastasis and is known as malignant tumor (1). The cancer phenotypes are characterized by a loss of control in normal cellular propagation, maturation and/or apoptosis mechanisms through altered cell proliferation, tissue specific characteristics, programmed cell death and/or cellular invasion (4, 5).

Although the cancer cells are originally derived from normal cells, they irreversibly escape from controlled mechanisms that regulate normal cell growth and death. Cells divide and multiply at uncontrolled rate and/or escape the programmed cell death events leading to increased number of cells to the extent that it results in complete loss of critical cellular functions. This uncontrolled cell population continues to rise at the expense of host, until the organism succumbs. Unlike hostile parasites, tumor originates directly from normal host cells and it exhibits almost similar structural and functional biology. The similar structure and function impose challenge on cancer therapeutics for the selective removal of few cancerous cells from wide population of normal host cells.

Most of the cancers are caused by defective genes and are diverse in nature with the involvement of either loss- or gain-of-function mutation. With current understanding of the mechanisms of cancer development and its genetic basis, cancers demonstrate greatest variety of disease state with its multifunctional complications at various intra-cellular events with almost every type of growing cell in the body. Cancer research has been at the center of attention for the scientific community of drug discovery and delivery.

Although conventional anticancer drugs act by different modes of action, the therapeutic effect is principally attributed to cytotoxic intervention, which is not selective for malignant cells but also affects all rapidly dividing normal host cells. As a consequence of this action, conventional anticancer drugs invariably affect the tumor as well as normal

host cells. Conventional chemotherapy is based on the premise that cancer cells divide more quickly than normal cells and repeated doses may present selective disadvantage for the cancer cells. However, several cancers arise due to cellular insensitivity towards the programmed cell death of tumor cells. Thus, the less significant role of cell proliferation rate leads to therapeutic failure of several conventional drugs in many cancers. Moreover, these drugs cause multiple side-effects because of their non-specific action on rapidly dividing normal host cells such as the bone marrow and the epithelial lining of the gut. Usually, these side effects limit the administration of a sufficient quantity of a drug to eradicate the tumor completely. In the last decade, cancer treatment has shifted from nonspecific high dose chemotherapy to highly specific and targeted therapy, posing challenges to formulations scientist for making better and selective drug delivery systems for anticancer drugs.

1.1.1 Incidence of cancer

Cancer is a major human health problem worldwide and is the second leading cause of death. It was reported by the World Health Organization that malignant tumors were responsible for 12% of total annual deaths worldwide from all causes, in the year 2000 (6). The world cancer report suggests that since 1990, there has been significant increase in cancer incidences (≈ 19%) and deaths (≈ 18%). Currently, more than a quarter of deaths are attributable to cancer in many developed and developing countries. Further, the world health organization has indicated the possibility of increase in cancer incidences by 50% to 15 million deaths per annum by the year 2020. The world cancer report published in 2003 has revealed that the cancer has emerged as a major public health problem in developing countries, matching its effect in industrialized nations (6). Thus, with more than 10 million new cases every year cancer remains the most devastating disease worldwide.

1.2 Modern cancer chemotherapy

Over the past few years, rapid advances in structural and molecular pharmacology, genomics, proteomics and biotechnology have enabled to explore the underlying critical biological processes of several diseases and helped to define the molecular mechanisms. Similarly, significant progress has been achieved in understanding the cellular and molecular biology of cancer that has aided in identifying several new potential targets for selective therapeutic interventions at various levels. With the emergence of rationally designed molecular targeted therapy, the traditional cytotoxic chemotherapy will have limited role in the advanced treatment. However, there remains a major possibility of

combination therapy of newer safe agents with older broad cytotoxic agents in the treatment of common solid tumors (7-9).

1.2.1 Molecular biology - exploring novel targets

Intercellular communication is of paramount importance in multi-cellular organisms and it contributes to critical links by regulating cell growth, differentiation, migration, survival and apoptosis (10). The molecules involved in cell-cell and cell-matrix interactions as well as extracellular signaling molecules are the mediators of cellular communication and transmit the information from the exterior of the cell to its cytoplasm or nucleus (4). The mediators activate a cascade of molecular events that are initiated by the specific binding of extracellular molecules to either cell adhesion molecules or transmembrane receptors on the cell surface leading to transfer of a signal (11). The regulated chain of events of transferring signal between the cells by stimulating specific cellular components is recognized as a signal transduction pathway. Thus, signal transduction pathways elicit a cellular response that may be involved in various critical processes such as gene expression, cell proliferation, cell survival, cell differentiation, protein trafficking, migration, cytoskeletal architecture, cellular adhesion, cellular metabolism and programmed cell death - apoptosis (12). Usually, the phosphorylation cascade of signal transduction is tightly controlled and well organized by enzymes such as kinases and phosphatases (11). However, frequent deregulation of any event leads to the constitutive activation of normal controlled pathways leading to the activation of other signaling proteins and secondary messengers subsequently disturb the regulatory functions of cellular responses leading to abnormality or dysfunction. Deregulation of the intracellular signal transduction pathways have been implicated as central pathogenic event in a number of diseases including human malignancies (12).

1.2.2 Protein kinases - as cancer targets

Conservative estimates based on the human genome project suggest that as much as 20% of human genes encode proteins involved in signal transduction. These include transmembrane receptors, G protein subunits and signal generating enzymes. The last group includes more than 700 protein kinases and 180 protein phosphatases. Protein kinases and phosphatases exist as transmembrane as well as intracellular signaling molecules.

A super-family of transmembrane cell surface receptors capable of intrinsic protein kinase activity is of particular importance for the regulation of intracellular signaling pathways. Protein kinases are the family of enzymes that catalyzes the transfer of

phosphate groups from adenosine triphosphate (ATP) to specific amino acids on substrate proteins (Fig. 1.1) (13). They are broadly classified into two sub-families, the protein serine threonine kinases (PSTK) and the protein tyrosine kinases (PTK).

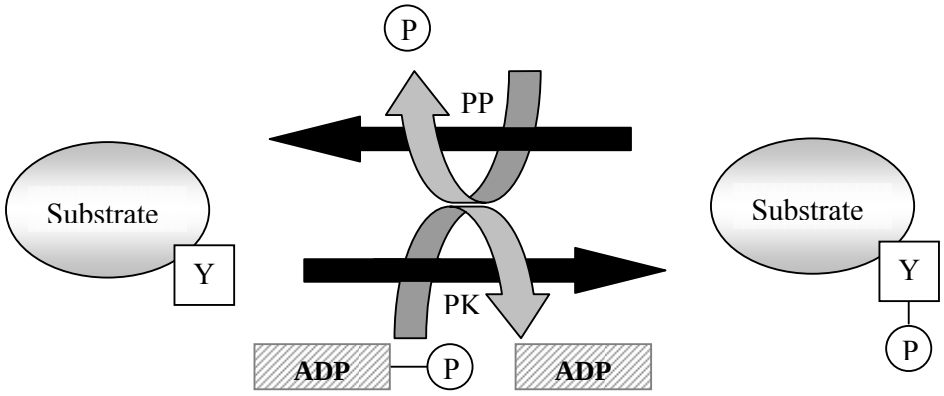

Fig. 1.1: Schematic representation of protein kinase activity; PK- protein kinase, PP - protein phosphatases, ADP - adinosine diphosphate, ATP - adinosine triphosphate

a) Protein tyrosine kinases

The PTKs are a family of enzymes that selectively phosphorylates tyrosine residue in a target (substrate) protein and are important mediators of various critical signal transduction events, which contribute in cellular communication and maintenance of homeostasis. Typically, PTKs are in non-phosphorylated condition at resting state and phosphorylation of the kinase domain leads to activation. Like other signaling mediators, these activated proteins initiate the cascading event of signal-transduction pathways and participate in the regulation of many critical biologic processes such as cell proliferation, differentiation, adhesion, migration and apoptosis (14).

Although rare in cells ($\leq 0.05\%$), tyrosine phosphorylation play a critical role in normal cell growth regulation. Apart from their normal function in cell, they also participate in preventing deregulated cellular proliferation or contribute in sensitizing apoptotic stimulus. This is evident from the fact that many of the PTKs are encoded by cellular proto-oncogenes (15). Proto-oncogenes are the normal cellular counterparts of oncogenes, the cancer-causing genes originally identified in RNA viruses.

While numerous retroviruses carrying oncogenes cause cancer and other malignancies in avian and rodent cells, so far only the human T-cell lymphotropic virus (HTLV-1) has been identified in human oncogenesis as T-cell lymphomas. On the other hand, several human proto-oncogenes are known to be altered or activated by stimulus such as irradiation (e.g., UV exposure), chemical carcinogens (e.g. cigarette smoke), unrepaired

replication errors or aging, resulting in the development of human malignancies. In literature, more than 150 proto-oncogenes are reported and most of them encode components of the signal transduction cascade such as GF Homologues, GFR of the RPTK type, cytoplasmic protein kinases (PTKs and PSTKs), small GTP binding proteins of the RAS super-family, nuclear proteins - transcription factors and cell cycle regulators.

In addition, tumor suppressor proteins caused by loss-of-function mutations can lead to malignant transformation. Although these proteins are usually not oncogenic, their normal function is vital in preventing oncogenesis by counteracting some of the oncogenic stimulus. PTKs comprise a major group of oncoproteins such as vERBβ (EGF receptor), vFMS (CSF-1 receptor) and vKIT (KIT/SCF receptor). According to one interesting observation, most of the PTKs have been identified as retroviral oncogene intermediates. The mechanisms for oncogenic activation of signaling molecules may be diverse in nature but they all have constitutive or deregulated protein activity in common. Thus, the normal intracellular regulation is perturbed resulting in activation of malignant transformations.

Extensive research in molecular biology of cancer during last two decades has revealed that the signaling pathways are often genetically or epigenetically altered in cancer cells. Although earlier it was believed that cancer arises via a long multi-step process with coordination between oncogenes and tumor suppressors proteins, this concept has been challenged by recent findings that constitutive activation of a single proto-oncogene is sufficient for malignant transformations without other detectable genomic alterations.

The activation or deregulation of proto-oncogenes in humans can occur via three well-known mechanisms viz. mutations in extracellular domain, chromosomal rearrangements caused by altered expression or activity of an oncogene and amplification; which results in proto-oncogene over-expression. There are several well established examples of proto-oncogenic conversion of signaling molecules which offer targeting advantage for selective inhibition or modulation of underpinning events of cancer progression.

The human genome encodes only 90 PTKs and several PTKs among them are oncogenes which are deregulated or over-expressed in human cancers. Protein tyrosine kinase is the largest protein kinase family reported to be implicated in many cellular events of neoplastic development and progression. The selective inhibition of oncogenic PTKs such as Bcr-Abl, PKC and the epidermal growth factor receptor is an attractive target for the treatment of several human malignancies (16). The Bcr-Abl tyrosine kinase of chronic myeloid leukemia represents one of the most extensively studied PTKs, which is now considered as a model of human malignancy.

Receptor protein tyrosine kinases

The PTKs family can be further categorized into receptor tyrosine kinases (RPTK) and non-receptor tyrosine kinases (nRPTK). The RPTKs are activated by the extracellular signaling factors (ligands) such as EGF, PDGF etc, which can specifically bind to their extracellular domain. Subsequently, they induce receptor dimerization and auto-phosphorylation of specific tyrosine residues creating a binding site for cytoplasmic substrates. The receptor dimerization is stabilized by various mechanisms and is usually ligand specific. Phosphotyrosine residues bind with high affinity to Src homology 2 (SH2) and phosphor-tyrosine binding (PTB) domains, thereby creating docking sites for various ligands. The intermediate signaling complexes thus formed are considered as a platform for recognition and recruitment of signaling proteins (17). The specificity for RPTK initiated signaling is found in several events such as the upstream activating event (binding of ligand to cognate RPTK), the catalytic specificity of the activated RPTK (kinases and phosphatases), the compartmentalization of signaling molecules (accurate subcellular localization) and the cell type specificity in signaling (specific molecules ascribed different roles).

Moreover, the duration, amplitude and kinetics of signals are critical for the cellular response. Protein phosphorylation is a key regulator as it can sustain or attenuate signals via amplification, feedback and cross talk. The ultimate outcome of a signaling cascade is alteration in gene expression through activation of transcription factors. In order to modulate RPTK activity, there are few possibilities of signal down-regulation such as receptor antagonists, soluble receptors, receptor endocytosis, ubiquitination and degradation, phosphatases and negative feedback loops.

The RPTK sub-family can be further divided into subgroups that have similar structural organization and sequence similarity within the kinase domain. The members of the type III group of RPTKs include α and β the platelet-derived growth factor receptors (PDGFRα and PDGFRβ), colony-stimulating factor receptor (CSF-1R, c-Fms), Flt-3 and stem cell or steel factor (SCF, cKIT) receptor. These receptor tyrosine kinases are characterized by five Ig-like domains in the extracellular domain and a cytoplasmic region containing a hydrophilic kinase insert domain (18).

b) Kinase inhibitors - the novel anti-cancer drugs

During last five years, several new anti-cancer drugs have been investigated for specific cancer targets such as unique protein targets expressed in any particular cancer cell (19).

These targets often include specific growth factor receptors that are over-expressed in particular types of cancer. These new drugs are inhibitors of the enzymatic intra-cytoplasmic domains and include small molecules and protein drugs such as Cetuximab, Trastuzumab, Bevacizumab, Imatinib, Gefitinib and monoclonal antibodies.

The kinase inhibitors represent a group of drugs that regulate kinase enzyme and its cellular activity by selective intervention of their phosphorylation. As discussed earlier, the intracellular signaling pathways that stimulate cell proliferation are frequently controlled by kinases. In chronic myeloid leukemia, a specific chromosome (Philadelphia chromosome) produces a damaged kinase fusion receptor protein BCR-ABL, which signals uncontrolled proliferation (20-22). Imatinib is a tyrosine kinase inhibitor that binds to the BCR-ABL receptor, preventing ATP binding and the resultant kinase activity (23-25). It is approved by the FDA for the treatment of chronic myeloid leukemia and also for gastrointestinal tumors. Similarly, the EGF receptors are over-expressed on the surface of some lung and colon cancer cells. Activation of these receptors by EGF and TGF-α (transforming growth factor α) is crucial for tumor cell proliferation. Gefitinib is a tyrosine kinase inhibitor that binds to the EGF receptor and inhibits the phosphorylation of the tyrosine residue by the tyrosine kinase enzyme. It is used clinically in the treatment of refractive non-small cell lung cancer.

1.3 Challenges in cancer chemotherapy

Most of the current anticancer drugs do not greatly differentiate between cancerous and normal cells, leading to systemic toxicity and adverse effects. Consequently, systemic applications of these drugs often cause severe side effects in other tissues (such as bone marrow suppression, cardio-myopathy and neurotoxicity), which greatly limits the maximal allowable dose of the drug. In addition, rapid elimination and widespread distribution into non-target organs and tissues require the administration of high dose, which is not economical and often complicated owing to nonspecific toxicity. Thus, another challenge is delivering sufficient amount of drug to target organs, which is otherwise poorly accessible to drugs e.g. poor brain penetration.

The physiological functions of human body present a variety of cellular and morphological barriers for transport of drug to its site of action. In oral administration, several natural barriers present in gastrointestinal tract such as enzymes, bacterial flora, mucus layers pose significant challenges to a drug to reach the systemic circulation apart from other cellular and epithelial transport barriers.

1.3.1 Chemotherapy and resistance

Chemotherapy is a major form of cancer treatment but majority of cancers become resistant or acquire resistance during treatment. The acquired resistance of several anticancer drugs is a major impediment to success of the treatment. A wide variety of structurally unrelated compounds such as Doxorubicin, Daunorubicin, Vincristine, Vinblasine, Etoposide, Teniposide, Paclitaxel, Docetaxel, Actinomycin-D, Mitomycin-C, Mitoxantone, Mithramycin, Topotecan, Irinotecan, Colchicine, Emetine, Puromycin, Tamoxifen etc. have shown acquired resistance during therapy. Multi-drug resistance (MDR) is identified as a cellular resistance to diverse array of structurally and functionally unrelated drugs with multiple mechanisms of action. In an estimate, it is reported that up to 5,00,000 new cases of cancer each year will eventually exhibit multi-drug resistance phenotype suggesting the magnitude of problem of resistance in cancer (26).

In chemotherapy, this non-specific cellular resistance utilizes several energy dependent transport mechanisms in order to overcome the cytotoxic affront. Cancer cells develop drug resistance through various mechanisms such as over-expression of efflux transport proteins, altered expression of apoptosis associated protein and tumor suppressor protein, changes in topoisomerase activity and modifications in glutathione S-transferase (27-32). However, in most of the cases, the main cause of resistance is over-expression of the membrane bound transport proteins that actively efflux drugs out of the cells leading to sub-therapeutic concentration and failure of the therapy. Often, two or more cellular mechanisms are involved concurrently, which offer cross-resistance in MDR to broader class of drugs (33-35). Amongst all the reported transport proteins, P-glycoproteins (P-gp) and multi-drug resistance-associated proteins (MRP) have been reported to mediate the cellular resistance in variety of cancers. As these proteins are expressed ubiquitously in the body tissues such as the brain, liver, lungs, kidney, intestine etc., they play an important role in the pharmacokinetics of a drug by actively changing its absorption, distribution, metabolism and elimination (36, 37). In addition, they may even change the pharmacodynamics of a drug by interfering in various cellular responses such as stimulation of DNA-damage repair, suppression of drug-induced apoptosis etc. For example, a decreased treatment response was observed with the over-expression of P-gp transport proteins in clinical settings (38, 39).

A wide range of chemicals such as HIV-protease inhibitors, antibiotics, immunosuppressants, antihypertensives, surfactants, polymers and copolymers etc are

reported to interact with efflux mechanism. These chemicals are of diverse structural and functional nature and most of them mediate through passive diffusion process. These compounds are broadly classified either as efflux substrates or efflux inhibitors, wherein, the former represent a class of drugs which undergo efflux mechanism, while the latter interact with transport proteins to inactivate efflux mechanism and are termed as MDR reversing, inhibiting or modulating agents (MDRM). It has been reported that the transport proteins demonstrate active elimination of several hydrophobic substrates with at least one anionic group at physiological pH. In addition, several drugs are also reported to be efflux substrates, which are co-transported by glutathione or sulfate conjugation (40-42).

1.4 Development of better cancer drug delivery - a rationale

Although chemotherapy has become an integral component of cancer treatment, chemotherapeutic drugs still exhibit poor specificity in reaching tumor tissue and are often restricted by dose-limiting toxicity.

The combination of developing controlled release technology and targeted drug delivery may provide a more efficient and less harmful solution to overcome the limitations found in conventional chemotherapy. Recent interest has been focused on developing nanoparticulate based drug delivery systems capable of delivering selectively to target organ and controlling the release of the drug. A drug may be encapsulated or attached to the nanoparticulate carriers in order to facilitate the distribution and control the release. Moreover, nanoparticles may offer a solution to the main barrier for successful chemotherapy such as the resistance of cancer cells to effective anticancer drugs and the destructive effect of these drugs on normal cells, tissues and organs. In order to deliver therapeutic agents to tumor cells in vivo, the drug resistance problem may be solved at the vascular, interstitial and cellular levels (43).

1.5 Nanotechnology - the power of small

The first original nanotechnology vision appeared during the mid of twentieth century as Sir Richard Feynman suggested the possibility of creating miniature machines build with a molecular accuracy for ultimate precision (44). Although today nanotechnology is used in a broader sense, earlier it was recognized as a production process termed as molecular manufacturing to get extra-high accuracy and ultra-fine dimensions with the preciseness and fineness at the order of billionth of a meter. Nanotechnology is now recognized as the design, characterization, production and application of structures, devices and systems by controlling shape and size at nanometer scale (45).

Extensive research in nanotechnology during last few decades has generated a substantial amount of technical literature (46, 47). The earlier articles proposed protein engineering as a path to nano-machine development and is cited as seminal in the field of computational protein engineering (48-51). The Feynman vision has also motivated the US National Nanotechnology Initiative (NNI). The most recent definition of nanotechnology was identified as the ability to manipulate material at the molecular level, with atom by atom precision, to create large structures with fundamentally new molecular organization (52). This vision generalizes the nano-machinery of living systems by promising a technology of unprecedented power that comes with plenty of opportunities and some dangers (53-57).

1.5.1 Nanotechnology - a revolution in drug delivery systems

In the past few years, the exponential growth of nanoscience and nanotechnology has surged into the foremost innovations in pharmaceutical sciences with tremendous impact on therapeutics and diagnostics (58-62). The advent of nanotechnology in pharmaceutical sciences has brought new dimensions to a century old concept of targeted DDS (63-66). The magic bullet as proposed by Sir Paul Ehrlich, which would offer benefits to patients in clinic, is now feasible to design in laboratory (67). The nanotechnology based DDSs are in the limelight of interest due to their outstanding potential to target physiological sites, organs, tissues or cells, where pharmacological activity of drug is desired (68-73).

At the nanoscale level, often the materials demonstrate significantly different quantum mechanical properties leading to a fundamental change in their physical, chemical and biological properties as compared to their bulk forms. Several scientists have indicated the possibility of manipulating the primary characteristics of a material such as melting point, magnetic properties, etc without altering its chemical composition. This ability to characterize, manipulate and/or organize matter systematically at the nanometer scale is spurring a revolution in science, engineering, technology and inevitably drug delivery and therapeutics (74).

In therapeutics, nanoparticles may show significant change in both pharmacokinetic and pharmacodynamic levels. Advances in nanotechnology during last two decades have suggested that nanoparticles are effective in altering the pharmacokinetics of drugs such as rapid and increased absorption, selective biodistribution, reduced degradation and elimination (75-80). Similarly, few groups have suggested the possibility of change in pharmacodynamics of drugs (81).

By virtue of their small size which is smaller than human cells (10-20 μm), nanoparticles can easily permeate through the biological and cellular barriers and enter most of the cells. As a result, these carriers can readily interact with biomolecules on both the cell surface and within the cell, often in ways that do not alter the behavior and biochemical properties of those molecules. Thus, nanoparticles show significant change in cellular interactions leading to noninvasive access to the interior of a living cell and present the opportunity for unprecedented gains on clinical and basic research frontiers. Moreover, the ability to simultaneously interact with critical drug targets such as proteins and nucleic acids at the molecular scale may provide better understanding of the complex regulatory and signaling networks that govern the behavior of cells in their normal state and as they undergo malignant transformation. Consequently, nanotechnology offers self-perpetuating opportunities to achieve the long cherished goal of precise delivery of drugs to a specific compartment in the target cell with a temporal pattern consistent with the underlying pathology (82).

Nanoparticles in therapeutics are identified as colloidal molecular assemblies designed in the size range of 10 nm to 1000 nm for entrapment, encapsulation and/or adsorption of the active therapeutic or diagnostic agent using either inorganic metals or organic macromolecular materials for the purpose of mitigation, prevention, cure or diagnosis of a disease. They are broadly classified as nanospheres or nanocapsules based on their physical nature such as solid core (monolithic) or vesicle (membranous) structure, respectively. It has been reported by several research groups that size and size distribution of nanoparticles play a crucial role in cell adhesion, trafficking and interaction e.g. penetration through a pore of a cellular membrane.

1.5.2 Nanotechnology - regulatory aspects

The National Science and Technology Council (NSTC) of the United States has taken a revolutionary and transformative step through the National Nanotechnology Initiative (NNI), which was a federal research and development program established to coordinate the multidisciplinary efforts in nanoscale science, engineering and technology (83-86). Similar efforts has been concerted by the National Cancer Institute (NCI) to harness the power of nanotechnology with a goal of eliminating the suffering and death due to cancer by 2015, through radical improvement in the way cancer is treated or diagnosed (87). In addition, considering the promising outcomes of extensive research and development over last two decades, the United States FDA has taken a leading breakthrough for promotion of nanotechnology in health sciences (88-90).

Many other drug controlling agencies over the entire world are now convinced with the potential of nanotechnology and are promoting research for the application of nanotechnology in health sciences. The United States FDA has approved the first nanoparticulate DDS, Abraxane®, for breast cancer treatment in January 2005. This nanotechnology based product contains the Albumin-bound nanoparticle of Paclitaxel, which showed better and faster cure rate, almost double when compared with solvent-based Taxol, in a clinical trial conducted in 460 patients with the metastic breast cancer (91-94).

1.6 Nanotechnology in chemotherapy - opportunities and challenges

There has been intensive research in the past few decades in the development of nanoparticles of biodegradable polymers as an effective DDS for medical practice, especially for chemotherapy and gene delivery (95, 96). The progress in nanoparticle technology, material science, in particular, biodegradable polymers along with cellular and molecular physiology have contributed to the advancements in chemotherapy and gene therapy of cancer and other diseases (97-103).

Based on the progress made during last few decades, nanotechnology seems to be one of the most promising disciplines for chemotherapy (103, 104). One of the main challenges in chemotherapy is the dosage form that is free from toxic adjuvants. Nanoparticles of biodegradable polymers, which have a size small enough to allow intra-capillary or trans-capillary passage and appropriate surface coating to escape from macrophage uptake and provide an ideal solution (105-108). Nanoparticles can also provide controlled and targeted delivery of the encapsulated anticancer drug resulting in increased efficacy and reduced side effects (109-115).

1.6.1 Nanoparticles and cellular barriers

Frequently, water-soluble small chemical molecules can passively diffuse through the intestinal barriers via water filled aqueous channels by the process termed as paracellular diffusion. In humans, these aqueous channels are reported to be as small as 4 to 8 Å and act as a barrier for water insoluble chemicals, macromolecules and particulate matters. However, recent findings have indicated the possibility of selective opening of these barriers reversibly by chemical treatment with penetration or permeation enhancers (116). The uptake of particulate matter is inversely proportional to the structural integrity of the tight junction barriers. Although the paracellular transport of macromolecules or nanoparticles is negligible because of their size, reversible opening of these tight junctions is possible with the use of permeation enhancers and mucoadhesive polymers.

The paracellular uptake via aqueous channels is one of the possible mechanisms for the transport of nanoparticles across the gastrointestinal wall.

Few authors have reported the translocation of nanoparticles across cellular barrier termed as a transcellular mode of absorption through M cells (117, 118). Transcellular transport of drug can be sub-divided into four distinct processes that are principally influenced by the particle size, surface charge, hydrophobicity and surface characteristics (119, 120).

Particle uptake via the Gut Associated Lymphoid Tissues (GALT) after oral delivery increases exponentially as particle size decreases from 5 μm to the submicron range (121). Similarly, in cases where it is desired that subcutaneously or intramuscularly injected particles circulate in tissues, particle size must be less than 5 μm. Therefore, creating submicron particles offer advantages of being taken up efficiently by the GALT and retaining within tissues providing the therapeutic drug concentrations for extended time period (122). However, the efficiency with which drug molecules can be encapsulated, particularly large, water-soluble molecules, decreases dramatically as particle diameter decreases below 1 μm (123).

Microfold cells (M cells) found in the follicle-associated epithelium of the Peyer's patch and have the unique ability to deliver foreign materials by trans-epithelial transport from the lumen to organized lymphoid tissues within the mucosa (118, 124-128). M cells are typical epithelial cells in that they are polarized and form tight junctions that define two major plasma membrane domains, apical and basolateral (129). The hallmark of M cells is the presence of an unusual sub-domain of the basolateral membrane that amplifies the cell surface and forms an intraepithelial pocket (124, 130). The apical membranes of M cells are designed to facilitate adherence, uptake of antigens and microorganisms, efficient delivery to the intraepithelial pocket and underlying lymphoid tissues. The apical surfaces of M cells generally lack a typical brush border and instead have variable microvilli or microfolds interspersed with large plasma membrane subdomains that are exposed to the lumen. Clathrin coated micro-domains are common within these areas and have been shown to mediate endocytosis of ligand-coated particles, adherent macromolecules and viruses (131-133). M cells also conduct fluid-phase pinocytosis, actin-dependent phagocytosis and macro-pinocytotic engulfment involving disruption of the apical cytoskeletal organization (124, 131, 132, 134, 135).

1.6.2 Enhanced permeation and retention effect

As tumor cells divide and multiply, angiogenesis is accelerated to cater to the needs of increasing oxygen and nutritional demands of growing tumor. Extensive studies have revealed that the neovasculature significantly differs from normal tissues in terms of microscopic anatomical architecture (136). Moreover, the structure and organization of endothelial cells, perivascular cells and vascular basement membrane of tumor vessels are all abnormal.

The blood vessels in tumor are irregular, dilated and defective with a leaky vasculature due to altered architecture. Endothelial cells are irregular in shape, loosely interconnected, disorganized with large fenestrations, wherein, size often ranges from 200-300 nm. Perivascular cells have less frequent and intimate association with endothelial cells, vascular basement membrane and smooth muscle layers are frequently defective and sometimes even absent. Thus, rapid tumor growth leads to formation of a physiologically and structurally defective vasculature.

One consistent functional change reported in the tumor blood vessels is that they have a wide lumen whereas tumor tissues have poor lymphatic drainage that contributes to gross anatomical defectiveness with significant functional abnormalities leading to enhanced permeability of plasma components inside the tumor tissues. Similarly, the macromolecules loaded with drug can easily infiltrate into tumor tissues.

On the other hand, poor lymphatic clearance coupled with slow venous return contributes in extensive retention of these macromolecules inside tumor tissues, while extravasation into tumor interstitium continues. The extravasations of macromolecules are reported to occur via intracellular gaps or the vesicular-vacuolar organelles (137, 138).

This architectural anarchy, combined with an overproduction of permeability enhancers and impairment of lymphatic drainage, results in the preferential extravasations and retention of high molecular weight macromolecules and colloids in developing tumors, a feature which has been termed Enhanced Permeation and Retention (EPR) effect (139, 140). This EPR effect of macromolecules contributes up to 10-50 fold increase in concentration in tumor tissues when compared with the normal tissues (141). With extensive research, EPR effect has become primary tumor targeting strategy in anticancer drug delivery with clinical products based on it (142). Like macromolecules, the nanoparticles prepared in a range of 200-300 nm can be preferentially taken into tumors as they are small enough to permeate through tumor vessels at the same time large enough for pores of normal blood vessels to affect normal cells (143) (Fig 1.2).

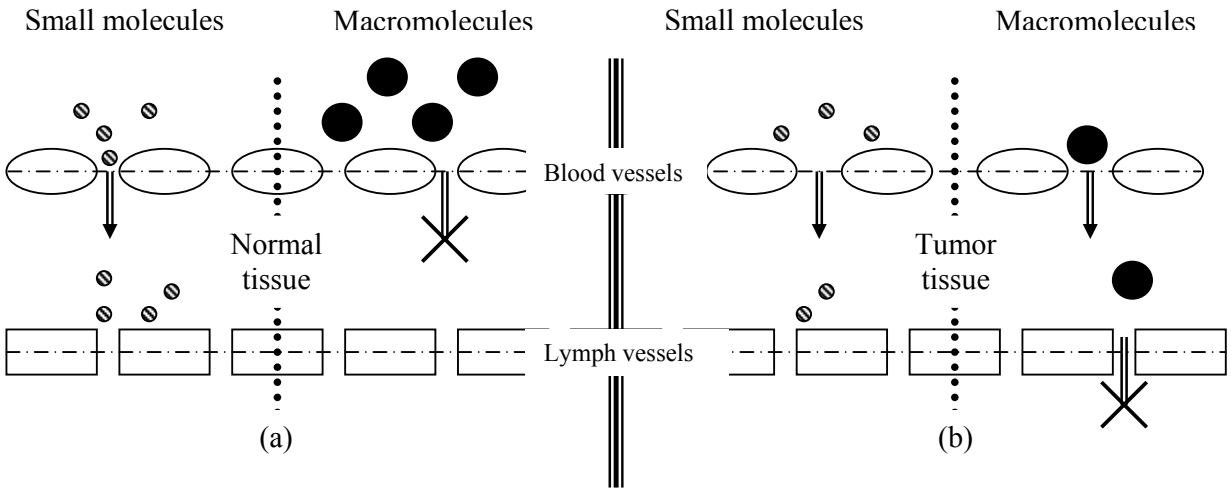

Fig. 1.2: Schematic representation of the EPR effect; a) normal tissue prevents extravasations of macromolecules, whereas low molecular weight agents are drained by the lymphatics; b) dysfunctional lymphatics and highly permeable vascular endothelium allow the preferential accumulation and retention of macromolecule in solid tumor.

Although low molecular weight drugs permeate into tumor interstitium, they are rapidly cleared by diffusion out into the bloodstream. Accumulation of nanoparticles inside tumor was found to be size dependent in animal models and cut-off size depends on various factors such as tumor type, anatomical location, progression stage, etc. (144). However, similar qualitative correlation may be assumed for human cancers. Type of tumor, progression stage and its unique micro-physiology may be exploited for targeting nanoparticles (145).

1.6.3 Surface treatments and modifications

Although nanoparticulate DDS inherently exhibit targetability towards RES organs, escaping RES remains the major challenge for site-specific drug delivery to one or more non-RES organs. During the past few years, several attempts were made to increase circulation half life by avoiding RES recognition (146-150). Most of these approaches demonstrate surface modification by treatment of suitable chemical agents, which would reduce or minimize the interaction with opsonins. As the protein adsorption on to the nanoparticles is the critical step in opsonization, approaches to reduce affinity of these proteins towards the nanoparticles are extensively investigated (151). It has been shown that many bacteria have a highly hydrophilic hydrated surface layer of protein, polysaccharide and glycoprotein that reduces interactions with blood components and inhibits phagocytosis (152, 153). Finding also indicate that poly (ethylene glycol) coating

of proteins may increase the systemic half life (154). Detailed investigation carried out by several authors suggests that the surface hydrophobicity of particles is crucial in opsonization (155). In order to reduce the affinity of the opsonin proteins towards the nanoparticles, most of the current approaches are based on chemical treatments that decrease surface hydrophobicity. Amongst all reported methods, the coating of biodegradable nanoparticles with poly (ethylene glycol), also known as pegylation, is the most efficient technique (156-158).

Few authors have shown that $PLGA_{dl}$ nanoparticles coated biodegradable PLA_l-PEG copolymer are less susceptible to hepatic uptake than uncoated $PLGA_{dl}$ nanoparticles (148). PEG-$PLGA_{dl}$ nanoparticles, methoxy-PEG-PLA nanoparticles and PLA-PEG nanoparticles have shown enhanced circulation half life (159-162). These characteristics of diblock copolymer nanoparticles are due to the reduction of protein adsorption owing to the formation of a hydrophilic layer and a low surface charge originating in PEG (148). Similar findings were also reported for the tri-block copolymers such as PLA-PEG-PLA, as it evaded the RES and remained in the circulation for a long time (163). The circulation half-life of the drug loaded PLA-PEG-PLA nanoparticles was found to increase by two folds, when compared with PLA nanoparticles (164, 165). Moreover, significant decrease in drug distribution to liver and spleen was reported in the same study. Thus, avoiding RES for increased circulation half-life is a good strategy for enhancing the therapeutic efficacy of anticancer drugs (159, 166-170).

1.6.4 Nanoparticles and blood brain barrier

The blood-brain barrier (BBB) represents an insurmountable obstacle for a large number of drugs including antibiotics, anticancer and a variety of central nervous system (CNS) - active drugs, especially hydrophilic drugs. One of the promising alley of nanotechnology is organ or cell-specific drug delivery mediated by nanoparticles (171-175). It is expected that transport of nanoparticles across the blood-brain barrier (BBB) is possible by either passive diffusion, carrier-mediated endocytosis or altering physical integrity of barriers (176). Coating of particles with polysorbates (e.g. polysorbate-80) results in anchoring of apolipoprotein E or other blood components (177-181).

Surface modified particles seem to mimic low density lipoproteins (LDL) and it can interact with the LDL receptor leading to uptake by endothelial cells. Subsequently, the drug (which was loaded in the particle) may be released in these cells and diffuse into the brain interior or the particles may be trans-cytosed. Also, other processes such as tight junction modulation or P-glycoprotein (P-gp) inhibition may also occur (182). In

addition, few authors have reported the translocation of inhaled nanoparticles via the olfactory nerves (183).

Thus, there is adequate evidence cited in literature that suggests that the colloidal nanoparticles can efficiently cross various cellular barriers in organs such as lungs, intestine, brain, skin etc. and almost freely penetrate in most of the organs (184, 185). The primary entry of nanoparticles into the human body depends on their ability to cross cellular barriers, which is principally governed by the size, size distribution and surface charge (186, 187). The biodistribution of nanoparticles is a strong function of surface properties. Although there is no enough clinical evidence that suggests the optimum particle size for effective drug delivery, few research groups have reported the primary requirement of particle size for selected organs in preclinical models. In addition, the pharmacokinetic behavior of different types of nanoparticles depends on several factors such as physicochemical properties of material, size and surface properties of carrier along with the properties of entrapped agent (188). Further, surface engineering can modulate the drug distribution as per requirement of individual disease conditions. Thus, there is certain evidence that nanoparticles affect the pharmacokinetics of many drugs and there exists a critical size limit beyond which the movement of the nanoparticles in various organs is restricted.

1.6.5 Nanoparticles and drug resistance

Nanoparticles can enhance the therapeutic efficacy of several drugs by overcoming drug resistance through various mechanisms (189-193). As the most common mechanism, Labhasetwar et al were first to report that the polymeric nanoparticles can be taken up by cells via endocytosis, resulting in higher cellular uptake of the entrapped therapeutic agent (194).

Subsequently, the migration of protons from the bulk liquid to the nanoparticle surface leads to surface charge reversal from anionic to cationic in the acidic pH of secondary endosomes / lysosomes. Further, the mechanistic studies confirmed that nanoparticles can escape the endo-lysosomal pathways, following cellular uptake and it can easily enter into the cytoplasm through a process of the surface charge reversal (Fig. 1.3). The change in surface charge results in the interaction with the anionic lysosomal membrane, causing the escape of nanoparticles into the cytoplasm (195). Once inside cytoplasm, nanoparticles act as intracellular drug depots leading to slow release of the encapsulated therapeutic agent in the cellular cytoplasm for a sustained period of time (196, 197)

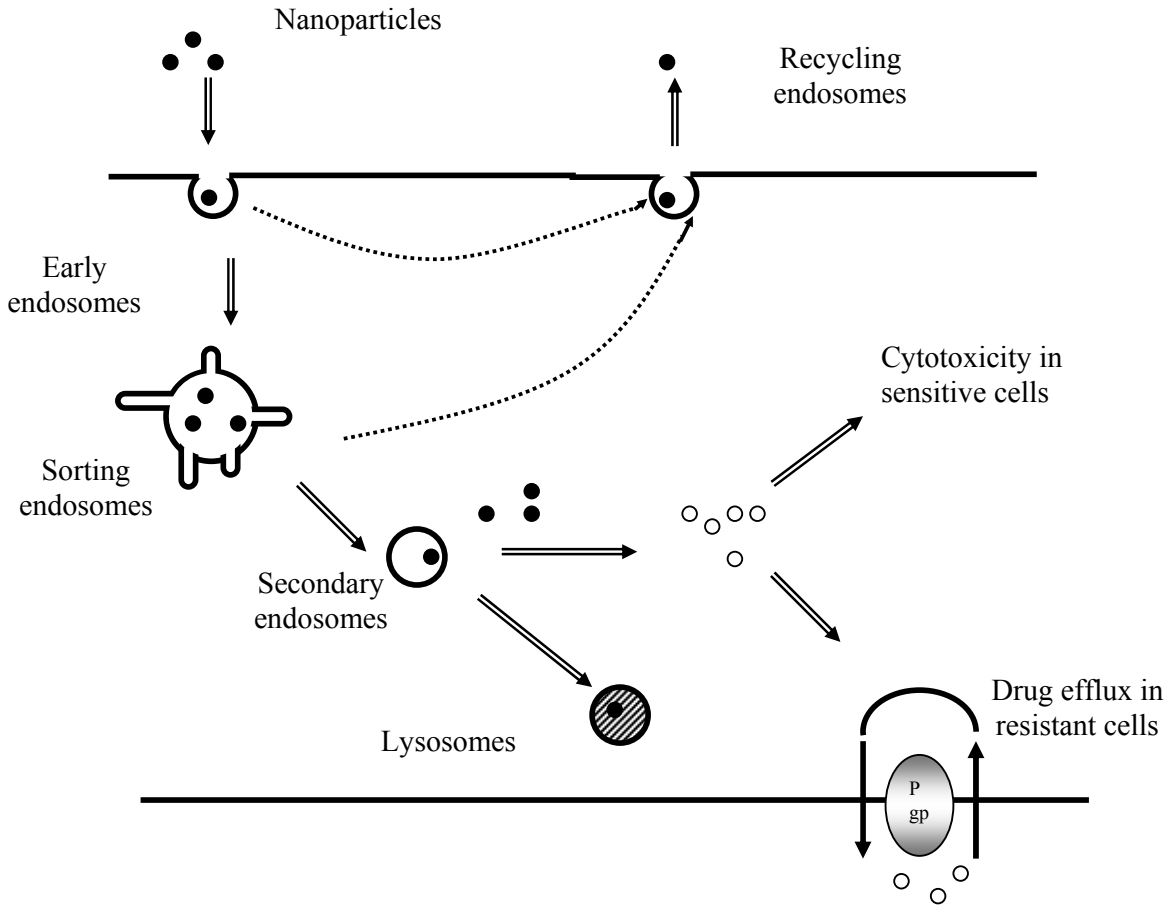

Fig. 1.3: Proposed scheme for cellular trafficking of polymeric nanoparticles in drug-resistant and sensitive cells

1.6.6 In vivo fate of nanoparticles

The in vivo fate of a drug after extravascular administration is determined by a combination of several processes such as absorption, distribution, metabolism and elimination (198). Regardless of the mechanisms involved, these pharmacokinetic processes are mainly attributed to the physicochemical properties of the drug and therefore on its chemical structure. During the last two decades, extensive research work has been carried out for the development of delivery systems which can modulate the in vivo fate of drugs for enhanced therapeutic actions (199-201). Although nanoparticles are reported to act principally on the drug distribution process in the body, they can also alter absorption, metabolism and elimination of a drug significantly (202, 203).

a) Intra-venous administration

Following intra-venous administration, the nanoparticles come in contact with the various blood components such as plasma proteins, blood cells, etc. Like all other xenobiotics entering into vascular compartment, most of the nanoparticulate DDS evoke similar

immune responses which in turn activate several mechanisms to eliminate nanoparticles out of the body. Several investigators have reported that nanoparticles are cleared immediately after systemic administration and this short half life is consistently observed with several different polymer types such as poly styrene, poly (lactic acid), albumin, poly (lactic acid-co-glycolic acid), poly (alkyl cyanoacrylate), poly (acryl starch) etc. irrespective of their chemical composistion (113, 204-207). Recognition of nanoparticulate DDS by the phagocytes is the principle mechanism for detection and elimination of these foreign products from systemic circulation.

A significant challenge in drug targeting is presented by the rapid uptake of nanoparticulate DDS by the cells of the reticulo-endothelial system (RES). Essentially, macrophages located in the RES, mainly comprises the cells of the mono-nuclear phagocyte system and the polymorpho-nuclear leukocytes, which play a crucial role in phagocytosis. Saba et al have reported that the Küpffer cells of the liver comprise 85-95% of the total elimination capacity (208-210). This scavenging mechanism also exists in the spleen and bone marrow and is found to play an important role in the elimination of nanoparticles (211, 212). Few authors have reported that the particle size plays critical role in systemic elimination of nanoparticulate DDS and nanoparticles larger than 200 nm are selectively screened by monocytes and macrophages of the liver, spleen etc. (212).

Several authors have reported that the rapid particle phagocytosis is principally governed by the process of opsonization. Mechanism is based on release of certain soluble proteins, also called opsonins, which tag all the foreign particles present inside the body by surface deposition (213). Immediately after tagging of nanoparticles, these proteins activate the cascade of events towards phagocytosis and elimination (214). The complement system plays a major in opsonization, while immunoglobulins and other proteins such as fibronectin, C-reactive protein, tuftsin etc. are also known to facilitate the elimination process. Few authors have identified that the serum complement protein C3, one of the most important components of the opsonin system of the body, strongly activates phagocytosis by macrophages (213). While, the other complement proteins such as C4 and C5 were also found to play a significant role in the phagocytic process (215).

b) Oral administration

The potential advantages of nanoparticles are enhancement of oral bioavailability, controlled release of a drug, site specific drug delivery, reduced gastric complications by overcoming one or more critical problems such as low solubility, poor permeability, gut wall metabolism, physical and chemical instability, first pass effect, absorption window,

etc (216, 217). The application of oral nanoparticulate DDSs is principally attributed to the fact that specific particulate uptake mechanisms exist in the gastrointestinal tract such as M cells of Peyer's patches, GALT and other mechanisms, as discussed previously (122, 218-221). From the surface of M cells, nanoparticles are taken up and transported to lymphocytes in the form of vesicles. The lymphatic absorption of a drug through GALT bypasses the portal blood circulation to the liver and the entrapped drug is protected from pre-systemic liver metabolism. This mechanism provides passive targeting of anticancer drug to lymphatics, which are primary targets of metastasis in any tumor. Moreover, after oral administration nanoparticles provide extended physical protection to the entrapped drug from hostile gastrointestinal tract environment and other bioenvironment along the way to the target site (222-224). Once inside the systemic circulation nanoparticles behave as administered via intra-venous route.

1.7 Preparation of nanoparticles

Although several methods are reported in literature for preparation of nanoparticles for various applications, principally these methods are classified in two broad categories as top-down and bottom-up techniques. The former technique represents class of methods based on breaking down materials or attrition to nanoscale, while the latter represent class of methods based on building up or assembling the supramolecular structures from the individual molecule.

1.7.1 Top-down techniques

Most of the top down techniques use conventional size reduction of material such as comminuting, milling or grinding methods for producing large quantity of nano-materials. However, application of this technique in nanoparticulate DDS is limited as the energy requirement is significantly high. Moreover, this technique is not suitable for heat and pressure sensitive materials such as proteins, peptides and several other small molecule drugs. In addition, agglomeration of nano-materials due to increased surface and stability of drug during process are of significant concern.

1.7.2 Bottom-up techniques

In bottom up technique, the drug is dissolved in a suitable solvent system to get molecular solution and the stable supramolecular structures containing drug molecules are formed by aid of self-assembling chemical agents. Although this technique require small amount of energy, gaining control over the procedure of assembling is much more critical for successful formation of stable nanoparticles. In the recent past, several bottom-up approaches have been extensively investigated and have become an integral part in

manufacturing nanoparticulate DDS. Further, this technique offers the advantage of selecting suitable chemical agents and solvents for sensitive drugs such as protein, peptide, vaccines, genes, etc. (225) However, in both, bottom-up and top-down techniques, the stabilization of prepared nanoparticles remains most challenging.

a) Polymeric nanoparticles

In general, most of the bottom-up approaches in the preparation of nanoparticle are based on polymers and are frequently termed as polymeric nanoparticles. Essentially, based on the mechanism of nanoparticle formation these methods can be further categorized as polymerization of dispersed monomers and emulsification of preformed polymers.

The critical quality properties of the nanoparticulate DDS such as average particle size, size distribution, morphology, loading and entrapment efficiency need process control in order to achieve high therapeutic success. However, manufacturing of nanoparticles involves several design variables such as drug(s), polymer(s), emulsifier(s) or surfactant(s), stabilizer(s), along with the processing variables such as sonication, evaporation, centrifugation, drying etc. which govern the final product quality and performance.

For a particular application, studies must be carried out to investigate the effect of individual system components, their strengths or magnitudes along with the impact of various processing parameters on the overall quality of the product. Design of experimentation technique may reduce the number of experiments required to be carried out in order to investigate relationship between individual variable and its effect on the final quality of the product. Moreover, studies can suggest magnitude of the individual effect and explain the first and second order interactions among two or more product and process variables. Application of these techniques may provide detailed insight into the formulation aspect of a new DDS and help to reduce experimental time and associated research costs.

Selection of a suitable method for the preparation of nanoparticles depends on the therapeutic application of the drug, site of administration, duration of therapy, physicochemical properties of the drug, polymer and individual excipients. The preparation techniques along with the selected polymer(s) largely determine the in vitro drug release characteristics and in vivo pharmacokinetic performance. Although several types of nano-structures are apparently possible with different types of preparation methods and polymers, all nanoparticles are largely classified as nanospheres or nanocapsules (Fig. 1.4). The former represents the nanoparticles with monolithic matrix

system wherein the drug can be adsorbed on to surface and dissolved or dispersed uniformly in the matrix, while the latter represents the reservoir type of system comprised of the drug containing non-polymeric core surrounded by uniform polymeric shell (102, 113, 194, 226).

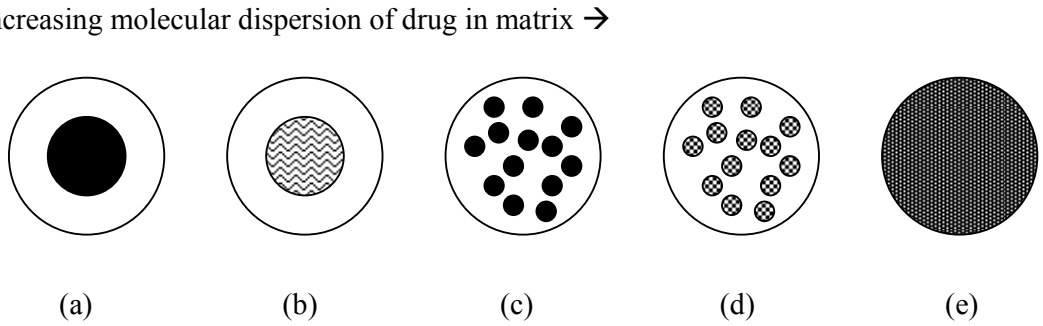

Fig. 1.4: Diagrammatic representation of the possible structures in nanoparticles; a) nanoparticle with solid shell and core; b) nanoparticle with solid shell and non-solid core; c) nanoparticle with solid sub-domains; d) nanoparticles with non-solid sub-domains; e) nanoparticles with polymeric matrix and molecular drug dispersion.

Method of preparation of nanoparticles can be classified as those based on macromolecule cross linking, polymerization and polymer precipitation. First category methods use amphiphilic macromolecules such as proteins, polysaccharides, etc. and techniques are based on aggregation of macromolecules followed by stabilization by heat treatment or chemical cross-linking (227). These processes may occur in biphasic *o/w* or *w/o* type of dispersed systems, which subdivides the amphiphilic macromolecules prior to aggregation stabilization. Aggregation and stabilization can be achieved by various techniques such as cross-linking in *w/o* emulsion, chemical dehydration in emulsion, phase separation (desolvation) in aqueous medium, pH induced aggregation, counter ion induced aggregation, etc. (228-232).

Second category of methods use in situ polymerization technique with polymers such as poly (methyl methacrylate), N-N' methylene-bis-acrylamide, poly (butyl cyanoacrylate), poly (acrylamide), etc. Four different types of techniques widely reported for the preparation are based in situ polymerization, dispersion polymerization, interfacial polymerization and interfacial complexation (233). The first technique uses monomer in non-solvent phase which is emulsified to entrap drug in internal phase. Second technique uses monomer dissolved in a solvent which acts as a non-solvent for formed polymer. Emulsion polymerization offers several advantages over the other techniques and follows

two mechanisms of nucleation during polymerization - micellar and homogenous nucleation. Earlier, emulsion polymerization method was extensively used for preparation of nanoparticles of water insoluble drugs by *w/o* emulsification technique. Briefly, water insoluble monomer is added an external phase with stabilizer. The monomer is polymerized by anionic polymerization method to get stable polymeric particles containing the drug. Recently, several modifications such as multiple emulsion (*w/o/w*), inverse emulsification polymerization based methods have been reported in literature to incorporate wide variety of drugs such as hydrophilic and lipophilic small molecules, macromolecules, biologicals etc. (234-236).

In dispersion polymerization technique, the monomer is introduced into a dispersion medium of emulsion or inversed emulsion into non-solvent based polymeric solution where nucleation is induced in aqueous monomer solution (237, 238). Interfacial polymerization technique uses two monomers each dissolved into two separate phases of the emulsion. The monomers present in internal phase react with the monomer present in external phase forming polymer at interface. The nanoparticles are formed as the interfacial polymerization process leads to encapsulation of the drug in internal phase. Similarly, interfacial complexation is initiated by competing poly-electrolyte solution which allows insoluble poly electrolyte complex to coacervate at the interface.

Third category represents the most widely accepted methods and involves precipitation of the preformed polymers. This technique is one of the most extensively studied techniques in nanoparticulate preparations. Briefly, hydrophobic polymer is dissolved in organic solvent, which is dispersed in external aqueous phase containing stabilizer leading to precipitation of polymer forming nanoparticles. Depending upon solvent miscibility, techniques are further classified as solvent extraction and solvent evaporation. Typical solvent extraction method involves the formation of conventional *o/w* micro-emulsion between partially water miscible solvent containing the polymer with drug and aqueous phase containing stabilizer. The subsequent addition of water, extracts the organic solvent leading to precipitation (239). Several modifications of the method have led to improved product performance such as use of high pressure homogenizer in the preparation of emulsion, various solvents for spontaneous diffusion etc (240-242).

Solvent displacement (nano-precipitation) technique involves the use of a polymer and drug dissolved in an organic phase, which is completely soluble in external aqueous phase. Upon addition to aqueous phase, the organic solvent diffuses instantaneously to the external aqueous phase with immediate polymer precipitation leading to formation of

nanoparticles (243, 244). Various modified methods are published by several authors in order to increase the loading of drug on to nanoparticles (245). Salting out is the most commonly adopted method for the preparation of nanoparticles and differs slightly from nano-precipitation technique as it involves saturation of aqueous phase to prevent miscibility of organic solvent into it. Precipitation of the polymer is initiated as the external aqueous phase is diluted to diffuse organic phase. This technique is also most suitable for hydrophilic drugs.

Double emulsion solvent evaporation method is a recent modification of solvent evaporation technique in order to increase loading efficiency of water soluble drugs and sensitive biologicals.

1.8 Characterization of nanoparticulate drug delivery system

A unique therapeutic advantage of nanoparticulate drug delivery principally originates from their changed physicochemical properties. The evaluation of the properties aids in enhancing the theoretic performance of nanoparticulate DDS. Like all other pharmaceutical formulations, in vivo performance of nanoparticulate formulations can be correlated with the critical product attributes such as particle size, size distribution, surface morphology and properties, drug loading efficiency, in vitro drug release behavior etc. Moreover, the in vitro evaluation of product properties provide better understanding of their in vivo performance and provides critical input to formulation design, development and optimization.

Although FDA has not released specific guidelines for characterization of nanoparticulate DDS, most of the methods currently employed are of similar nature as that of their sub-micronic colloidal associates such as micelles, liposomes, emulsion etc. Several unique properties of nanoparticulate DDS offers distinct advantages as compared to conventional DDS, which are extensively investigated during their characterization.

1.8.1 Sizing and morphological properties

Most of the advantages offered by nanoparticulate DDS are based on the assumption that they exist in a sub-micronic range. As discussed earlier, the particle size offers a unique advantage to these DDS and it is the most important parameter for the characterization of nanoparticulate DDS (246, 247). However, there is significant analytical challenge in accurately estimating particle size at a sub-micronic level as it is affected by process variability and critical surface properties. Moreover, size of nanoparticles may exist in a homogeneous (mono-dispersed) or heterogeneous (poly dispersed) form imposing additional challenges.

Two main methods being used currently for the determination of particle size and size distribution are based on light scattering (static or dynamic) and imaging (electron microscopy) techniques (248). The former class represents the advanced spectroscopic techniques such as photon correlation spectroscopy (PCS), quasi-elastic light scattering (QELS) etc.; while, the latter methods represent advanced imaging techniques such as scanning electron microscopy (SEM), transmission electron microscopy (TEM), scanning tunneling electron microscopy (STEM), atomic force microscopy (AFM) etc.

a) Dynamic light scattering

Dynamic light scattering (DLS) based instruments records the variation in the intensity of scattered light, resulting from interference of light scattered by individual particles due to Brownian motion, on time scale (μs). Using a standard assumption of spherical size, low concentration and known viscosity of the suspending medium, the particle size is calculated from the diffusion coefficient calculated from a decay constant, which is obtained from the autocorrelation function. The photon correlation spectroscopy (PCS) represent the most frequently used technique for accurate estimation of the particle size and size distribution based on DLS (249).

b) Electron microscopy

Scanning electron microscopy (SEM) offers advantage of morphological examination with direct visualization of particulate surface (250-253). Transmission electron microscopy (TEM) operates at relatively smaller size range and it provides structural information using electron diffraction. TEM permits differentiation among nanocapsules, nanospheres, liposomes, emulsions etc. The techniques based on electron microscopy offer several advantages in morphological and sizing analysis; however, they provide limited information about the size distribution and true population average. Moreover, these techniques are time consuming, costly and frequently need complementary information about sizing distribution.

c) Atomic force microscopy

Atomic force microscopy (AFM) offer ultra-high resolution in particle size measurement and is based on a physical scanning of samples at sub-micron level using a probe tip of atomic scale (254-256). Instrument provides a topographical map of sample based on forces between the tip and the sample surface. Samples are usually scanned in contact or non-contact mode depending on their properties. In contact mode, the topographical map is generated by tapping the probe on to the surface across the sample and probe hovers over the conducting surface in non-contact mode. AFM provides the most accurate

description of size and size distribution and requires no mathematical treatment. Moreover, particle size obtained by AFM technique provides real picture which helps understand the effect of various biological conditions (249).

1.8.2 Surface properties

Surface properties of nanoparticulate DDSs are critical in determining their drug delivery potential, as these properties govern the overall in vivo performance of the DDS. These properties also modulate the in vitro performance such as stability, drug entrapment efficiency, drug release kinetics, etc. The specific surface area, surface charge and surface hydrophobicity are important properties of nanoparticle as these govern the physicochemical and electrostatic interactions with biological components and overall biodistribution of drug loaded nanoparticles.

a) Surface charge

Surface charge of the colloidal drug carriers can be determined by the electrophoretic mobility of nanoparticles. The surface charge is represented as the zeta potential, which can be obtained from the electrophoretic mobility by using Helmholtz-Smoluchowski equation. Electrophoretic mobility is medium specific and generally measured in phosphate buffer saline at pH 7.4.

Frequently, laser scattering technique such as Laser Doppler Anemometry (Velocimetry) is used to determine the particle velocity in electric field (257). The Zeta potential measurements can be a useful tool for characterizing colloidal DDS, especially when it is used in conjunction with other techniques like size determination by quasi-elastic light scattering. Together, these techniques provide information about the overall surface charge of the particles and the way it is affected by changes in the environment (e.g. pH, presence of counter-ions, adsorption of proteins). Moreover, these measurements provide information about the organization of molecular assembly such as polymer, surfactant, drug, other excipients etc. and the mode of association with drug (entrapment, adsorption and both). In addition, this information may be useful in predicting the effectiveness of the barrier function against opsonization under in vivo conditions after surface modification or treatment. Although the role of zeta potential measurement is critical in characterizing nanoparticulate DDSs, there are only a few investigations carried out for specifying the surface charges.

b) Surface hydrophobicity

Surface hydrophobicity can be determined by several techniques such as hydrophobic-interaction chromatography, biphasic partitioning, adsorption of probes, contact angle

measurements etc. Frequently, nanoparticles are surface engineered to decrease surface hydrophobicity as it leads to opsonization, as described earlier. Recently, several sophisticated analytical techniques are reported in literature for surface analysis of nanoparticles. X-ray photon correlation spectroscopy permits the identification of specific chemical groups on the surface of nanoparticles (258).

c) Specific surface area and other properties

The specific surface area of dried nanoparticles can be determined by the sorptometric techniques using the following equation. Frequently, surface modifications or treatments need this information in order to optimize various processing parameter in the preparation of nanoparticles. Together with density measurements, these data provide critical information about the porosity, density distribution within the particle, structural properties (smoothness, imperfections) etc. The later studies can be carried out by gas Pycnometer as described by Kreuter (203). In order to confirm the effect of surface engineering, surface characterization demands additional investigations such as molecular weight analysis. Molecular weight of the polymer used affects surface properties and it can be conveniently determined by gel permeation chromatography (GPC) with refractive index (RI) detector.

1.8.3 Bulk properties

Most of the bulk properties indicate the ability of nanoparticulate DDSs to efficiently deliver the drug to the site of action. However, the ultimate in vivo performance of the nanoparticulate systems is a complex function of all critical properties. The bulk properties of nanoparticulate systems govern the gross product performance including drug loading and entrapment efficiency, drug release kinetics, drug stability and compatibility etc. In vitro evaluations for these properties provide a better understanding of various pharmaceutical considerations, which may aid in development and optimization of the product.

a) Drug loading and entrapment efficiency

Therapeutic success of nanoparticulate DDS is attributed to its ability to release the drug within the vicinity of site of action at required rate over the extended duration. The drug associated with nanoparticles offer unique advantages, which are not available with free drug. Thus, the extent of incorporation of the drug in nanoparticles is the most critical factor in determining in vivo efficacy and is represented as the drug loading efficiency (drug content). Frequently, it is determined as the amount of drug present per unit weight

of the final product by analyzing the recovered drug from the nanoparticles using suitable extraction method.

The ability of the manufacturing process and components to incorporate or associate the drug efficiently in nanoparticles is represented as drug entrapment efficiency, which can be conveniently expressed by analyzing the free drug and entrapped drug or total drug. As discussed earlier, the drug can be either entrapped within the reservoir (nanocapsules) or uniformly dispersed within the matrix (nanospheres) and/or it may be associated with the surface of nanoparticles. Loosely associated and adsorbed drugs can be separated by mild washing treatment with suitable solvent media. The overall efficiency of the manufacturing process is represented as a recovery of the obtained product.

b) In vitro drug release kinetics

In a conventional DDS, the drug is released from the formulation at the site of administration or absorption and the released free drug migrate across the various biological barriers reaching the desired site of action. Mathematical model for the release studies are based on the premise that the rate and extent of drug available at the site of action is a function of the free drug release at the site of absorption or administration. Unlike conventional DDS, the nanoparticulate systems have ability to cross various biological barriers as they permeate inside systemic circulation and other tissues with differential affinity. So, the mathematical model used in modeling of the release data from conventional DDS may not be suitable for nanoparticulate DDS. Moreover, selected models should explain the drug release during the transit of the particle from the site of administration to the site of action.

Although several researchers around the world have investigated the effect of various formulation parameters on the release behavior of drug for conventional DDS, only a few studies have been carried out to investigate the release behavior of the drug from nanoparticulate DDS with suitable mathematical models. Crank et al and Polakoviĉ et al have made significant contributions in explaining the release behavior of drugs from the DDS (259, 260). Many previous attempts to model diffusion-controlled drug delivery from nanoparticulate DDS are largely based on empirically determined diffusion coefficients. For the first time, Polakoviĉ et al have suggested two main possible models to investigate the release rate of the drug from the polymeric nanoparticulate DDS and are based on the diffusion and the dissolution phenomenon. Usually, the drug is homogeneously mixed within the polymeric matrix in monolithic devices and can be either in a dissolved or dispersed state.

Frequently, the release kinetics of the drug can be explained by Fickian kinetics, if the drug is in dissolved state or by the Higuchi's square-root kinetics, if the drug is uniformly dispersed in the polymer matrix. Recently, Jo et al have reported a revised mathematical expression for diffusion models based on Fick's second law for diffusion phenomenon (261). Further, the coefficient reported by Jo et al are significantly different than those previously reported by Crank et al and Polakovič et al and gives more accurate mathematical expression. Unlike conventional models, these mathematical models are applicable to nanoparticulate DDS and can explain the controlled-release behavior during circulation in the blood stream and localization on the target site.

Jalil et al have suggested that the various formulation factors such as diffusion through particle pores, intact polymers, water swollen polymers and surface desorption along with surface or bulk erosion of the polymeric matrix influence the release mechanism of the drug from spherical DDS (262-270). Often, one or more such mechanisms contribute in the process of drug release. To some extent, the polymer matrix erosion contributes in drug release, while the other factors indirectly influence the rate of release through diffusion mechanisms as they affect the particle morphology. In addition, the swelling of polymer network and solid drug dissolution are also reported to play significant role in modulation of drug release from nanoparticulate DDS. Similar factors are extendable to nanoparticulate DDS based on their spherical and polymeric nature. Moreover, significance of individual mechanism of drug release varies with the factors such as molecular weight of the polymer, composition, crystallinity, the loading amounts of the drug, interaction between polymer and drug etc. These factors can be adjusted in a formulation design to achieve the desired release profile of the drug. The accurate mathematical modeling of the drug release rate is a key input in design and development of nanoparticulate DDS.

1.8.4 Drug stability and other properties

Nanoparticulate DDS provides extended protection to the entrapped drug by reducing interaction with external factors such as enzymatic, proteolytic, hydrolytic, oxidative stress etc. This protective function of nanoparticulate DDS is assessed by the in vitro characterization for stability of free drug and encapsulated drug. Like conventional DDS, the preparation of nanoparticles involve several processing steps, wherein, the drug is exposed to various stress conditions such as solvents, homogenization, high speed shear, heat treatment, freeze-drying etc. Stability of drug during and after preparation is analyzed in a similar way to that of a conventional DDS.

a) Thermal properties and crystallinity

Nanoparticulate materials provide significantly different properties as compared to free drugs. Thermal properties provide good understanding about the nanomaterials such as the physicochemical properties of polymer, drug, stabilizer and other excipients and their compatibility with each other. Moreover, the measurement of thermal properties such as glass transition temperature, melting temperature and their associated enthalpies offers unique advantage, which can be used to determine the nature and speciation of crystallinity within the nanoparticles. These techniques always provide complement information to X-ray diffraction analysis and it can be used to determine the relative extent of multiple phases in the nanomaterial and their possible interaction. Differential scanning calorimetry (DSC) represents the most frequently used analytical tool for thermal analysis of samples (271).

In summary, nanotechnology is playing critical role in DDS for enhancing the therapeutic efficacy of several drugs. The increased availability of novel polymers in DDS and advanced techniques in nanotechnology may lead to development and extension of the applications of nanoparticulate DDS in therapeutics which will continue to grow in the future. However, better characterization tools are essential in vitro evaluation of nanoparticulate products, which subsequently aid in predicting the in vivo response and efficacy.

1.8.5 In vivo characterization in animal models

From a regulatory point of view, an important consideration for the development of any DDS is the quantity of evidence needed in particular circumstances to substantiate the proof of therapeutic effectiveness. Although the possible alternative approaches are described in the Modernization Act (FDA MA), all are based on extrapolation of data obtained from the conventional drug delivery systems (CDDS) to novel drug delivery systems (NDDS). Ordinarily, this takes into account the other supporting data such as in vitro characterization and drug release kinetics which provide the evidence of effectiveness for a new drug product application.

Considering the fact that the formulations based on nanoparticulate DDS have capability to modulate the in vivo absorption, distribution, metabolism and elimination behavior of the drug, the pharmacokinetic profile of nanoparticulate DDS and CDDS may not be identical. In most of the cases, effectiveness of a developed nanoparticulate DDS as a new drug product cannot be demonstrated without additional pharmacokinetic studies. Moreover, the release kinetics of the drug from these formulations may significantly

differ from that of the CDDS. It is important to have complete understanding of the relationship of plasma concentration to response and the time course of this relationship, in the preclinical animal models before exploring its final clinical effects.

Although currently no specific guidelines are available for nanotechnology based formulations are available, the pharmacokinetic requirements for NDDS covered under 21-CFR-320.25(f) are applicable to these formulations. Further, these regulations indicate that pharmacokinetic data obtained from the plasma concentration time profile of a drug under investigation is sufficient for its regulatory approval as NDDS. As there exist ample evidence to define the predictive relationship between the plasma concentrations of a drug and its therapeutic response, both regarding the safety and efficacy. Thus, the products based on nanotechnology may be claimed therapeutically effective on the basis of its in vitro characterization and in vivo pharmacokinetic data.

1.9 Summary

Despite the enormous development in molecular biology of cancer, even the rationally designed molecular approaches suffer from major problems such as - poor physicochemical properties leading to instability and/or poor bioavailability, nonspecific biodistribution leading to poor site-specific bioavailability, permeation across various biological barriers, intra- and inter-subject pharmacokinetic variations, emergence of inherent and acquired resistance, sub-optimal drug levels from activated efflux systems and recurrence of disease. Most of these reasons are interlinked but need to be addressed individually. Aspects of this disease will remain as a formidable challenge in drug delivery, in order to translate new techniques into clinical practice, for ultimate success of the therapy**.**

On the other hand, nanotechnology and nanoscience are becoming increasingly important for various drug delivery applications in several therapeutic and diagnostic segments. Considering the fact that the diameter of the smallest blood capillary is 4 μm, the US FDA has approved use of nanoparticles of less than 1 μm diameter for intra-venous applications (102, 113, 272). Similar size requirements are also applicable for intra-muscular and subcutaneous administration of nanoparticulate DDS in order to reduce possible irritation reaction (273).

However, the properties of the nanoparticles should be optimized in order to meet the specific requirements of the drug and disease condition. Nanoparticles provide substantial advantages such as modulation of physicochemical properties (stability, solubility, release etc.), pharmacokinetics (drug absorption, distribution, metabolism and elimination) and

pharmacodynamics (drug action) of the drug. Moreover, several novel materials and advanced engineering approaches are available for preparation and characterization of nanoparticles. Moreover, the preparation of tailor-made nanoparticles may offers significant advantage in cancer drug delivery.

1.10 Problem definition and research objectives

Imatinib represents the prototype of protein tyrosine kinase inhibitors that have replaced the earlier class of drugs with low efficacy and high toxicity. Although Imatinib offers enhanced pharmacodynamic benefits, currently marketed formulations of Imatinib present several clinical limitations. It has been reported that activation of P-gp efflux reduces bioavailability of Imatinib with subsequent dosing leading to poor prognosis of the disease with frequent resistance and relapse. Unlike classical chemotherapy, Imatinib requires continuous treatment regimen extending over a period of time demanding frequent administration. It also undergoes efflux mechanisms leading to reduced cytotoxic effect with subsequent exposure. Moreover, intra- and inter-subject pharmacokinetic variability affects its in vivo biodistribution. A non-specific biodistribution presents significant therapeutic challenge for successful therapy e.g. the poor biodistribution to the organs and deep tissues like brain results in subtherapeutic levels of the drug leading to resistance in metastic tumors.

During the past few years, the interest in NDDS has been increased due to their potential in drug delivery application such as controlled and targeted drug delivery, enhanced stability etc. Nanoparticulate DDS have already been validated for better therapeutic efficacy by the enhanced permeation and retention effect, which allows selective targeting to the cancer cells. Thus, the principle objective of the present research work was to design and develop nanoparticulate DDS using biodegradable and biocompatible polymers for improved therapeutic efficacy of Imatinib mesylate by controlling its release characteristics and modifying biodistribution behavior with enhanced and selective distribution to brain. To achieve this broad objective, following specific studies were carried out in the present work.

Design and development of nanoparticulate DDS for Imatinib mesylate. Quality parameters of the prepared drug product and substance were evaluated by well established methods and protocols. Suitable analytical and bioanalytical methods were developed based on spectrophotometric and liquid chromatography for determination of the drug in formulation and biological matrix.

For efficient product development, the preformulation studies were performed to establish necessary physicochemical data of Imatinib mesylate prior to formulation development. Studies were performed to address the product specific questions related to drug solubility, stability, drug-excipient compatibility, etc.

Formulation development was carried out by identifying and optimizing the critical factors in the design and the process using optimization techniques. The prepared nanoparticles were extensively characterized for surface morphology and shape, particle size and size distribution, drug content (loading and entrapment efficiency) and in vitro drug release. Further, the optimized formulations were studied for the drug product stability and reproducibility.

Pharmacokinetic studies were performed to investigate in vivo performance of the prepared nanoparticles in healthy rat model. In situ rat intestinal absorption studies were performed to investigate the significance of the efflux transport processes and effect of efflux modulators on the absorption profile of pure drug. The model was also employed to study the relative absorption behavior of the pure drug and drug loaded nanoparticles.

Biodistribution studies were carried out to investigate the overall systemic and tissue (brain and lungs) specific bioavailability of the pure drug and optimized nanoparticulate formulations. The in vivo biodistribution behavior of Imatinib mesylate loaded nanoparticles after oral and intra-venous administration was studied in comparison with the pure drug. Obtained pharmacokinetic data was modeled using non compartmental analysis to predict the preclinical and clinical efficacy of formulations in the diseased subjects.

References

1. M.P. Kamps. Differentiation and cancer: Basic research. In J.R. Bertino (ed.), Encyclopedia of Cancer, Vol. 2, Elsevier Science, New York, 2002, pp. 49-63.
2. R.Y.C. Poon. Cell cycle control. In J.R. Bertino (ed.), Encyclopedia of Cancer, Vol. 1, Elsevier Science, New York, 2002, pp. 393-403.
3. C.H. McGowan. Cell cycle checkpoints. In J.R. Bertino (ed.), Encyclopedia of Cancer, Vol. 1, Elsevier Science, New York, 2002, pp. 383-391.
4. L.A. Culp, R. Judware, P. Kogerman, J.L. Holleran, and C.J. Miller. Extracellular matrix and matrix receptors: Alterations during tumor pogression. In J.R. Bertino (ed.), Encyclopedia of Cancer, Vol. 2, Elsevier Science, New York, 2002, pp. 215-233.

5. D.L. Vaux and A. Strasser. The molecular biology of apoptosis. Proc Natl Acad Sci U S A. 93:2239-2244 (1996).
6. B.W. Stewart and P. Kleihues. World Cancer Report - International Agency for Research on Cancer (IARC), *Non-serial Publication*, World Health Organization, Geneva, Switzerland, 2003.
7. L. Gao, L. Chen, X.H. Fei, H.Y. Qiu, H. Zhou, and J.M. Wang. STI571 combined with vincristine greatly suppressed the tumor formation of multidrug-resistant K562 cells in a human-nude mice xenograft model. Chin Med J. 119:911-918 (2006).
8. X.W. Wang, J.R. Zhang, Y. Shen, G. Zheng, and C.C. Zhong. Glivec enhances the down-regulated cytotoxicity of adriamycin in acquired tamoxifen-resistant MCF-7 cell line. Di Yi Jun Yi Da Xue Xue Bao. 23:731-733 (2003).
9. J. Jakubowska, M. Stasiak, A. Szulawska, A. Bednarek, and M. Czyz. Combined effects of doxorubicin and STI571 on growth, differentiation and apoptosis of CML cell line K562. Acta Biochim Pol. 54:839-846 (2007).
10. R.A. Schwartzman and J.A. Cidlowski. Apoptosis: the biochemistry and molecular biology of programmed cell death. Endocr Rev. 14:133-151 (1993).
11. P. Blume-Jensen and T. Hunter. Signal transduction mechanisms initiated by receptor tyrosine kinases. In J.R. Bertino (ed.), Encyclopedia of Cancer, Vol. 4, Elsevier Science, New York, 2002, pp. 213-234.
12. A. Levitzki. Tyrosine kinases as targets for cancer therapy. Eur J Cancer. 38 Suppl 5:S11-18 (2002).
13. M.K. Pauland A.K. Mukhopadhyay. Tyrosine kinase - Role and significance in Cancer. Int J Med Sci. 1:101-115 (2004).
14. D.R. Robinson, Y.M. Wu, and S.F. Lin. The protein tyrosine kinase family of the human genome. Oncogene. 19:5548-5557 (2000).
15. T.G. Lugo, A.M. Pendergast, A.J. Muller, and O.N. Witte. Tyrosine kinase activity and transformation potency of bcr-abl oncogene products. Science. 247:1079-1082 (1990).
16. B.J. Druker, S. Tamura, E. Buchdunger, S. Ohno, G.M. Segal, S. Fanning, J. Zimmermann, and N.B. Lydon. Effects of a selective inhibitor of the Abl tyrosine kinase on the growth of Bcr-Abl positive cells. Nat Med. 2:561-566 (1996).
17. T. Pawson. Signal transduction--a conserved pathway from the membrane to the nucleus. Dev Genet. 14:333-338 (1993).

18. C.H. Heldin. Dimerization of cell surface receptors in signal transduction. Cell. 80:213-223 (1995).
19. K.S. Kolibaba and B.J. Druker. Protein tyrosine kinases and cancer. Biochim Biophys Acta. 1333:F217-248 (1997).
20. J.B. Konopka, S.M. Watanabe, and O.N. Witte. An alteration of the human c-abl protein in K562 leukemia cells unmasks associated tyrosine kinase activity. Cell. 37:1035-1042 (1984).
21. R. Kurzrock, J.U. Gutterman, and M. Talpaz. The molecular genetics of Philadelphia chromosome-positive leukemias. N Engl J Med. 319:990-998 (1988).
22. A. Hermans, N. Heisterkamp, M. von Linden, S. van Baal, D. Meijer, D. van der Plas, L.M. Wiedemann, J. Groffen, D. Bootsma, and G. Grosveld. Unique fusion of bcr and c-abl genes in Philadelphia chromosome positive acute lymphoblastic leukemia. Cell. 51:33-40 (1987).
23. E. Buchdunger, J. Zimmermann, H. Mett, T. Meyer, M. Muller, U. Regenass, and N.B. Lydon. Selective inhibition of the platelet-derived growth factor signal transduction pathway by a protein-tyrosine kinase inhibitor of the 2-phenylaminopyrimidine class. Proc Natl Acad Sci U S A. 92:2558-2562 (1995).
24. E. Buchdunger, J. Zimmermann, H. Mett, T. Meyer, M. Muller, B.J. Druker, and N.B. Lydon. Inhibition of the Abl protein-tyrosine kinase in vitro and in vivo by a 2-phenylaminopyrimidine derivative. Cancer Res. 56:100-104 (1996).
25. J. Zimmermann, G. Caravatti, H. Mett, T. Meyer, M. Muller, N.B. Lydon, and D. Fabbro. Phenylamino-pyrimidine (PAP) derivatives: a new class of potent and selective inhibitors of protein kinase C (PKC). Arch Pharm (Weinheim). 329:371-376 (1996).
26. J.A. Shabbits, R. Krishna, and L.D. Mayer. Molecular and pharmacological strategies to overcome multidrug resistance. Expert Rev Anticancer Ther. 1:585-594 (2001).
27. N. Krishnamachary and M.S. Center. The MRP gene associated with a non-P-glycoprotein multidrug resistance encodes a 190-kDa membrane bound glycoprotein. Cancer Res. 53:3658-3661 (1993).
28. V. Kirkin, S. Joos, and M. Zornig. The role of Bcl-2 family members in tumorigenesis. Biochim Biophys Acta. 1644:229-249 (2004).

29. K. Viktorsson, L. De Petris, and R. Lewensohn. The role of p53 in treatment responses of lung cancer. Biochem Biophys Res Commun. 331:868-880 (2005).

30. K. Viktorsson, R. Lewensohn, and B. Zhivotovsky. Apoptotic pathways and therapy resistance in human malignancies. Adv Cancer Res. 94:143-196 (2005).

31. A.M. Deffie, J.K. Batra, and G.J. Goldenberg. Direct correlation between DNA topoisomerase II activity and cytotoxicity in adriamycin-sensitive and -resistant P388 leukemia cell lines. Cancer Res. 49:58-62 (1989).

32. Y. Zhangand P. Talalay. Mechanism of differential potencies of isothiocyanates as inducers of anticarcinogenic Phase 2 enzymes. Cancer Res. 58:4632-4639 (1998).

33. A.T. Nies, G. Jedlitschky, J. Konig, C. Herold-Mende, H.H. Steiner, H.P. Schmitt, and D. Keppler. Expression and immunolocalization of the multidrug resistance proteins, MRP1-MRP6 (ABCC1-ABCC6), in human brain. Neuroscience 129:349-360 (2004).

34. S.E. Bates, S. Bakke, M. Kang, R.W. Robey, S. Zhai, P. Thambi, C.C. Chen, S. Patil, T. Smith, S.M. Steinberg, M. Merino, B. Goldspiel, B. Meadows, W.D. Stein, P. Choyke, F. Balis, W.D. Figg, and T. Fojo. A phase I/II study of infusional vinblastine with the P-glycoprotein antagonist valspodar (PSC 833) in renal cell carcinoma. Clin Cancer Res. 10:4724-4733 (2004).

35. P. Heffeter, M. Pongratz, E. Steiner, P. Chiba, M.A. Jakupec, L. Elbling, B. Marian, W. Korner, F. Sevelda, M. Micksche, B.K. Keppler, and W. Berger. Intrinsic and acquired forms of resistance against the anticancer ruthenium compound KP1019 [indazolium trans-[tetrachlorobis(1H-indazole)ruthenate (III)] (FFC14A). J Pharmacol Exp Ther. 312:281-289 (2005).

36. A. Hanafy, H. Spahn-Langguth, G. Vergnault, P. Grenier, M. Tubic Grozdanis, T. Lenhardt, and P. Langguth. Pharmacokinetic evaluation of oral fenofibrate nanosuspensions and SLN in comparison to conventional suspensions of micronized drug. Adv Drug Deliv Rev. 59:419-426 (2007).

37. J.C. Leroux, R. Cozens, J.L. Roesel, B. Galli, F. Kubel, E. Doelker, and R. Gurny. Pharmacokinetics of a novel HIV-1 protease inhibitor incorporated into biodegradable or enteric nanoparticles following intravenous and oral administration to mice. J Pharm Sci. 84:1387-1391 (1995).

38. B.J. Trock, F. Leonessa, and R. Clarke. Multidrug resistance in breast cancer: a meta-analysis of MDR1/gp170 expression and its possible functional significance. J Natl Cancer Inst. 89:917-931 (1997).
39. Chintamani, J.P. Singh, M.K. Mittal, S. Saxena, A. Bansal, A. Bhatia, and P. Kulshreshtha. Role of p-glycoprotein expression in predicting response to neoadjuvant chemotherapy in breast cancer--a prospective clinical study. World J Surg Oncol. 3:61 (2005).
40. J. Renes, E.G. de Vries, P.L. Jansen, and M. Muller. The (patho)physiological functions of the MRP family. Drug Resist Updat. 3:289-302 (2000).
41. P. Borst, R. Evers, M. Kool, and J. Wijnholds. A family of drug transporters: the multidrug resistance-associated proteins. J Natl Cancer Inst. 92:1295-1302 (2000).
42. J. Konig, A.T. Nies, Y. Cui, I. Leier, and D. Keppler. Conjugate export pumps of the multidrug resistance protein (MRP) family: localization, substrate specificity, and MRP2-mediated drug resistance. Biochim Biophys Acta. 1461:377-394 (1999).
43. M. Links and R. Brown. Clinical relevance of the molecular mechanisms of resistance to anti-cancer drugs. Expert Rev Mol Med. 1999:1-21 (1999).
44. R.P. Feynman. There's plenty of room at the bottom. Journal of Microelectromechanical Systems. 1:60-66 (1967).
45. Promotional Brochure. National Nanotechnology Initiative National Science & Technology Council, 2000.
46. J. Kreuter. Nanoparticles--a historical perspective. Int J Pharm. 331:1-10 (2007).
47. P. Couvreur, G. Barratt, E. Fattal, P. Legrand, and C. Vauthier. Nanocapsule technology: a review. Crit Rev Ther Drug Carrier Syst. 19:99-134 (2002).
48. K.E. Drexler. Molecular engineering: An approach to the development of general capabilities for molecular manipulation. Proc Natl Acad Sci U S A. 78:5275-5278 (1981).
49. H.W. Hellinga. Computational protein engineering. Nat Struct Biol. 5:525-527 (1998).
50. C.O. Pabo and E.G. Suchanek. Computer-aided model-building strategies for protein design. Biochemistry. 25:5987-5991 (1986).
51. P.D. Vogel. Nature's design of nanomotors. Eur J Pharm Biopharm. 60:267-277 (2005).

52. Report. Nanotechnology, The Royal Society & The Royal Academy of Engineering, 2004.
53. J.M. Balbus, K. Florini, R.A. Denison, and S.A. Walsh. Getting it right the first time: developing nanotechnology while protecting workers, public health, and the environment. Ann N Y Acad Sci. 1076:331-342 (2006).
54. O.M. Koo, I. Rubinstein, and H. Onyuksel. Role of nanotechnology in targeted drug delivery and imaging: a concise review. Nanomedicine. 1:193-212 (2005).
55. C. Zandonella. Cell nanotechnology: The tiny toolkit. Nature. 423:10-12 (2003).
56. J.W. Choi, B.K. Oh, Y.K. Kim, and J. Min. Nanotechnology in biodevices. J Microbiol Biotechnol. 17:5-14 (2007).
57. N.A. Peppas. Intelligent therapeutics: biomimetic systems and nanotechnology in drug delivery. Adv Drug Deliv Rev. 56:1529-1531 (2004).
58. R. Paull, J. Wolfe, P. Hebert, and M. Sinkula. Investing in nanotechnology. Nat Biotechnol. 21:1144-1147 (2003).
59. L. Mazzola. Commercializing nanotechnology. Nat Biotechnol. 21:1137-1143 (2003).
60. T.M. Allen and P.R. Cullis. Drug delivery systems: entering the mainstream. Science. 303:1818-1822 (2004).
61. K. Kostarelos. Rational design and engineering of delivery systems for therapeutics: biomedical exercises in colloid and surface science. Adv Colloid Interface Sci. 106:147-168 (2003).
62. S.M. Moghimi and T. Kissel. Particulate nanomedicines Adv Drug Deliv Rev. 58:1451-1455 (2006).
63. O. Salata. Applications of nanoparticles in biology and medicine. J Nanobiotechnology 2:3 (2004).
64. M. Ferrariand G. Downing. Medical nanotechnology: shortening clinical trials and regulatory pathways? BioDrugs. 19:203-210 (2005).
65. M. Yokoyama. Drug targeting with nano-sized carrier systems. J Artif Organs. 8:77-84 (2005).
66. J. Kreuter. Nanoparticulate systems in drug delivery and targeting. J Drug Target. 3:171-173 (1995).
67. M. Ferrari. Cancer nanotechnology: opportunities and challenges. Nat Rev Cancer. 5:161-171 (2005).

68. M. Sprintz, C. Benedetti, and M. Ferrari. Applied nanotechnology for the management of breakthrough cancer pain. Minerva Anestesiol. 71:419-423 (2005).
69. S.M. Moghimi and A.R. Rajabi-Siahboomi. Recent advances in cellular, sub-cellular and molecular targeting. Adv Drug Deliv Rev. 41:129-133 (2000).
70. N. Surtiand A. Misra. Wheat germ agglutinin-conjugated nanoparticles for sustained cellular and lung delivery of budesonide. Drug Deliv. 15:81-86 (2008).
71. L.H. Reddy. Drug delivery to tumours: recent strategies. J Pharm Pharmacol. 57:1231-1242 (2005).
72. A.T. Florence. Pharmaceutical nanotechnology: more than size. Ten topics for research. Int J Pharm. 339:1-2 (2007).
73. K. Park. Nanotechnology: What it can do for drug delivery. J Control Release. 120:1-3 (2007).
74. O.C. Farokhzad and R. Langer. Nanomedicine: developing smarter therapeutic and diagnostic modalities. Adv Drug Deliv Rev. 58:1456-1459 (2006).
75. I. Brigger, J. Morizet, G. Aubert, H. Chacun, M.J. Terrier-Lacombe, P. Couvreur, and G. Vassal. Poly(ethylene glycol)-coated hexadecylcyanoacrylate nanospheres display a combined effect for brain tumor targeting. J Pharmacol Exp Ther. 303:928-936 (2002).
76. J. Alper. Drug delivery. Breaching the membrane. Science. 296:838-839 (2002).
77. J. Darius, F.P. Meyer, B.A. Sabel, and U. Schroeder. Influence of nanoparticles on the brain-to-serum distribution and the metabolism of valproic acid in mice. J Pharm Pharmacol. 52:1043-1047 (2000).
78. T.K. Jain, M.K. Reddy, M.A. Morales, D.L. Leslie-Pelecky, and V. Labhasetwar. Biodistribution, Clearance, and Biocompatibility of Iron Oxide Magnetic Nanoparticles in Rats. Mol Pharm *In press* (2008).
79. F. Esmaeili, M.H. Ghahremani, B. Esmaeili, M.R. Khoshayand, F. Atyabi, and R. Dinarvand. PLGA nanoparticles of different surface properties: preparation and evaluation of their body distribution. Int J Pharm. 349:249-255 (2008).
80. S. Kommareddy and M. Amiji. Biodistribution and pharmacokinetic analysis of long-circulating thiolated gelatin nanoparticles following systemic administration in breast cancer-bearing mice. J Pharm Sci. 96:397-407 (2007).
81. J.V. Aukunuru, S.P. Ayalasomayajula, and U.B. Kompella. Nanoparticle formulation enhances the delivery and activity of a vascular endothelial growth

factor antisense oligonucleotide in human retinal pigment epithelial cells. J Pharm Pharmacol. 55:1199-1206 (2003).

82. S.M. Moghimi. Recent developments in polymeric nanoparticle engineering and their applications in experimental and clinical oncology. Anticancer Agents Med Chem. 6:553-561 (2006).
83. J.L. Fox. Researchers discuss NIH's nanotechnology initiative. Nat Biotechnol. 18:821 (2000).
84. M.C. Roco. Nanotechnology: convergence with modern biology and medicine. Curr Opin Biotechnol. 14:337-346 (2003).
85. R. Sandler and W.D. Kay. The national nanotechnology initiative and the social good. J Law Med Ethics. 34:675-681 (2006).
86. J. Alper. US NCI launches nanotechnology plan. Nat Biotechnol. 22:1335-1336 (2004).
87. E.S. Kawasaki and A. Player. Nanotechnology, nanomedicine, and the development of new, effective therapies for cancer. Nanomedicine. 1:101-109 (2005).
88. S.L. Fluckiger. Industry's challenge to academia: changing the bench to bedside paradigm. Exp Biol Med. 231:1257-1261 (2006).
89. R.P. Kulkarni. Nano-Bio-Genesis: tracing the rise of nanotechnology and nanobiotechnology as 'big science'. J Biomed Discov Collab. 2:3 (2007).
90. D. Ho, D. Garcia, and C.M. Ho. Nanomanufacturing and characterization modalities for bio-nano-informatics systems. J Nanosci Nanotechnol. 6:875-891 (2006).
91. A. Moreno-Aspitia and E.A. Perez. North Central Cancer Treatment Group N0531: Phase II Trial of weekly albumin-bound paclitaxel (ABI-007; Abraxane) in combination with gemcitabine in patients with metastatic breast cancer. Clin Breast Cancer. 6:361-364 (2005).
92. T.E. Stinchcombe, M.A. Socinski, C.M. Walko, B.H. O'Neil, F.A. Collichio, A. Ivanova, H. Mu, M.J. Hawkins, R.M. Goldberg, C. Lindley, and E. Claire Dees. Phase I and pharmacokinetic trial of carboplatin and albumin-bound paclitaxel, ABI-007 (Abraxane) on three treatment schedules in patients with solid tumors. Cancer Chemother Pharmacol. 60:759-766 (2007).
93. K. Altundag, D.S. Dede, and T. Purnak. Albumin-bound paclitaxel (ABI-007; Abraxane) in the management of basal-like breast carcinoma. J Clin Pathol. 60:958 (2007).

94. M.R. Green, G.M. Manikhas, S. Orlov, B. Afanasyev, A.M. Makhson, P. Bhar, and M.J. Hawkins. Abraxane, a novel Cremophor-free, albumin-bound particle form of paclitaxel for the treatment of advanced non-small-cell lung cancer. Ann Oncol. 17:1263-1268 (2006).

95. E. Mathiowitz, J.S. Jacob, Y.S. Jong, G.P. Carino, D.E. Chickering, P. Chaturvedi, C.A. Santos, K. Vijayaraghavan, S. Montgomery, M. Bassett, and C. Morrell. Biologically erodable microspheres as potential oral drug delivery systems. Nature. 386:410-414 (1997).

96. M.A. Moses, H. Brem, and R. Langer. Advancing the field of drug delivery: taking aim at cancer. Cancer Cell. 4:337-341 (2003).

97. J. Kreuter. Drug targeting with nanoparticles. Eur J Drug Metab Pharmacokinet. 19:253-256 (1994).

98. N.A. Peppas and J.R. Robinson. Bioadhesives for optimization of drug delivery. J Drug Target. 3:183-184 (1995).

99. R. Langer, J.L. Cleland, and J. Hanes. New advances in microsphere-based single-dose vaccines. Adv Drug Deliv Rev. 28:97-119 (1997).

100. J.T. Santini, Jr., A.C. Richards, R.A. Scheidt, M.J. Cima, and R.S. Langer. Microchip technology in drug delivery. Ann Med. 32:377-379 (2000).

101. R.S. Langer and N.A. Peppas. Present and future applications of biomaterials in controlled drug delivery systems. Biomaterials. 2:201-214 (1981).

102. K.S. Soppimath, T.M. Aminabhavi, A.R. Kulkarni, and W.E. Rudzinski. Biodegradable polymeric nanoparticles as drug delivery devices. J Control Release. 70:1-20 (2001).

103. I. Brigger, C. Dubernet, and P. Couvreur. Nanoparticles in cancer therapy and diagnosis. Adv Drug Deliv Rev. 54:631-651 (2002).

104. M.J. Alonso. Nanomedicines for overcoming biological barriers. Biomed Pharmacother. 58:168-172 (2004).

105. F. Ahsan, I.P. Rivas, M.A. Khan, and A.I. Torres Suarez. Targeting to macrophages: role of physicochemical properties of particulate carriers--liposomes and microspheres--on the phagocytosis by macrophages. J Control Release. 79:29-40 (2002).

106. M.F. Zambaux, F. Bonneaux, R. Gref, E. Dellacherie, and C. Vigneron. Protein C-loaded monomethoxypoly (ethylene oxide)-poly(lactic acid) nanoparticles. Int J Pharm. 212:1-9 (2001).

107. R. Gref, P. Quellec, A. Sanchez, P. Calvo, E. Dellacherie, and M.J. Alonso. Development and characterization of CyA-loaded poly(lactic acid)-poly(ethylene glycol)PEG micro- and nanoparticles. Comparison with conventional PLA particulate carriers. Eur J Pharm Biopharm. 51:111-118 (2001).

108. C. Evora, I. Soriano, R.A. Rogers, K.N. Shakesheff, J. Hanes, and R. Langer. Relating the phagocytosis of microparticles by alveolar macrophages to surface chemistry: the effect of 1,2-dipalmitoylphosphatidylcholine. J Control Release. 51:143-152 (1998).

109. R.S. Langer. An audience with Robert S. Langer [interviewed by Kenneth J. Germeshausen]. Nat Rev Drug Discov. 3:546 (2004).

110. Z. Ahmad, R. Pandey, S. Sharma, and G.K. Khuller. Pharmacokinetic and pharmacodynamic behaviour of antitubercular drugs encapsulated in alginate nanoparticles at two doses. Int J Antimicrob Agents. 27:409-416 (2006).

111. M.E. Akerman, W.C. Chan, P. Laakkonen, S.N. Bhatia, and E. Ruoslahti. Nanocrystal targeting in vivo. Proc Natl Acad Sci U S A. 99:12617-12621 (2002).

112. C. Alexiou, R.J. Schmid, R. Jurgons, M. Kremer, G. Wanner, C. Bergemann, E. Huenges, T. Nawroth, W. Arnold, and F.G. Parak. Targeting cancer cells: magnetic nanoparticles as drug carriers. Eur Biophys J. 35:446-450 (2006).

113. E. Allemann, J. Leroux, and R. Gurny. Polymeric nano- and microparticles for the oral delivery of peptides and peptidomimetics. Adv Drug Deliv Rev. 34:171-189 (1998).

114. T. Ameller, V. Marsaud, P. Legrand, R. Gref, and J.M. Renoir. In vitro and in vivo biologic evaluation of long-circulating biodegradable drug carriers loaded with the pure antiestrogen RU 58668. Int J Cancer. 106:446-454 (2003).

115. T.A. Elbayoumiand V.P. Torchilin. Tumor-specific antibody-mediated targeted delivery of Doxil((R)) reduces the manifestation of auricular erythema side effect in mice. Int J Pharm *In press* (2008).

116. C.M. Lehr. Lectin-mediated drug delivery: the second generation of bioadhesives. J Control Release. 65:19-29 (2000).

117. E. Sanders and C.T. Ashworth. A study of particulate intestinal absorption and hepatocellular uptake. Use of polystyrene latex particles. Exp Cell Res. 22:137-145 (1961).

118. M. Garinot, V. Fievez, V. Pourcelle, F. Stoffelbach, A. des Rieux, L. Plapied, I. Theate, H. Freichels, C. Jerome, J. Marchand-Brynaert, Y.J. Schneider, and V. Preat. PEGylated PLGA-based nanoparticles targeting M cells for oral vaccination. J Control Release. 120:195-204 (2007).

119. M.H. El-Shabouri. Positively charged nanoparticles for improving the oral bioavailability of cyclosporin-A. Int J Pharm. 249:101-108 (2002).

120. O. Harush-Frenkel, E. Rozentur, S. Benita, and Y. Altschuler. Surface charge of nanoparticles determines their endocytic and transcytotic pathway in polarized MDCK cells. Biomacromolecules. 9:435-443 (2008).

121. F. Delie. Evaluation of nano- and micro-particle uptake by the gastrointestinal tract. Adv Drug Deliv Rev. 34:221-233 (1998).

122. S. McClean, E. Prosser, E. Meehan, D. O'Malley, N. Clarke, Z. Ramtoola, and D. Brayden. Binding and uptake of biodegradable poly-DL-lactide micro- and nanoparticles in intestinal epithelia. Eur J Pharm Sci. 6:153-163 (1998).

123. P. Jani, G.W. Halbert, J. Langridge, and A.T. Florence. Nanoparticle uptake by the rat gastrointestinal mucosa: quantitation and particle size dependency. J Pharm Pharmacol. 42:821-826 (1990).

124. M.R. Neutra, A. Frey, and J.P. Kraehenbuhl. Epithelial M cells: Gateways for mucosal infection and immunization. Cell. 86:345-348 (1996).

125. R.L. Owen. And now pathophysiology of M cells: Good news and bad news from Peyer's patches. Gastroenterology. 85:468-470 (1983).

126. M.A. Clark, M.A. Jepson, and B.H. Hirst. Exploiting M cells for drug and vaccine delivery. Adv Drug Deliv Rev. 50:81-106 (2001).

127. T.H. Ermak and P.J. Giannasca. Microparticle targeting to M cells. Adv Drug Deliv Rev. 34:261-283 (1998).

128. M.A. Jepson, M.A. Clark, N. Foster, C.M. Mason, M.K. Bennett, N.L. Simmons, and B.H. Hirst. Targeting to intestinal M cells. J Anat. 189 (Pt 3):507-516 (1996).

129. J.S. Trier. Structure and function of intestinal M cells. Gastroenterol Clin North Am. 20:531-547 (1991).

130. Y. Fujimura, T. Kihara, K. Ohtani, R. Kamoi, T. Kato, K. Kozuka, N. Miyashima, and J. Uchida. Distribution of microfold cells (M cells) in human follicle-associated epithelium. Gastroenterol Jpn. 25:130 (1990).

131. M.R. Neutra, T.L. Phillips, E.L. Mayer, and D.J. Fishkind. Transport of membrane-bound macromolecules by M cells in follicle-associated epithelium of rabbit Peyer's patch. Cell Tissue Res. 247:537-546 (1987).

132. P. Sicinski, J. Rowinski, J.B. Warchol, Z. Jarzabek, W. Gut, B. Szczygiel, K. Bielecki, and G. Koch. Poliovirus type 1 enters the human host through intestinal M cells. Gastroenterology. 98:56-58 (1990).

133. D.J. Brayden and A.W. Baird. Apical membrane receptors on intestinal M cells: potential targets for vaccine delivery. Adv Drug Deliv Rev. 56:721-726 (2004).

134. D.E. Bockman and M.D. Cooper. Pinocytosis by epithelium associated with lymphoid follicles in the bursa of Fabricius, appendix, and Peyer's patches. An electron microscopic study. Am J Anat. 136:455-477 (1973).

135. R.L. Owen. Sequential uptake of horseradish peroxidase by lymphoid follicle epithelium of Peyer's patches in the normal unobstructed mouse intestine: an ultrastructural study. Gastroenterology. 72:440-451 (1977).

136. E. Ruoslahti. Specialization of tumour vasculature. Nat Rev Cancer. 2:83-90 (2002).

137. H. Hashizume, P. Baluk, S. Morikawa, J.W. McLean, G. Thurston, S. Roberge, R.K. Jain, and D.M. McDonald. Openings between defective endothelial cells explain tumor vessel leakiness. Am J Pathol. 156:1363-1380 (2000).

138. D. Feng, J.A. Nagy, H.F. Dvorak, and A.M. Dvorak. Ultrastructural studies define soluble macromolecular, particulate, and cellular transendothelial cell pathways in venules, lymphatic vessels, and tumor-associated microvessels in man and animals. Microsc Res Tech. 57:289-326 (2002).

139. H. Maeda, J. Wu, T. Sawa, Y. Matsumura, and K. Hori. Tumor vascular permeability and the EPR effect in macromolecular therapeutics: a review. J Control Release. 65:271-284 (2000).

140. H. Maeda, T. Sawa, and T. Konno. Mechanism of tumor-targeted delivery of macromolecular drugs, including the EPR effect in solid tumor and clinical overview of the prototype polymeric drug SMANCS. J Control Release. 74:47-61 (2001).

141. H. Maeda. The enhanced permeability and retention (EPR) effect in tumor vasculature: the key role of tumor-selective macromolecular drug targeting. Adv Enzyme Regul. 41:189-207 (2001).

142. S. Modi, J. Prakash Jain, A.J. Domb, and N. Kumar. Exploiting EPR in polymer drug conjugate delivery for tumor targeting. Curr Pharm Des. 12:4785-4796 (2006).

143. S. Sengupta, D. Eavarone, I. Capila, G. Zhao, N. Watson, T. Kiziltepe, and R. Sasisekharan. Temporal targeting of tumour cells and neovasculature with a nanoscale delivery system. Nature. 436:568-572 (2005).

144. D.A. Sanan, D.L. Newland, R. Tao, S. Marcovina, J. Wang, V. Mooser, R.E. Hammer, and H.H. Hobbs. Low density lipoprotein receptor-negative mice expressing human apolipoprotein B-100 develop complex atherosclerotic lesions on a chow diet: no accentuation by apolipoprotein(a). Proc Natl Acad Sci U S A. 95:4544-4549 (1998).

145. Y. Bae, W.D. Jang, N. Nishiyama, S. Fukushima, and K. Kataoka. Multifunctional polymeric micelles with folate-mediated cancer cell targeting and pH-triggered drug releasing properties for active intracellular drug delivery. Mol Biosyst. 1:242-250 (2005).

146. L. Illum and S.S. Davis. The organ uptake of intravenously administered colloidal particles can be altered using a non-ionic surfactant (Poloxamer 338). FEBS Lett. 167:79-82 (1984).

147. J.H. Senior, K.R. Trimble, and R. Maskiewicz. Interaction of positively-charged liposomes with blood: implications for their application in vivo. Biochim Biophys Acta. 1070:173-179 (1991).

148. S. Stolnik, S.E. Dunn, M.C. Garnett, M.C. Davies, A.G. Coombes, D.C. Taylor, M.P. Irving, S.C. Purkiss, T.F. Tadros, S.S. Davis, and et al. Surface modification of poly(lactide-co-glycolide) nanospheres by biodegradable poly(lactide)-poly(ethylene glycol) copolymers. Pharm Res. 11:1800-1808 (1994).

149. S.M. Moghimi, A.E. Hawley, N.M. Christy, T. Gray, L. Illum, and S.S. Davis. Surface engineered nanospheres with enhanced drainage into lymphatics and uptake by macrophages of the regional lymph nodes. FEBS Lett. 344:25-30 (1994).

150. M. Luck, B.R. Paulke, W. Schroder, T. Blunk, and R.H. Muller. Analysis of plasma protein adsorption on polymeric nanoparticles with different surface characteristics. J Biomed Mater Res. 39:478-485 (1998).

151. S.M. Moghimi, A.C. Hunter, and J.C. Murray. Long-circulating and target-specific nanoparticles: theory to practice. Pharmacol Rev. 53:283-318 (2001).

152. C.J. van Oss. Phagocytosis as a surface phenomenon. Annu Rev Microbiol. 32:19-39 (1978).

153. C.J. van Oss. Phagocytosis: an overview. Methods Enzymol. 132:3-15 (1986).

154. A. Abuchowski, J.R. McCoy, N.C. Palczuk, T. van Es, and F.F. Davis. Effect of covalent attachment of polyethylene glycol on immunogenicity and circulating life of bovine liver catalase. J Biol Chem. 252:3582-3586 (1977).

155. D. Kim, H. El-Shall, D. Dennis, and T. Morey. Interaction of PLGA nanoparticles with human blood constituents. Colloids Surf B Biointerfaces. 40:83-91 (2005).

156. R. Gref, M. Luck, P. Quellec, M. Marchand, E. Dellacherie, S. Harnisch, T. Blunk, and R.H. Muller. 'Stealth' corona-core nanoparticles surface modified by polyethylene glycol (PEG): influences of the corona (PEG chain length and surface density) and of the core composition on phagocytic uptake and plasma protein adsorption. Colloids Surf B Biointerfaces. 18:301-313 (2000).

157. V.C. Mosqueira, P. Legrand, J.L. Morgat, M. Vert, E. Mysiakine, R. Gref, J.P. Devissaguet, and G. Barratt. Biodistribution of long-circulating PEG-grafted nanocapsules in mice: effects of PEG chain length and density. Pharm Res. 18:1411-1419 (2001).

158. R. Gref, Y. Minamitake, M.T. Peracchia, A. Domb, V. Trubetskoy, V. Torchilin, and R. Langer. Poly(ethylene glycol)-coated nanospheres: potential carriers for intravenous drug administration. Pharm Biotechnol. 10:167-198 (1997).

159. R. Gref, Y. Minamitake, M.T. Peracchia, V. Trubetskoy, V. Torchilin, and R. Langer. Biodegradable long-circulating polymeric nanospheres. Science. 263:1600-1603 (1994).

160. D. Bazile, C. Prud'homme, M.T. Bassoullet, M. Marlard, G. Spenlehauer, and M. Veillard. Stealth Me.PEG-PLA nanoparticles avoid uptake by the mononuclear phagocytes system. J Pharm Sci. 84:493-498 (1995).

161. M. Vittaz, D. Bazile, G. Spenlehauer, T. Verrecchia, M. Veillard, F. Puisieux, and D. Labarre. Effect of PEO surface density on long-circulating PLA-PEO nanoparticles which are very low complement activators. Biomaterials. 17:1575-1581 (1996).

162. S.M. Moghimi and J. Szebeni. Stealth liposomes and long circulating nanoparticles: critical issues in pharmacokinetics, opsonization and protein-binding properties. Prog Lipid Res. 42:463-478 (2003).

163. G. He, L.L. Ma, J. Pan, and S. Venkatraman. ABA and BAB type triblock copolymers of PEG and PLA: a comparative study of drug release properties and "stealth" particle characteristics. Int J Pharm. 334:48-55 (2007).

164. Y. Nakada, K. Sakurai, M. Horiushi, R. Tudomi, T. Nakamura, and Y. Takahashi. Long-circulating nanoparticles using biodegradable ABA triblock copolymers containing of poly(L-lactic acid) A-blocks attached to central poly(oxyethylene) B-blocks. Pharm Sci. 3:1-4 (1997).

165. J. Matsumoto, Y. Nakada, K. Sakurai, T. Nakamura, and Y. Takahashi. Preparation of nanoparticles consisted of poly(L-lactide)-poly(ethylene glycol)-poly(L-lactide) and their evaluation in vitro. Int J Pharm. 185:93-101 (1999).

166. S.M. Moghimi, I.S. Muir, L. Illum, S.S. Davis, and V. Kolb-Bachofen. Coating particles with a block co-polymer (poloxamine-908) suppresses opsonization but permits the activity of dysopsonins in the serum. Biochim Biophys Acta. 1179:157-165 (1993).

167. H. Otsuka, Y. Nagasaki, and K. Kataoka. PEGylated nanoparticles for biological and pharmaceutical applications. Adv Drug Deliv Rev. 55:403-419 (2003).

168. A. Bogdanov, Jr., S.C. Wright, E.M. Marecos, A. Bogdanova, C. Martin, P. Petherick, and R. Weissleder. A long-circulating co-polymer in "passive targeting" to solid tumors. J Drug Target. 4:321-330 (1997).

169. V.S. Trubetskoy, G.S. Gazelle, G.L. Wolf, and V.P. Torchilin. Block-copolymer of polyethylene glycol and polylysine as a carrier of organic iodine: design of long-circulating particulate contrast medium for X-ray computed tomography. J Drug Target. 4:381-388 (1997).

170. J. Vandorpe, E. Schacht, S. Dunn, A. Hawley, S. Stolnik, S.S. Davis, M.C. Garnett, M.C. Davies, and L. Illum. Long circulating biodegradable poly(phosphazene) nanoparticles surface modified with poly(phosphazene)-poly(ethylene oxide) copolymer. Biomaterials. 18:1147-1152 (1997).

171. R.N. Alyaudtin, A. Reichel, R. Lobenberg, P. Ramge, J. Kreuter, and D.J. Begley. Interaction of poly(butylcyanoacrylate) nanoparticles with the blood-brain barrier in vivo and in vitro. J Drug Target. 9:209-221 (2001).

172. S.K. Pulfer, S.L. Ciccotto, and J.M. Gallo. Distribution of small magnetic particles in brain tumor-bearing rats. J Neurooncol. 41:99-105 (1999).

173. S. Azarmi, W.H. Roa, and R. Lobenberg. Targeted delivery of nanoparticles for the treatment of lung diseases. Adv Drug Deliv Rev *In press* (2008).

174. Y.C. Kuo and H.H. Chen. Effect of nanoparticulate polybutylcyanoacrylate and methylmethacrylate-sulfopropylmethacrylate on the permeability of zidovudine and lamivudine across the in vitro blood-brain barrier. Int J Pharm. 327:160-169 (2006).

175. A. Prokop and J.M. Davidson. Nanovehicular intracellular delivery systems. J Pharm Sci *In Press* (2008).

176. P.R. Lockman, M.O. Oyewumi, J.M. Koziara, K.E. Roder, R.J. Mumper, and D.D. Allen. Brain uptake of thiamine-coated nanoparticles. J Control Release. 93:271-282 (2003).

177. A. Ambruosi, A.S. Khalansky, H. Yamamoto, S.E. Gelperina, D.J. Begley, and J. Kreuter. Biodistribution of polysorbate 80-coated doxorubicin-loaded [14C]-poly(butyl cyanoacrylate) nanoparticles after intravenous administration to glioblastoma-bearing rats. J Drug Target. 14:97-105 (2006).

178. A. Ambruosi, H. Yamamoto, and J. Kreuter. Body distribution of polysorbate-80 and doxorubicin-loaded [14C]poly(butyl cyanoacrylate) nanoparticles after i.v. administration in rats. J Drug Target. 13:535-542 (2005).

179. P.R. Lockman, J.M. Koziara, R.J. Mumper, and D.D. Allen. Nanoparticle surface charges alter blood-brain barrier integrity and permeability. J Drug Target. 12:635-641 (2004).

180. I. Kratzer, K. Wernig, U. Panzenboeck, E. Bernhart, H. Reicher, R. Wronski, M. Windisch, A. Hammer, E. Malle, A. Zimmer, and W. Sattler. Apolipoprotein A-I coating of protamine-oligonucleotide nanoparticles increases particle uptake and transcytosis in an in vitro model of the blood-brain barrier. J Control Release. 117:301-311 (2007).

181. R.N. Alyautdin, V.E. Petrov, K. Langer, A. Berthold, D.A. Kharkevich, and J. Kreuter. Delivery of loperamide across the blood-brain barrier with polysorbate 80-coated polybutylcyanoacrylate nanoparticles. Pharm Res. 14:325-328 (1997).

182. J. Kreuter. Nanoparticulate systems for brain delivery of drugs. Adv Drug Deliv Rev. 47:65-81 (2001).

183. G. Oberdorster, Z. Sharp, V. Atudorei, A. Elder, R. Gelein, A. Lunts, W. Kreyling, and C. Cox. Extrapulmonary translocation of ultrafine carbon particles following whole-body inhalation exposure of rats. J Toxicol Environ Health A. 65:1531-1543 (2002).

184. B. Muller and J. Kreuter. Enhanced transport of nanoparticle associated drugs through natural and artificial membranes: A general phenomenon? Int J Pharm. 178:23-32 (1999).

185. J. Lademann, H. Richter, A. Teichmann, N. Otberg, U. Blume-Peytavi, J. Luengo, B. Weiss, U.F. Schaefer, C.M. Lehr, R. Wepf, and W. Sterry. Nanoparticles--an efficient carrier for drug delivery into the hair follicles. Eur J Pharm Biopharm. 66:159-164 (2007).

186. Y. Jallouli, A. Paillard, J. Chang, E. Sevin, and D. Betbeder. Influence of surface charge and inner composition of porous nanoparticles to cross blood-brain barrier in vitro. Int J Pharm. 344:103-109 (2007).

187. C. Chouly, D. Pouliquen, I. Lucet, J.J. Jeune, and P. Jallet. Development of superparamagnetic nanoparticles for MRI: effect of particle size, charge and surface nature on biodistribution. J Microencapsul. 13:245-255 (1996).

188. M. Shakweh, M. Besnard, V. Nicolas, and E. Fattal. Poly (lactide-co-glycolide) particles of different physicochemical properties and their uptake by peyer's patches in mice. Eur J Pharm Biopharm. 61:1-13 (2005).

189. I.M. Adcock, K. Ito, and P.J. Barnes. Histone deacetylation: an important mechanism in inflammatory lung diseases. COPD. 2:445-455 (2005).

190. J. Panyamand V. Labhasetwar. Targeting intracellular targets. Curr Drug Deliv. 1:235-247 (2004).

191. J. Panyamand V. Labhasetwar. Sustained cytoplasmic delivery of drugs with intracellular receptors using biodegradable nanoparticles. Mol Pharm. 1:77-84 (2004).

192. J. Zhao, J.E. Kim, E. Reed, and Q.Q. Li. Molecular mechanism of antitumor activity of taxanes in lung cancer (Review). Int J Oncol. 27:247-256 (2005).

193. C. Vauthier, C. Dubernet, C. Chauvierre, I. Brigger, and P. Couvreur. Drug delivery to resistant tumors: the potential of poly(alkyl cyanoacrylate) nanoparticles. J Control Release. 93:151-160 (2003).

194. J. Panyam and V. Labhasetwar. Biodegradable nanoparticles for drug and gene delivery to cells and tissue. Adv Drug Deliv Rev. 55:329-347 (2003).

195. J. Panyam, W.Z. Zhou, S. Prabha, S.K. Sahoo, and V. Labhasetwar. Rapid endo-lysosomal escape of poly(DL-lactide-co-glycolide) nanoparticles: implications for drug and gene delivery. FASEB J. 16:1217-1226 (2002).

196. J. Panyam, S.K. Sahoo, S. Prabha, T. Bargar, and V. Labhasetwar. Fluorescence and electron microscopy probes for cellular and tissue uptake of poly(D,L-lactide-co-glycolide) nanoparticles. Int J Pharm. 262:1-11 (2003).

197. J. Panyam and V. Labhasetwar. Dynamics of endocytosis and exocytosis of poly(D,L-lactide-co-glycolide) nanoparticles in vascular smooth muscle cells. Pharm Res. 20:212-220 (2003).

198. J. Kreuter, M. Nefzger, E. Liehl, R. Czok, and R. Voges. Distribution and elimination of poly(methyl methacrylate) nanoparticles after subcutaneous administration to rats. J Pharm Sci. 72:1146-1149 (1983).

199. S.A. Galindo-Rodriguez, E. Allemann, H. Fessi, and E. Doelker. Polymeric nanoparticles for oral delivery of drugs and vaccines: a critical evaluation of in vivo studies. Crit Rev Ther Drug Carrier Syst. 22:419-464 (2005).

200. M.A. Radwan, I.Y. Zaghloul, and Z.H. Aly. In vivo performance of parenteral theophylline-loaded polyisobutylcyanoacrylate nanoparticles in rats. Eur J Pharm Sci. 8:95-98 (1999).

201. E.S. Park, J.D. Shaughnessy, Jr., S. Gupta, H. Wang, J.S. Lee, H.G. Woo, F. Zhan, J.D. Owens, Jr., M. Potter, S. Janz, and J.F. Mushinski. Gene expression profiling reveals different pathways related to Abl and other genes that cooperate with c-Myc in a model of plasma cell neoplasia. BMC Genomics. 8:302 (2007).

202. J. Kreuter. Evaluation of nanoparticles as drug-delivery systems. II: Comparison of the body distribution of nanoparticles with the body distribution of microspheres (diameter greater than 1 micron), liposomes, and emulsions. Pharm Acta Helv. 58:217-226 (1983).

203. J. Kreuter. Evaluation of nanoparticles as drug-delivery systems. III: materials, stability, toxicity, possibilities of targeting, and use. Pharm Acta Helv. 58:242-250 (1983).

204. L. Illum, S.S. Davis, R.H. Muller, E. Mak, and P. West. The organ distribution and circulation time of intravenously injected colloidal carriers sterically stabilized with a block copolymer--poloxamine 908. Life Sci. 40:367-374 (1987).

205. D.V. Bazile, C. Ropert, P. Huve, T. Verrecchia, M. Marlard, A. Frydman, M. Veillard, and G. Spenlehauer. Body distribution of fully biodegradable [14C]-poly(lactic acid) nanoparticles coated with albumin after parenteral administration to rats. Biomaterials. 13:1093-1102 (1992).

206. P. Artursson, P. Edman, T. Laakso, and I. Sjoholm. Characterization of polyacryl starch microparticles as carriers for proteins and drugs. J Pharm Sci. 73:1507-1513 (1984).

207. J. Williams, R. Lansdown, R. Sweitzer, M. Romanowski, R. LaBell, R. Ramaswami, and E. Unger. Nanoparticle drug delivery system for intravenous delivery of topoisomerase inhibitors. J Control Release. 91:167-172 (2003).

208. T.M. Saba. Physiology and physiopathology of the reticuloendothelial system. Arch Intern Med. 126:1031-1052 (1970).

209. T.M. Allen, C. Hansen, and J. Rutledge. Liposomes with prolonged circulation times: factors affecting uptake by reticuloendothelial and other tissues. Biochim Biophys Acta. 981:27-35 (1989).

210. S.M. Moghimiand H.M. Patel. Serum opsonins and phagocytosis of saturated and unsaturated phospholipid liposomes. Biochim Biophys Acta. 984:384-387 (1989).

211. S.M. Moghimiand H.M. Patel. Differential properties of organ-specific serum opsonins for liver and spleen macrophages. Biochim Biophys Acta. 984:379-383 (1989).

212. S.M. Moghimi, C.J. Porter, I.S. Muir, L. Illum, and S.S. Davis. Non-phagocytic uptake of intravenously injected microspheres in rat spleen: influence of particle size and hydrophilic coating. Biochem Biophys Res Commun. 177:861-866 (1991).

213. J.F. Scieszka and M.J. Cho. Cellular uptake of a fluid-phase marker by human neutrophils from solutions and liposomes. Pharm Res. 5:352-358 (1988).

214. D.E. Owens, 3rdand N.A. Peppas. Opsonization, biodistribution, and pharmacokinetics of polymeric nanoparticles. Int J Pharm. 307:93-102 (2006).

215. J.F. Scieszka, L.L. Maggiora, S.D. Wright, and M.J. Cho. Role of complements C3 and C5 in the phagocytosis of liposomes by human neutrophils. Pharm Res. 8:65-69 (1991).

216. T. Musumeci, C.A. Ventura, I. Giannone, B. Ruozi, L. Montenegro, R. Pignatello, and G. Puglisi. PLA/PLGA nanoparticles for sustained release of docetaxel. Int J Pharm. 325:172-179 (2006).

217. R.H. Muller, S. Runge, V. Ravelli, W. Mehnert, A.F. Thunemann, and E.B. Souto. Oral bioavailability of cyclosporine: solid lipid nanoparticles (SLN) versus drug nanocrystals. Int J Pharm. 317:82-89 (2006).

218. C. Damge, M. Aprahamian, W. Humbert, and M. Pinget. Ileal uptake of polyalkylcyanoacrylate nanocapsules in the rat. J Pharm Pharmacol. 52:1049-1056 (2000).

219. S. Jain, R.K. Sharma, and S.P. Vyas. Chitosan nanoparticles encapsulated vesicular systems for oral immunization: preparation, in-vitro and in-vivo characterization. J Pharm Pharmacol. 58:303-310 (2006).

220. M.I. Papisov, A. Yurkovetskiy, S. Syed, N. Koshkina, M. Yin, A. Hiller, and A.J. Fischman. A systemic route for drug loading to lymphatic phagocytes. Mol Pharm. 2:47-56 (2005).

221. K. Yoncheva, L. Guembe, M.A. Campanero, and J.M. Irache. Evaluation of bioadhesive potential and intestinal transport of pegylated poly(anhydride) nanoparticles. Int J Pharm. 334:156-165 (2007).

222. C.P. Reis, F.J. Veiga, A.J. Ribeiro, R.J. Neufeld, and C. Damge. Nanoparticulate biopolymers deliver insulin orally eliciting pharmacological response. J Pharm Sci *In press* (2008).

223. C.P. Reis, A.J. Ribeiro, S. Houng, F. Veiga, and R.J. Neufeld. Nanoparticulate delivery system for insulin: design, characterization and in vitro/in vivo bioactivity. Eur J Pharm Sci. 30:392-397 (2007).

224. U. Bilati, E. Allemann, and E. Doelker. Strategic approaches for overcoming peptide and protein instability within biodegradable nano- and microparticles. Eur J Pharm Biopharm. 59:375-388 (2005).

225. L.J. Peek, C.R. Middaugh, and C. Berkland. Nanotechnology in vaccine delivery. Adv Drug Deliv Rev *In press* (2008).

226. Y. Nishioka and H. Yoshino. Lymphatic targeting with nanoparticulate system. Adv Drug Deliv Rev. 47:55-64 (2001).

227. K. Widder, G. Flouret, and A. Senyei. Magnetic microspheres: synthesis of a novel parenteral drug carrier. J Pharm Sci. 68:79-82 (1979).

228. P.A. Kramer. Letter: Albumin microspheres as vehicles for achieving specificity in drug delivery. J Pharm Sci. 63:1646-1647 (1974).

229. Y. Nakagawa, K. Takayama, H. Ueda, Y. Machida, and T. Nagai. Preparation of bovine serum albumin nanospheres as drug targeting carriers. Drug Des Deliv. 2:99-107 (1987).

230. K. Bhargavaand H.Y. Ando. Immobilization of active urokinase on albumin microspheres: use of a chemical dehydrant and process monitoring. Pharm Res. 9:776-781 (1992).

231. M. Rajaonarivony, C. Vauthier, G. Couarraze, F. Puisieux, and P. Couvreur. Development of a new drug carrier made from alginate. J Pharm Sci. 82:912-917 (1993).

232. U. Bilati, E. Allemann, and E. Doelker. Development of a nanoprecipitation method intended for the entrapment of hydrophilic drugs into nanoparticles. Eur J Pharm Sci. 24:67-75 (2005).

233. M. Aboubakar, F. Puisieux, P. Couvreur, and C. Vauthier. Physico-chemical characterization of insulin-loaded poly(isobutylcyanoacrylate) nanocapsules obtained by interfacial polymerization. Int J Pharm. 183:63-66 (1999).

234. M.R. Gasco, S. Morel, M. Trotta, and I. Viano. Doxorubicine englobed in polybutylcyanoacrylate nanocapsules: behaviour in vitro and in vivo. Pharm Acta Helv. 66:47-49 (1991).

235. M.S. el-Samaligy, P. Rohdewald, and H.A. Mahmoud. Polyalkyl cyanoacrylate nanocapsules. J Pharm Pharmacol. 38:216-218 (1986).

236. R. Carpignano, M.R. Gasco, and S. Morel. Optimization of doxorubicine incorporation and of the yield of polybutylcyanacrylate nanoparticles. Pharm Acta Helv. 66:28-32 (1991).

237. J. Kreuter and P.P. Speiser. In vitro studies of poly(methyl methacrylate) adjuvants. J Pharm Sci. 65:1624-1627 (1976).

238. F. Stieneker, J. Kreuter, and J. Lower. High antibody titres in mice with polymethylmethacrylate nanoparticles as adjuvant for HIV vaccines. AIDS. 5:431-435 (1991).

239. A. Lamprecht, N. Ubrich, M. Hombreiro Perez, C. Lehr, M. Hoffman, and P. Maincent. Biodegradable monodispersed nanoparticles prepared by pressure homogenization-emulsification. Int J Pharm. 184:97-105 (1999).

240. D. Quintanar-Guerrero, E. Allemann, H. Fessi, and E. Doelker. Pseudolatex preparation using a novel emulsion-diffusion process involving direct displacement of partially water-miscible solvents by distillation. Int J Pharm. 188:155-164 (1999).

241. D. Quintanar-Guerrero, E. Allemann, E. Doelker, and H. Fessi. Preparation and characterization of nanocapsules from preformed polymers by a new process based on emulsification-diffusion technique. Pharm Res. 15:1056-1062 (1998).

242. H. Murakami, M. Kobayashi, H. Takeuchi, and Y. Kawashima. Preparation of poly(DL-lactide-co-glycolide) nanoparticles by modified spontaneous emulsification solvent diffusion method. Int J Pharm. 187:143-152 (1999).

243. J. Molpeceres, M. Guzman, M.R. Aberturas, M. Chacon, and L. Berges. Application of central composite designs to the preparation of polycaprolactone nanoparticles by solvent displacement. J Pharm Sci. 85:206-213 (1996).

244. T. Govender, S. Stolnik, M.C. Garnett, L. Illum, and S.S. Davis. PLGA nanoparticles prepared by nanoprecipitation: drug loading and release studies of a water soluble drug. J Control Release. 57:171-185 (1999).

245. C. Losa, L. Marchal-Heussler, F. Orallo, J.L. Vila Jato, and M.J. Alonso. Design of new formulations for topical ocular administration: polymeric nanocapsules containing metipranolol. Pharm Res. 10:80-87 (1993).

246. M. Gaumet, A. Vargas, R. Gurny, and F. Delie. Nanoparticles for drug delivery: The need for precision in reporting particle size parameters. Eur J Pharm Biopharm *In press* (2007).

247. J.A. Champion, Y.K. Katare, and S. Mitragotri. Particle shape: a new design parameter for micro- and nanoscale drug delivery carriers. J Control Release. 121:3-9 (2007).

248. V. Villari and N. Micali. Light scattering as spectroscopic tool for the study of disperse systems useful in pharmaceutical sciences. J Pharm Sci. 97:1703-1730 (2007).

249. D.N. de Assis, V.C. Mosqueira, J.M. Vilela, M.S. Andrade, and V.N. Cardoso. Release profiles and morphological characterization by atomic force microscopy and photon correlation spectroscopy of 99mTechnetium-fluconazole nanocapsules. Int J Pharm. 349:152-160 (2008).

250. K. Jores, W. Mehnert, M. Drechsler, H. Bunjes, C. Johann, and K. Mader. Investigations on the structure of solid lipid nanoparticles (SLN) and oil-loaded solid

lipid nanoparticles by photon correlation spectroscopy, field-flow fractionation and transmission electron microscopy. J Control Release. 95:217-227 (2004).

251. M. Tobio, R. Gref, A. Sanchez, R. Langer, and M.J. Alonso. Stealth PLA-PEG nanoparticles as protein carriers for nasal administration. Pharm Res. 15:270-275 (1998).
252. P. Calvo, J.L. Vila-Jato, and M.J. Alonso. Comparative in vitro evaluation of several colloidal systems, nanoparticles, nanocapsules, and nanoemulsions, as ocular drug carriers. J Pharm Sci. 85:530-536 (1996).
253. J. Molpeceres, M.R. Aberturas, and M. Guzman. Biodegradable nanoparticles as a delivery system for cyclosporine: preparation and characterization. J Microencapsul. 17:599-614 (2000).
254. A. zur Muhlen, E. zur Muhlen, H. Niehus, and W. Mehnert. Atomic force microscopy studies of solid lipid nanoparticles. Pharm Res. 13:1411-1416 (1996).
255. I. Montasser, H. Fessi, and A.W. Coleman. Atomic force microscopy imaging of novel type of polymeric colloidal nanostructures. Eur J Pharm Biopharm. 54:281-284 (2002).
256. H.G. Shi, L. Farber, J.N. Michaels, A. Dickey, K.C. Thompson, S.D. Shelukar, P.N. Hurter, S.D. Reynolds, and M.J. Kaufman. Characterization of crystalline drug nanoparticles using atomic force microscopy and complementary techniques. Pharm Res. 20:479-484 (2003).
257. C. Sestier, M.F. Da-Silva, D. Sabolovic, J. Roger, and J.N. Pons. Surface modification of superparamagnetic nanoparticles (Ferrofluid) studied with particle electrophoresis: application to the specific targeting of cells. Electrophoresis. 19:1220-1226 (1998).
258. P.D. Scholes, A.G. Coombes, L. Illum, S.S. Davis, J.F. Watts, C. Ustariz, M. Vert, and M.C. Davies. Detection and determination of surface levels of poloxamer and PVA surfactant on biodegradable nanospheres using SSIMS and XPS. J Control Release. 59:261-278 (1999).
259. M. Polakovic, T. Gorner, R. Gref, and E. Dellacherie. Lidocaine loaded biodegradable nanospheres. II. Modelling of drug release. J Control Release. 60:169-177 (1999).
260. J. Crank. The Mathematics of Diffusion, Oxford University Press, New York, 1975.

261. Y.S. Jo, M.-C. Kim, D.K. Kim, C.-J. Kim, Y.-K. Jeong, K.-J. Kim, and M. Muhammed. Mathematical modelling on the controlled-release of indomethacin-encapsulated poly(lactic acid-co-ethylene oxide) nanospheres. Nanotechnology. 15:1186-1194 (2004).

262. R. Jalil and J.R. Nixon. Microencapsulation using poly(L-lactic acid). I: Microcapsule properties affected by the preparative technique. J Microencapsul. 6:473-484 (1989).

263. R. Jalil and J.R. Nixon. Microencapsulation using poly(DL-lactic acid). IV: Effect of storage on the microcapsule characteristics. J Microencapsul. 7:375-383 (1990).

264. R. Jalil and J.R. Nixon. Microencapsulation using poly(DL-lactic acid). III: Effect of polymer molecular weight on the release kinetics. J Microencapsul. 7:357-374 (1990).

265. R. Jalil and J.R. Nixon. Biodegradable poly(lactic acid) and poly(lactide-co-glycolide) microcapsules: problems associated with preparative techniques and release properties. J Microencapsul. 7:297-325 (1990).

266. R. Jalil and J.R. Nixon. Microencapsulation using poly(DL-lactic acid). II: Effect of polymer molecular weight on the microcapsule properties. J Microencapsul. 7:245-254 (1990).

267. R. Jalil and J.R. Nixon. Microencapsulation using poly(DL-lactic acid). I: Effect of preparative variables on the microcapsule characteristics and release kinetics. J Microencapsul. 7:229-244 (1990).

268. R. Jalil and J.R. Nixon. Microencapsulation using poly(L-lactic acid) IV: Release properties of microcapsules containing phenobarbitone. J Microencapsul. 7:53-66 (1990).

269. R. Jalil and J.R. Nixon. Microencapsulation using poly (L-lactic acid) III: Effect of polymer molecular weight on the microcapsule properties. J Microencapsul. 7:41-52 (1990).

270. R. Jalil and J.R. Nixon. Microencapsulation using poly (L-lactic acid) II: Preparative variables affecting microcapsule properties. J Microencapsul. 7:25-39 (1990).

271. D.J. van Drooge, W.L. Hinrichs, M.R. Visser, and H.W. Frijlink. Characterization of the molecular distribution of drugs in glassy solid dispersions at the nano-meter scale, using differential scanning calorimetry and gravimetric water vapour sorption techniques. Int J Pharm. 310:220-229 (2006).

272. H.J. Jeon, Y.I. Jeong, M.K. Jang, Y.H. Park, and J.W. Nah. Effect of solvent on the preparation of surfactant-free poly(DL-lactide-co-glycolide) nanoparticles and norfloxacin release characteristics. Int J Pharm. 207:99-108 (2000).

273. T. Gorner, R. Gref, D. Michenot, F. Sommer, M.N. Tran, and E. Dellacherie. Lidocaine-loaded biodegradable nanospheres. I. Optimization Of the drug incorporation into the polymer matrix. J Control Release. 57:259-268 (1999).

2. Drug Profile

2.1 Introduction

Imatinib mesylate (IM) is a potent inhibitor of several protein-tyrosine kinases such as Abelson proto-oncogene, platelet derived growth factor and cKIT receptor (1-7). The deregulated tyrosine kinase activity has been implicated as a central pathogenic event in a number of human malignancies as it plays a critical role in tumor cell proliferation (8-10). Selective inhibition of the kinase enzymes offers therapeutic benefit with fewer side effects in comparison with the conventional anticancer chemotherapy (11, 12).

IM is first molecularly targeted drug that is rationally designed for the treatment of chronic myeloid leukemia (CML) and gastrointestinal stromal tumors (GIST), both cancers are considered as models for oncology (13-18). The US FDA has given accelerated approval for IM in the first-line treatment of CML and GIST (19-25). IM is also a selective inhibitor of several important cancer targets including Abelson proto-oncogene, Abelson related gene, platelet derived growth factor receptor, stem cell factor receptor etc. Recently, IM has shown promising activity in the treatment of brain tumors such as mixed recurrent gliomas, oligodendroglioma, oligoastrogliomas, etc. (26-30).

2.2 Drug information

Parameters	**Description**
Drug name:	Imatinib
Category:	Anti-neoplastic
Therapeutic class:	1. Protein tyrosine kinase (PTK) inhibitor 2. Signal transduction inhibitor (STI)
Chemical class:	2-phenylaminopyrimidine derivative
Approval status:	US, UK, EU, JP, IN and other countries
Chemical name:	4-(4-methyl-piperazin-1-yl-methyl)-N-[4-methyl-3- (4 -pyridin-3-yl-pyrimidin-2-yl-amino)-phenyl]-benzamide methane sulfonate salt (IUPAC)
Chemical formula:	$C_{29}H_{31}N_7O$
Generic name:	Imatinib (INN, USAN, BAN)
Salts:	Mesylate ($\cdot CH_4SO_3$)
Proprietary names:	Glivec® (US), Gleevec® (UK, EU and Other)

Chemical structure:

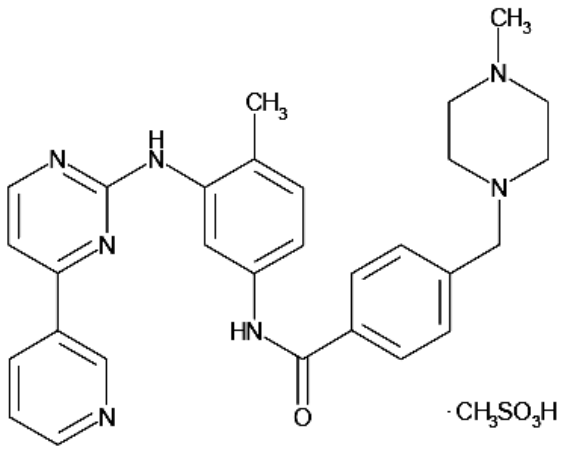

Proprietors:	Novartis Pharmaceuticals, Switzerland
Pre-approval names:	CGP57148B and STI 571 [ATC Code: L01XX28]
CAS registry number:	Imatinib : 152459-95-5 ; mesylate salt : 220127-57-1
Melting point:	226°C[#]
Molecular weight:	base : 493.603 g mol^{-1} salt : 571.48 g mol^{-1}
Water solubility profile:	Water soluble[#] (below pH 5.5)
Physical state:	Solid (white or cream color, odorless powder)
pH of 1% *w/v* solution:	5.5 (aqueous)
Hydrophobicity:	clog P 2.48 ± 0.73
Ionization constant:	1.71 ± 0.02, 3.10 ± 0.01, 3.88 ± 0.03 and 7.7 ± 0.1
Optical activity	Nil (no chiral center)
Hygroscopicity	Not significant (for β-polymorph)
Physical stability:	Fairly stable in solid and liquid states[#]
Photo stability:	Fairly photo stable[#]

INN: International Non-proprietary Names; ATC Code: Anatomical Therapeutic Chemical Classification System; USAN: United States Adopted Names; BAN: British Approved Names; IUPAC: International Union of Pure and Applied Chemistry; US, UK, EU, JP, IN - United States, United kingdom, European Union, Japan, India respectively. [#] *Conclusions based on preformulation studies*

2.3 Pharmacodynamics and therapeutic applications

2.3.1 Chronic myeloid leukemia

IM targets tyrosine kinase protein produced by DNA translocation (the "Philadelphia chromosome") that appears central to CML disease (31). Imatinib is specific for the tyrosine kinase domain in Abl (the Abelson proto-oncogene), c-KIT and PDGFR (platelet derived growth factor receptors) (32, 33). The Philadelphia chromosome leads to a fusion protein of Abl (Abelson) with Bcr (breakpoint cluster region), termed Bcr-Abl. As it is a continuously active tyrosine kinase, Imatinib decreases Bcr-Abl activity (34, 35). The Bcr-Abl tyrosine kinase is a constitutively active kinase that functions by binding ATP and transferring phosphate from ATP to tyrosine residues on various substrates (Fig. 2.1) (36, 37). This activity causes the excessive proliferation of myeloid cells, a characteristic of CML (38-40). IM acts by blocking the binding of ATP to the Bcr-Abl tyrosine kinase thereby inhibiting kinase activity, substrates required for Bcr-Abl function cannot be phosphorylated (41-43). Imatinib has also been found to be effective in patients with blast crises including chronic phase CML.

Pharmacodynamics and mechanism of action

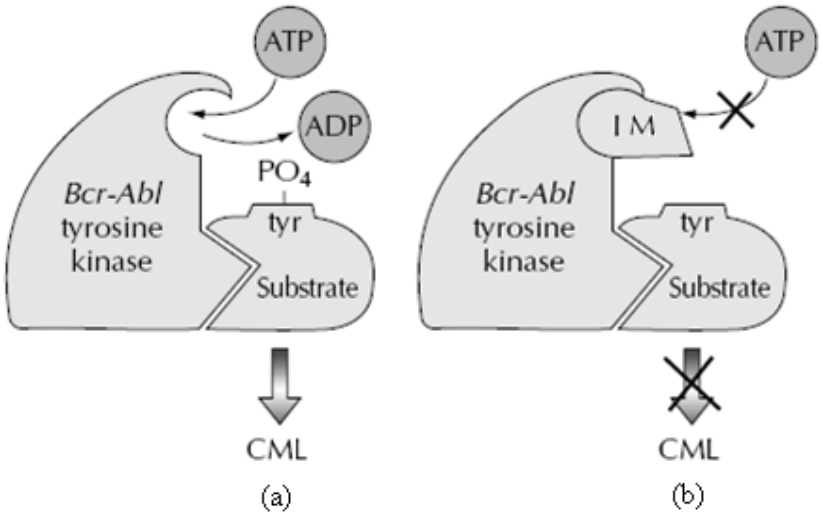

Fig. 2.1: Bcr-Abl tyrosine kinase activity in chronic myeloid leukemia a) a constitutively active kinase functions by binding of ATP to Bcr-Abl tyrosine kinase producing a defective CML protein; b) Imatinib mesylate inhibits binding of ATP to the Bcr-Abl tyrosine kinase blocking the production of defective CML protein.

In a recent Indian report, patients in chronic phase received IM in the dose of 400 mg daily, while those in accelerated phase and blast crisis received 600 to 800 mg daily (44). Of the 97 patients with chronic phase, 49 patients (50.5%) achieved a complete

cytogenetic response. Of the 47 patients in accelerated phase, 10 patients (21.3%) achieved a major cytogenetic response and in 30 patients with blast crisis, 7 (23.3%) achieved a major cytogenetic response.

2.3.2 Gastrointestinal stromal tumors

Gastrointestinal stromal tumors (GIST) is a neoplasm of the gastrointestinal tract, mesentery, or omentum that expresses the protein-tyrosine kinase KIT (45). Most advanced GISTs are resistant to chemotherapy with poor success rate (< 5%). Imatinib, also acts as a c-KIT tyrosine kinase inhibitor and it is reported to be useful in treating GISTs, leading to a 40-70% response rate in metastatic or inoperable cases (46-48). It has increased survival rates up to 1 year in high risk GISTS to more than 90% and also improved survival rates up to 5 years after surgical resection.

2.3.3 Acute lymphoid leukemia

Philadelphia chromosome positive acute lymphoid leukemia (Ph^+ ALL) is a form of adult acute leukemia that has a poor prognosis (49). Moreover, ALL has low response to intensive chemotherapy and high degree of early refractory relapse. Imatinib has been found to be a promising drug in all type of ALL. In a recent study, after a median follow-up period of 25 months in sequential chemotherapy with Imatinib administration prior to bone marrow transplantation, the estimated probability of disease free survival and overall survival was 78% and relapse rate was low at 4% (50, 51).

2.3.4 Clonal eosinophilic disorders and other cancers

Mutations involving the platelet-derived growth factor receptor genes (PDGFR-A and PDGFR-B) have been pathogenetically linked to clonal eosinophilia and their presence predicts complete as well as durable treatment responses to IM (52, 53). These disorders include systemic mastocytosis, chronic eosinophilic leukemia, chronic myelomonocytic leukemia and atypical chronic myelo-proliferative disorder (54, 55). Presence of either PDGFR-A or PDGFR-B mutations necessitates the use of Imatinib in clonal eosinophilia. In hypereosinophilic syndrome, Prednisone, Hydroxyurea and Interferon-α constitute first-line therapy, whereas Imatinib, Cladribine, and Monoclonal antibodies to either interleukin-5 (Mepolizumab) or CD52 (Alemtuzumab) are under clinical investigation.

2.3.5 Therapeutic extensions

Therapeutic applications of IM beyond CML and GIST are being investigated for various other malignancies. Recently, FDA has given simultaneous approval for IM monotherapy in five life-threatening disorders including systemic mastocytosis, myelodysplastic

diseases, hypereosinophilic syndrome and refractory acute lymphoblastic leukemia. It is also approved in solid tumors like unresectable dermatofibrosarcoma protuberans (56, 57).

In a case of chronic neutrophilic leukemia, after failure of alpha interferon and Hydroxyurea therapy, a durable and complete clinical and cytogenetic remission was induced by IM at dose of 400 mg daily. Imatinib in combination with Hydroxyurea proved to be a promising therapy for grade IV progressive glioblastoma multiforme (29). Patients experiencing response or stable disease yielded a combined clinical benefit rate of 57% (26, 28).

Amyloid-β peptides, metabolites of the amyloid precursor protein, are reported to be the central pathological determinants of Alzheimer's disease (58). Newer therapies are targeted to achieve reduction in amyloid-β peptides and/or their accumulation or accumulation in the brain (59, 60). Few authors have provided in vitro and in vivo evidence that IM is effective in reducing the amyloid-β peptide without affecting Notch-1 cleavage (61). Thus, IM may prove clinically useful as a basis for developing novel therapies for Alzheimer's disease (62).

IM treatment was found to be effective in lung cancer as it could suppress the cell growth by inhibiting PDGFRα phosphorylation in a dose dependent manner with the inhibitory concentration of 2-3 μM (IC_{50}) for A549 cell growth (63, 64). Further, the authors also suggested that the drug could potentiate the effect of Cisplatin with synergistic effect indicating a potential role of IM as adjuvant therapeutic agent for the treatment of non-small cell lung cancer. Although role of IM in late phase of lung cancer is unclear, there remains a possibility of successful targeting the early events (65, 66).

Considering the fact that PDGFR and c-KIT play a critical role in the development of Kaposi's sarcoma, Imatinib therapy was proposed as an effective strategy for treating the disease (67). Few authors have reported that IM (10 μM over 48 h) attenuated the activity of T-cell factor/lymphoid enhancer factor, reduced cyclin D1 levels and suppressed thyrocyte proliferation (68). The authors have proposed the Wnt/β-Catenin signaling mediated molecular mechanism as stabilization of adherens junctions by increasing β-catenin/E-cadherin binding and thereby reduction of the invasive potential of anaplastic thyroid cancer.

The preclinical investigations have indicated the importance of inhibition of Abl and PDGFR phosphorylation in the treatment of patients with endometrial carcinoma (69).

Similarly, few authors have supported the rational for clinical trial of IM against uveal melanoma by recording the decrease in proliferation and invasion rates in human uveal melanoma cell lines (70).

The dual inhibition of the transforming growth factor β (TGF_β) and PDGF pathways have reported to results in potent antifibrotic effects (71). The authors have proposed that IM is a promising candidate for the treatment of fibrotic diseases such as systemic sclerosis. In a case report, a need for the clinical trials against rheumatoid arthritis is strongly indicated by few authors (72). Similarly, the promising results obtained in preliminary investigations against chordoma were sufficient to initiate Phase II trials (73).

Several groups have suggested that IM also has activity in mast-cell disease, even in the absence of associated eosinophilia (74-76). The potential of targeting c-KIT and $PDGFR_\beta$ kinases as a primary treatment target in uterine sarcomas is reported in literature (77). IM also found to inhibit spontaneous rhythmic contractions of human uterus and intestine (78). A dose-dependent suppression of neointimal hyperplasia is observed with IM treatment. Moreover, the synergistic effect of co-administration with Rapamycin is also documented by the authors (79). A randomized double-blind placebo-controlled trial is being conducted for effectiveness of IM in restenosis prevention (80). IM also modulates the tumor necrotic factor α (TNFα) in monocytes and macrophages and there by acts as a potent anti-inflammatory agent (81).

2.4 Pharmacokinetics

2.4.1 Absorption

Pharmacokinetic studies in humans demonstrated that Imatinib was absorbed rapidly after oral administration, with a peak concentration (C_{max}) reaching within 2 to 4 h and the detectable amount in plasma was observed within 30 min of dosing (82-84). Mean C_{max} ranged from 72 ng mL^{-1} (25 mg dose) to 3,016 ng mL^{-1} (750 mg dose) after once-daily administration and from 2,315 ng mL^{-1} (800 mg dose) to 3,380 ng mL^{-1} (1,000 mg dose) after twice-daily administration.

Following oral administration of ^{14}C-labeled Imatinib, the radioactivity observed in plasma was more than 80% of the dose (85). After oral administration, the absolute bioavailability of Imatinib was reported in the range of 80-113% (86). Although there was no significant change in pharmacokinetic parameters of IM when administered with a high-fat diet, it delayed the time to reach peak plasma concentration (T_{max}) by approximately one hour and reduced the peak plasma concentration (C_{max}).

2.4.2 Distribution

Imatinib is reported to be extensively bound to plasma proteins with 89% to 96% bound fraction. Plasma protein binding studies performed using in vitro models revealed that Imatinib preferentially binds to albumin and α-1-acid glycoproteins (87, 88). Although, there is no in vivo study reported in humans to investigate the extent and variability of plasma protein binding, several investigators have indicated the possibility of variable plasma protein binding as a reason for pharmacokinetic variability.

The steady-state mean plasma-trough concentration at 24 h post dosing was reported to be 0.72 μg mL^{-1} (1.46 μM) with 400 mg oral administration, which is significantly greater than that required to inhibit proliferation of Bcr-Abl positive leukemic cells obtained from patients with CML. The concentration of Imatinib required to inhibit 50% of cellular phosphorylation by Bcr-Abl (IC_{50}) is reported to be 0.25 μM.

2.4.3 Metabolism

Imatinib is metabolized primarily in liver as it is a good substrate of the cytochrome P450 isoenzymes. Among all cytochrome P450 isoenzymes, CYP3A4 isoenzyme plays a major role in metabolism, while the other isoenzymes such as CYP1A2, CYP2D6, CYP2C9 and CYP2C19 contribute to a little extent. However, Imatinib is a potent competitive inhibitor of CYP2D6 and there are potential chances of drug-drug interactions with co-administered drugs, which are substrates of CYP2D6 (89).

The drug is principally metabolized by CYP3A4 isoenzyme into its N-demethylated piperazine derivative, which was earlier recognized as CGP74588. This main circulating metabolite is also called as N-desmethyl-imatinib ($C_{29}H_{33}N_7SO_4$). In literature, there was no information available either on the in vivo efficacy or pharmacokinetic profiles of N-desmethyl-imatinib. However, Novartis internal reports suggested that the principle metabolite has shown comparable biologic activity in the in vitro models for Bcr-Abl, c-Abl, PDGFR and c-KIT tyrosine kinases (90).

Few authors have reported a correlation between the dose administered and the dynamics of hematologic response in chronic-phase CML patients, however, these results were associated with considerable inter-subject variability in drug exposure (% RSD, 40-60), which was attributed to a major metabolizing enzyme i.e. CYP3A4 and variable plasma protein binding (91). Similar findings were also reported by few other authors at steady-state conditions, wherein, the mean ratio of the plasma concentration of Imatinib to its metabolite was found to be 5.18 (92).

The principle metabolite of Imatinib i.e. N-desmethyl-imatinib has shown mean half-life of 40 h and 74.3 h in two separate studies. Only 5 to 10% of Imatinib and N-desmethyl-imatinib has been reported to be excreted via renal elimination with plasma AUC of about 15% of the AUC of Imatinib (83). Further, the authors have reported that the N-desmethyl-imatinib to Imatinib ratio was 17% with a distinct inter-subject variability of 74%, probably reflecting different metabolic behavior among individual patients (83). Thus, marked inter-subject variability in plasma area under the curve compared with administered dose of IM has been documented by several authors, independently. Although there were no detailed investigations carried out for explaining the intra- and inter-subject variability, it has been attributed to the variability of metabolizing enzymes, efflux systems, protein binding etc.

2.4.4 Elimination

Elimination of Imatinib was reported to be primarily as a metabolite via fecal route with 65-70% of the dose recovered in the feces and 10-15% in the urine, within seven days of administration. Wherein, unchanged Imatinib accounted for 25% of the recovered dose (≈ 5% urine, 20% feces). Accumulation is approximately 1.5 to 3 fold at steady-state with once daily administration. In a study of the 24 h urine elimination, few authors have reported a total elimination of Imatinib as 5.6% and N-desmethyl-imatinib as 2.2% of the administered dose (83). The mean plasma half-life of Imatinib was found to be 12-18 hours and Cl/F was about 12.5 L h^{-1} with 400 mg oral administration (83, 93). The elimination half-life of its major active metabolite, the N-desmethyl derivative, is approximately 40-75 h, which accounted for approximately 18% of the Imatinib dose (93, 94). Pharmacokinetic study of IM in humans suggested that the 5-10% of the administered dose under goes renal elimination with a clearance rate of about 10 mL min^{-1} (83). Further, the authors indicated that the high volume of distribution and plasma binding may not significantly affect the pharmacokinetics in patients with renal failure. In summary, based on overall findings it may be suggested that the main elimination route for Imatinib and its main metabolite is via the intestine.

2.4.5 Single-dose and multi-dose pharmacokinetics

General pharmacokinetic characteristics of Imatinib were reported on day one in the plasma of CML patients after once-daily (400 and 750 mg per day) and twice-daily (400 and 500 mg twice a day) oral administration. The mean T_{max} ranged from 3.1 to 3.9 h with a proportional increase in C_{max} from 508 to 803 ng mL^{-1} for once-daily oral administration (400 and 750 mg per day) (93). Similarly, with twice-daily oral

administration, the mean T_{max} ranged from 5.5 to 9 h with C_{max} from 664 to 882 ng mL^{-1}. The steady state pharmacokinetic parameters during one month Imatinib therapy investigated in phase I clinical trials have been reported.

In the dose proportionality study, relationship between dose and plasma exposure on day one was compared with one month steady-state levels. It was observed that the increase in mean plasma AUC was proportional to the drug exposure up to 1000 mg per day, however, it was associated with a very large intra- and inter-subject variability. The intra-subject (inter-occasions) variability in Cl/F was approximately 37% and the inter-subject variability was about 49% (93). The authors observed high degree of correlations between Cl/F and V_d/F for both day one and day 28 with the correlation coefficient of 0.71 and 0.80, respectively and the underlying reason for this correlation was attributed to the variability in protein binding. Surprisingly, the authors have observed a very high mean plasma $T_{1/2}$ at a steady-state, the reason for which was not reported. Comparison of the steady-state $AUC_{0\text{-}24h}$ with day one $AUC_{0\text{-}24h}$ confirmed a 1.5 to 3 fold drug accumulation for once-daily dosing. After administration of 350 mg of Imatinib at steady-state, the mean plasma trough concentration was found to be approximately 570 ng mL^{-1} or higher (≈ 1 μM) (93). Previously, in vitro studies confirmed that the IM concentration of 1 μM was sufficiently higher than that required to demonstrate cytotoxic effect in the Bcr-Abl positive cell lines. In summary, although Imatinib showed good and proportional oral absorption, the observations were associated with high degree of inter-occasions and inter-subject variability.

2.4.6 Dose escalation

Few authors have investigated the effect of increasing the dose of IM in acute and chronic phase CML patients who have previously been treated with IM. The outcome revealed that the increasing IM dose did not result in a proportional increase in response. The investigators rather observed either the clinically suboptimal response or disease progression despite continuous therapy (95).

2.4.7 Pharmacokinetics and pharmacodynamics correlation

Results of Phase I clinical trials in CML patients used to explore the relationship between the various pharmacokinetic parameters and the pharmacodynamic effects of the drug during one month continuous therapy (93). A simple inhibition E_{max} model was used to describe the correlation between the WBC count reduction as a pharmacodynamic effect with various pharmacokinetic parameters such as daily dose, trough-plasma concentrations, AUC, C_{max} and duration above MEC (1 μM) (96, 97). The analysis of the

pharmacokinetics and pharmacodynamics correlation (PK/PD) of Imatinib indicated that various drug exposure parameters (PK parameters) such as AUC, C_{max}, trough-plasma concentrations and duration above MEC were well correlated with the hematological response (PD effects) and established relationship was adequately described by considering the total daily dose administered.

The average WBC count in CML patients at baseline was found to be 49.7×10^9 L^{-1}, which were compared with the estimated WBC E_{max} values (26 to 58×10^9 L^{-1}) for dose and other PK parameters. These estimated values represent a significant reduction in the WBC count after one month treatment. E_{max} model (E_{max} and ED_{50} parameters) was used to simulate the WBC count in 1,000 future patients. These simulations predicted that one month treatment of 400 mg per day would lead to normalization of WBC count in approximately 76% of the CML patients. The analysis of the PK/PD correlation between the haematological response and various pharmacokinetic parameters at steady-state indicated that a dose of 400 mg per day or greater is required for maximal PD effect (93).

2.4.8 Population pharmacokinetics

The International Randomized Interferon versus STI-571 (IRIS) study results have reported the findings of Phase III clinical trials in CML patients, wherein, authors have discussed the population pharmacokinetic parameters of IM (84). On the first day of Imatinib treatment, the mean population estimates for apparent clearance (Cl) was 14 L h^{-1} and apparent volume of distribution (V_d) was 252 L. The estimate of absorption parameter (K_{01}) observed with a one-compartment model with first-order absorption was approximately 1.1 h^{-1}.

Population modelling revealed that Imatinib clearance decreased by 25% from first day of treatment to 4 L h^{-1} within a month with significant inter-subject variability of 32%, whereas the apparent volume of distribution remained almost unchanged with high inter-subject variability of 31%. In a separate study with GIST patients over 12 months, the European Organization for Research and Treatment of Cancer - soft tissue bone sarcoma group have reported similar findings that there was a significant increase in clearance with chronic exposure to Imatinib, which was attributed to the intra-subject variability by the authors (98).

2.4.9 Imatinib therapy and resistance

Although the chimeric oncoprotein remains good therapeutic target, Imatinib develops intrinsic and acquired resistance over a period of treatment leading to subtherapeutic drug concentrations after oral administration (99). Important underlying causes are the

compromised and variable bioavailability of Imatinib, which can be principally attributed to drug efflux mechanisms (100).

Few authors have recently reported high degree of inter-subject pharmacokinetic variability, in particular, 73% variation in the apparent oral clearance of Imatinib in GIST patients (93, 98). Several research groups have reported that Imatinib is a substrate for various efflux pumps including the breast cancer resistant protein (ABCG2), which is a highly polymorphic transporter protein that influences the absorption and disposition of various drugs (101-104). Few authors have demonstrated the role of P-gp over BCRP, in limiting brain penetration of Imatinib using BCRP1 knockout mice and MDR1a and MDR1b double knockout mice (101, 105). Similar findings have also been reported for other PKI drugs such as Gefitinib, wherein, the use of BCRP inhibitors was proposed for brain metastasis originating from non-small cell lung cancer (106, 107). Thus, clinical use of the efflux inhibitors for enhancing therapeutic efficacy of an anticancer drug may be a promising strategy for the management of chemotherapy.

In vitro studies carried out by few investigators have revealed that Imatinib is principally transported by P-gp (ABCB1) and extensively metabolized by cytochrome P450 isoenzymes such as CYP2C9, CYP2C19, CYP2D6, CYP3A4, and CYP3A5 (108, 94). ABCB1 (P-gp) and ABCG2 act as an efflux transporter possibly by decreasing the amount of substrate drug absorbed after oral administration, which resulted in its localization on the apical surface of intestinal epithelial cells. Furthermore, ABCG2 may increase systemic drug elimination as it is expressed in proximal renal tubular cells and the biliary surface of hepatocytes (109).

Few authors have reported that there was clinically no significant influence of ABCG2, when studied in a functional single-nucleotide polymorphism on exon 5 of the ABCG2 gene, a common genetic variant (110). However, there was no comprehensive review available on homozygous variants of ABCG2 and CYP2D6 genotypes in patients treated with Imatinib. Thus, the extensive inter-subject variability in the pharmacokinetics of Imatinib may be associated with the polymorphism in transporter proteins of patients with GIST and CML.

Although, few authors have reported a significant inverse correlation between the absolute oral bioavailability and the inter-subject variation of a drug but these findings may not be extendable to drugs like Imatinib, as there is significant inter-subject variation reported despite good oral bioavailability (111).

Further, the good oral bioavailability with significant inter-subject variation may show severe toxicity, as the window of fluctuation is relatively broad. In addition, the most cytotoxic drugs have a narrow therapeutic window and are often prescribed at the highest tolerated dose. In such cases, due to the high inter-subject variation cells may be exposed to a broad range of drug concentrations, which would initiate acquired and intrinsic resistance or activate various efflux mechanisms leading to failure of the therapy.

2.4.10 Drug-drug and drug-food interactions

Previously, in vitro studies had shown that Imatinib is mainly transformed by CYP3A4 and, in addition, it competitively inhibits CYP2C9, CYP2D6 and CYP3A4/5. In a drug-drug interaction study with a CYP3A4 inhibitor (Ketoconazole), the average C_{max}, $AUC_{0\text{-}24h}$ and AUC_{∞}, increased significantly by 26%, 40% and 40%, respectively. Statistically significant decrease is reported in Cl/F with an average reduction of 28.6%. Similarly, the corresponding decrease in the metabolite concentration was recorded with 22.6 and 13% decrease in the average C_{max} and $AUC_{0\text{-}24\ h}$ of the N-desmethyl-imatinib. In a drug-drug interaction study with a CYP3A4 substrate (Simvastatin), Imatinib showed the average two fold increase in C_{max} value of simvastatin with more than three fold increase in AUC_{∞}. Moreover, the mean plasma half life of Simvastatin was prolonged from 1.4 h to 3.2 h. Considering these facts following drugs might demand dosage adjustment or special monitoring during treatment with Imatinib - antifungals like Itraconazole or Ketoconazole; antibiotics like Clarithromycin, Erythromycin or Troleandomycin; Rifampicin, Rifabutin; Prednisolone and Dexamethasone; anticonvulsants like Phenytoin, Carbamazepine, Clonazepam, or Phenobarbital; antihypertensives like Nifedipine, Amlodipine, Felodipine, Isradipine, Nimodipine; anti-anxiety agents like Alprazolam, Diazepam, or Triazolam; cholesterol lowering drugs like Lovastatin, Atorvastatin, Simvastatin, Cyclosporin, Pimozide, Warfarin etc. IM also demonstrates P-gp level drug-drug interactions with several drugs including Methotrexate and Benzimidazoles (112) .

The effect of food on bioavailability was investigated at steady state (400 mg day^{-1}) under fed state with a standardized high fat meal and fasted condition. The mean pharmacokinetic parameters indicated that the AUC and C_{max} were affected with the insignificant prolongation of T_{max}.

2.4.11 Cost of therapy

In a cost effectiveness analysis, Imatinib was more economic and efficacious than currently available alternative therapy in most of the cases (113). Several drugs have been

used to treat CML including cytotoxic drugs such as Busulfan, Hydroxyurea, and Cytosine Arabinoside (Ara-C). However, the treatment of CML remained challenging until arrival of IM, especially in the accelerated and blast crises phase. Previously established high toxicity and poor prognostic effect is less applicable to Imatinib therapy.

At current prices, one year treatment with Imatinib 400 mg per day costs £18,948 per patient in UK (114). Its medical and economic value supported a high US retail price of INR 1,000,000 (≈ USD 30,000 annually) as the only treatment alternatives are interferon-alpha INR of 1,400,000 (≈ USD 40,000 annually) and bone-marrow transplants which could cost up to INR of 7,000,000 (≈ USD 200,000). Gleevec patent for its initial CML indication is valid until 2017 (87).

2.4.12 Pharmaceutical formulations

Brand Names: Glivec® and Gleevec® [Novartis Pharmaceuticals]

Dosage form: Film-coated tablets, hard gelatin capsule

Type: single-ingredient preparations

Dose: 100 mg and 400 mg per Unit

2.5 Summary

The concept behind cancer treatment has evolved over the past decade from systemic, nonspecific, high-dose chemotherapy to targeted therapy (115). However, the progress in fundamental cancer biology has not yet been met by a comparable advancement in its clinical treatment. The inability to selectively reach and eliminate tumor tissue with marginal damage in healthy organs, rather than the availability of potent chemotherapeutics, is a fundamental reason (116). Although modern chemotherapy is highly selective and effective, the drugs are characterized by variable and low tissue specific bioavailability. Moreover, these drugs have limited cellular permeability and demonstrate high drug efflux. The identification and elimination of these contributing factors to variability and resistance would facilitate the individualization of doses. Moreover, it would enhance the tissue specific bioavailability for the successful treatment of cancers.

References

1. M. Carroll, S. Ohno-Jones, S. Tamura, E. Buchdunger, J. Zimmermann, N.B. Lydon, D.G. Gilliland, and B.J. Druker. CGP 57148, a tyrosine kinase inhibitor, inhibits the growth of cells expressing BCR-ABL, TEL-ABL, and TEL-PDGFR fusion proteins. Blood 90:4947-4952 (1997).

2. E. Buchdunger, T. O'Reilly, and J. Wood. Pharmacology of imatinib (STI571). Eur J Cancer 38 Suppl 5:S28-36 (2002).
3. D.G. Savage and K.H. Antman. Imatinib mesylate : A new oral targeted therapy. N Engl J Med. 346:683-693 (2002).
4. R. Schwartz. A molecular star in the wars against cancer. N Engl J Med. 347:462-463 (2002).
5. A.M. Carella and E. Lerma. Imatinib mesylate in chronic myeloid leukemia. Curr Stem Cell Res Ther. 2:249-251 (2007).
6. K.T. Carpiuc, J.M. Stephens, M.F. Botteman, W. Feng, and J.W. Hay. A review of the clinical and economic outcomes of imatinib in Philadelphia chromosome-positive acute lymphoblastic leukemia. Expert Opin Pharmacother. 8:2775-2787 (2007).
7. J. Siehl and E. Thiel. C-kit, GIST, and imatinib. Recent Results Cancer Res. 176:145-151 (2007).
8. M.E. O'Dwyer and B.J. Druker. Status of bcr-abl tyrosine kinase inhibitors in chronic myelogenous leukemia. Curr Opin Oncol. 12:594-597 (2000).
9. K. Peggs and S. Mackinnon. Imatinib mesylate: The new gold standard for treatment of chronic myeloid leukemia. N Engl J Med. 348:1048-1050 (2003).
10. A. Quintas-Cardama, H. Kantarjian, and J. Cortes. Tyrosine kinase inhibitors for chronic myelogenous leukemia. N Engl J Med. 357:1557-1558 (2007).
11. J. Marx. Molecular biology. Cancer fighter's modus operandi revealed. Science. 289:1857-1859 (2000).
12. I. Shchemelinin, L. Sefc, and E. Necas. Protein kinase inhibitors. Folia Biol. 52:137-148 (2006).
13. L.M. Toledo, N.B. Lydon, and D. Elbaum. The structure-based design of ATP-site directed protein kinase inhibitors. Curr Med Chem. 6:775-805 (1999).
14. R. Capdeville, E. Buchdunger, J. Zimmermann, and A. Matter. Glivec (STI571, imatinib), a rationally developed, targeted anticancer drug. Nat Rev Drug Discov. 1:493-502 (2002).
15. Y. Corujo and W. Caceres. Signal transduction inhibitors (STI571): Molecularly targeted therapy. P R Health Sci J. 21:203-205 (2002).
16. B.J. Druker. Imatinib as a paradigm of targeted therapies. Adv Cancer Res. 91:1-30 (2004).

17. R. Hehlmann, U. Berger, and A. Hochhaus. Chronic myeloid leukemia: a model for oncology. Ann Hematol. 84:487-497 (2005).
18. S. Sleijfer, E. Wiemer, and J. Verweij. Drug Insight: Gastrointestinal stromal tumors (GIST) - The solid tumor model for cancer-specific treatment. Nat Clin Pract Oncol. 5:102-111 (2008).
19. K. Arnold. After 30 years of laboratory work, a quick approval for STI571. J Natl Cancer Inst. 93:972 (2001).
20. B.J. Druker, C.L. Sawyers, H. Kantarjian, D.J. Resta, S.F. Reese, J.M. Ford, R. Capdeville, and M. Talpaz. Activity of a specific inhibitor of the BCR-ABL tyrosine kinase in the blast crisis of chronic myeloid leukemia and acute lymphoblastic leukemia with the Philadelphia chromosome. N Engl J Med. 344:1038-1042 (2001).
21. A.T. van Oosterom, I. Judson, J. Verweij, S. Stroobants, E. Donato di Paola, S. Dimitrijevic, M. Martens, A. Webb, R. Sciot, M. Van Glabbeke, S. Silberman, and O.S. Nielsen. Safety and efficacy of imatinib (STI571) in metastatic gastrointestinal stromal tumours: A phase I study. Lancet 358:1421-1423 (2001).
22. M.H. Cohen, M.L. Moses, and R. Pazdur. Gleevec for the treatment of chronic myelogenous leukemia: US. Food and Drug Administration regulatory mechanisms, accelerated approval, and orphan drug status. Oncologist 7:390-392 (2002).
23. R. Dagher, M. Cohen, G. Williams, M. Rothmann, J. Gobburu, G. Robbie, A. Rahman, G. Chen, A. Staten, D. Griebel, and R. Pazdur. Approval summary: imatinib mesylate in the treatment of metastatic and/or unresectable malignant gastrointestinal stromal tumors. Clin Cancer Res. 8:3034-3038 (2002).
24. R. Dagher, J. Johnson, G. Williams, P. Keegan, and R. Pazdur. Accelerated approval of oncology products: a decade of experience. J Natl Cancer Inst. 96:1500-1509 (2004).
25. M.W. Wiedmann and K. Caca. Molecularly targeted therapy for gastrointestinal cancer. Curr Cancer Drug Targets 5:171-193 (2005).
26. D.A. Reardon, M.J. Egorin, J.A. Quinn, J.N. Rich, S. Gururangan, J.J. Vredenburgh, A. Desjardins, S. Sathornsumetee, J.M. Provenzale, J.E. Herndon, 2nd, J.M. Dowell, M.A. Badruddoja, R.E. McLendon, T.F. Lagattuta, K.P. Kicielinski, G. Dresemann, J.H. Sampson, A.H. Friedman, A.J. Salvado, and H.S. Friedman. Phase II study of imatinib mesylate plus hydroxyurea in adults with recurrent glioblastoma multiforme. J Clin Oncol. 23:9359-9368 (2005).

27. R. Stupp, M.E. Hegi, M.J. van den Bent, W.P. Mason, M. Weller, R.O. Mirimanoff, and J.G. Cairncross. Changing paradigms: An update on the multidisciplinary management of malignant glioma. Oncologist 11:165-180 (2006).

28. P.Y. Wen, W.K. Yung, K.R. Lamborn, P.L. Dahia, Y. Wang, B. Peng, L.E. Abrey, J. Raizer, T.F. Cloughesy, K. Fink, M. Gilbert, S. Chang, L. Junck, D. Schiff, F. Lieberman, H.A. Fine, M. Mehta, H.I. Robins, L.M. DeAngelis, M.D. Groves, V.K. Puduvalli, V. Levin, C. Conrad, E.A. Maher, K. Aldape, M. Hayes, L. Letvak, M.J. Egorin, R. Capdeville, R. Kaplan, A.J. Murgo, C. Stiles, and M.D. Prados. Phase I/II study of imatinib mesylate for recurrent malignant gliomas: North American Brain Tumor Consortium Study 99-08. Clin Cancer Res. 12:4899-4907 (2006).

29. A. Desjardins, J.A. Quinn, J.J. Vredenburgh, S. Sathornsumetee, A.H. Friedman, J.E. Herndon, R.E. McLendon, J.M. Provenzale, J.N. Rich, J.H. Sampson, S. Gururangan, J.M. Dowell, A. Salvado, H.S. Friedman, and D.A. Reardon. Phase II study of imatinib mesylate and hydroxyurea for recurrent grade III malignant gliomas. J Neurooncol. 83:53-60 (2007).

30. I.F. Pollack, R.I. Jakacki, S.M. Blaney, M.L. Hancock, M.W. Kieran, P. Phillips, L.E. Kun, H. Friedman, R. Packer, A. Banerjee, J.R. Geyer, S. Goldman, T.Y. Poussaint, M.J. Krasin, Y. Wang, M. Hayes, A. Murgo, S. Weiner, and J.M. Boyett. Phase I trial of imatinib in children with newly diagnosed brainstem and recurrent malignant gliomas: a Pediatric Brain Tumor Consortium report. Neuro Oncol. 9:145-160 (2007).

31. N.B. Heaney and T.L. Holyoake. Therapeutic targets in chronic myeloid leukaemia. Hematol Oncol. 25:66-75 (2007).

32. T. Kilic, J.A. Alberta, P.R. Zdunek, M. Acar, P. Iannarelli, T. O'Reilly, E. Buchdunger, P.M. Black, and C.D. Stiles. Intracranial inhibition of platelet-derived growth factor-mediated glioblastoma cell growth by an orally active kinase inhibitor of the 2-phenylaminopyrimidine class. Cancer Res. 60:5143-5150 (2000).

33. M. Talpaz, R.T. Silver, B.J. Druker, J.M. Goldman, C. Gambacorti-Passerini, F. Guilhot, C.A. Schiffer, T. Fischer, M.W. Deininger, A.L. Lennard, A. Hochhaus, O.G. Ottmann, A. Gratwohl, M. Baccarani, R. Stone, S. Tura, F.X. Mahon, S. Fernandes-Reese, I. Gathmann, R. Capdeville, H.M. Kantarjian, and C.L. Sawyers. Imatinib induces durable hematologic and cytogenetic responses in patients with accelerated phase chronic myeloid leukemia: results of a phase 2 study. Blood 99:1928-1937 (2002).

34. C.R. Bartram, A. de Klein, A. Hagemeijer, T. van Agthoven, A. Geurts van Kessel, D. Bootsma, G. Grosveld, M.A. Ferguson-Smith, T. Davies, M. Stone, and et al. Translocation of c-ab1 oncogene correlates with the presence of a Philadelphia chromosome in chronic myelocytic leukaemia. Nature 306:277-280 (1983).

35. N. Heisterkamp, J.R. Stephenson, J. Groffen, P.F. Hansen, A. de Klein, C.R. Bartram, and G. Grosveld. Localization of the c-ab1 oncogene adjacent to a translocation break point in chronic myelocytic leukaemia. Nature 306:239-242 (1983).

36. P. le Coutre, L. Mologni, L. Cleris, E. Marchesi, E. Buchdunger, R. Giardini, F. Formelli, and C. Gambacorti-Passerini. In vivo eradication of human BCR/ABL-positive leukemia cells with an ABL kinase inhibitor. J Natl Cancer Inst. 91:163-168 (1999).

37. D. Raina, N. Mishra, S. Kumar, S. Kharbanda, S. Saxena, and D. Kufe. Inhibition of c-Abl with STI571 attenuates stress-activated protein kinase activation and apoptosis in the cellular response to 1-beta-D-arabinofuranosylcytosine. Mol Pharmacol. 61:1489-1495 (2002).

38. J.D. Rowley. Letter: A new consistent chromosomal abnormality in chronic myelogenous leukaemia identified by quinacrine fluorescence and Giemsa staining. Nature 243:290-293 (1973).

39. E. Shtivelman, B. Lifshitz, R.P. Gale, and E. Canaani. Fused transcript of abl and bcr genes in chronic myelogenous leukaemia. Nature 315:550-554 (1985).

40. Y. Ben-Neriah, G.Q. Daley, A.M. Mes-Masson, O.N. Witte, and D. Baltimore. The chronic myelogenous leukemia-specific P210 protein is the product of the bcr/abl hybrid gene. Science 233:212-214 (1986).

41. M. Beran, X. Cao, Z. Estrov, S. Jeha, G. Jin, S. O'Brien, M. Talpaz, R.B. Arlinghaus, N.B. Lydon, and H. Kantarjian. Selective inhibition of cell proliferation and BCR-ABL phosphorylation in acute lymphoblastic leukemia cells expressing Mr 190,000 BCR-ABL protein by a tyrosine kinase inhibitor (CGP-57148). Clin Cancer Res. 4:1661-1672 (1998).

42. T. Schindler, W. Bornmann, P. Pellicena, W.T. Miller, B. Clarkson, and J. Kuriyan. Structural mechanism for STI-571 inhibition of abelson tyrosine kinase. Science 289:1938-1942 (2000).

43. T. Maekawa, E. Ashihara, and S. Kimura. The Bcr-Abl tyrosine kinase inhibitor imatinib and promising new agents against Philadelphia chromosome-positive leukemias. Int J Clin Oncol. 12:327-340 (2007).

44. C. Deshmukh, T. Saikia, A. Bakshi, P. Amare-Kadam, C. Baisane, and P. Parikh. Imatinib mesylate in chronic myeloid leukemia: a prospective, single arm, non-randomized study. J Assoc Physicians India 53:291-295 (2005).

45. H. Joensuu and L.G. Kindblom. Gastrointestinal stromal tumors A review. Acta Orthop Scand Suppl. 75:62-71 (2004).

46. N. Kosmadakis, E.E. Visvardis, P. Kartsaklis, M. Tsimara, A. Chatziantoniou, I. Panopoulos, P. Erato, and P. Capsambelis. The role of surgery in the management of gastrointestinal stromal tumors (GISTs) in the era of imatinib mesylate effectiveness. Surg Oncol. 14:75-84 (2005).

47. D.M. Steinert, J.C. McAuliffe, and J.C. Trent. Imatinib mesylate in the treatment of gastrointestinal stromal tumour. Expert Opin Pharmacother. 6:105-113 (2005).

48. D.M. Steinert, M. Oyarzo, X. Wang, H. Choi, P.F. Thall, L.J. Medeiros, A.K. Raymond, R.S. Benjamin, W. Zhang, and J.C. Trent. Expression of Bcl-2 in gastrointestinal stromal tumors: correlation with progression-free survival in 81 patients treated with imatinib mesylate. Cancer 106:1617-1623 (2006).

49. S.S. Clark, J. McLaughlin, M. Timmons, A.M. Pendergast, Y. Ben-Neriah, L.W. Dow, W. Crist, G. Rovera, S.D. Smith, and O.N. Witte. Expression of a distinctive BCR-ABL oncogene in Ph1-positive acute lymphocytic leukemia (ALL). Science 239:775-777 (1988).

50. K.H. Lee, J.H. Lee, S.J. Choi, M. Seol, Y.S. Lee, W.K. Kim, J.S. Lee, E.J. Seo, S. Jang, C.J. Park, and H.S. Chi. Clinical effect of imatinib added to intensive combination chemotherapy for newly diagnosed Philadelphia chromosome-positive acute lymphoblastic leukemia. Leukemia 19:1509-1516 (2005).

51. S. Lee, Y.J. Kim, C.K. Min, H.J. Kim, K.S. Eom, D.W. Kim, J.W. Lee, W.S. Min, and C.C. Kim. The effect of first-line imatinib interim therapy on the outcome of allogeneic stem cell transplantation in adults with newly diagnosed Philadelphia chromosome-positive acute lymphoblastic leukemia. Blood 105:3449-3457 (2005).

52. A. Tefferi and A. Pardanani. Imatinib therapy in clonal eosinophilic disorders, including systemic mastocytosis. Int J Hematol. 79:441-447 (2004).

53. A. Tefferi. Modern diagnosis and treatment of primary eosinophilia. Acta Haematol. 114:52-60 (2005).

54. A. Tefferi, R.A. Mesa, L.A. Gray, D.P. Steensma, J.K. Camoriano, M.A. Elliott, A. Pardanani, S.M. Ansell, T.G. Call, G. Colon-Otero, G. Schroeder, C.A. Hanson, G.W. Dewald, and S.H. Kaufmann. Phase 2 trial of imatinib mesylate in myelofibrosis with myeloid metaplasia. Blood 99:3854-3856 (2002).

55. I.K. Choi, B.S. Kim, K.A. Lee, S. Ryu, H.Y. Seo, H. Sul, J.G. Choi, H.J. Sung, K.H. Park, S.Y. Yoon, S.C. Oh, J.H. Seo, C.W. Choi, S.W. Shin, Y. Cho, Y.K. Kim, Y.H. Kim, and J.S. Kim. Efficacy of imatinib mesylate (STI571) in chronic neutrophilic leukemia with t(15;19): case report. Am J Hematol. 77:366-369 (2004).

56. C.L. Sawyers. Imatinib GIST keeps finding new indications: successful treatment of dermatofibrosarcoma protuberans by targeted inhibition of the platelet-derived growth factor receptor. J Clin Oncol. 20:3568-3569 (2002).

57. G.A. McArthur. Molecular targeting of dermatofibrosarcoma protuberans: a new approach to a surgical disease. J Natl Compr Canc Netw. 5:557-562 (2007).

58. Y.S. Eisele, M. Baumann, B. Klebl, C. Nordhammer, M. Jucker, and E. Kilger. Gleevec increases levels of the amyloid precursor protein intracellular domain and of the amyloid-beta degrading enzyme neprilysin. Mol Biol Cell. 18:3591-3600 (2007).

59. J. Hardy and D.J. Selkoe. The amyloid hypothesis of Alzheimer's disease: progress and problems on the road to therapeutics. Science 297:353-356 (2002).

60. C.H. Rojas-Fernandez, M. Chen, and H.L. Fernandez. Implications of amyloid precursor protein and subsequent beta-amyloid production to the pharmacotherapy of Alzheimer's disease. Pharmacotherapy. 22:1547-1563 (2002).

61. W.J. Netzer, F. Dou, D. Cai, D. Veach, S. Jean, Y. Li, W.G. Bornmann, B. Clarkson, H. Xu, and P. Greengard. Gleevec inhibits beta-amyloid production but not Notch cleavage. Proc Natl Acad Sci U S A. 100:12444-12449 (2003).

62. D. Gianni, N. Zambrano, M. Bimonte, G. Minopoli, L. Mercken, F. Talamo, A. Scaloni, and T. Russo. Platelet-derived growth factor induces the beta-gamma-secretase-mediated cleavage of Alzheimer's amyloid precursor protein through a Src-Rac-dependent pathway. J Biol Chem. 278:9290-9297 (2003).

63. P. Zhang, W.Y. Gao, S. Turner, and B.S. Ducatman. Gleevec (STI-571) inhibits lung cancer cell growth (A549) and potentiates the cisplatin effect in vitro. Mol Cancer 2:1 (2003).

64. T. Yokoyama, K. Miyazawa, T. Yoshida, and K. Ohyashiki. Combination of vitamin K2 plus imatinib mesylate enhances induction of apoptosis in small cell lung cancer cell lines. Int J Oncol. 26:33-40 (2005).

65. G.W. Krystal, S. Honsawek, J. Litz, and E. Buchdunger. The selective tyrosine kinase inhibitor STI571 inhibits small cell lung cancer growth. Clin Cancer Res. 6:3319-3326 (2000).

66. C. Gambacorti-Passerini, R. Piazza, L. Tornaghi, S. Pilotti, and E. Pogliani. Development of c-Kit-expressing small-cell lung cancer in a chronic myeloid leukemia patient during imatinib treatment. J Natl Cancer Inst. 96:1723-1724 (2004).

67. H.B. Koon, G.J. Bubley, L. Pantanowitz, D. Masiello, B. Smith, K. Crosby, J. Proper, W. Weeden, T.E. Miller, P. Chatis, M.J. Egorin, S.R. Tahan, and B.J. Dezube. Imatinib-induced regression of AIDS-related Kaposi's sarcoma. J Clin Oncol. 23:982-989 (2005).

68. A.S. Rao, N. Kremenevskaja, R. von Wasielewski, V. Jakubcakova, S. Kant, J. Resch, and G. Brabant. Wnt/beta-catenin signaling mediates antineoplastic effects of imatinib mesylate (gleevec) in anaplastic thyroid cancer. J Clin Endocrinol Metab. 91:159-168 (2006).

69. B.M. Slomovitz, R.R. Broaddus, R. Schmandt, W. Wu, J.C. Oh, L.M. Ramondetta, T.W. Burke, D.M. Gershenson, and K.H. Lu. Expression of imatinib mesylate-targeted kinases in endometrial carcinoma. Gynecol Oncol. 95:32-36 (2004).

70. P.R. Pereira, A.N. Odashiro, J.C. Marshall, Z.M. Correa, R. Belfort, Jr., and M.N. Burnier, Jr. The role of c-kit and imatinib mesylate in uveal melanoma. J Carcinog. 4:19 (2005).

71. J.H. Distler, A. Jungel, L.C. Huber, U. Schulze-Horsel, J. Zwerina, R.E. Gay, B.A. Michel, T. Hauser, G. Schett, S. Gay, and O. Distler. Imatinib mesylate reduces production of extracellular matrix and prevents development of experimental dermal fibrosis. Arthritis Rheum. 56:311-322 (2007).

72. K. Miyachi, A. Ihara, R.W. Hankins, R. Murai, S. Maehiro, and H. Miyashita. Efficacy of imatinib mesylate (STI571) treatment for a patient with rheumatoid

arthritis developing chronic myelogenous leukemia. Clin Rheumatol. 22:329-332 (2003).

73. P.G. Casali, A. Messina, S. Stacchiotti, E. Tamborini, F. Crippa, A. Gronchi, R. Orlandi, C. Ripamonti, C. Spreafico, R. Bertieri, R. Bertulli, M. Colecchia, E. Fumagalli, A. Greco, F. Grosso, P. Olmi, M.A. Pierotti, and S. Pilotti. Imatinib mesylate in chordoma. Cancer 101:2086-2097 (2004).

74. A. Pardanani, M. Elliott, T. Reeder, C.Y. Li, E.J. Baxter, N.C. Cross, and A. Tefferi. Imatinib for systemic mast-cell disease. Lancet 362:535-536 (2003).

75. A. Pardanani, T. Reeder, L.F. Porrata, C.Y. Li, H.D. Tazelaar, E.J. Baxter, T.E. Witzig, N.C. Cross, and A. Tefferi. Imatinib therapy for hypereosinophilic syndrome and other eosinophilic disorders. Blood 101:3391-3397 (2003).

76. A. Pardanani, T.L. Reeder, T.K. Kimlinger, J.Y. Baek, C.Y. Li, J.H. Butterfield, and A. Tefferi. Flt-3 and c-kit mutation studies in a spectrum of chronic myeloid disorders including systemic mast cell disease. Leuk Res. 27:739-742 (2003).

77. S.F. Adams, J.A. Hickson, J.Y. Hutto, A.G. Montag, E. Lengyel, and S.D. Yamada. PDGFR-alpha as a potential therapeutic target in uterine sarcomas. Gynecol Oncol. 104:524-528 (2007).

78. L.M. Popescu, C. Vidulescu, A. Curici, L. Caravia, A.A. Simionescu, S.M. Ciontea, and S. Simion. Imatinib inhibits spontaneous rhythmic contractions of human uterus and intestine. Eur J Pharmacol. 546:177-181 (2006).

79. J.E. Vamvakopoulos, L. Petrov, S. Aavik, S. Lehti, E. Aavik, and P. Hayry. Synergistic suppression of rat neointimal hyperplasia by rapamycin and imatinib mesylate: implications for the prevention of accelerated arteriosclerosis. J Vasc Res. 43:184-192 (2006).

80. D. Zohlnhofer, J. Hausleiter, A. Kastrati, J. Mehilli, C. Goos, H. Schuhlen, J. Pache, G. Pogatsa-Murray, U. Heemann, J. Dirschinger, and A. Schomig. A randomized, double-blind, placebo-controlled trial on restenosis prevention by the receptor tyrosine kinase inhibitor imatinib. J Am Coll Cardiol. 46:1999-2003 (2005).

81. A.M. Wolf, D. Wolf, H. Rumpold, S. Ludwiczek, B. Enrich, G. Gastl, G. Weiss, and H. Tilg. The kinase inhibitor imatinib mesylate inhibits TNF-{alpha} production in vitro and prevents TNF-dependent acute hepatic inflammation. Proc Natl Acad Sci U S A. 102:13622-13627 (2005).

82. C. Gambacorti. STI571 (Glivec): A new paradigm for the development of innovative therapies in onco-hematology Tumori. 87:S10-12 (2001).

83. P. le Coutre, K.A. Kreuzer, S. Pursche, M. Bonin, T. Leopold, G. Baskaynak, B. Dorken, G. Ehninger, O. Ottmann, A. Jenke, M. Bornhauser, and E. Schleyer. Pharmacokinetics and cellular uptake of imatinib and its main metabolite CGP74588. Cancer Chemother Pharmacol. 53:313-323 (2004).

84. H. Schmidli, B. Peng, G.J. Riviere, R. Capdeville, M. Hensley, I. Gathmann, A.E. Bolton, and A. Racine-Poon. Population pharmacokinetics of imatinib mesylate in patients with chronic-phase chronic myeloid leukaemia: results of a phase III study. Br J Clin Pharmacol. 60:35-44 (2005).

85. H.P. Gschwind, U. Pfaar, F. Waldmeier, M. Zollinger, C. Sayer, P. Zbinden, M. Hayes, R. Pokorny, M. Seiberling, M. Ben-Am, B. Peng, and G. Gross. Metabolism and disposition of imatinib mesylate in healthy volunteers. Drug Metab Dispos. 33:1503-1512 (2005).

86. B. Peng, C. Dutreix, G. Mehring, M.J. Hayes, M. Ben-Am, M. Seiberling, R. Pokorny, R. Capdeville, and P. Lloyd. Absolute bioavailability of imatinib (Glivec) orally versus intravenous infusion. J Clin Pharmacol. 44:158-162 (2004).

87. Internal Report. Gleevec®. Novartis Pharmaceuticals, 2002.

88. N. Widmer, L.A. Decosterd, C. Csajka, S. Leyvraz, M.A. Duchosal, A. Rosselet, B. Rochat, C.B. Eap, H. Henry, J. Biollaz, and T. Buclin. Population pharmacokinetics of imatinib and the role of alpha-acid glycoprotein. Br J Clin Pharmacol. 62:97-112 (2006).

89. Package Insert. Gleevec. Novartis Pharmaceuticals Corporation, East Hanover, New Jersey, 2002.

90. J.M. Ford. Investigators Brochure - Imatinib Mesilate. Novartis Pharmaceuticals, 2002.

91. B. Peng, M. Hayes, A. Racine-Poon, B.J. Druker, M. Talpaz, and C.L. Sawyers. Clinical Investigation of the Pharmacokinetic / Pharmacodynamic Relationship for Glivec® (STI571): a Novel Inhibitor of Signal Transduction. ASCO Proceedings. 20:280 (2001).

92. M. Bornhauser, N. Kroger, R. Schwerdtfeger, K. Schafer-Eckart, H.G. Sayer, C. Scheid, M. Stelljes, J. Kienast, P. Mundhenk, S. Fruehauf, M.G. Kiehl, H. Wandt, C. Theuser, G. Ehninger, and A.R. Zander. Allogeneic haematopoietic cell

transplantation for chronic myelogenous leukaemia in the era of imatinib: a retrospective multicentre study. Eur J Haematol. 76:9-17 (2006).

93. B. Peng, M. Hayes, D. Resta, A. Racine-Poon, B.J. Druker, M. Talpaz, C.L. Sawyers, M. Rosamilia, J. Ford, P. Lloyd, and R. Capdeville. Pharmacokinetics and pharmacodynamics of imatinib in a phase I trial with chronic myeloid leukemia patients. J Clin Oncol. 22:935-942 (2004).
94. B. Peng, P. Lloyd, and H. Schran. Clinical pharmacokinetics of imatinib. Clin Pharmacokinet. 44:879-894 (2005).
95. J.A. Zonder, P. Pemberton, H. Brandt, A.N. Mohamed, and C.A. Schiffer. The effect of dose increase of imatinib mesylate in patients with chronic or accelerated phase chronic myelogenous leukemia with inadequate hematologic or cytogenetic response to initial treatment. Clin Cancer Res. 9:2092-2097 (2003).
96. E. Buchdunger, J. Zimmermann, H. Mett, T. Meyer, M. Muller, B.J. Druker, and N.B. Lydon. Inhibition of the Abl protein-tyrosine kinase in vitro and in vivo by a 2-phenylaminopyrimidine derivative. Cancer Res. 56:100-104 (1996).
97. B.J. Druker, S. Tamura, E. Buchdunger, S. Ohno, G.M. Segal, S. Fanning, J. Zimmermann, and N.B. Lydon. Effects of a selective inhibitor of the Abl tyrosine kinase on the growth of Bcr-Abl positive cells. Nat Med. 2:561-566 (1996).
98. I. Judson, P. Ma, B. Peng, J. Verweij, A. Racine, E.D. di Paola, M. van Glabbeke, S. Dimitrijevic, M. Scurr, H. Dumez, and A. van Oosterom. Imatinib pharmacokinetics in patients with gastrointestinal stromal tumour: a retrospective population pharmacokinetic study over time. EORTC Soft Tissue and Bone Sarcoma Group. Cancer Chemother Pharmacol. 55:379-386 (2005).
99. A. Hochhaus, S. Kreil, A.S. Corbin, P. La Rosee, M.C. Muller, T. Lahaye, B. Hanfstein, C. Schoch, N.C. Cross, U. Berger, H. Gschaidmeier, B.J. Druker, and R. Hehlmann. Molecular and chromosomal mechanisms of resistance to imatinib (STI571) therapy. Leukemia 16:2190-2196 (2002).
100. J. Thomas, L. Wang, R.E. Clark, and M. Pirmohamed. Active transport of imatinib into and out of cells: implications for drug resistance. Blood. 104:3739-3745 (2004).
101. H. Dai, P. Marbach, M. Lemaire, M. Hayes, and W.F. Elmquist. Distribution of STI-571 to the brain is limited by P-glycoprotein-mediated efflux. J Pharmacol Exp Ther. 304:1085-1092 (2003).

102. H. Burger and K. Nooter. Pharmacokinetic resistance to imatinib mesylate: role of the ABC drug pumps ABCG2 (BCRP) and ABCB1 (MDR1) in the oral bioavailability of imatinib. Cell Cycle 3:1502-1505 (2004).

103. H. Burger, H. van Tol, A.W. Boersma, M. Brok, E.A. Wiemer, G. Stoter, and K. Nooter. Imatinib mesylate (STI571) is a substrate for the breast cancer resistance protein (BCRP)/ABCG2 drug pump. Blood 104:2940-2942 (2004).

104. P. Breedveld, J.H. Beijnen, and J.H. Schellens. Use of P-glycoprotein and BCRP inhibitors to improve oral bioavailability and CNS penetration of anticancer drugs. Trends Pharmacol Sci. 27:17-24 (2006).

105. P.J. Houghton, G.S. Germain, F.C. Harwood, J.D. Schuetz, C.F. Stewart, E. Buchdunger, and P. Traxler. Imatinib mesylate is a potent inhibitor of the ABCG2 (BCRP) transporter and reverses resistance to topotecan and SN-38 in vitro. Cancer Res. 64:2333-2337 (2004).

106. A.B. Heimberger, C.A. Learn, G.E. Archer, R.E. McLendon, T.A. Chewning, F.L. Tuck, J.B. Pracyk, A.H. Friedman, H.S. Friedman, D.D. Bigner, and J.H. Sampson. Brain tumors in mice are susceptible to blockade of epidermal growth factor receptor (EGFR) with the oral, specific, EGFR-tyrosine kinase inhibitor ZD1839 (iressa). Clin Cancer Res. 8:3496-3502 (2002).

107. G.L. Ceresoli, F. Cappuzzo, V. Gregorc, S. Bartolini, L. Crino, and E. Villa. Gefitinib in patients with brain metastases from non-small-cell lung cancer: a prospective trial. Ann Oncol. 15:1042-1047 (2004).

108. A. Hamada, H. Miyano, H. Watanabe, and H. Saito. Interaction of imatinib mesilate with human P-glycoprotein. J Pharmacol Exp Ther. 307:824-828 (2003).

109. E.R. Lepper, K. Nooter, J. Verweij, M.R. Acharya, W.D. Figg, and A. Sparreboom. Mechanisms of resistance to anticancer drugs: the role of the polymorphic ABC transporters ABCB1 and ABCG2. Pharmacogenomics 6:115-138 (2005).

110. E.R. Gardner, H. Burger, R.H. van Schaik, A.T. van Oosterom, E.A. de Bruijn, G. Guetens, H. Prenen, F.A. de Jong, S.D. Baker, S.E. Bates, W.D. Figg, J. Verweij, A. Sparreboom, and K. Nooter. Association of enzyme and transporter genotypes with the pharmacokinetics of imatinib. Clin Pharmacol Ther. 80:192-201 (2006).

111. E.T. Hellriegel, T.D. Bjornsson, and W.W. Hauck. Interpatient variability in bioavailability is related to the extent of absorption: implications for bioavailability and bioequivalence studies. Clin Pharmacol Ther. 60:601-607 (1996).

112. P. Breedveld, N. Zelcer, D. Pluim, O. Sonmezer, M.M. Tibben, J.H. Beijnen, A.H. Schinkel, O. van Tellingen, P. Borst, and J.H. Schellens. Mechanism of the pharmacokinetic interaction between methotrexate and benzimidazoles: potential role for breast cancer resistance protein in clinical drug-drug interactions. Cancer Res. 64:5804-5811 (2004).

113. G.H. Skrepnek and E.E. Ballard. Cost-efficacy of imatinib versus allogeneic bone marrow transplantation with a matched unrelated donor in the treatment of chronic myelogenous leukemia: a decision-analytic approach. Pharmacotherapy 25:325-334 (2005).

114. Summary Sheet. Midland Therapeutic Review & Advisory Committee : Signal Transduction Inhibitor for the Treatment of Chromic Myeloid Leukemia. Department of Medicines Management, Keele University, 2001.

115. R. Abou-Jawde, T. Choueiri, C. Alemany, and T. Mekhail. An overview of targeted treatments in cancer. Clin Ther. 25:2121-2137 (2003).

116. M. Ferrari. Cancer nanotechnology: opportunities and challenges. Nat Rev Cancer. 5:161-171 (2005).

3. Analytical and Bioanalytical Methods

3.1 Introduction

The primary goal of any pharmaceutical product development is to provide design and process that would consistently deliver a product of predetermined quality. In order to evaluate a product or assess the quality, suitable analytical methods are essential. Analytical methods significantly influence the product design and development process and it is essential to ensure that the employed analytical method(s) provide accurate and reliable information. Thus, it is important to develop a simple, sensitive and accurate analytical method for assessing critical quality and performance attributes (1-3).

The science of analyzing chemical characteristics such as identity and purity is well established and still advancing with the use of hyphenated analytical techniques coupled with mathematical principles such as multivariate design, design of experimentation etc (4, 5). Although estimation of pure drug(s) in pharmaceutical products is complex with one or more product components such as excipients and degradation substances, the liquid chromatography with ultraviolet detection remains the most common technique for potency and impurity analysis. Most of the regulatory agencies across the globe emphasize the use of stability indicating methods to monitor the stability profiles of drug substances and drug products (6). Requirements also demand the strict monitoring of impurities and degradation products. Such analytical methods are also useful in preformulation and product stability studies (7). Similarly, the presence of complex biological environment demands specific considerations for estimation of pure drug in biological samples for accurate determination of in vivo pharmacokinetic parameters (8, 9).

With the FDA's process analytical technology initiative, the current view of 'quality by design' is further strengthened by stating that the quality should be built in product and should not be inspected within. Drug control and regulatory agencies of several countries have recognized the importance of analytical sciences in product design and development and have released extensive guidelines on validation requirements in recent years (10-13). Although analytical validation requirements depend upon the type of analyte and analytical instrument, it broadly includes specificity and selectivity, linearity and range, accuracy and precision, sensitivity, reproducibility, stability etc (14).

Few analytical methods are reported in literature for the determination of IM in bulk and formulations. Amongst the reported liquid chromatographic methods, a very few include use of UV detector for quantitation (15-17). However, none of these methods demonstrate adequate sensitivity and peak symmetry. Moreover, these chromatographic methods used

either a complex gradient system or ion-pair agents leading to higher variations and cost of analysis. Moreover, extensive literature survey did not reveal any simple UV-spectrophotometric method for analysis of IM. A sensitive, rapid and cost effective analytical method is required for routine analysis of IM in bulk and pharmaceutical formulations.

Although few analytical methods are reported for determination of IM in biological matrix, the extensive literature survey did not reveal any bioanalytical method suitable for determination of IM in rat serum (18-20). For Amongst the reported bioanalytical methods, only a few include use of UV detector for quantification (18, 20, 21); while other methods use sophisticated analytical instruments such as mass spectrophotometer, thus making them unsuitable for routine analysis (22-28).

Moreover, most of the methods use either complex gradient system or ion-pairing agents leading to higher analytical variations and increased cost of analysis. In addition, HPLC-UV methods demonstrate inadequate sensitivity, poor peak symmetry and use complex extraction protocols. Most of the reported methods used sophisticated analytical instruments and there was no simple, rapid, cost effective analytical method based on spectrophotometry in literature, which could be used for routine analysis of IM.

The objective of the present study was to develop a simple, accurate and robust spectrophotometric analytical method for routine drug analysis. In addition, a sensitive and stability indicating liquid chromatographic method was required for determination of IM in the presence of its degradation products for stability studies. Moreover, for in vivo evaluation of prepared nanoparticles in animal model, a selective and sensitive bioanalytical method for determination of IM in rat biomatrices was essential. In the present work, in-house developed methods used most of the common mathematical and statistical treatments for analytical method validation with modern techniques of experimental design and orthogonality (29). Moreover, in-house developed methods were validated as per the current regulatory guidelines for analytical and bioanalytical methods using suitable statistical tests (10, 12, 13, 30). Further, the methods were successfully assessed for the determination of IM in respective matrices.

3.2 Materials

Imatinib mesylate (Assay 99.95%) was obtained as a gift sample from Cipla, India. Extra pure analytical grade acetonitrile, methanol, trifluroacetic acid, triethylamine, n-hexane, methylene chloride were purchased from Spectrochem, India. All buffer salts were of analytical grade and purchased from S.D. Fine Chemicals Ltd., India. Ultra pure water

was prepared fresh using a Milli-Q® water purification system (Millipore Co., USA) and filtered (0.22 μm) before use. All excipients used for the preparation of placebo formulations such as diluent (Avicel PH101 NF), glidant (Aerosil NF), lubricant (magnesium stearate NF), disintegrant (Polyplasdone XL-10 NF), binder (Hypromellose USP), etc. were gift from Medreich Pharmaceuticals, India. All chemicals and reagents were of either spectroscopic or analytical grade.

One commercially available tablet preparation - Imalek 100 (Sun Pharmaceutical Ltd., India), labeled to contain 100 mg equivalent Imatinib, was selected from local Indian market. IM loaded PLGA nanoparticles were prepared in-house. Similarly, blank PLGA nanoparticles prepared without drug was used as placebo standards.

For bioanalytical method, drug free serum pool was obtained from healthy male Wistar rats and it was stored at −80°C in sealed cryovials.

3.3 Method I: Spectroscopic method

3.3.1 Experimental

a) Spectrophotometer and spectrophotometric conditions

The analysis was carried out using a V-570 double beam UV-VIS spectrophotometer (Jasco, Japan) in 10 mm matched quartz cells. Data acquisition and analysis were performed using Spectra Manager® workstation (Jasco, Japan). Absorption spectra were recorded from 190 to 800 nm at a speed of 400 nm min^{-1} with 0.2 nm data interval, using medium response and 1 nm bandwidth. The quantitative analysis was carried out in the photometric mode at a fixed wavelength.

b) Preparation of stock and standards

A primary stock solution of 100 μg mL^{-1} was prepared by dissolving 10 mg of IM in 100 mL of solvent media consisting of methanol and phosphate buffer (pH 7.4, 100 mM) (50:50 *v/v*). Seven calibration standards containing 2.5, 5, 7.5, 10, 15, 20 and 25 μg mL^{-1} of IM were prepared by transferring aliquots of stock solution into series of 10 mL standard flasks and volume was made up with solvent media. On each day of validation, five separate series of seven calibration standards were prepared fresh and absorbance values were recorded in photometric mode at 285 nm against blank solvent system.

Formulation standards were prepared by adding known amount of drug to both the placebo blend of tablets and blank nanoparticles at five levels - 50, 75, 100, 125 and 150% of the labeled claim. Similarly, placebo standards were prepared in both the

matrices without adding drug. Prepared standards were processed as described in the sample preparation section and analyzed.

c) Sample preparation

A quantity of the product, powdered tablets or nanoparticles, equivalent to 10 mg of IM was weighed and transferred to 100 mL calibrated flask. Only in case of nanoparticles, preparations were digested with 10 mL acetonitrile by ultra-sonication (15 min, 25°C); while, tablet samples were processed without additional treatment. The volume was made up to 100 mL with solvent media and samples were centrifuged (10,000 rpm, 15 min, 20°C) after mixing for 5 min. Finally, 1 mL of clear supernatant was transferred to 10 mL calibrated flask and diluted to volume with solvent media.

d) Spectroscopic method development

Initially, different solvent systems were studied to develop a selective and sensitive UV-spectrophotometric method for the analysis of IM in formulations. The criteria employed for solvent selection were the ease in sample preparation, analyte stability, preparation time, cost of sample processing and comprehensive applicability. The wavelength was selected by assessing critical performance parameters such as sensitivity, reproducibility, selectivity and robustness. Absorbance of IM standard solutions was determined in selected media at optimized wavelength and molar absorptivity, specific absorptivity and Sandell's coefficient were calculated according to standard formulae. Robustness of the method was analyzed by studying the effect of change in pH, buffer strength and composition of the solvent media. Analysis was performed at ambient temperature (25°C) after instrument stabilization for at least 15 min.

e) Spectroscopic method validation

The developed spectrophotometric method was validated for selectivity, linearity, range, precision, accuracy and sensitivity. The method was also applied for the drug content analysis from commercial tablets and in-house prepared nanoparticles.

i) Selectivity

Placebo and formulation (spiked-placebo) standards of tablets and nanoparticles were used to study selectivity of the method. On three consecutive days, two sets of placebo and formulation standards were prepared in triplicate (n = 3, at each level). On each day of validation, one set of standards was used to study the absorption spectrum from 190 to 800 nm. While, the other sets of standards (n = 3, at each level) were used for absorbance measurement at 285 nm for quantitative estimation of IM. The obtained spectra were

compared for change in absorption profile with the spectra of fresh calibration standards. The mean absorbance at each concentration level was compared using paired t-test at 95% level of significance.

ii) Linearity and range

Calibration standards prepared at seven concentration levels ranging from 2.5 to 25 µg mL^{-1} were analyzed for establishing linearity of the method. The least square linear regression analysis was performed on calculated average absorbance values at each concentration level. Obtained linear regression equation was used to calculate the corresponding predicted concentrations. One-way analysis of variance (ANOVA) was performed on each replicate measurement obtained at seven concentration levels. The analysis of residuals was performed to establish the analytical range of the method and test of the intercept was carried out using t-statistic.

iii) Accuracy and precision

Placebo spiking and standard addition techniques were used to assess accuracy of the method. Two different techniques of recovery study were carried out for both the formulations viz. tablets and nanoparticles, separately. In placebo spiking technique, a known amount of pure drug standard, at five concentration levels viz. 50, 75, 100, 125 and 150% of the labeled claim of the individual products, was added to placebo blank. Similarly, a known amount of the pure drug standard was added to the sample solution at two concentration levels viz. 50 and 100% of the labeled claim of the individual products in standard addition technique. On three consecutive days, each concentration level was processed in six replicates and the results were expressed as mean absolute recovery, % RSD and % Bias.

Quality control (QC) standards prepared at lower (LQC = 2.5 µg mL^{-1}), medium (MQC = 10 µg mL^{-1}) and higher (HQC = 25 µg mL^{-1}) concentration levels were used to evaluate the repeatability (intra-batch) and intermediate (inter-batch) precision of the method. Six series of three QC standards were prepared fresh and analyzed for assessing repeatability (intra-batch). Similarly, standards were prepared and analyzed on three consecutive days for evaluation of intermediate precision (inter-batch). The intra-batch and inter-batch % RSD obtained at three QC levels were calculated to establish repeatability and intermediate precision of the method respectively.

iv) Sensitivity

Calibration standards were prepared at seven concentration levels and used to assess the sensitivity of the method. Sensitivity was expressed as a limit of detection (LOD) and

limit of quantitation (LOQ), which were determined using standard deviation of intercept (σ) and slope (s) of the calibration curve. The LOD and LOQ of the method were calculated using a standard formulae 3.3 σ/s and 10 σ/s, respectively.

v) Robustness

Robustness of the method was evaluated by making small variations to the internal method parameters. The effect of critical operating parameters such as pH (± 1 units), buffer strength (± 100 mM) and changing organic solvent composition such as methanol (–20% *v/v*) and addition of acetonitrile (+20% *v/v*) were investigated. At each media condition (pH, buffer strength and organic solvent), one set of QC standards (LQC, MQC and HQC) was prepared in triplicate and the results were expressed as mean absolute recovery, % RSD and % Bias. In addition, one-way ANOVA was performed to investigate the effect of individual factor.

vi) System precision and drug stability

Fresh calibration standards in ten replicates were analyzed for the purpose of system precision. Calibration standards in triplicates were analyzed over duration of 48 h to establish stability of IM in the solvent media.

vii) Analysis of formulations

For tablet samples, the average weight of twenty tablets was recorded and tablets were powdered and blended. A quantity of powder blend equivalent to 10 mg of IM was weighed accurately and processed as described in sample processing section. For nanoparticle samples, a quantity of freeze dried nanoparticles equivalent to 10 mg of IM was weighed accurately and processed as described in the sample processing section.

3.3.2 Results and Discussion

a) Spectroscopic method development

In preliminary investigations, UV absorbance profile of IM has shown insignificant change at 285 nm in different solvent systems such as pure water, methanol, acetonitrile, 0.1 N HCl, 0.1 N NaOH, phosphate buffer of different pH and various organic with aqueous solvent combinations. Although a pH dependent UV absorption profile was observed with a significant change in the absorbance values, magnitude of change in UV absorbance was lowest at 285 nm (Fig. 3.1). Therefore, the wavelength of 285 nm providing high repeatability and sensitivity was selected for further method development. Moreover, it has also shown selectivity in the presence of different components of formulation matrix offering accurate estimation even with the change in pH of the solvent

system. Finally, the selected solvent system consisting of 50:50 *v/v* methanol: PBS (pH 7.4, 100 mM) demonstrated advantages in terms of ease in sample preparation, analyte stability, time and cost of sample processing and wide applicability.

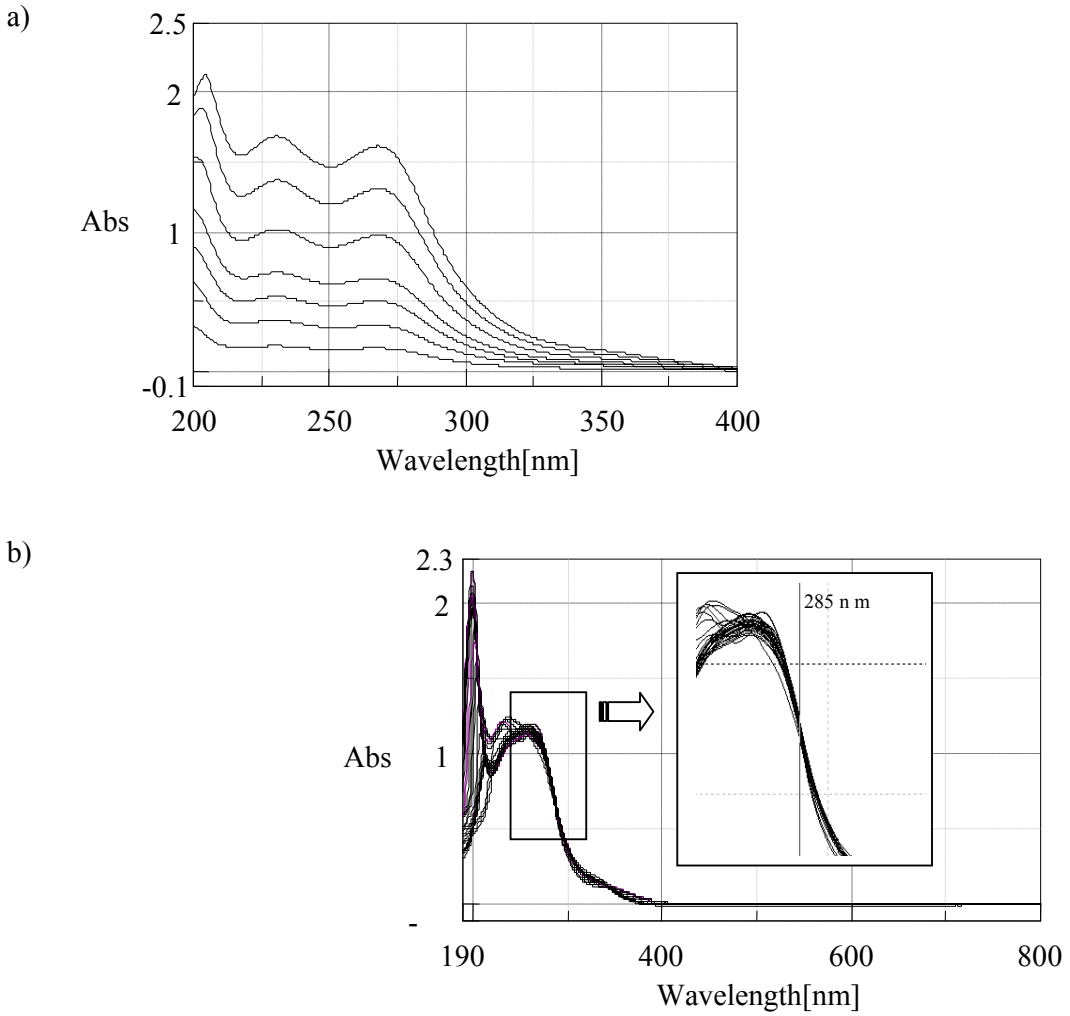

Fig. 3.1: UV-Visible absorption spectrum of Imatinib mesylate in a) 50:50 *v/v* methanol: PBS (1-25 µg mL^{-1}) and b) different buffer phases (pH 1-13)

The molar and specific absorptivity of IM was found to be 2.75×10^3 L M^{-1} cm^{-1} and 4.66×10^2 mL gm^{-1} cm^{-1} in the optimized solvent system while the Sandell's coefficient was found to be 2.15×10^{-2} µg cm^{-2}. Thus, the optimized wavelength has not only demonstrated merits in terms of better sensitivity and repeatability but also selectivity in the presence of formulation matrix with significant pH tolerance. The UV-Visible spectrum of IM in buffer system at various pH is shown in Fig. 3.1(b).

b) Spectroscopic method validation

i) Selectivity

The UV absorption spectrum of placebo samples of both the formulations did not show significant interference in determination of IM. Moreover, formulation standards and test samples showed no significant change in absorption spectrum when compared with the calibration standards. The method has demonstrated high and consistent recoveries at all concentration levels. Moreover, the calculated t-values were found to be much lower than that of the critical t-value confirming statistically insignificant difference between the mean absorbance of formulation and calibration standards (Table 3.1).

Table 3.1: Statistical data summary for spectroscopic method

Parameter	Spectrophotometric Method
Calibration range	2.5-25 µg mL^{-1}
Linearity (Regression coefficient)	$R^2 = 0.9995$
Regression equation	Absorbance (AU) = 0.047 × Conc. (µg mL^{-1}) + 0.008
Confidence interval of slope [a]	0.0456 to 0.0485 (Std. error = 0.001)
Confidence interval of intercept [a]	−0.0299 to 0.0146 (Std. error = 0.008)
Standard deviation of intercept ($Ś_c$)	5.76×10^{-3}
t-value for intercept [a, b] (tab = 2.57)	0.955 (P-value 0.39)
F-value (tab) [c]	2.88×10^{-4} (1.80) [c]
Standard error of estimate	8.10×10^{-3} (0.300 µg mL^{-1})
Limit of detection	0.568 µg mL^{-1}
Limit of quantification	1.705 µg mL^{-1}
Absolute recovery	99.18-102.04%
Precision (% RSD)	Repeatability - 2.21% (intra-batch)
	Intermediate Precision - 0.80% (inter-batch)
System suitability	System Precision - 0.85% (n = 10)
	Molar Absorptivity - 2.75×10^3 L M^{-1} cm^{-1}
	Specific Absorptivity - 4.66×10^2 mL gm^{-1} cm^{-1}
	Sandell's Coefficient - 2.15×10^{-2} µg cm^{-2}
Selectivity (resolution)	selective at 285 nm
Robustness	Organic component ± 20%
	Buffer strength ± 100 mM
	pH ± 1%

[a] calculated at 0.05 level of significance; [b] calculated using the test of the intercept (t_{df} = | C – α | / $Ś_c$); [c] calculated using Fisher test with one-way ANOVA (P-value < 0.05).

These observations suggested that the proposed method demonstrates adequate selectivity for IM in presence of formulation excipients and other impurities.

ii) Linearity and range

The least square regression analysis indicated excellent linearity over the range of 2.5-25 µg mL^{-1} with regression coefficient of 0.9995. The best-fit linear equation obtained was absorbance (AU) = 0.047 × concentration (µg mL^{-1}) + 0.008. Across the analytical range, a low standard deviation and % RSD (< 5) was observed in absorbance values (Table 3.2). Selected linear model with univariant regression showed minimum % Bias, indicating goodness of fit which was further supported by low standard error of estimate (1.94×10^{-1}) and mean sum of the squared residuals (3.76×10^{-2}).

Table 3.2: Calibration curve of Imatinib mesylate by the spectrophotometric method

Concentrations (µg mL^{-1})	Average absorbance [a] ± Standard deviation	% RSD	% Bias
2.5	0.1137 ± 0.004	3.87	2.01
5	0.2276 ± 0.001	0.19	–0.48
7.5	0.3522 ± 0.006	1.64	1.74
10	0.4565 ± 0.003	0.55	–1.48
15	0.6889 ± 0.003	0.43	–1.32
20	0.9447 ± 0.003	0.28	1.26
25	1.1646 ± 0.002	0.21	–0.26

[a] Each value represents the average of six independent determinations.

The effect of formulation matrix was statically insignificant as the intercept was not different from zero, which was confirmed by the test of the intercept using t-statistic ($t_{df} = 0.955 << t_{tab} = 2.57$). Finally, one-way ANOVA was performed on individual absorbance recorded at all concentration levels and calculated F-value was found to be much below the critical F-value at 5% level of significance (Table 3.1).

iii) Accuracy and precision

In recovery studies, the method showed consistent and high absolute recoveries at all five concentration levels and mean absolute recovery ranged from 99.18 to 102.04% (Table 3.3). Placebo spiking technique indicated that the obtained absolute recoveries were normally distributed around the mean (≈ 100%) with uniform and low % RSD (< 3) across five concentration levels, which suggested the suitability of univariant regression model. Thus, it can be summarized that there was no significant interference of excipients and the method was found to be accurate with low % Bias (< 2). Moreover, the results of

standard addition technique were in agreement with placebo spiking technique as it also resulted in consistent and high absolute recoveries. Recovery study indicated that the method was suitable for determination of IM from tablets and nanoparticles (Table 3.3).

Table 3.3: Recovery studies by placebo spiking and standard addition technique

Products	Technique	Amount of drug added (% of label claim)	Mean absolute recovery (%)	% RSD	% Bias
Tablets	Placebo spiking [b]	50	100.78 ± 1.58	1.57	0.78
		75	99.67 ± 1.63	1.64	−0.33
		100	99.18 ± 1.42	1.43	−0.82
		125	100.71 ± 2.01	2.00	0.71
		150	99.75 ± 1.02	1.02	−0.25
	Standard addition [d]	50	99.40 ± 0.58	0.58	−0.60
		100	100.05 ± 0.42	0.42	0.05
Nanoparticles	Placebo spiking [c]	50	101.47 ± 2.56	2.52	1.47
		75	101.91 ± 3.10	3.04	1.91
		100	101.94 ± 1.01	0.99	1.94
		125	100.99 ± 1.77	1.75	0.99
		150	101.08 ± 1.64	1.62	1.08
	Standard addition [e]	50	102.04 ± 3.16	3.10	2.04
		100	101.68 ± 3.15	3.10	1.68

[a] Each level was processed independently and analyzed in six replicates; [b] Placebo tablet matrix equivalent to unit dose weight; [c] Placebo nanoparticulate preparation equivalent to unit dose; [d] Commercial tablet preparation containing 100 mg of equivalent Imatinib; [e] In-house prepared nanoparticulate preparation containing 10 mg of equivalent Imatinib.

Precision was determined as repeatability and intermediate precision. Freshly prepared three QC standards (n = 6; at each level) showed no significant variation in measured response demonstrating repeatability of the method with low % RSD (≤ 2.21). Similarly, inter-batch % RSD was significantly low (≤ 0.80) indicating intermediate precision of the method. Low % RSD demonstrated the repeatability and intermediate precision of the method (Table 3.4).

Table 3.4: Results of repeatability and intermediate precision study

QC Levels	Repeatability (Intra-batch)						Intermediate precision (Inter-batch)	
	Batch (I)		Batch (II)		Batch (III)			
	Mean [a]	% RSD	Mean [a]	% RSD	Mean [a]	% RSD	Mean	% RSD
LQC	2.53	1.76	2.53	2.21	2.50	1.22	2.52	0.80
MQC	10.04	1.29	9.94	1.31	10.05	1.05	10.01	0.61
HQC	25.28	1.30	25.23	1.11	25.31	1.09	25.28	0.16

[a] Each value represents the average of six independent determinations.

iv) Sensitivity

The LOD and LOQ of the method were found to be 0.57 and 1.71 µg mL^{-1}, respectively. The method has shown high magnitude of slope with low standard error (Table 3.2). Upon repeated analysis at quantitation limit, the mean absolute recovery was consistently high with low % Bias and % RSD. Thus, the method was found to be highly sensitive as small change in the drug concentration can be accurately determined by the proposed method.

v) Robustness

The statistical analysis indicated that the obtained response remains unaffected by small variations in critical method parameters such as pH, buffer strength and composition of solvent media.

Table 3.5: Robustness studies - mean absolute recovery from quality control standards

Treatments		LQC	MQC	HQC
pH	(pH 6.5)	100.4 ± 1.47	101.0 ± 0.81	101.3 ± 0.69
	(pH 8.4)	100.9 ± 0.91	100.9 ± 1.82	100.5 ± 1.00
Buffer Strength	(0 mM)	97.9 ± 2.02	98.3 ± 1.06	99.7 ± 0.73
	(200 mM)	102.3 ± 1.41	101.6 ± 1.14	101.5 ± 0.81
Composition	A	102.7 ± 1.62	102.6 ± 2.09	101.7 ± 0.63
	B	103.6 ± 1.73	103.4 ± 1.25	102.1 ± 0.68

Each value represents the average of three independent determinations. Composition A is methanol and phosphate buffer (pH 7.4, 100 mM) (30:80 *v/v*) and B is acetonitrile, methanol and phosphate buffer (pH 7.4, 100 mM) (20:50:30 *v/v*)

In addition, there was no significant change in absorption spectrum of IM in the near vicinity of detection wavelength (275-295 nm) (Fig. 3.1). The results obtained from the statistical analysis of individual treatment showed that the obtained F-values were much lower than tabulated. This indicated that there was no significant difference between the treated and untreated groups as far as accuracy and precision of the method are concerned. The method was found to be robust with consistent mean absolute recovery values and low % RSD for individual treatments (Table 3.5).

vi) System precision and drug stability

The method was found to be suitable in terms of system repeatability as the results were consistent with low variability in absorbance (% RSD < 1). Further, the absorption spectrum of drug exhibited no significant change for 48 h at room temperature when compared with freshly prepared standards. The results indicated that the drug was stable in the solvent media at ambient temperature with less than 2.5% change in concentrations of stability samples.

vii) Analysis of formulations

The mean recoveries were found to be in good agreement with the labeled claim of individual products. The method was found to be accurate and precise with consistently high analytical recoveries of 99.52 ± 0.66% and 100.22 ± 3.37% for tablets and nanoparticles, respectively. Moreover, both the formulations showed low % Bias indicating insignificant interference from the formulation excipients. Thus, the method was found to be suitable for determination of IM from both formulations.

3.4 Method II: Chromatographic analytical method

3.4.1 Experimental

a) Chromatographic system and conditions

An HPLC system (Shimadzu, Japan) consisted of pump system (LC-10AT*VP*), integrated system controller with auto-sampler (SIL-HT*A*) and UV detector (SPD-10A*VP*) was used. Data acquisition and analysis was done using 21 CFR part 11 compliant work station LCsolutions® (Shimadzu, Japan).

Optimized mobile phase consisted of methanol and aqueous triethylamine (pH 10.5; 1% *v/v*) (60:40 *v/v*), where aqueous pH was adjusted with hydrochloric acid. Mobile phase was delivered in isocratic elution mode at a flow rate of 1 mL min^{-1}. The chromatographic separation was achieved on Zorbax Extend-C18 (250 × 4.6 mm, 5 µm, 80 Å) double end-capped RP-HPLC column (Agilent, USA) fitted with guard column

(12 × 4.6 mm) of the same material. The quantitation was carried out at 285 nm with injection volume of 50 µL. Analysis was performed at ambient temperature (25°C) after baseline stabilization for at least 30 min.

b) Preparation of stocks and standards

A primary stock solution of 1 mg mL^{-1} was prepared in solvent media consisting of methanol: TDW (60:40 *v/v*). Secondary stock solution of 10 µg mL^{-1} was prepared by diluting 1 mL of primary stock solutions to 100 mL of the solvent media. Three separate series of seven calibration standards containing 25, 50, 100, 200, 400, 800, and 1600 ng mL^{-1} of IM were prepared fresh by serial dilution in mobile phase on three different days of validation.

Formulation standards were prepared by adding known amount of the drug in placebo blend of tablets and blank nanoparticulate preparation at five levels - 50, 75, 100, 125 and 150% of the labeled claim. Similarly, placebo standards were prepared without adding drug. Prepared standards were processed independently, as described below in their respective sample preparation section and analyzed.

c) Sample preparation

For tablets, a quantity of the product equivalent to 10 mg of IM was weighed and transferred to 100 mL calibrated flask and volume was made up with solvent media. Samples were filtered through Whatman® filter paper after vortex mixing for 5 min. Finally, 0.5 mL of filtrate was transferred to 100 mL calibrated flask and diluted to volume with mobile phase.

For nanoparticulate preparations, a quantity of the product equivalent to 10 mg of IM was weighed and transferred to 100 mL calibrated flask and nanoparticles were digested with 10 mL of acetonitrile by ultrasonication (15 min & 25°C). The volume was made with solvent media and the samples were centrifuged (10,000 rpm, 15 min & 20°C). Finally, 0.5 mL of clear supernatant was transferred to 100 mL calibrated flask and diluted to volume with mobile phase.

d) Analytical method development

In order to develop a selective and sensitive analytical method, primary concern during development was to achieve maximum height to area ratio and peak symmetry. Different buffer type and pH media such as phosphate buffer (pH 3-7 & 20 mM), citrate buffer (pH 3-5 & 20 mM), ammonium acetate buffer (pH 3-5 & 20 mM) and acetic acid buffer (pH 3-5 & 20 mM) were studied in combination with methanol (30, 50 & 70% *v/v*).

Effect of various organic modifiers such as acetonitrile, methanol and their combinations, on peak properties (peak height & symmetry) and response function were investigated. Various ion pairing agents such as trifluoroacetic acid (1% *v/v*), triethylamine (1% *v/v*), sodium dodecyl sulfate (10 mM) and 1-octanesulfonic acid sodium salt (10 mM) were tested to improve peak properties such as peak height, tailing factor (T_f) etc. In addition, chromatographic parameters such as retention factor (k), number of theoretical plates (N), height equivalent to theoretical plates (HETP) etc. were also recorded. Further, robustness study was conducted during final phase of method development by using design of experimentation technique.

e) Analytical method validation

The developed chromatographic method was validated for selectivity, linearity, range, precision, accuracy, sensitivity, robustness and system suitability. Additionally, stability indicating capability was determined by forced degradation study. The method was also applied for the drug content analysis from commercial tablets and in-house prepared nanoparticle formulations.

i) Selectivity

Selectivity was assessed by placebo and spiked-placebo analysis technique. On three consecutive days, placebo and formulation standards were prepared and analysed. Each standard (tablets and nanoparticles) was prepared in triplicate and processed as described in the respective sample processing section. Obtained chromatograms were compared with the fresh calibration standards.

Further, forced degradation study was carried out by exposing the drug to acidic, alkaline and neutral hydrolytic as well as thermal, photo and oxidative stress conditions. A novel, fast and effective microwave based degradation technique was designed and employed for hydrolytic forced degradation study. For each stress treatment, 10 mg of the drug was weighed accurately and transferred to 10 mL clear calibrated flask.

For hydrolytic treatments, 2 mL of either 2M hydrochloric acid or 2M sodium hydroxide or TDW was added in each flask containing 10 mg of drug. Prepared solutions were vortex mixed and subjected to microwave radiation (15 sec/cycle, 2.45 GHz, 300 W & 80% intensity) for 15 min. After the treatment, samples were allowed to cool and neutralized.

For thermal and photolytic stress treatments in liquid state, 2 mL of TDW was added in each flask containing 10 mg of drug, while dry state samples were processed as such.

Prepared samples were subjected to either a controlled heating at 90°C or natural sun light for 12 h over a period of two days (≈ 6 h day^{-1}).

For oxidative stress treatment, 2 mL of hydrogen peroxide (6% *v/v*) solution was added in each flask containing 10 mg of drug and vortex mixed for 5 min. Prepared drug solutions were subjected to controlled-temperature at 25°C for 12 h, protected from light. After each treatment, samples were suitably diluted in mobile phase and analyzed by the proposed method.

An orthogonal method was developed to increase selectivity of the method on the same column by replacing methanol with acetonitrile. The ratio of organic phase was optimized (25% *v/v*) to obtain significant change in selectivity, while all other chromatographic conditions were kept constant. All degradation samples were subjected to orthogonal separation and degree of orthogonality was determined.

ii) Linearity and range

To establish linearity, calibration standards prepared at seven concentration levels ranging from 25-1600 ng mL^{-1} were analyzed. Average peak area at each concentration level was subjected to linear regression analysis with the least square method. Calibration equation obtained from regression analysis was used to calculate the corresponding predicted concentrations. One-way analysis of variance (ANOVA) was performed on each replicate response obtained at seven concentration levels. Analytical range of the method was established by the analysis of residuals and test of the intercept was carried out using t-statistic.

iii) Accuracy and precision

For determination of accuracy, recovery study was carried out by two different techniques viz. placebo spiking and standard addition method for tablets and nanoparticles, separately. In placebo spiking method, a known amount of standard solution was added to placebo blank at five concentration levels 50, 75, 100, 125 and 150% of the labeled claim. In standard addition technique, a known amount of pure drug was added in sample solution at 50 and 100% concentration level of the labeled claim of previously analyzed tablets and nanoparticulate preparations. Each concentration level was processed in six replicates on three different days and the results were expressed as mean absolute recovery, % RSD and % Bias.

Precision was determined through repeatability (intra-batch) and intermediate (inter-batch) precision. Study was conducted using quality control (QC) standards prepared at lower (LQC = 25 ng mL^{-1}), medium (MQC = 200 ng mL^{-1}) and higher

(HQC = 1600 ng mL^{-1}) concentration levels. Precision of the method was expressed as percent relative standard deviation (% RSD) of the assay results.

For repeatability (intra-batch), six series of three QC standards were prepared fresh and analyzed. Similarly, standards were prepared and analyzed on three consecutive days for intermediate precision (inter-batch). The intra-batch and inter-batch assay % RSD obtained at three QC levels were used to assess repeatability and intermediate precision, respectively.

iv) Sensitivity

Sensitivity was determined based on standard deviation of intercept (σ) and slope (s) of the calibration curve. The limit of detection (LOD) and limit of quantitation (LOQ) were determined using formulae 3.3 σ/s and 10 σ/s, respectively.

v) Robustness

Robustness study was conducted by making small but deliberate changes to the optimized method parameters. The design of experimentation technique was used to identify critical chromatographic factors and their effect on method performance. Critical sources of variability in operating procedure such as percent organic component, buffer strength and pH were identified. The critical factors were investigated in a range that covers the variation due to intra- and inter-laboratory conditions. A three-factor face-centered design consisting of total eighteen experiments was carried out. Three selected factors were percentage of methanol (MET: X_1, 55-65% *v/v*), percentage of triethylamine in aqueous component (TEA: X_2, 0.5-1.5% *v/v*) and pH of aqueous phase (pH: X_3, 10-11), adjusted with hydrochloric acid. For each experiment, analytical standard of IM (1000 ng mL^{-1}) was analyzed in triplicate after baseline stabilization. Chromatographic parameters such as retention time, peak area and peak height along with system suitability parameters (k, T_f, N and HETP) were recorded as experimental responses. For statistical analysis, one-way ANOVA and lack of fit analysis were carried out for data fitting and model validation.

vi) System suitability and drug stability

As an integral part of the analytical procedure, various chromatographic performance parameters (k, T_f, N and HETP) were recorded in system suitability study. System precision was evaluated by performing injection repeatability of the calibration standards with ten replicates. Further, stability of the drug in mobile phase was tested by injecting calibration standards and formulation standards at 0, 6, 12, 24 and 48 h, in triplicates.

vii) Analysis of formulations

As a part of validation procedure, the method was tested for drug content analysis of test samples such as marketed tablets and in-house prepared nanoparticulate preparations. For commercial tablets of IM, the average weight of twenty tablets was recorded and tablets were powdered and mixed. A quantity of powder equivalent to 10 mg of IM was weighed accurately and processed as described in the sample processing section.

Finally, 50 µL of resulting solution was injected in triplicate and analyzed by the method. For in-house prepared nanoparticulate preparations, a quantity of freeze dried nanoparticulate preparation equivalent to 10 mg of IM was weighed accurately and processed as described in sample processing section. Finally, 50 µL of the resulting solution was injected in triplicate and analyzed.

3.4.2 Results and Discussion

a) Analytical method development

In the preliminary study, peak properties and response function were optimized by changing type of organic modifier, organic to aqueous ratio, buffer type, buffer strength and pH. Use of ion-pairing agents showed varying degree of improvement in peak symmetry ($T_f \approx 1.35$ to 1.65) over simple buffer systems ($T_f > 1.85$). Amongst the various ion pairing agents studied, trifluroacetic acid (pH 2; 1% *v/v*) and triethylamine (pH 10; 0.5% *v/v*) with methanol (50:50 *v/v*) provided acceptable peak symmetry ($T_f \approx 1.35$) but triethylamine offered advantage of better sensitivity and reproducibility. Considering chromatographic parameters, triethylamine was found to be the most suitable ion pairing agent. Use of triethylamine (pH 10.5; 1% *v/v*) in combination with methanol (40:60 *v/v*) produced a symmetric peak ($T_f \approx 1.15$) with sensitive and reproducible results. Reduction in pH led to peak asymmetry ($T_f \approx 1.65$), where pH below 4 showed poor peak properties and loss in selectivity with incomplete resolution from degradation products. Double end-capped C_{18} column was used for better peak symmetry and enhanced stability at higher pH. Moreover, wavelength was optimized at 285 nm for better sensitivity and selectivity from degradation products. Thus, the mobile phase was optimized to methanol and aqueous triethylamine (pH 10.5; 1% *v/v*) (60:40 *v/v*) and it was found to provide good retention ($R_t \approx 8 \pm 0.25$ min) with better peak properties, selectivity and reproducibility.

b) Analytical method validation

i) Selectivity

Placebo samples showed no interference within the vicinity of IM peak, which indicated selectivity of the method for IM in presence of formulation excipients (Fig. 3.2a).

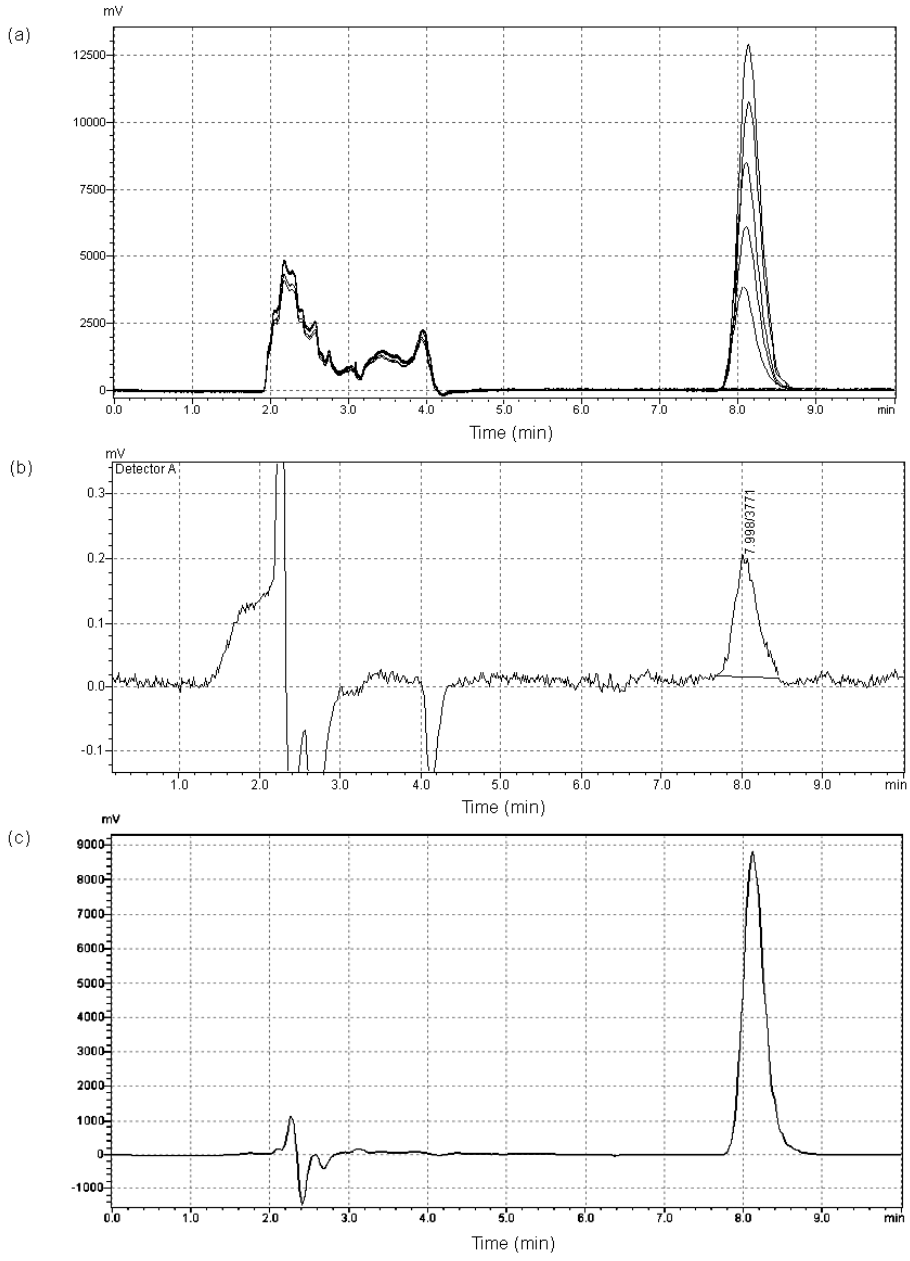

Fig. 3.2: Representative chromatograms of standards demonstrating selectivity (a) placebo and formulation standards - nanoparticles, (b) standard at quantitation limit and (c) test sample - commercial tablets

At LOQ level, drug spiked placebo samples in comparison with calibration standards showed no significant change in response and peak properties (Fig. 3.2b).

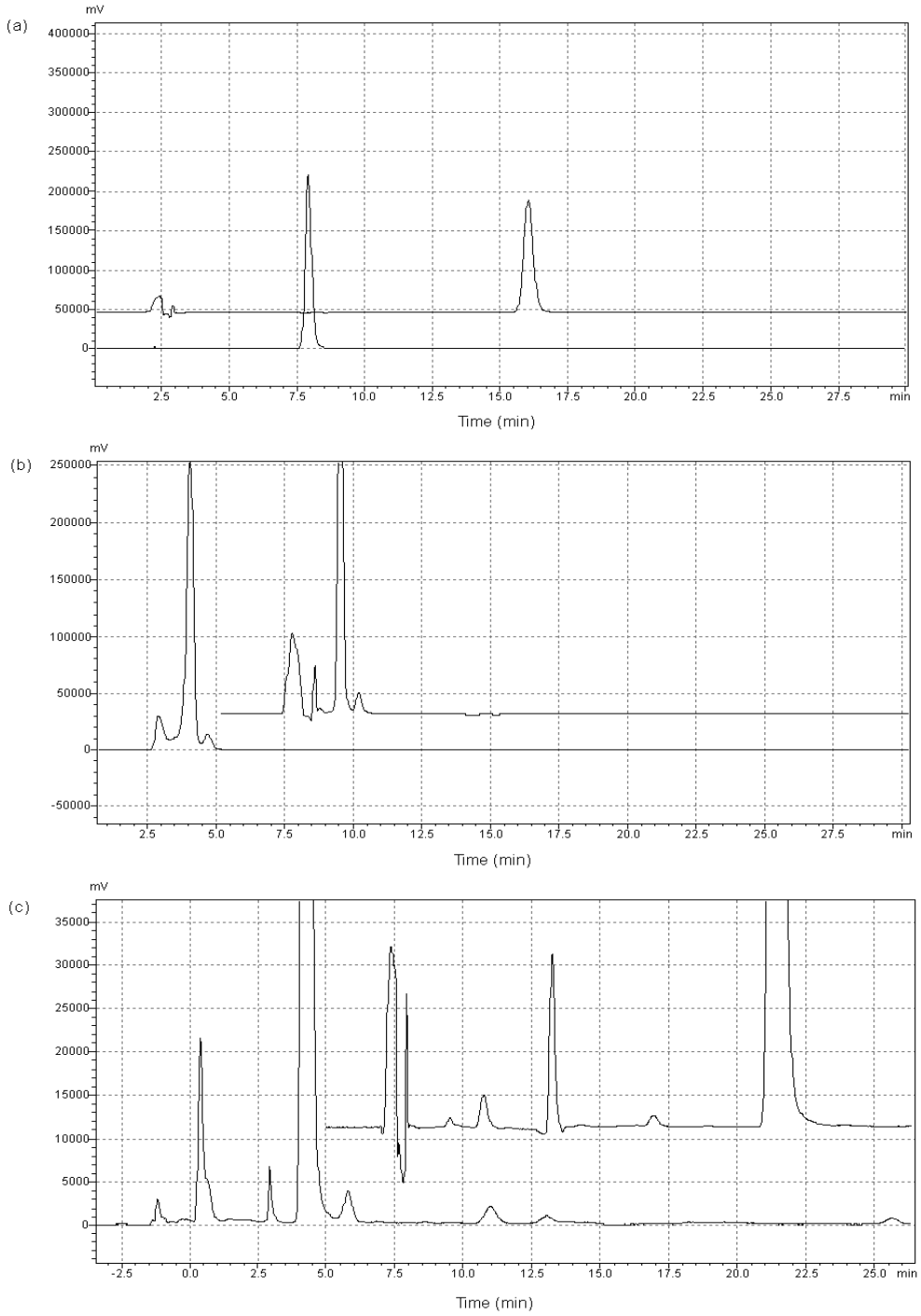

Fig. 3.3: Representative chromatograms of samples analyzed by the proposed and orthogonal method (a) calibration standards (b) forced degradation samples - oxidative stress and (c) forced degradation samples - acid stress conditions

Stress testing study under various conditions demonstrated that degradation products of IM could be well separated without significant interference in IM estimation. Further, orthogonal separation technique demonstrated that there were no co-eluting components at the retention time of IM (Fig. 3.3a to 3.3c). Insignificant degradation of IM was observed with the heat treatment in dry state. In the aqueous solution at 90°C showed one prominent degradation product eluting before IM at 4.3 min, which indicates that the degradation product may be hydrophilic in nature. The same degradation product was also found in the dry state degradation along with one additional impurity eluting at 22.9 min. IM has shown good stability in dry and liquid state photo-stability without detectable degradation products. There were two degradation products observed at retention time of 4.3 and 22.5 min, which indicates that obtained degradation products may be of similar nature as found under heat treatment study.

Although liquid state stability of IM under neutral pH condition showed low extent of degradation, obtained degradation products were of similar nature as those observed under heat and photo treatment with retention time of 4.3 and 22.7 min. IM has shown significant degradation under acidic and alkaline conditions with overall eight degradation products. Under alkaline conditions, three degradation products were found to be hydrophilic in nature as they eluted before IM with retention time of 4.1, 4.6 and 6.6 min, while the other two hydrophobic products were eluted at 12.3 and 16.1 min. Under acidic conditions, two hydrophilic degradation products were observed at retention time of 4.1 and 6.6 min and one additional degradation product eluted at 2.5 min merged into the solvent front (2.2 min). Further, two hydrophobic degradation products were observed at retention time of 9.4 and 14.6 min, which may be of different nature as compared to the degradation products obtained under alkali treatment. IM has shown significant sensitivity towards the treatment of hydrogen peroxide leading to three prominent degradation products eluting at 3.6, 4.2 min and one degradation product merging into solvent front at 2.4 min. The degradation products may be relatively hydrophilic in nature as retention time for all the three products was less than retention time of IM.

The orthogonal separation technique was employed as an additional selectivity tool to ensure the purity of analyte peak in presence of its degradation products (29). In this technique, the same forced-degraded sample was separated by two separate systems of markedly different selectivity (≥ 1.5). In order to ensure selectivity of the proposed method the degree of orthogonality was calculated by plotting log k “orthogonal method”

versus log k "proposed method" of each degradation product and IM. Linearity equation obtained was log k (orthogonal method) = 1.534 × log k (proposed method) – 0.104 with regression coefficient of 0.9277 and standard error of 0.125 (SE). The value for $| \delta \log \alpha |_{avg}$ (1.4 × SE = 0.175) was significantly more than 0.1 which suggests that the orthogonal separation was adequate to separate any overlapping peaks. Thus, the developed orthogonal method was sufficient to disengage two overlapping peaks, if unresolved by the proposed method.

Table 3.6: Statistical data summary for chromatographic method

Parameter	Chromatographic Method
Calibration range	25-1600 ng mL^{-1}
Linearity (Regression coefficient)	$R^2 = 0.9998$
Regression equation	Peak area (μV s) = 285.7 × Conc. (ng mL^{-1}) + 176.3
Confidence interval of slope [a]	283.23 to 288.22 (Std. error = 0.972)
Confidence interval of intercept [a]	−1567.85 to 1920.51 (Std. error = 678.52)
Standard deviation of intercept ($Ś_c$)	2.87×10^2
t-value for intercept [a, b] (tab = 2.57)	0.607 (P-value 0.29)
F-value [c]	4.76×10^{-12}
Standard error of estimate	4.39×10^2 (0.92 ng mL^{-1})
Limit of detection	3.35 ng mL^{-1}
Limit of quantification	10.16 ng mL^{-1}
Absolute recovery	99.35-100.69%
Precision (% RSD)	Repeatability - 2.39 % (intra-batch)
	Intermediate Precision - 2.08 % (inter-batch)
System suitability	System Precision - 0.77% (n = 10)
	Capacity Factor - 2.65 (± 0.002)
	Tailing Factor - 1.14 (± 0.005)
	Number of Plates - 3975 (± 52.31)
Selectivity (resolution)	> 2 (nearest impurity)
Robustness	%MET ± 2.5
	%TEA ± 0.25
	pH ± 0.25

[a] calculated at 0.05 level of significance; [b] calculated using the test of the intercept ($t_{df} = | C - \alpha | / Ś_c$); [c] calculated using Fisher test with one-way ANOVA (P-value <0.05)

Forced-degraded samples were also analyzed by the orthogonal method which showed retention time of 16.1 min for pure IM. There was no statistically significant change in the average peak area observed between the proposed method and orthogonal method,

which suggests that there was no possibility of any overlapping peaks in the proposed method. In addition, the number of degradation products eluting before and after the drug retention time were constant in both the methods which indicate the suitability of the proposed method for effective separation of the degradation products. Thus, it can be concluded that the proposed method demonstrates adequate selectivity of IM from formulation excipients, impurities and degradation products.

ii) Linearity and range

Calibration curve obtained by the least square regression analysis between average peak area and the concentration showed linear relationship with regression coefficient of 0.9998. The best-fit linear equation obtained was average peak area (μV s) = 285.7 × concentration (ng mL^{-1}) + 176.3. At all concentration levels, standard deviation and % RSD of peak area was significantly low. Analysis of residuals indicated that the residuals were normally distributed around the mean with uniform variance across all concentrations, suggesting the homoscedastic nature of data. Selected linear model with univariant regression showed minimum % Bias indicating the goodness of fit and it was further supported by low standard error of estimate and mean sum of the squared residuals (Table 3.6). The statistical analysis indicated excellent linearity over the range 25-1600 ng mL^{-1}. Test of the intercept revealed that intercept was not significantly different from zero at 95% confidence interval using t-statistic (t_{df} = 0.607). Finally, one-way ANOVA was performed for peak area obtained at individual concentration levels and calculated F-value was found to be less than the critical F-value at 5% level of significance.

Table 3.7: Calibration curve of Imatinib mesylate by the chromatographic method

Concentrations (ng mL^{-1})	Average peak area [a] ± Standard deviation	% RSD	% Bias
25	7408 ± 153.5	2.07	1.25
50	14396 ± 272.3	1.89	–0.46
100	28797 ± 554.1	1.92	0.17
200	57697 ± 859.0	1.49	0.65
400	113962 ± 1540.3	1.35	–0.44
800	227736 ± 2562.8	1.13	–0.45
1600	456262 ± 4600.7	1.01	–0.24

[a] Each value represents the average of six independent determinations.

iii) Accuracy and precision

The method showed consistent and high absolute recoveries at all five concentration levels with mean absolute recovery ranging from 99.35 to 100.69% (Table 3.8). Placebo spiking method indicated that the obtained absolute recoveries were normally distributed around the mean with uniform % RSD across five concentration levels suggesting homoscedastic nature of the data. Thus, it can be summarized that there was no significant interference of excipients and the method was found to be accurate with low % Bias (< 1). Further, consistent and high absolute recoveries obtained from the standard addition method were in agreement with placebo spiking technique. Recovery study indicated that the method was suitable for determination of IM from tablets and nanoparticulate preparations.

Table 3.8: Recovery studies by placebo spiking and standard addition technique

Products	Technique	Amount of drug added (% of label claim)	Mean absolute recovery (%)	% RSD	% Bias
Tablets	Placebo spiking [b]	50	100.24 ± 1.52	1.52	0.24
		75	100.48 ± 1.31	1.30	0.48
		100	100.22 ± 1.34	1.34	0.22
		125	100.34 ± 1.09	1.09	0.34
		150	100.40 ± 0.74	0.74	0.40
	Standard addition [d]	50	100.21 ± 0.97	0.97	0.21
		100	100.39 ± 0.89	0.89	0.39
Nanoparticles	Placebo spiking [c]	50	100.28 ± 1.84	1.83	0.28
		75	100.56 ± 1.63	1.62	0.56
		100	100.69 ± 1.06	1.05	0.69
		125	100.62 ± 1.02	1.01	0.62
		150	100.40 ± 0.75	0.75	0.40
	Standard addition [e]	50	99.39 ± 0.86	0.87	−0.61
		100	99.35 ± 1 .22	1.23	−0.65

[a] Each level was processed independently and analyzed in six replicates; [b] Placebo tablet matrix equivalent to unit dose weight; [c] Placebo nanoparticulate preparation equivalent to unit dose; [d] Commercial tablet preparation containing 100 mg of equivalent Imatinib; [e] In-house prepared nanoparticulate preparation containing 10 mg of equivalent Imatinib.

Freshly prepared six standards at three QC levels showed insignificant variation in measured response (% RSD < 2.39) demonstrating the method repeatability. Similarly, inter-batch % RSD was significantly low (≤ 2.08) for intermediate precision. Low % RSD indicated the repeatability and intermediate precision of the method (Table 3.9).

Table 3.9: Results of repeatability and intermediate precision study

QC Levels	Repeatability (Intra-batch)						Intermediate precision (Inter-batch)	
	Batch (I)		Batch (II)		Batch (III)			
	Mean [a]	%RSD	Mean [a]	%RSD	Mean [a]	%RSD	Mean	%RSD
LQC	25.44	2.16	25.55	2.10	25.17	2.39	25.33	2.08
MQC	202.58	0.91	201.71	1.05	198.01	0.91	201.29	1.45
HQC	1600.6	1.02	1595.7	0.89	1585.5	0.90	1597.0	1.04

[a] Each value represents the average of six independent determinations.

iv) Sensitivity

The LOD and LOQ of the method were found to be 3.35 and 10.16 ng mL^{-1}, respectively. The method has shown high magnitude of slope and low standard error (Table 3.6). Upon repeated injection at quantitation limit, the peak properties (retention time, peak area and tailing factor) were not affected and mean absolute recovery was consistently high and acceptable with low % Bias and % RSD. Thus, the method was found to be highly sensitive as compared to other reported methods.

v) Robustness

Analysis of response surface plots revealed that the obtained response remains unaffected by the small changes in critical method parameters such as percent organic component, buffer strength and pH. The statistical analysis showed that there was good agreement between experimental and predicted values. The developed quadratic model showed good correlation between obtained responses and studied factors. The model coefficients obtained by least square regression analysis were successfully used to determine qualitative and quantitative relationship between the critical method parameters and chromatographic response function using the following equation.

$$\hat{Y} = \beta_0 + \beta_1X_1 + \beta_2X_2 + \beta_3X_3 + \beta_{12}X_1X_2 + \beta_{13}X_1X_3 + \beta_{23}X_2X_3 + \beta_{11}X_1^2 + \beta_{22}X_2^2 + \beta_{33}X_3^2$$

Where, $\hat{Y}$: predicted response; X: coded variables: β: model coefficients

Fig. 3.4a to 3.4f show the 3-D surface plots of predicted responses (on Z-axis) for IM as a function of two significant factors (on X- and Y-axis) while the third factor, i.e. the least

significant factor was held constant at optimum level. Fig. 3.4a and 3.4b show peak area of IM against %MET versus %TEA and %TEA versus pH, where there was no significant change in the mean peak area over studied range of all three factors indicating robustness of response for studied factors. However, %MET showed significant effect on retention time of IM as shown in Fig. 3.4c and 3.4d indicating sensitivity of retention time for %MET amongst studied factors.

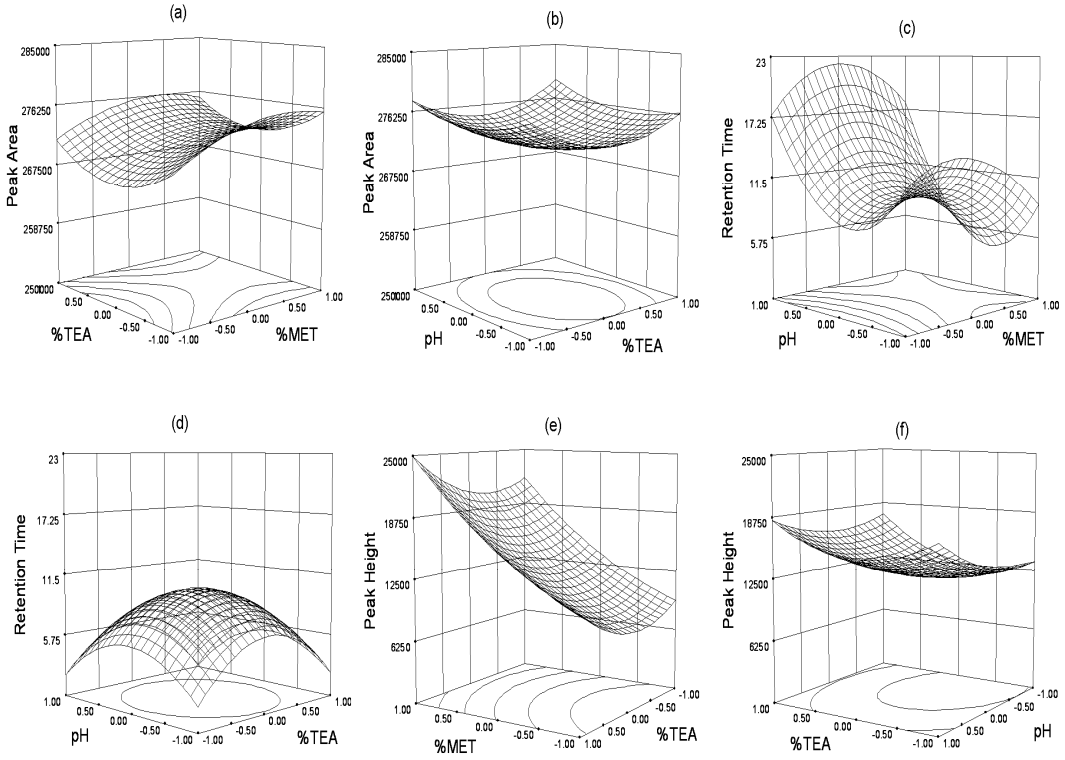

Fig. 3.4: Three-dimensional surface plots of predicted responses. *Z*, peak area (mV s) (a) as a function of *X*, % methanol (*v/v*) and *Y*, % triethylamine (*v/v*); (b) as a function of *X*, % triethylamine (*v/v*) and *Y*, pH; *Z*, retention time (min) (c) as a function of *X*, % methanol (*v/v*) and *Y*, pH; (d) as a function of *X*, % triethylamine (*v/v*) and *Y*, pH; *Z*, peak height (mV) (e) as a function of *X*, % methanol (*v/v*) and *Y*, % triethylamine (*v/v*); (f) as a function of *X*, % triethylamine (*v/v*) and *Y*, pH

The peak height has showed sensitivity towards %MET with significant drop in retention time and retention factor as shown in Fig. 3.4e and 3.4f. Selected factors did not show significant effect on peak symmetry (T_f) within the range of optimized parameters. Further, none of the factors studied showed significant effect on system efficiency. Although few factors have shown effect on retention time and peak symmetry (T_f), the

principle chromatographic response function - peak area was almost unaffected by any of the studied factors suggesting that the proposed method was robust.

vi) System suitability and drug stability

The method was found to be suitable in terms of system performance as obtained values for primary system suitability parameters such as retention factor ($k \geq 2.5$), resolution ($R_s \geq 2$), number of theoretical plates ($N \geq 3900$) were above acceptable limit and height equivalent to theoretical plates ($HETP \leq 60$ µm) was well below limit. The method has shown better peak symmetry ($T_f \approx 1.135$) and injection repeatability was found to be consistent with low variability in peak area and retention time. System suitability study confirmed that the method was specific, precise and stable for determination of IM.

Further, the drug peak exhibited no chromatographic or response change for 48 h at room temperature when compared against freshly prepared standards. The results indicated that the drug was stable in mobile phase at ambient temperature with less than 0.74% RSD.

vii) Analysis of formulations

A typical chromatogram of IM extracted from commercial tablet and in-house prepared nanoparticulate preparation is shown in Fig. 3.2c. The mean recoveries for each formulation were found to be in good agreement with the labeled claim of individual products. The method was found to be accurate with mean absolute recovery of 100.53 and 99.36% for tablet and nanoparticulate preparations, respectively and precise with % RSD not exceeding 0.60 and 1.77 for tablet and nanoparticulate preparations, respectively. Moreover, formulation excipients did not show interference in determination of IM as % Bias was below 0.53 and 0.64 for tablet and nanoparticulate preparations, respectively. Thus, the method was found to be suitable for determination of IM from both the formulations.

3.5 Method III: Chromatographic bioanalytical method

3.5.1 Experimental

a) Chromatographic system and conditions

The same HPLC system as mentioned under method II was used with the same optimized chromatographic conditions including mobile phase and stationary phase compositions. Quantification was carried out at 285 nm with 50 µL injection volume and analysis was performed at ambient temperature (25°C) after baseline stabilization for at least 60 min.

b) Preparations of stocks and standards

A primary stock solution of 1 mg mL^{-1} was prepared in reconstitution solution consisting of methanol: water (60:40 *v/v*). A series of seven working stocks containing 1, 2, 4, 8, 16, 32 and 64 µg mL^{-1} of IM was prepared by serial dilution of primary stock in reconstitution solution. Seven analytical standards containing 25, 50, 100, 200, 400, 800 and 1600 ng mL^{-1} of IM were prepared fresh by diluting 250 µL of each working stock to 10 mL with reconstitution solution, in triplicate on three different days of validation.

Seven serum standards containing 25, 50, 100, 200, 400, 800 and 1600 ng mL^{-1} of IM were prepared fresh by spiking 25 µL of each working stock in 975 µL of blank rat serum. The standards were vortex mixed for 1 min and allowed to equilibrate with the drug. Similarly, four quality control (QC) standards were prepared at lower limit of quantification (LLOQ = 25 ng mL^{-1}), low (LQC = 100 ng mL^{-1}), medium (MQC = 400 ng mL^{-1}) and high (HQC = 1600 ng mL^{-1}) concentration levels of calibration curve.

Similarly, brain and lungs standards were prepared at 25 to 800 and 50 to 1600 mL^{-1} concentration level of IM with three QC standards each at low (LQC = 50 ng mL^{-1}), medium (MQC = 400 ng mL^{-1}) and high (HQC = 1600 ng mL^{-1}) concentration levels of calibration curve. Each standard (serum, brain and lungs) was prepared fresh in five replicates on three different days of validation. The QC standards were prepared fresh in five replicates on each day of validation. Serum and QC standards were processed as described in the sample preparation section and analyzed by the proposed method.

c) Sample preparation

Aliquot of serum sample (100 µL) or tissue homogenate (200 µL) was transferred to a clean glass tube and 1.5 mL of methylene chloride was added to it. Samples were vortex mixed for 1 min and methylene chloride was separated by centrifugation (10,000 rpm, 5 min, 20°C). The upper aqueous layer was removed by aspiration and organic layer was transferred to a fresh tube. Separated organic layer was dried using a vacuum concentrator and dry residue was reconstituted in 100 µL of the reconstitution solution by vortex mixing for 1 min. Resultant solution was centrifuged (10,000 rpm, 2 min, 4°C) and the clear supernatant was transferred to auto-sampler micro-vials.

d) Bioanalytical method development

Successful analysis of an analyte in biological fluids relies on the optimization of sample preparation, chromatographic separation and interference free detection. Each step was optimized for developing sensitive, selective and reproducible method. For selectivity

purpose, the principle metabolite of the drug was synthesized by N-demethylation of Imatinib as reported elsewhere (31). Briefly, Imatinib was dissolved in dry 1, 2-dichloroethane and the drug solution was refluxed with four equivalents of α-chloroethyl chloroformate for 24 h under nitrogen. The obtained carbamate intermediate was hydrolyzed by treating with methanol at 50°C for 2 h. The separation and purification was carried out using thin layer chromatography over a distance of 10 cm with mobile phase consisting of toluene, acetone, ethanol and ammonia (45:45:06:04 *v/v*). After separation and drying, the N-desmethyl derivative was extracted with solvent phase consisting of methylene chloride, propranol and ammonia (95:4:1 *v/v*).

For sample clean up, various techniques such as simple one-step precipitation with methanol or acetonitrile, single and multi stage liquid-liquid extraction with organic solvents were investigated. In addition to this, acidification and basification of biomatrix for enhancement of recovery were also studied. Considering the physicochemical properties of drug such as ionization coefficient, partition coefficient and solubility in aqueous and organic solvents, various extraction solvents such as n-hexane, diethyl ether, chloroform, methylene chloride and ethyl acetate were studied individually and in combinations. Finally, injection volume and wavelength of detection were optimized for better sensitivity and selectivity.

e) Bioanalytical method validation

The developed liquid chromatographic method was validated with respect to various validation parameters viz. selectivity, linearity, range, recovery, accuracy, precision, sensitivity and drug stability in serum. Partial validation was carried out in brain and lungs for analysis of IM. As a part of validation, intra- and inter-batch variability were studied by repeating the analysis on three different occasions. Method was also applied for the determination of IM in real world serum (test) samples, in order to study in vivo pharmacokinetics in rats.

i) Selectivity

Selectivity of the method was studied by investigating the interference from various endogenous proteins and other impurities present in bio-matrix. Blank rat serum, brain and lungs samples collected from six different rats were processed independently and analyzed by the proposed method. Obtained chromatograms of blank serum samples were compared against analytical and calibration standards for investigating interference in determination.

ii) Linearity and range

Linearity and range of the method was assessed by three separate series of seven serum standards (25-1600 ng mL^{-1}) prepared and analyzed on three consecutive days. Similarly, three separate series of six standards each of brain (25-800 ng mL^{-1}) and lungs (50-1600 ng mL^{-1}) were used for linearity and range. Average peak area at each level was plotted against concentration and the curves were subjected to linear regression analysis by least square method. Calibration equation was used to calculate the corresponding predicted concentrations. One-way analysis of variance (ANOVA) was performed on each replicate response obtained at seven concentration levels.

iii) Recovery studies

Recovery studies in serum were conducted at four QC levels using LLOQ, LQC, MQC and HQC standards, prepared in five replicates on three consecutive days. Similarly, three QC levels were selected for each of brain and lungs sample for recovery study. All QC standards were processed as described in sample preparation section. Absolute recovery at each QC level was calculated by comparing the peak area obtained from QC and analytical standards.

iv) Accuracy and precision

Accuracy and precision of the method in individual matrix was determined by analyzing QC standards prepared at LLOQ, LQC, MQC and HQC levels. Each QC standard was processed and analyzed in five replicates and analysis was repeated on three different occasions to study intra- and inter-batch accuracy and precision. Concentration of IM in QC standards was calculated from the calibration equation. Accuracy was expressed as % Bias and precision was determined as intra and inter-batch variations as percent relative standard deviation (% RSD).

v) Sensitivity

Sensitivity of the method was obtained by determining the lowest concentration of IM that can be estimated with acceptable accuracy and precision (% RSD < 20) and it was expressed as a lower limit of quantitation (LLOQ), in the individual matrix. The QC standards were prepared at LLOQ concentration (25 ng mL^{-1}) in pentaplates and analyzed by the proposed method, on three different occasions. Concentrations of IM in QC standards were calculated from calibration equation and parameters such as mean calculated concentration, % Bias and % RSD were determined.

vi) Stability studies

In order to investigate the integrity of drug under storage and different operational conditions of the proposed method - short term, long term, dry residue and freeze thaw stability studies were carried out at four QC levels of serum standard, in triplicate. Since the developed method was extended to different tissue sample of same animal species, as per standard partial validation protocol stability studies in these matrix were excluded.

For short term stability studies, prepared QC standards were kept at room temperature and each set of QC standards was analyzed at 1, 3, 6, 12 and 24 h of post-spiking. Long term stability of IM in rat serum was investigated over a period of 90 days. Prepared QC standards were stored at −20°C and they were processed and analyzed on 7, 15, 30, 60 and 90 days. Post extraction stability of IM in dry residue was investigated for 15 days. For this purpose, all QC standards were prepared, extracted and stored at −20 °C. One set of QC standards (n = 3) was analyzed on day 1, 3, 5, 10 and 15, immediately after reconstitution with dilution phase.

Freeze thaw stability studies were conducted to investigate the integrity of drug after exposing it to alternate freezing (at least 24 h) and thawing cycles (at least 2 h). For this purpose, prepared QC standards were stored in sealed glass tubes at −20°C. Upon completion of required freeze thaw cycles, respective set of QC standards were processed and analyzed as described earlier. The stability results were expressed as accuracy in terms of % Bias against fresh serum standards.

vii) Over-curve dilution integrity

To study the over-curve dilution integrity, three dilution integrity (DI) standards were prepared in serum at higher (over-curve) concentrations. Before extraction, these standards were diluted in rat serum to bring the concentrations within the calibration range. Five series of DI standards were prepared in rat serum at 5, 10 and 15 μg mL^{-1} concentrations and they were diluted 5, 10 and 15 times, respectively. The DI standards were vortex mixed for 5 min and processed as mentioned previously.

vii) Analysis of in vivo samples

Various pharmacokinetic studies including serum pharmacokinetics and biodistribution in brain and lungs were performed using the validated method and the detailed procedures are mentioned in Chapter 6.

3.5.2 Results and Discussion

a) Bioanalytical method development

A doubled end-capped reversed phase column with bidentate silane (Zorbax Extend-C18, Agilent, USA) was selected for enhanced stability, which is reported to protect silica from dissolution at extreme alkaline conditions (32). Previously, few authors have reported that the nor-metabolites synthesized obtained from this selective procedure can directly be used as qualitative standards for analytical purpose without extensive purification (33). The purified product was used to prepare standards of the N-desmethyl Imatinib, which showed retention time of 5.67 ± 0.29 min indicating clear peak resolution from IM in the optimized mobile phase.

A simple one-step precipitation with methanol or acetonitrile led to a higher protein load and inefficient sample clean up. It was found that even a double extraction with n-hexane, diethyl ether, ethyl acetate and their combination showed poor recovery of the drug. Further, basification of serum showed only a marginal improvement in the drug recovery, there was significant interference from matrix components. Chloroform and methylene chloride showed high extraction efficiency with reproducible and consistent recovery (> 90%). However, extraction with chloroform showed a little interference due to endogenous component of serum in the near vicinity of drug retention time. Single extraction with 1.5 mL methylene chloride resulted in the high extraction efficiency. Optimized injection volume (50 µL) led to sensitive method with interference-free determination at 285 nm. Thus, optimized extraction protocol showed consistent and high recovery at all concentration levels without any interference from endogenous components and impurities. Moreover, brain and lungs samples showed consistent and acceptable recoveries.

b) Bioanalytical method validation

i) Selectivity

Chromatograms of six blank samples revealed that there was no peak present in elution windows of IM. A lack of response in blank biological matrix confirmed the selectivity of the method from endogenous components. Further, test samples obtained from oral pharmacokinetic studies proved that there was no interference from metabolites or degradation products in the near vicinity of drug peak. Comparison of chromatograms of blank, spiked and test serum samples indicate selectivity of the method (Fig. 3.5). Thus, the proposed method was found to be selective in the determination of IM from spiked as well as test samples.

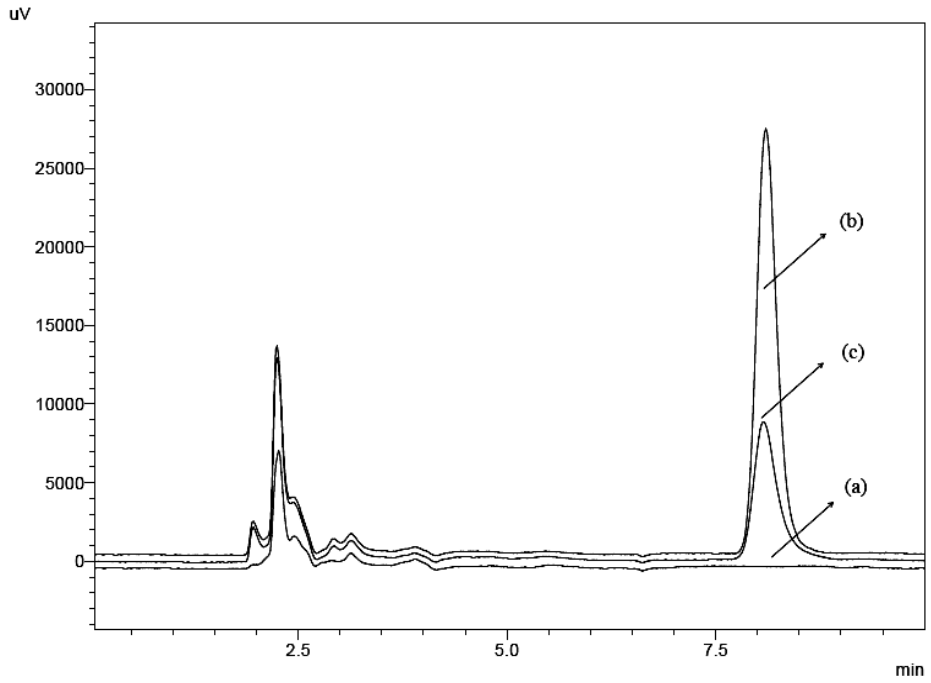

Fig. 3.5: Representative chromatograms of Imatinib mesylate in rat serum (a) blank serum, (b) spiked serum (1600 ng mL^{-1}) and (c) test samples in overlay mode.

ii) Linearity and range

The linear regression analysis indicated linear relationship between the average peak area and concentration in serum over the range 25-1600 ng mL^{-1} with high regression coefficient ($R^2 \geq 0.9995$). The best-fit linear equation was average peak area (μV s) = 263.98 × concentration (ng mL^{-1}) + 44.51 with low standard error of estimate (6.88×10^2) and mean sum of the squared residuals (4.74×10^5).

Table 3.10: Calibration data for serum standards of Imatinib mesylate

Concentration (ng mL^{-1})	Mean peak area [a] (μVs)	% RSD	% Bias
25	6506.14 ± 681.03	10.45	–2.09
50	12670.52 ± 885.36	7.01	–4.34
100	26518.98 ± 933.17	3.52	0.29
200	53788.21 ± 2498.48	4.65	1.79
400	109138.74 ± 3919.95	3.59	3.31
800	205575.40 ± 6995.69	3.40	–2.68
1600	424281.28 ± 19418.47	4.58	0.44

[a] Each value represents the average of nine independent determinations (n = 3 on three occasions).

Mean response obtained for individual concentrations are indicated in Table 3.10. Further, 95% confidence interval and standard error (SE) of the slope was found to be 258.26 to 269.72 (SE ± 2.23). The standard deviation of peak area was significantly low across the analytical range and % RSD was less than 10.5.

Good linear relationship existed between the average peak area and concentration in brain over the range 25-800 ng mL^{-1} with high regression coefficient ($R^2 \geq 0.9997$) (Table 3.11). The best-fit linear equation was average peak area (µV s) = 250.9 × concentration (ng mL^{-1}) + 263.8.

Table 3.11: Calibration data for brain standards of Imatinib mesylate

Concentration (ng mL^{-1})	Mean peak area [a] (µVs)	% RSD	% Bias
25	5918.27 ± 584.13	9.87	–4.45
50	12125.61 ± 883.27	7.28	–5.33
100	24367.05 ± 1186.67	4.87	–3.89
200	50610.96 ± 1862.48	3.68	0.33
400	104581.81 ± 4162.35	3.98	3.93
800	199152.31 ± 5715.67	2.87	–0.91

[a] Each value represents the average of nine independent determinations (n = 3 on three occasions).

The best-fit linear equation for lungs calibration standards was average peak area (µV s) = 219.7 × concentration (ng mL^{-1}) + 856.4 with high regression coefficient ($R^2 \geq 0.9997$) (Table 3.12).

Table 3.12: Calibration data for lungs standards of Imatinib mesylate

Concentration (ng mL^{-1})	Mean peak area [a] (µVs)	% RSD	% Bias
50	10706.59 ± 1131.69	10.57	–4.58
100	22403.03 ± 1675.75	7.48	–1.85
200	45533.91 ± 2581.77	5.67	1.65
400	92274.19 ± 4558.34	4.94	3.99
800	173006.11 ± 5380.49	3.11	–2.04
1600	353261.11 ± 13318.23	3.77	0.25

[a] Each value represents the average of nine independent determinations (n = 3 on three occasions).

In homoscedasticity test, analysis of residuals indicated that the residuals are normally distributed around the mean observed response with uniform variance across all concentrations suggesting homoscedastic nature of data. In addition, selected linear model with univariant regression showed acceptable % Bias indicating the goodness of fit which was further supported by low values of standard error of estimate and mean sum of squared residuals. Test of the intercept revealed that intercept of serum calibration was not significantly different from zero as t_{df} value was 0.0286 (tabulated 2.57) at 5% level of significance. Finally, one-way ANOVA was performed for peak area obtained at individual concentration levels and F-value (7.21×10^{-3}) was found to be much lower than the theoretical F-value (2.12) at 5% level of significance.

iii) Recovery studies

The proposed method showed high and consistent recovery of IM from rat serum at all concentrations studied and use of internal standard was not necessary. Mean absolute recovery values in serum were ranged from 90.32 to 95.86% over the calibration range (Table 3.13).

Table 3.13: Mean absolute recovery of Imatinib mesylate from serum QC standards

Quality control standard		Mean absolute recovery [a;b] (%)	% RSD
Serum QC Standards	LLOQ	90.32 ± 6.97	7.71
	LQC	92.20 ± 3.43	3.72
	MQC	95.86 ± 3.34	3.48
	HQC	93.75 ± 3.36	3.58

[a] Each value represents the average of fifteen independent determinations (n = 5 on three occasions); [b] Recovery = [(Peak area of serum standard / peak area of analytical standard) × 100]

In addition, the method was found to be precise with low % RSD at all QC levels (Table 3.13). Simple liquid-liquid extraction procedure with methylene chloride was found to be efficient and reproducible. The high and consistent recovery results indicated that the method was sensitive and precise for quantitative analysis of IM in the rat serum.

The proposed method also showed consistent and acceptable drug recovery from brain and lungs tissues of rat at all concentrations studied. Mean absolute recovery values in brain and lungs were ranged from 85.48 to 88.79% and 73.81 to 79.52% over the calibration range (Table 3.14).

Table 3.14: Mean absolute recovery of Imatinib mesylate from brain and lung tissues

Quality control standard		Mean absolute recovery [a;b] (%)	% RSD
Brain QC Standards	LQC	85.48 ± 5.62	6.57
	MQC	88.79 ± 3.24	3.65
	HQC	87.35 ± 2.63	3.01
Lungs QC Standards	LQC	73.81 ± 5.92	8.02
	MQC	79.52 ± 3.01	3.79
	HQC	77.43 ± 2.76	3.56

[a] Each value represents the average of fifteen independent determinations (n = 5 on three occasions); [b] Recovery = [(Peak area of serum standard / peak area of analytical standard) × 100]

iv) Accuracy and precision

The obtained results confirmed the accuracy of the proposed method, as the percent deviation was significantly less. At all QC levels, intra-batch % Bias ranged from −2.34 to 3.42 and inter-batch % Bias ranged from −2.17 to 3.45. Results obtained for % Bias and % RSD at each QC level is presented in Table 3.15. The method was found to be precise with % RSD not exceeding 8.53 and 8.01 at LLOQ for intra- and inter-batch, respectively.

In addition, test of the intercept along with homoscedasticity test suggested that there was no significant interference from matrix components in analysis of IM.

Table 3.15: Intra- and inter-batch accuracy and precision of the proposed method

Quality control standards	Accuracy (% Bias)		Precision (% RSD)	
	Intra-batch [a]	Inter-batch [b]	Intra-batch [a]	Inter-batch [b]
LLOQ	–2.34	–2.17	8.53	8.01
LQC	0.42	–0.19	3.55	3.76
MQC	3.42	3.45	4.19	3.49
HQC	0.87	1.43	3.29	3.59

[a] Each value represents the average of five independent determinations; [b] Each value represents the average of fifteen independent determinations (n = 5 on three occasions)

Consistent and high recovery observed at four QC levels was in agreement with the above findings. Results of accuracy and precision study were in acceptable limits and indicated that the method was accurate and precise (Table 3.15).

v) Sensitivity

Serum standards prepared at LLOQ showed quantifiable amount of IM, when analyzed in pentaplates on three different days (Fig. 3.6). Further, it confirmed that the method was precise and accurate at LLOQ with % RSD less than 8.53 and % Bias not exceeding −2.34. The method was found to be sensitive with a high signal-to-noise ratio at 285 nm detection wavelength. It can be suggested that the present method is suitable for various pharmacokinetic investigations in the rat, which demand high sensitivity.

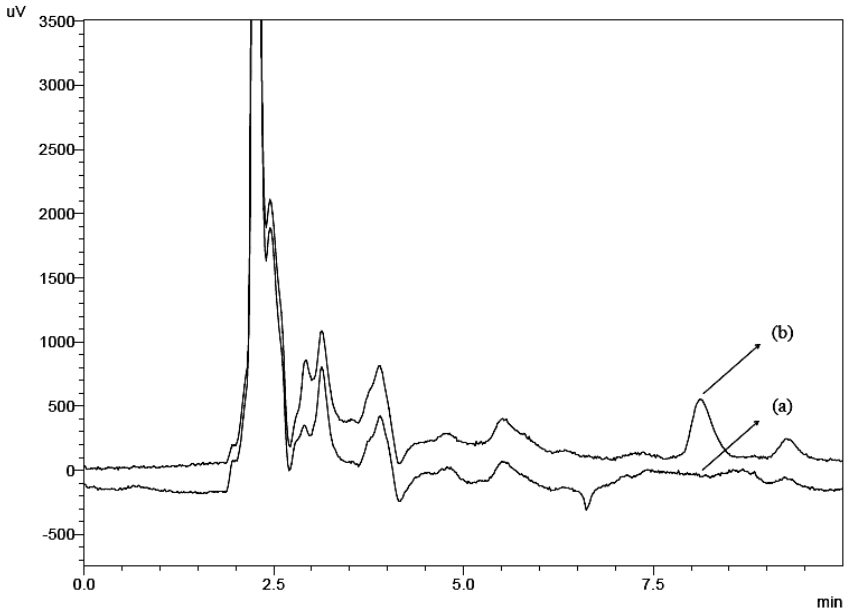

Fig. 3.6: Representative chromatograms of Imatinib mesylate in rat serum (a) blank and (b) spiked serum standards at LLOQ

vi) Stability studies

Results obtained for short term stability studies at all QC levels demonstrate that IM was stable in rat serum under bench top conditions. IM does not show significant change (% RSD < 5) in response up to 24 h at room temperature, when compared with the response obtained from fresh standards (Fig. 3.7a). Similarly, in long term stability study, IM was found to be stable in rat serum at −20°C for all QC levels, as there was no significant difference between the response of standards at zero time and during 90 days. The maximum deviation observed was within acceptable limits at all QC levels (Fig. 3.7b). In dry residue stability study, obtained results have indicated that IM was stable under post-extraction storage conditions up to 15 days at −20 °C (Fig. 3.7c).

There was no significant degradation detected in QC standards prepared at all four QC levels up to five freeze-thaw cycles. Results are expressed as accuracy in terms of % Bias,

which was below 10% at LLOQ and below 8% at other concentration levels and the deviation observed during five freeze thaw cycles was within acceptable limits (Fig. 3.7d). Thus, the drug was found to be stable for five freeze thaw cycles making it suitable for subzero storage conditions. Percent deviation calculated for all stability samples were well within the acceptance range of ± 20% at LLOQ and ± 15% at other concentration levels demonstrating the stability of IM under various processing and storage conditions stated in the method.

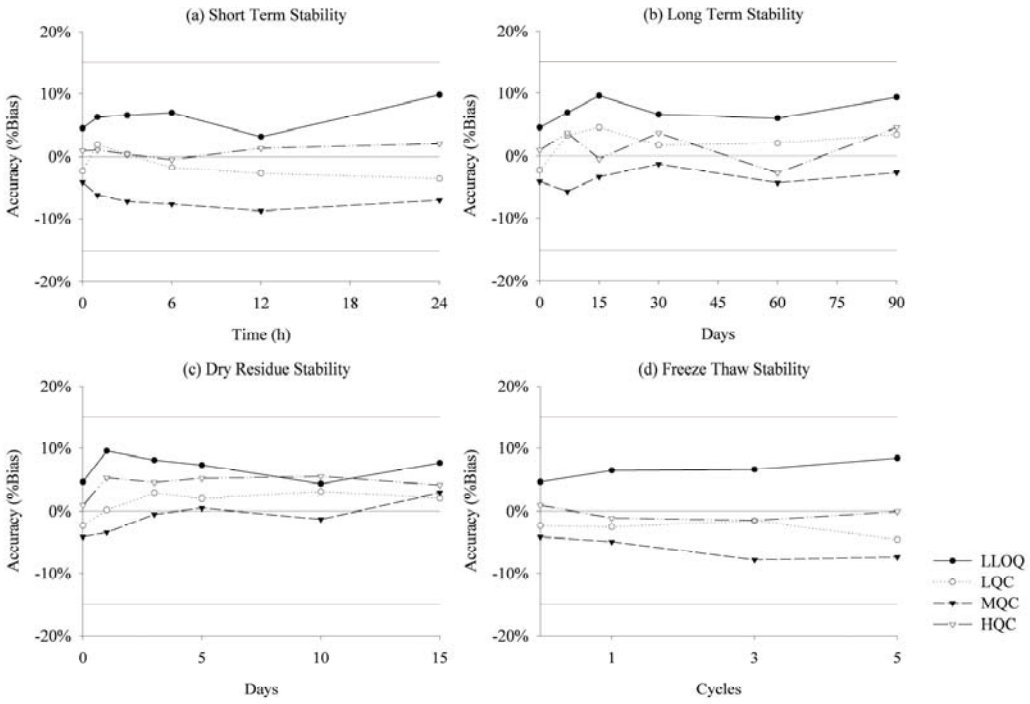

Fig. 3.7: Stability study of Imatinib mesylate in rat serum (a) short term stability, (b) long term stability, (c) dry residue stability and (d) freeze thaw stability

vii) Over-curve dilution integrity

The dilution integrity of the method was found to be acceptable with accuracy (% Bias) of −2.34, 3.18 and 0.61 for respective 5, 10 and 15 μg mL^{-1} concentration levels. Precision for 5, 10 and 15 times dilution was within acceptable limits with % RSD 4.55, 4.62 and 3.61, respectively. Thus, the results demonstrated that the method was suitable for over-curve dilution up to 15 times in the rat serum.

viii) Analysis of in vivo samples

The validated method was successfully applied to study pharmacokinetic disposition of IM in rats (Chapter 6).

3.6 Conclusions

A new, sensitive and selective UV-spectrophotometric method was successfully developed for the determination of IM from pharmaceutical formulations. Moreover, the simple composition of solvent medium and easy extraction procedure offered rapid and cost effective analysis of IM. The method demonstrated adequate accuracy and precision with high and consistent recoveries across the calibration range. Robustness studies confirmed that the method can be extended to various other applications as method performance remained unaffected by a significant change in the composition of solvent media. Further, it may be used for routine analysis of IM from bulk drug, pharmaceutical preparations and other quality control samples of the product development.

A new, sensitive and stability indicating chromatographic method was successfully developed for determination of IM. For the first time, orthogonal separation technique was successfully used to demonstrate selectivity in forced degradation study. A novel microwave assisted degradation technique was found to be fast, effective and accurate as compared to conventional refluxing method of forced degradation. A three-factor face-centered design demonstrated that the developed method has significant tolerance for any change in critical chromatographic factors. In addition, simple isocratic elution and easy extraction procedure offered rapid and cost effective analysis of IM. The method was found to be accurate and precise with high and consistent recoveries at all levels studied. Further, it has demonstrated high resolution from degradation products, impurities and formulation excipients. The validated method may be used for routine analysis of IM from bulk drug, pharmaceutical preparations and other quality control samples of the product development.

A new, simple and sensitive reversed-phase high performance liquid chromatographic method has been successfully developed and validated for determination of IM in rat serum, brain and lung tissue samples. Simple liquid-liquid extraction technique provided consistent and high recovery with selective determination of IM. The method was found to be accurate, precise and reproducible with good stability of IM under various processing and storage conditions. In addition, the method was successfully employed for in vivo pharmacokinetic investigations of pure drug. All the developed methods were used for different analytical and pharmacokinetic studies of the present research work.

References

1. J. Ermer. Validation in pharmaceutical analysis. Part I: an integrated approach. J Pharm Biomed Anal. 24:755-767 (2001).

2. J. Ermer and H.J. Ploss. Validation in pharmaceutical analysis. Part II: Central importance of precision to establish acceptance criteria and for verifying and improving the quality of analytical data. J Pharm Biomed Anal. 37:859-870 (2005).
3. J. Ermer, C. Arth, P. De Raeve, D. Dill, H.D. Friedel, H. Hower-Fritzen, G. Kleinschmidt, G. Koller, H. Koppel, M. Kramer, M. Maegerlein, U. Schepers, and H. Watzig. Precision from drug stability studies. Investigation of reliable repeatability and intermediate precision of HPLC assay procedures. J Pharm Biomed Anal. 38:653-663 (2005).
4. J. Wieling, G. Hendriks, W.J. Tamminga, J. Hempenius, C.K. Mensink, B. Oosterhuis, and J.H. Jonkman. Rational experimental design for bioanalytical methods validation. Illustration using an assay method for total captopril in plasma. J Chromatogr A. 730:381-394 (1996).
5. J. Ermer. The use of hyphenated LC-MS technique for characterisation of impurity profiles during drug development. J Pharm Biomed Anal. 18:707-714 (1998).
6. E. Rozet, A. Ceccato, C. Hubert, E. Ziemons, R. Oprean, S. Rudaz, B. Boulanger, and P. Hubert. Analysis of recent pharmaceutical regulatory documents on analytical method validation. J Chromatogr A. 1158:111-125 (2007).
7. M. Bakshi and S. Singh. Development of validated stability-indicating assay methods - critical review. Journal of Pharmaceutical and Biomedical Analysis. 28:1011-1040 (2002).
8. S. Braggio, R.J. Barnaby, P. Grossi, and M. Cugola. A strategy for validation of bioanalytical methods. J Pharm Biomed Anal. 14:375-388 (1996).
9. S. Bansal and A. DeStefano. Key elements of bioanalytical method validation for small molecules. AAPS J. 9:E109-114 (2007).
10. Food and Drug Administration. Guidance for industry: Bioanalytical method validation, United States Department of Health and Human Services, Maryland, USA, 2001.
11. International Union of Pure and Applied Chemistry. Harmonized Guidelines for single laboratory validation of methods of analysis, IUPAC, North Carolina, USA, 2002, pp. 835-855.
12. United States Pharmacopoeia. Validation of compendial procedures United States Pharmacopoeial Convention Inc., Maryland, USA, 2005.

13. International Conference on Harmonization. Technical requirements for registration of pharmaceuticals for human use, Harmonized tripartite guidelines - Validation of analytical procedures: Text and methodology, ICH Steering Committee, Geneva, Switzerland, 2005.
14. S. Chandran and R.S. Singh. Comparison of various international guidelines for analytical method validation. Pharmazie 62:4-14 (2007).
15. V.V. Vivekan and, D. Sreenivas Rao, G. Vaidyanathan, N.M. Sekhar, S. Avijit Kelkar, and P. Ramachandra Puranik. A validated LC method for imatinib mesylate. J Pharm Biomed Anal. 33:879-889 (2003).
16. D. Ivanovic, M. Medenica, B. Jancic, and A. Malenovic. Reversed-phase liquid chromatography analysis of imatinib mesylate and impurity product in Glivec capsules. J Chromatogr B Analyt Technol Biomed Life Sci. 800:253-258 (2004).
17. W.J. Szczepek, B. Kosmacinska, A. Bielejewska, W. Luniewski, M. Skarzynski, and D. Rozmarynowska. Identification of imatinib mesylate degradation products obtained under stress conditions. J Pharm Biomed Anal. 43:1682-1691 (2007).
18. T. Velpandian, R. Mathur, N.K. Agarwal, B. Arora, L. Kumar, and S.K. Gupta. Development and validation of a simple liquid chromatographic method with ultraviolet detection for the determination of imatinib in biological samples. J Chromatogr B Analyt Technol Biomed Life Sci. 804:431-434 (2004).
19. G. Guetens, H. Prenen, G. De Boeck, M. Highley, I. de Wever, A.T. van Oosterom, and E.A. de Bruijn. Imatinib (Gleevec, Glivec) tumour tissue analysis by measurement of sediment and by liquid chromatography tandem mass spectrometry. J Sep Sci. 29:453-459 (2006).
20. N. Widmer, A. Beguin, B. Rochat, T. Buclin, T. Kovacsovics, M.A. Duchosal, S. Leyvraz, A. Rosselet, J. Biollaz, and L.A. Decosterd. Determination of imatinib (Gleevec) in human plasma by solid-phase extraction-liquid chromatography-ultraviolet absorbance detection. J Chromatogr B Analyt Technol Biomed Life Sci. 803:285-292 (2004).
21. R.L. Oostendorp, J.H. Beijnen, J.H. Schellens, and O. Tellingen. Determination of imatinib mesylate and its main metabolite (CGP74588) in human plasma and murine specimens by ion-pairing reversed-phase high-performance liquid chromatography. Biomed Chromatogr. 21:747-754 (2007).

22. R. Bakhtiar, L. Khemani, M. Hayes, T. Bedman, and F. Tse. Quantification of the anti-leukemia drug STI571 (Gleevec) and its metabolite (CGP 74588) in monkey plasma using a semi-automated solid phase extraction procedure and liquid chromatography-tandem mass spectrometry. J Pharm Biomed Anal. 28:1183-1194 (2002).

23. R. Bakhtiar, J. Lohne, L. Ramos, L. Khemani, M. Hayes, and F. Tse. High-throughput quantification of the anti-leukemia drug STI571 (Gleevec) and its main metabolite (CGP 74588) in human plasma using liquid chromatography-tandem mass spectrometry. J Chromatogr B Analyt Technol Biomed Life Sci. 768:325-340 (2002).

24. G. Guetens, G. De Boeck, M. Highley, H. Dumez, A.T. Van Oosterom, and E.A. de Bruijn. Quantification of the anticancer agent STI-571 in erythrocytes and plasma by measurement of sediment technology and liquid chromatography-tandem mass spectrometry. J Chromatogr A. 1020:27-34 (2003).

25. R.A. Parise, R.K. Ramanathan, M.J. Hayes, and M.J. Egorin. Liquid chromatographic-mass spectrometric assay for quantitation of imatinib and its main metabolite (CGP 74588) in plasma. J Chromatogr B Analyt Technol Biomed Life Sci. 791:39-44 (2003).

26. K. Neville, R.A. Parise, P. Thompson, A. Aleksic, M.J. Egorin, F.M. Balis, L. McGuffey, C. McCully, S.L. Berg, and S.M. Blaney. Plasma and cerebrospinal fluid pharmacokinetics of imatinib after administration to nonhuman primates. Clin Cancer Res. 10:2525-2529 (2004).

27. Y. Tsutsumi, H. Kanamori, H. Yamato, N. Ehira, T. Miura, T. Kawamura, S. Obara, J. Tanaka, M. Asaka, M. Imamura, and N. Masauzi. Monitoring of plasma imatinib concentration for the effective treatment of CML patients. Leuk Res. 28:1117-1118 (2004).

28. K. Titier, S. Picard, D. Ducint, E. Teilhet, N. Moore, P. Berthaud, F.X. Mahon, and M. Molimard. Quantification of imatinib in human plasma by high-performance liquid chromatography-tandem mass spectrometry. Ther Drug Monit. 27:634-640 (2005).

29. J. Pellett, P. Lukulay, Y. Mao, W. Bowen, R. Reed, M. Ma, R.C. Munger, J.W. Dolan, L. Wrisley, K. Medwid, N.P. Toltl, C.C. Chan, M. Skibic, K. Biswas, K.A. Wells, and L.R. Snyder. "Orthogonal" separations for reversed-phase liquid chromatography. J Chromatogr A. 1101:122-135 (2006).

30. S. Bolton and C. Bon. Pharmaceutical statistics: Practical and clinical applications, Marcel Dekker, Inc., New York, 2004.
31. A. Olofson, K. Yakushijin, and D.A. Horne. Synthesis of Mauritiamine. J Org Chem. 62:7918-7919 (1997).
32. J.J. Kirkland, J.W. Henderson, J.J. DeStefano, M.A. van Straten, and H.A. Claessens. Stability of silica-based, endcapped columns with pH 7 and 11 mobile phases for reversed-phase high-performance liquid chromatography. J Chromatogr A. 762:97-112 (1997).
33. A. Pelander, I. Ojanpera, and T.A. Hase. Preparation of N-demethylated drug metabolites for analytical purpose using 1-chloroethyl chloroformate. Forensic Sci Int 85:193-198 (1997).

4. Preformulation Studies

4.1 Introduction

A successful formulation design takes into account the prior information of physical, chemical and biological properties of the drug to produce an effective, stable, safe and marketable product (1). Frequently, this prior information minimizes the efforts in the later stages of product design and development by reducing cost and time to market. Preformulation study is designed to investigate specific drug characteristics, which addresses the identity, purity and strength of the drug substances and quality of the drug products. Moreover, this exploratory activity, at the early stage of product development cycle, aid in establishing a correlation between the physicochemical properties of a drug substance and the biopharmaceutical parameters, such as the prediction of the in vivo product performance.

Although the Food and Drug Administration has not released any specific guidelines for nanotechnology based products, these pharmaceutical and analytical investigations were carried out as per standard product development guidelines. Typically, a standard pharmaceutical product development study includes comprehensive drug characterization such as determination of dissociation constant, partition coefficient, solubility, polymorphism and hydrates, powder properties, thermal behavior, molecular spectroscopic profile, drug-excipient compatibility, stability etc (2-5). However, considering the scope of nanoparticulate formulations, methods were selected to investigate product specific questions, which offer a rational basis for nanotechnology based product design and the developmental strategies (6).

Although IM is widely used in several research investigations and clinical applications, the information about its physicochemical properties is scarce in literature. An extensive literature search did not reveal important properties of the drug. Thus, broad goal of the study was to evaluate physicochemical properties, determine the drug-excipient compatibility, investigate the drug stability and characterize drug substance in a manner that would regulate the subsequent developmental events.

4.2 Experimental

4.2.1 Materials

Poly (lactic-*co*-glycolic acid) (PLGA 50/50, MW 10,000), Poloxamer 188 (Pluronic® F-68, MW 8400), Poly vinyl alcohol (PVA, MW 13,000-23,000, 98% hydrolyzed) and Poly (ε-caprolactone) (PCL, MW 40,000) were purchased from Sigma Aldrich Chemicals. Sodium chloride, anhydrous sodium phosphate dibasic and anhydrous potassium

dihydrogen phosphate, glycine, polyethylene glycol (PEG, MW 300 & 400) and all other chemicals and reagents used were of analytical grade.

4.2.2 Instruments and equipments

A digital pH meter (pH Tutor, Eutech Instruments, Singapore) equipped with glass electrode and automatic thermal compensation probe; digital analytical balance (AG135, Mettler Toledo, Switzerland) with sensitivity ± 0.01 mg; water bath shaker (MSW-275, Macro Scientific Works, India) with a temperature control ± 0.05°C; humidity and temperature control cabinet (MSW-125, Macro Scientific Works, India); refrigerator (Frost-free 200L, Godrej, India); rotary flask shaker (REMI Instruments, India); ultrasonicator (1201, Systronics Instruments, India); vortex mixer (Spinix, India) were used for analysis. While, all other analytical instruments were of standard grade and used after calibration.

4.2.3 Methods

Frequently, wide ranges of analytical methods are required to perform the preformulation studies. For present study, analysis of drug was carried out using either the reversed phase liquid chromatographic method or the UV-spectroscopic method as described in Chapter 3.

A Fourier transform infrared spectrophotometer model IRPrestige-21 (Shimadzu, Japan) equipped with a diffuse reflectance attachment was used to record infrared absorption spectrum of all samples. The individual samples were suitably mixed with moisture-free spectral grade potassium bromide. The infrared absorption spectra were recorded in a range of 400 to 4000 cm^{-1} with a resolution of 4 cm^{-1} using a high-energy ceramic source, CsI beam splitter and DLATGS detector. The diffuse reflectance FTIR spectra were acquired using a Labsolutions® workstation (CreonLab Control, Japan) and the data was transformed using Kubelka-Munk conversion before interpretations.

Thermal analysis was carried out using a previously calibrated differential scanning calorimeter - DSC-60 (Shimadzu, Japan) with TA-60WS thermal analyzer. For each measurement, 5 ± 2 mg of individual sample was loaded into aluminium pan and covered by crimping the lid. Considering the melting point of individual component, each sample was suitably scanned between 25 to 300°C at 5°C min^{-1} heating rate. Inert environment was ensured by purging nitrogen gas at 30 mL min^{-1} flow rate. The thermograms were acquired using a TA-60WS workstation (Shimadzu, Japan) and the melting temperatures (T_m) were recorded.

For statistical analysis, the concentrations of IM in the stability samples were plotted as a function of time. The order and reaction rate constants were determined after modeling the obtained data using a linear and non-linear regression analysis using the statistical package S-Plus® (Insightful Corporations, USA).

4.2.4 Bulk characterization

Imatinib is not listed in pharmacopoeia or official compendia of any country. Few in-house tests were performed to establish identification and characterization of Imatinib mesylate.

a) Assay and purity

For assay and percent purity purpose, in-house UV-spectroscopic and stability indicating liquid chromatographic methods were developed and validated as described earlier.

b) pH

Aqueous solution of IM (1% *v/v*) was prepared fresh and pH was recorded at 25°C.

c) Spectral analysis

i) Ultra-violet visible absorption spectrum

Aqueous solution of IM (10 μg mL^{-1}) was prepared fresh and UV-Visible spectrum was recorded as described earlier.

ii) Fourier-transform infrared absorption spectrum

Pure drug FTIR absorption spectrum was recorded using diffuse reflectance spectroscopy as described previously.

d) Thermal analysis

Thermal analysis of pure drug was studied using a previously calibrated differential scanning calorimeter as described earlier.

4.2.5 Physical form

In the present study, physical form of the drug was determined using thermal behavior and spectral absorption study. The thermal properties of the drug were studied using differential scanning calorimetry and the integrity of the functional groups was confirmed using the infrared absorption spectroscopy. Pure drug was subjected to recrystallization from selected solvents and obtained crystalline forms were analysed for physical and chemical integrity. In addition, samples were also given heat treatment to investigate possible alterations in the crystalline form of drug. In a separate study, the samples were also subjected to multiple heating cycles (25°C → first heating cycle → 300°C → cooling cycle → 25°C → second heating cycle → 300°C) and changes in thermal properties of samples were recorded.

4.2.6 Solubility analysis

In the present work, the solubility study of IM was carried out in selected aqueous and non-aqueous solvents using the shake-flask method. Selection of various non-aqueous solvents was according to product development needs, while the pH range selected for aqueous solubility analysis was in accordance with the in vivo physiological conditions. Initially, saturation solubility of IM was determined in buffered and unbuffered media at selected pH conditions. In addition, solubility analysis was also carried out in some selected aqueous and non aqueous media such as n-hexane, ethyl acetate, acetone, diethyl ether, dimethyl formamide, acetonitrile, dimethyl sulfoxide, n-octanol, methylene chloride, chloroform, isopropyl alcohol, poly ethylene glycol (300 & 400), methanol, simulated intestinal fluid and simulated gastric fluid.

For pH-solubility profile, unbuffered solutions were prepared by adjusting pH of pure water using hydrochloric acid or sodium hydroxide solutions and the ionic strength was adjusted using sodium chloride solution (0.5% *w/v*). While, buffered solutions of same ionic strength with pH range between 1 and 12 were prepared by mixing two solutions and the extreme pH conditions were adjusted by using hydrochloric acid or sodium hydroxide solutions (7).

In the shake-flask method, an excess of the drug was added to 5 mL of each solvent measured into glass flasks and the mixture was vortex-mixed for 5 min. Samples were agitated in a water bath shaker maintained at 37 ± 2°C for 24 h. Previously, a pilot study with small scale (1 mL) was carried out to study the equilibration time at low, medium and high pH conditions. At each time point, samples were withdrawn, filtered (Whatman® No. 40) and diluted at isothermal conditions to ensure they were free from particulate matter before analysis. Processed samples were suitably diluted with mobile phase and analysed by liquid chromatographic method. All solubility experiments were performed in triplicate and the average solubility of IM in various solvents is presented.

4.2.7 Dissociation constants

For determination of the acid dissociation constant, a primary stock solution of 1000 µg mL^{-1} was prepared by dissolving 100 mg of IM in 100 mL of pure water. Different pH media were prepared fresh and ionic strength was adjusted to 0.3 M using sodium chloride. Immediately after pH adjustment, 100 µL of stock solution was transferred to 10 mL standard volumetric flask to prepare 10 µg mL^{-1} of the drug in different pH media. Each sample was prepared in triplicate and the spectrum was recorded independently at 25 ± 0.5°C. The absorbance values obtained at each wavelength were

plotted as a function of pH and the data was processed to identify a suitable wavelength, which demonstrates differential UV-Vis absorbance with significant effect of ionization. First derivative of absorbance respective to pH (ΔAbsorbance/ΔpH) was plotted against media pH and the pKa was determined (8).

4.2.8 Partition coefficient

For lipophilicity analysis, the partition coefficient of IM was determined by shake flask method using the n-octanol-water and chloroform-water systems with a modification of the reported procedure (40-CFR-799, 2005) (9). All the phases were pre-saturated with the other solvent for at least 24 h, prior to start of the experiment and saturated phases were separated by centrifugation (1000 rpm, 2 min & 25°C). In separate glass vials, 10 mL of water-saturated organic phase was transferred and mixed with equal proportion of pure water, pre-saturated with respective organic solvent. After the drug addition, prepared solvent mixtures were placed on rotary flask shaker and maintained at controlled temperature (25 ± 0.5°C) for 12 h. In a separate study, it was established that the 12 h time period was sufficient for attaining complete equilibrium in all cases. On completion of 12 h, samples were centrifuged (1000 rpm, 10 min & 25°C) to separate aqueous layer and IM concentration was determined by HPLC method. The partition coefficient of IM was calculated using following formula.

$$P_{o/w} = C_{[n\text{-octanol}]} / C_{[water]}$$

Where, $C_{[n\text{-octanol}]}$ and $C_{[water]}$ are the concentration of the IM in n-octanol and pure water, respectively.

Similarly, the pH partition coefficient ($D_{o/w}$) was determined in the n-octanol-water ($pH_{1\text{-}12}$) systems. Before starting the experiment, all the pH solutions were pre-saturated with n-octanol for at least 24 h and saturated phases were separated by centrifugation (1000 rpm, 2 min & 25°C). In separate glass vials, 10 mL of each pre-saturated pH solution was transferred and mixed with equal proportion of n-octanol, pre-saturated with respective pH solution. The prepared solvent mixture was placed on rotary flask shaker and maintained at controlled temperature (25 ± 0.5°C) for 12 h. On completion of 12 h, samples were processed as mentioned above. All the experiments were carried out in triplicate and results are expressed as log $P_{o/w}$ and log $D_{o/w,\ pH}$ by taking logarithm of the partition coefficient and distribution coefficient at individual pH, respectively.

4.2.9 Stability analysis

In order to investigate the integrity of drug molecule under various pH conditions during the product manufacturing and in vivo biological environment, the stability studies were performed in liquid and solid state.

a) Liquid state stability

Liquid state stability of IM was studied in a various un-buffered and buffered pH solutions. For this purpose, a stock solution of IM prepared in pure water was spiked in various buffered and un-buffered solutions at pH 0.5, 1, 1.2, 3, 5, 6.2, 6.8, 7, 7.4, 9, 11 and 13 to get a final concentration of 10 $\mu g\ mL^{-1}$ in the respective media. In addition, two sets of liquid state samples prepared in pure water were subjected to thermal stress (90 ± 5°C) and oxidative stress (H_2O_2 solution) conditions.

The prepared solutions were stored at 25 ± 2°C in 20 mL glass vials on a temperature controlled water bath shaker with sufficient flux. At predetermined time intervals (0, 2, 4, 6, 12 & 24 h and 2, 4, 8, 15, 30, 45 & 60 days), the samples were withdrawn and analysed for the drug content using HPLC method. The amount of the drug remaining in solution was plotted as a function of time. The order of degradation kinetics and the rate constants were determined for respective buffered and un-buffered solutions.

b) Solid state stability

For solid state thermal- and photo-stability studies, IM was subjected to various thermal conditions with humidity and photo-stress conditions, separately. The pure drug was stored in a clear glass vial and maintained at ambient (RT: 25 ± 2°C, 60 ± 5% RH) and accelerated (AT: 40 ± 2°C, 75 ± 5% RH) conditions, while the control was kept at a refrigerated (FT: 5 ± 3°C) condition. At predetermined time intervals (0, 0.5, 1, 1.5, 2, 3, 4.5 & 6 months for AT; two additional 9 & 12 months for RT; and two additional at 18 & 24 months for FT) samples were withdrawn and analysed. In a separate study, one set of vials was kept at dry thermal conditions (90 ± 2°C, dry conditions) and samples were withdrawn at 0, 0.5, 1, 2, 3, 6, 9, 12, 18 and 24 h and analyzed for the drug content. The amount of the drug remaining was plotted as a function of time. The order of degradation kinetics and the rate constants were determined. In addition, all the stability samples were also analysed for physical (DSC) and chemical (HPLC & FTIR) integrity on completion of stability period (6-12 months).

4.2.10 Drug-excipients compatibility study

Solid state interactions between drug and various excipients were studied by subjecting physical admixtures of drug and individual excipient to different stress conditions. The prepared mixtures were studied for physical observation (color, odor & physical state), drug content (assay, degradation products), thermal analysis (DSC) and spectroscopic analysis (FTIR) etc.

The drug and excipient were weighed accurately and mixed pharmaceutically (1:10 proportion) by sieving (mesh #80) and blending process. The prepared admixtures were transferred to a set of glass vials and each vial was kept at a refrigerated (FT: 5 ± 3°C), ambient (RT: 25 ± 2°C, 60 ± 5% RH) or accelerated (AT: 40 ± 2°C, 75 ± 5% RH) conditions. The pure drug stability data obtained at each condition was used as a control. At predetermined time interval, samples were withdrawn in triplicate and physical observations, drug content and impurity analysis were performed. The drug content results were plotted as a function of time and the data was fitted to determine the order of reaction. The degradation kinetics of IM was studied and degradation rate constants were expressed as $T_{90\%}$, which signifies the time duration required to retain 90% of the drug potency, in presence of individual excipient at respective stress condition. At the end of stability period (12 months), thermal and spectroscopic analysis was performed to investigate possible physical and chemical interactions.

4.3 Results and Discussion

4.3.1 Bulk characterization

a) Assay and purity

The studied sample showed that IM was 99.95% pure.

b) pH

Aqueous solution of IM (1% *w/v*) showed pH of 5.5 at 25°C.

c) Spectral analysis

i) Ultra-violet visible absorption spectrum

IM showed maximum absorption at 256 nm for a concentration of 10 μg mL^{-1} in triple distilled water.

ii) Fourier-transform infrared absorption spectrum

The infrared absorption spectrum of the pure drug showed characterisitic IR bands, which were in aggreement with the reported data (10). In brief, a broad shaped singlet at $3258_{(m)}$ cm^{-1} was attributed to N-H stretching vibrations. A sharp peak at $1656_{(s)}$ cm^{-1} was

identified as C=O stretching vibrations of amide linkage. A strong signal at 1557 cm^{-1} was assigned for N-H deformations of a secondary acyclic amide. A prominent peak at $1417_{(s)}$ cm^{-1} was attributed to C=N stretching vibrations of aromatic rings (pyridine and pyrimidine).

d) Thermal analysis

The DSC thermograms of the pure drug demonstrated a single sharp endothermic peak onset (T_s) at 212°C for β-polymorphic form and the average melting temperature (T_m) was found to be 217°C (Fig. 4.1).

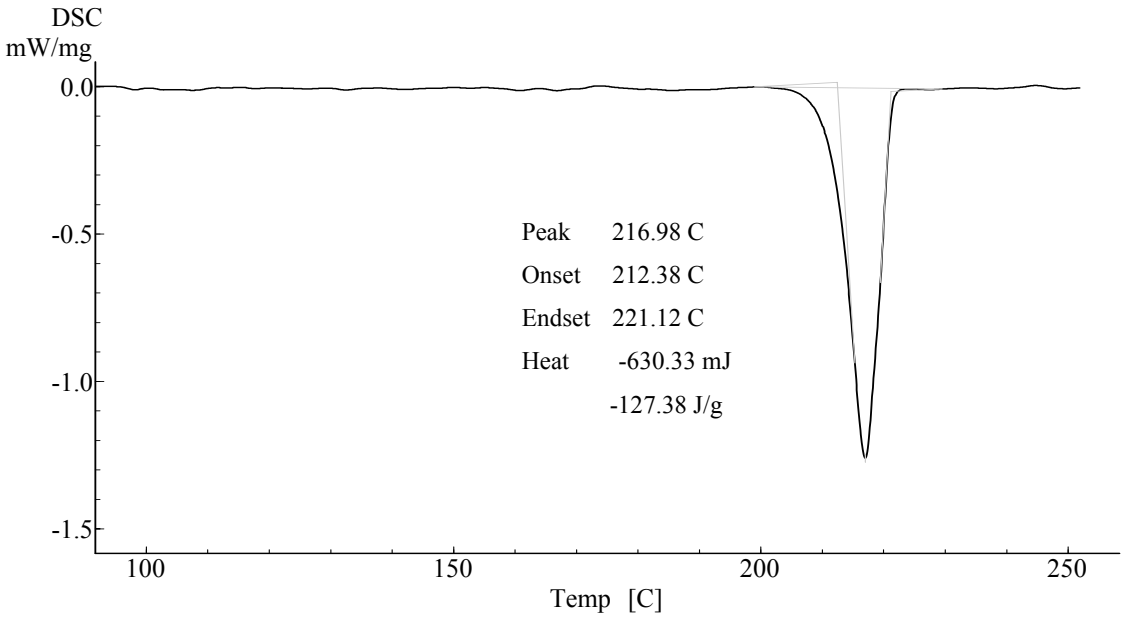

Fig. 4.1: Thermograms of pure Imatinib mesylate (β-polymorph)

Interpretation of thermograms provided melting enthalpy (ΔH) of –127 J g^{-1} and the drug was found to decompose at its melting point. The repeated measurement of same sample did not record any endothermic event between 210-225°C indicating complete decomposition of the drug.

4.3.2 Physical form

The infrared absorption spectrum of the drug was in agreement with the reported spectrum of β-polymorphic form (10). Moreover, these studies support the observations of thermal analysis and confirm the crystalline structure as a β-polymorphic form (Fig 4.1).

Previously, it has been reported that IM exists in two different anhydrous polymorphic forms, which are represented as α- and β-polymorphic form (10, 11). Both the polymorphic forms belong to the triclinic crystal system with P-1 space group but have

markedly different cell parameters. The α-polymorphic form has a lower melting enthalpy, which indicates an enantiotropic relationship between these polymorphic forms (12). Both the α- and β-polymorphic forms have been reported to be stable at room temperature with less than 2% change in the crystalline structure. Moreover, these polymorphic forms maintain the structural integrity even after subjecting to heat treatment (60-70°C, ≈ 12 h). However, prolonged heating (> 24 h) of either polymorphic form above 70°C may result in the partial conversions. One reported method suggests the inversion of polymorphic form (β to α) upon extreme heat treatment (175°C) for prolonged duration (> 12 h). However, several authors have reported that β-polymorphic form is extremely stable and may not be converted back into α-polymorphic form easily (13). It has also been reported that the α-polymorphic form is more hygroscopic in comparison with the β-polymorphic form with rapid adsorption of water at 25°C. Although both the polymorphic forms liquefy at 97% relative humidity, the α-polymorphic form showed high water adsorption rate with 0.18% water adsorption at 33% RH against 0.10% for β-polymorphic form (14). Lower hygroscopicity of the β-polymorphic form provides advantage of processability and stability in storage.

Thus, β-polymorphic form has been reported to demonstrate better pharmaceutical properties such as high flow properties, low hygroscopicity, relatively high solubility, stability etc. apart from its stability aspects over other polymorphs (15). Considering these facts, the β-polymorphic form was selected for design and development of nanoparticulate drug delivery systems. Moreover, β-polymorphic form has same biological activity as other polymorphs and is available commercial preparations in several countries.

4.3.3 Solubility analysis

The pH-solubility observations indicated that the aqueous solubility of IM is highly charge dependent (Fig. 4.2-4.4). In both un-buffered and buffered systems, a trend of decreasing solubility with increasing pH was observed. IM has shown higher solubility (756 ± 76.15 mg mL^{-1}) in acidic media (pH 1) and lower (0.04 ± 0.004 mg mL^{-1}) at alkaline media (pH 12), in buffered state (Fig. 4.2-4.3).

A decreasing relationship was observed between pH and solubility with relatively constant behavior at acidic side (pH 1-5) and alkaline side (pH 10-12). The aqueous solubility of Imatinib freebase prepared in-house was found to be very low (≈ 50 ng mL^{-1}, unbuffered, 25 ± 2°C).

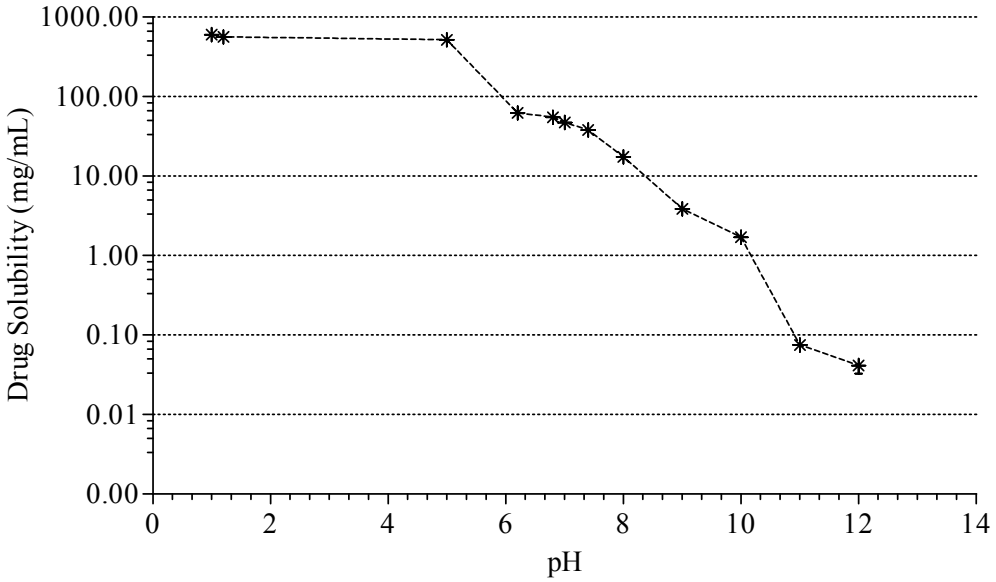

Fig. 4.2: pH solubility profile of Imatinib mesylate in unbuffered media

Similar finding were also observed in solvent solubility studies as the drug showed poor solubility in non-polar solvents such as n-hexane (0.02 µM), diethyl ether (0.55 M), chloroform (1.15 µM), ethyl acetate (0.05 µM) and methylene chloride (1.15 µM). However, a typical trend of increasing solubility with increasing polarity was observed among the selected non-polar solvents (Fig. 4.4). IM showed highest solubility in methylene chloride (ε = 9.1) and lowest in n-hexane (ε = 2).

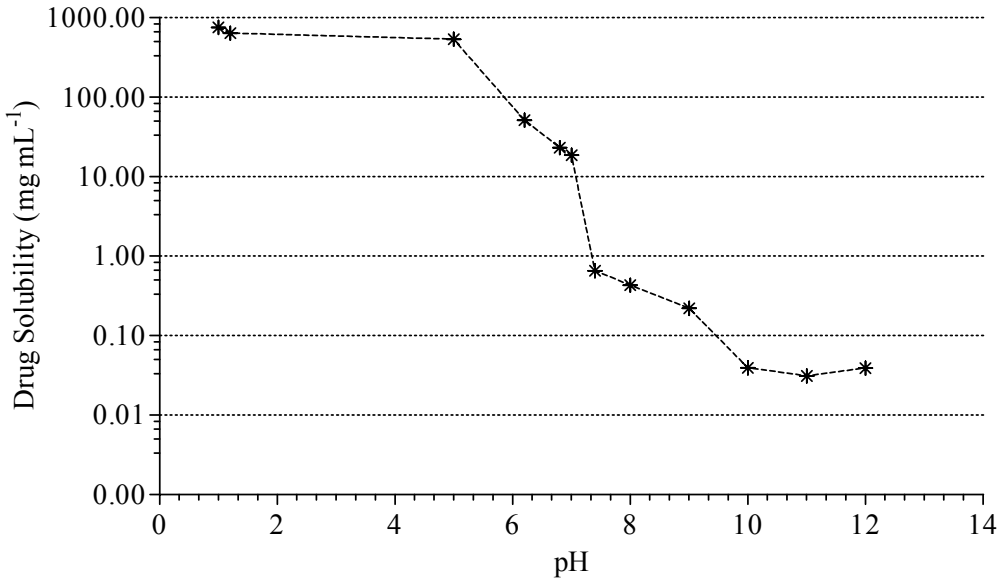

Fig. 4.3: pH solubility profile of Imatinib mesylate in buffered media

Frequently, a protic polar solvent such as methanol demonstrates specific interactions with the drug by acting mainly as a hydrogen donor in establishing hydrogen bonds, while, a nonpolar solvent such as n-hexane acts as an inert solvent and interacts with the drug molecules exclusively by nonspecific interactions such as dispersion forces. Thus, the comparative solubility profile in nonpolar, aprotic- and protic-polar solvents provided evaluation of solute-solvent interactions. Among the selected polar solvents, polar aprotic solvents showed poor drug solubility in comparison with the polar protic solvents (Fig 4.4). A similar trend of increasing solubility with increasing polarity was also observed in aprotic polar solvents such as acetone (0.17 μM), acetonitrile (0.66 μM), dimethyl formamide (0.59 μM), dimethyl sulfoxide (0.90 μM).

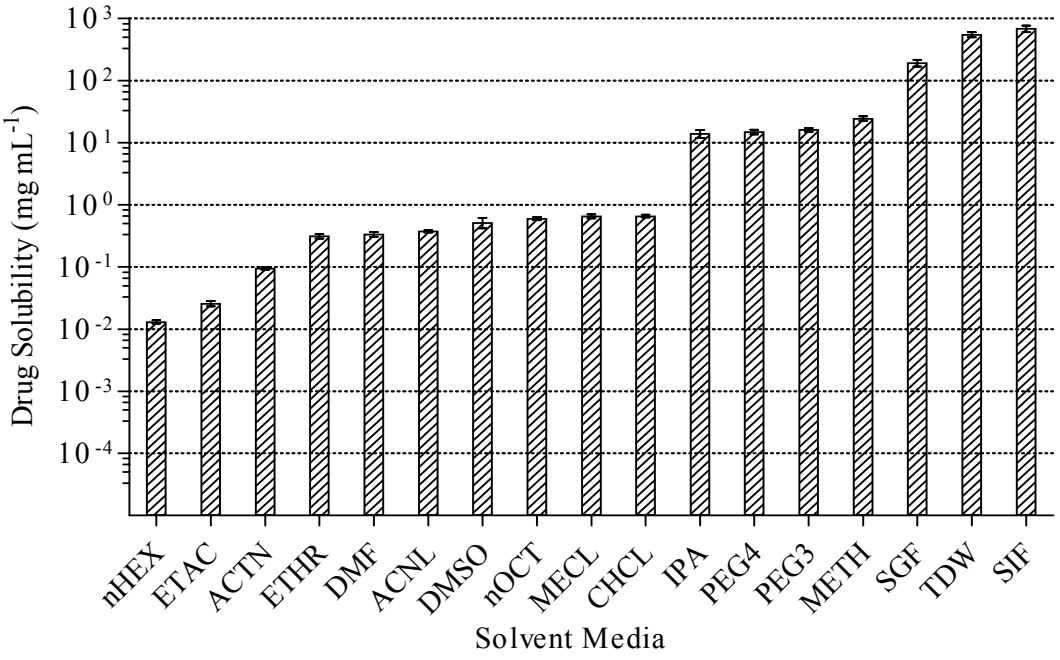

Fig. 4.4: Solubility profile of Imatinib mesylate in different solvents : TWD - triple distilled water, nHEX - n-Hexane, ETAC - Ethyl acetate, ETHR - Ether, DMF - Dimethyl formamide, ACNL - Acetonitrile, DMSO - Dimethyl sulfoxide, nOCT - n-Octanol, METH - Methylene chloride, CHCL - Chloroform, IPA - Isopropyl alcohol, PEG4 & PEG3 – Poly (ethylene glycol) 400 and 300, METH - Methanol and SGF and SIF - Simulated gastric and intestinal fluids.

Interestingly, one significant observation was the polar aprotic solvents like acetone have shown poor aqueous solubility despite high polarity (ε = 21) over the non-polar solvents e.g. diethyl ether with low polarity (ε = 4.3). Independent on polarity of organic solvents, IM showed a high solubility in all protic solvents over aprotic solvents indicating

significance of charge in the drug solubilization. Within the class of protic solvents, a linear increase in solubility was observed with increasing polarity e.g. isopropyl alcohol (24.54 μM), methanol (42.95 μM) and water (961.48 μM) was observed.

Considering these facts, it can be inferred that the pH, protic nature and polarity plays critical role in the solubilization process of the drug, Szakács et al have extensively studied the ionization behavior of IM and its selected fragments using the nuclear magnetic resonance technique (16). The authors have reported the log K protonation constants of Imatinib and proposed that the fraction of the mono-, di-, tri- and tetra-protonated forms of Imatinib increases with decreasing pH. Thus, it may be concluded that the increasing formation of different protonated species with decreasing pH conditions may have resulted in pH dependent solubility profile of IM. Moreover, the poor aqueous solubility of the freebase at room temperature confirmed that the uncharged molecules might be practically insoluble in water.

4.3.4 Dissociation constants

At a fixed concentration, the UV spectra acquired at different pH were analysed for maximal pH dependent change in the absorbance values. The mean absorbance value of three independent determinations at a selected wavelengths and its first derivative (ΔAbsorbance/ΔpH) were plotted as a function of pH of the medium. Peaks and/or valley in the first derivative method were considered as pKa. The results indicated four pKa vales each at pKa_1 (1.47 ± 0.23), pKa_2 (3.92 ± 0.37), pKa_3 (7.61 ± 0.28) and pKa_4 (9.25 ± 0.34). The UV-spectrophotometric method was found to be reliable and reproducible with low % RSD.

Previously, few authors have reported site-specific basicity profile of Imatinib quantified in terms of its protonation macroconstants, microconstants and group constants by NMR-pH and pH-potentiometric titrations (16). The authors have reported macroscopic protonation constants as 1.71 ± 0.02 (log K_1), 3.10 ± 0.01 (log K_2), 3.88 ± 0.03 (log K_3) and 7.7 ± 0.1 (log K_4) in pure water at 25°C [I = 0.15 M NaCl]. Although the obtained values of pKa were in agreement with the reported data, the slight discrepancy may have resulted from the limitation of UV-spectroscopic method in differentiating close values at pKa2 and pKa3 of 3.88 ± 0.03 and 3.1 ± 0.01, respectively. In addition, fourth pKa observed at 9.45 ± 0.34 in the present study was unexplored in the reported study.

$$L \overset{K_1}{\rightleftharpoons} HL^{+} \overset{K_2}{\rightleftharpoons} H_2L^{++} \overset{K_3}{\rightleftharpoons} H_3L^{+++} \overset{K_4}{\rightleftharpoons} H_4L^{+++}_{+}$$

Considering these protonation constants, the predicted population of ionized species at various biological pH can be as follows - 33% mono-cationic (HL^{+}) species in blood (pH 7.4) with single proton on piperazine site, 80% in mono-cationic (HL^{+}) species in duodenum (pH 6.8) with fraction of di-cationic (H_2L^{++}) species and 63% tri-cationic (H_3L^{+++}) species in stomach (pH 2) with abundance (≈ 33%) of fully protonated (H_4L^{++++}) species.

4.3.5 Partition coefficient

The partition or distribution coefficient was expressed as a ratio of the molar concentrations of a drug between the organic phase (e.g. n-octanol, chloroform etc.) and aqueous phase (pure water, buffered phase etc.), in dilute solution (< 0.01M) at a given temperature. These dimensionless constants are presented as the decadic logarithm – log P ($\log_{10} P_{o/w}$) and log D $_{pH}$ ($\log_{10} D_{o/w, pH}$).

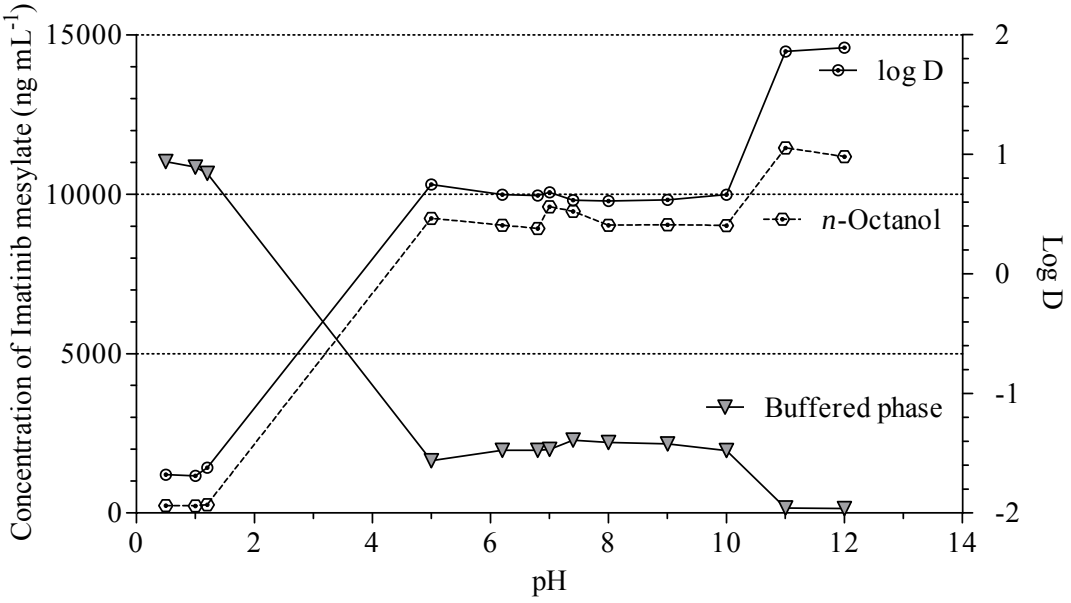

Fig. 4.5: n-octanol - buffered phase - distribution of Imatinib mesylate

In shake flask method, both the oil-water systems (chloroform-water and n-octanol-water) showed rapid partitioning of IM with equilibrium reaching within 6 h. Study was conducted at increasing concentrations of IM with 12 h equilibration time. The partition coefficients for chloroform-water system was found to be 2.02 ± 0.56 and for n-octanol-water system was 0.20 ± 0.16.

In order to ensure complete partitioning of unionized state of IM, an additional study was conducted after adjusting pH of aqueous phase to 12, which showed n-octanol-water

partition coefficient of 1.90 ± 0.34. The theoretical partition coefficient of IM calculated using ACD Labs was 2.48 ± 0.73 (ACD/Labs, USA). Relatively high solubility of IM in chloroform (0.66 mg mL^{-1}) as compared to n-octanol (0.62 mg mL^{-1}) would have resulted in increased partitioning of the drug. A sigmoidal relationship was observed between fraction distributed to oil phase and buffered phase over a pH range (Fig. 4.5). The charge dependent behavior of IM was observed in oil-water distribution studies. Moreover, these findings correlate well with the obtained solubility data. The fraction partitioned into oil phase decreased with increasing ionization at acidic pH.

4.3.6 Stability analysis

a) Liquid state stability

IM was found to be sensitive towards various pH conditions with similar degradation kinetics (Fig. 4.6). The decadic logarithm of the percent unchanged drug was plotted as a function of time and slope was used to determine the first order degradation rate constants (K_d) at the respective pH condition (Fig. 4.7). The obtained degradation data could be well described by the first order degradation kinetics with high correlation coefficient, low mean sum of squared residuals and low information criterion (AIC and BIC) values (Table 4.1). The shelf life was expressed as $T_{90\%}$ which indicates the period of storage of the drug without significant loss of the potency.

The first order degradation over the pH range indicated that IM is most sensitive to acidic environment with the first order degradation rate constant of 13.40 day^{-1} and $T_{90\%}$ of 0.79 days. Similarly, extreme basic conditions were found to be detrimental on the stability of the drug with the first order degradation rate constant of 1.74 day^{-1} and $T_{90\%}$ of 6.07 days. However, the degradation rate was found minimal at neutral conditions with the first order degradation rate constant of 0.40 day^{-1} and $T_{90\%}$ of 26.57 days.

The drug demonstrated good thermal stability at liquid state with the first order degradation rate constant of 10.01 day^{-1} and $T_{90\%}$ of 1.05 days, even at 90°C. Chromatographic results indicated no signs of oxidative degradation of IM in aqueous solution at various pH and temperature conditions as oxidative degradation products were not observed in respective chromatograms. However, IM showed highest sensitivity towards oxidative stress under forced degradation conditions with the first order degradation rate constant of 387.03 day^{-1} and $T_{90\%}$ of 0.03 days.

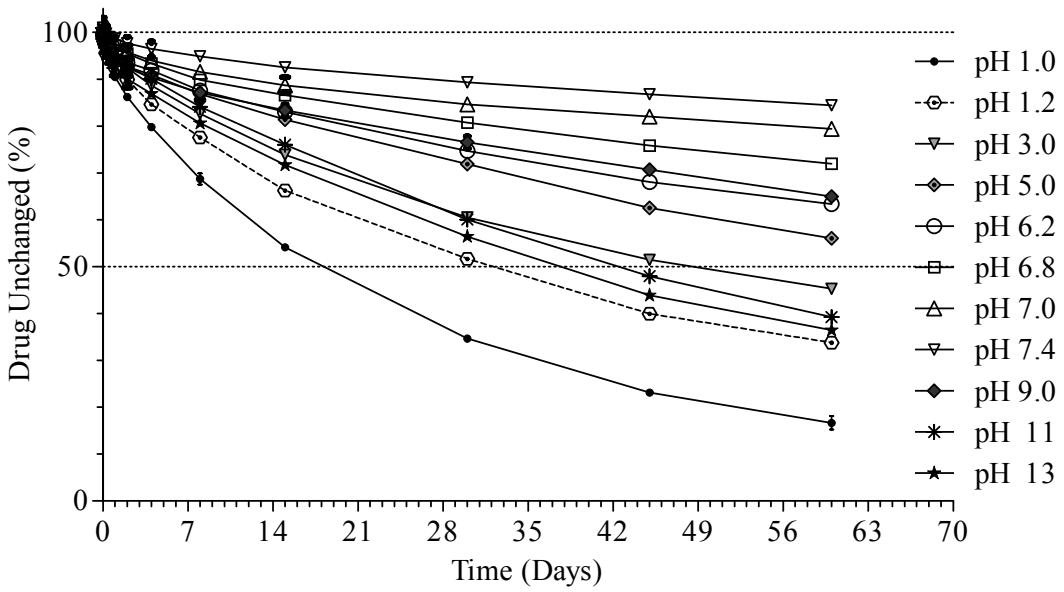

Fig. 4.6: pH stability profile of Imatinib mesylate in buffered media

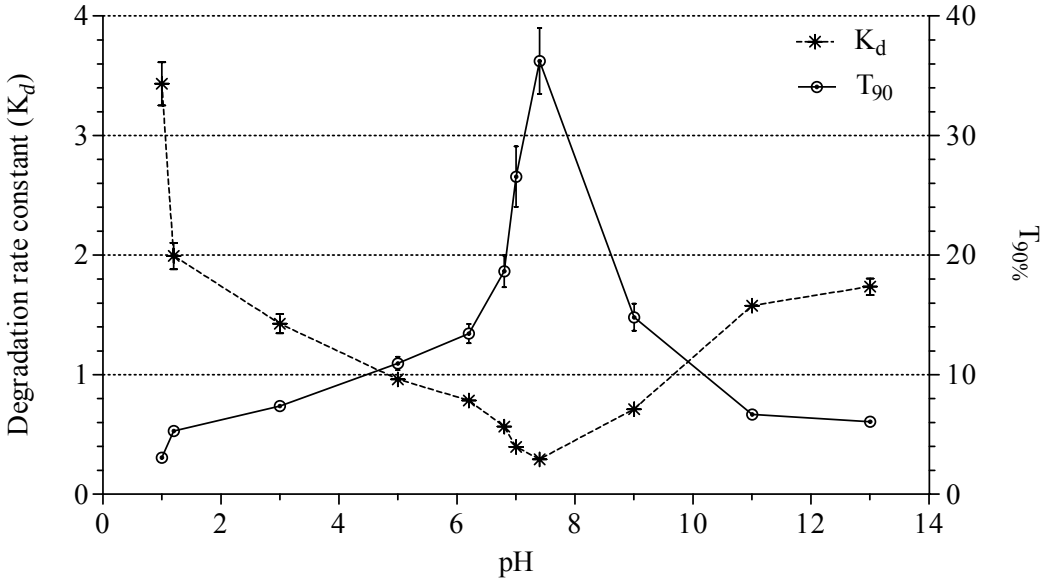

Fig. 4.7: Degradation rate constants versus pH profile of Imatinib mesylate in buffered media

The rapid degradation at acidic pH may be due to hydrogen ion catalysis of the fully charged (H_4L^{++++}) Imatinib species. Similarly, at alkaline conditions rate of degradation may have been accelerated by hydroxide ion catalysis of neutral (L) species of Imatinib (17). Although, during its transit through the gastrointestinal tract, IM would be exposed to

extreme acidic environment for 2 to 4 h, the fraction degrading during this exposure would be less significant (< 2%).

Table 4.1: pH, thermal and oxidation stability data of Imatinib mesylate in liquid state

Treatment	$K_d \times 10^2$ (day^{-1})	$T_{90\%}$ (days)	R^2	MSSR	AIC
pH - 0.5	13.40 ± 1.21	0.79 ± 0.07	0.9943	18.55	75.31
pH - 1.0	3.43 ± 0.18	3.07 ± 0.16	0.9952	8.61	65.34
pH - 1.2	1.99 ± 0.11	5.29 ± 0.30	0.9912	9.00	65.90
pH - 3.0	1.43 ± 0.08	7.39 ± 0.42	0.9891	7.42	63.40
pH - 5.0	0.96 ± 0.02	10.95 ± 0.56	0.9895	4.07	55.60
pH - 6.2	0.78 ± 0.04	13.44 ± 0.81	0.9845	4.36	56.50
pH - 6.8	0.57 ± 0.04	18.65 ± 1.34	0.9767	3.92	55.10
pH - 7.0	0.40 ± 0.03	26.57 ± 2.53	0.9579	3.92	55.10
pH - 7.4	0.29 ± 0.02	36.23 ± 2.75	0.9719	1.50	42.62
pH - 9.0	0.71 ± 0.05	14.81 ± 1.13	0.9747	6.11	60.88
pH - 11	1.58 ± 0.05	6.68 ± 0.20	0.9972	2.25	47.89
pH - 13	1.74 ± 0.07	6.07 ± 0.26	0.9944	4.86	57.89
Heat	10.0 ± 1.61	1.05 ± 0.17	0.9634	0.22	4.40
H_2O_2	387.0 ± 19.5	0.03 ± 0.001	0.9982	3.85	18.78

K_d - first order degradation rate constant; MSSR - mean sum of squared residuals; Heat - temperature (90 ± 5°C) treatment; H_2O_2 - hydrogen peroxide treatment .

Moreover, it can be suggested that IM need to be processed at neutral pH conditions in liquid state and prolonged exposure to extreme acidic and alkaline conditions (pH < 5 & pH < 9) may lead to significant degradation of the drug. Moreover, the drug was found to be sensitive for oxidizing agent with more than 90% degradation within 24 h.

b) Solid-state stability

Solid-state stability samples analysed by the liquid chromatographic method suggested that the drug is stable at freeze temperature and controlled room temperature with first order degradation rate constants of 0.79×10^{-3} $month^{-1}$ (HL 877.6 months) and 1.79×10^{-3} (HL 386 months) (Table 4.2). Moreover, FTIR studies revealed that there is no change in main infrared absorptions peaks even at the end of 12 months. In addition, the thermal analysis using DSC suggested that there is no evidence of change in polymorphs as there was no significant change in melting temperature (onset, peak & endset) and enthalpy (Table 4.3). Similarly, photo-stability samples did not show significant degradation

(< 2%, 1 month) suggesting that the drug is the photo-stable. Thus, solid-state stability studies for drug content (HPLC), chemical (FTIR) and physical (DSC) analysis confirmed that β-polymorphic form of IM is stable at thermal and photo-stress conditions.

Table 4.2: Thermal and photo stability data of Imatinib mesylate in solid state

Treatments	K_d ($\times 10^{-3}$ month^{-1})	$T_{90\%}$ (months)	R	MSSR	AIC
5 ± 3°C	0.79 ± 0.07	133.46 ± 11.65	0.9641	0.025	−10.47
25 ± 2°C	1.79 ± 0.02	58.74 ± 6.14	0.9592	0.039	−5.47
40 ± 2°C	2.84 ± 0.04	37.07 ± 4.68	0.9554	0.028	−7.75
90 ± 5°C	176.56 ± 57.6	0.59 ± 0.19	0.9307	0.032	−7.43
Photo	1.85 ± 0.04	57.11 ± 2.96	0.9432	0.035	−7.99

Drug-excipients compatibility study

The drug was found to follow first order degradation kinetics in the binary mixture, which was supported by high correlation coefficient and low information criterion (AIC & BIC) values (Table 4.3). IM showed good stability at controlled room temperature and accelerated temperature conditions with the highest first order degradation rate constant of 2.46×10^{-3} month^{-1} and 5.02×10^{-3} month^{-1}, respectively.

In thermal analysis, the sharp melting endothermic peak of the drug was found to be preserved in all binary mixtures, which suggested the physical compatibility of the drug with all studied excipients. All physical mixtures in stability showed same onset and endset temperature as that of pure drug with the melting peak at 217 ± 0.9°C, without any additional thermal events. In few cases, a broad endothermic peak approximately at 100°C was observed and it was attributed to residual moisture in sample. The melting enthalpy values were proportional to the amount of pure drug in the binary mixtures. Thus, the stability samples demonstrated that the binary mixtures have similar thermal properties as that of the initial samples (Table 4.3).

Further, these findings were supported by the infrared absorption spectrum as it confirmed the absence of possible chemical interactions between the drug and selected excipients. Thus, the drug-excipients compatibility study did not reveal any unfavorable chemical interactions between drug and various selected excipients. The drug was found to be stable in all physical mixtures at ambient and accelerated stress conditions. Thus, all binary mixtures analysed for drug content, chemical and physical integrity confirmed the stability of IM in presence of individual excipients at various stress conditions studied.

Table 4.3: Compatibility analysis of Imatinib mesylate with selected excipients

		Parameters	Drug-excipient compatibility studies					
			(IM)	(IM : PLGA)	(IM : PCL)	(IM : PECA)	(IM : PVA)	(IM : PF-68)
Degradation kinetics	Storage at 25 ± 2°C	$K_d \times 10^3$ (Month^{-1})	1.79 ± 0.19	2.32 ± 0.03	1.55 ± 0.14	1.785 ± 0.03	2.32 ± 0.24	2.46 ± 0.22
		$T_{90\%}$ (Months)	58.74 ± 6.15	45.44 ± 0.59	67.99 ± 5.98	59.045 ± 1.09	45.42 ± 4.72	42.81 ± 3.79
		R	0.9591	0.9934	0.9776	0.9987	0.9596	0.9702
		MSSR	0.039	0.009	0.033	0.012	0.064	0.051
		AIC	−5.47	−42.22	−23.31	−40.27	−0.54	−2.56
	Storage at 40 ± 2°C	$K_d \times 10^3$ (Month^{-1})	2.84 ± 0.36	4.33 ± 0.30	1.68 ± 0.05	2.49 ± 0.24	4.19 ± 0.32	5.02 ± 0.41
		$T_{90\%}$ (Months)	37.07 ± 4.68	24.37 ± 1.67	62.76 ± 2.01	42.28 ± 4.04	25.18 ± 1.92	21.01 ± 1.70
		R	0.9554	0.9863	0.9962	0.9737	0.9831	0.9811
		MSSR	0.028	0.015	0.032	0.010	0.018	0.028
		AIC	−7.75	-	−30.47	−14.41	−9.82	−6.08
Thermal analysis	Pure Component	Onset (°C)	212.4	-	60.5	183.3	208.0	48.8
		Peak (°C)	217.0	Tg, 43.1	64.6	196.9	221.9	53.6
		Endset (°C)	221.1	-	67.1	204.2	225.8	56.1
		Enthalpy (J g^{-1})	−127.4	-	-	−219.1	-	-
	Physical mixture	Onset	-	212.2	211.7	213.4	211.4	212.8
		Peak	-	216.6	218.2	216.3	217.7	218.6
		Endset	-	222.4	220.8	222.1	221.4	221.7
		Enthalpy (J g^{-1})	-	−132.9	−125.9	−128.7	−129.6	−128.8

Each value represents average of three independent measurements: $T_{90\%} = 0.10538 / K_d$; R - Correlation coefficient; IM - Imatinib mesylate; PLGA - Poly (lactic-*co*-glycolic acid); PCL - Poly (ε-caprolactone); PECA - Poly (ethyl cyanoacrylate); PVA - Polyvinyl alcohol; PF-68 - Poloxamer 188.

4.4 Conclusions

IM showed a pH dependent solubility profile with high solubility in acidic environment and low solubility in alkaline environment. Similarly, the drug showed high solubility in protic organic solvents in comparison with aprotic organic solvents. However, the drug was found to be poorly soluble in non-polar organic solvents.

The lipophilicity analysis indicated that unionized drug is well partitioned in oil phase, however, ionization of drug molecules significantly affects the fraction distributed to oil phase. This is evident with the sigmoidal nature of pH-partition curve with poor partitioning towards the acidic side. Considering the protonation constants of IM it can be stated that the drug would show high permeability at intestinal pH with significant unionized species. However, fully protonated species at gastric pH may limit the absorption of IM in stomach.

Liquid state stability studies revealed that the drug follows first order degradation kinetics. Stability studies indicated that IM is sensitive for acidic and alkaline environment as the degradation constants were found to be high at extreme pH conditions. However, drug was found to be most stable at 7.4 pH in buffered phase. Solid-state stability studies confirmed that the drug is stable at refrigerated and ambient temperature. Moreover, the photo-stability studies indicated that the drug could be processed without strict photo-protection.

The drug-excipient compatibility studies indicated that IM is stable in presence of various excipients at ambient and accelerated storage conditions. In addition, there were no polymorphic transformations observed during the study. Thus, drug-excipient compatibility studies would support the rationale for selection of various excipients and justify the product life span.

Although poor aqueous solubility of drug has been known to cause bioavailability related problems, frequently these challenges may simply be overcome by conventional formulation development approaches such as preparations with co-solvents, polymers and cyclodextrins, solid dispersions etc. (18, 19). Conversely, non-solubility related pharmacokinetic challenges need to be addressed specifically after detailed in vivo investigations. Considering the solubility data of IM, it can be predicted that the drug solubilization processes would not be a rate limiting state in the intestinal absorption of IM, upon oral dosing. Thus, the possibility of poor absorption and subsequent therapeutic failure due to poor solubility may be excluded and the drug related problems may be attributed to pharmacokinetics of the drug. These pharmacokinetic challenges may be

overcome by delivering the drug in nanoparticulate drug delivery systems. Thus, preformulation data provided the strategic input to formulation design and optimization.

References

1. J.T. Carstensen. Pharmaceutical Preformulation, Technomic Publishing Company, Inc., Lancaster, USA, 1998.
2. W.N. Charman, C.J.H. Porter, S. Mithani, and J.B. Dressman. Physicochemical and physiological mechanisms for the effects of food on drug absorption: The role of lipids and pH. Journal of Pharmaceutical Sciences. 86:269-282 (1997).
3. D.R. Flanagan, J.L. Lach, and L.E. Matheson. Preformulation and Formulation Investigational Drugs, University of Iowa College of Pharmacy, 1990.
4. P.C. Mora, M. Cirri, and P. Mura. Differential scanning calorimetry as a screening technique in compatibility studies of DHEA extended release formulations. J Pharm Biomed Anal. 42:3-10 (2006).
5. P.J. Sinko. Martin's Physical Pharmacy and Pharmaceutical Sciences: Physical Chemical and Biopharmaceutical Principles in the Pharmaceutical Sciences, Lippincott Williams & Wilkins, Philadelphia, 2006.
6. R.H. Müller, C. Jacobs, and O. Kayser. Nanosuspensions as particulate drug formulations in therapy Rationale for development and what we can expect for the future. Advanced Drug Delivery Reviews. 47:3-19 (2001).
7. P. Kole. Studies on some novel approaches for enhancement of solubility and bioavailability of rifapentine, a newer anti-tubercular drug, *Birla Institute Technology and Science, Pilani*, Vol. Ph. D. Thesis, Rajasthan, 2006, pp. 1-242.
8. S. Pinsuwan, F.A. Alvarez-Nunez, S.E. Tabibi, and S.H. Yalkowsky. Spectrophotometric determination of acidity constants of 4-dedimethylamino sancycline (Col-3), a new antitumor drug. J Pharm Sci. 88:535-537 (1999).
9. Federal Register. 40 CFR Part 799 - Partition coefficient (n-octanol/water), generator column method. National Archives and Records Administration, USA (2005).
10. W. Szczepek, D. Samson-lazinska, B. Zagrodzki, M. Glice, W. Maruszak, K. Korczak, R. Modzelewski, M. Lawecka, L. Kaczmarek, W. Szelejewski, U. Fraczek, and P. Cmoch. Crystalline polymorphs of methanesulfonic acid addition salts of Imatinib. In United States Patent and Trademark Office (ed.), Instytut Farmaceutyczny, Poland, United States, 2007.

11. A.k. Kompella, B.R. Adibhatla Kali Satya, K. Podili, and N. Venkaiah Chowdary. Polymorphs of Imatinib mesylate. In World Intellectual Property Organization (ed.), Natco Pharma Limited, India, Switzerland, 2006.
12. J. Zimmermann, B. Sutter, and H.M. Burger. Crystal modification of a N-phenyl-2-pyrimidineamine derivative, processes for its manufacture and its use. In World Intellectual Property Organization (ed.), Novartis AG, Switzerland, Switzerland, 1999.
13. W. Szczepek, D. Samson-lazinska, B. Zagrodzki, M. Glice, W. Maruszak, K. Korczak, R. Modzelewski, M. Lawecka, L. Kaczmarek, W. Szelejewski, U. Fraczek, and P. Cmoch. Crystalline methanesulfonic acid addition salts of Imatinib. In World Intellectual Property Organization (ed.), Instytut Farmaceutyczny, Poland, Switzerland, 2005.
14. S.L. Pathi, R. Puppala, R.N. Kankan, and D.R. Rao. Stable crystal form of Imatinib mesylate and process for the preparation there of In World Intellectual Property Organization (ed.), Cipla Limited, India, Switzerland, 2006.
15. M. Vasanthavada, J.P. Lakshman, W.Q. Tong, and A. Serajuddin. Pharmaceutical compositions comprising Imatinib and a release retardant. In World Intellectual Property Organization (ed.), Novartis AG, Switzerland, Switzerland, 2006.
16. Z. Szakacs, S. Beni, Z. Varga, L. Orfi, G. Keri, and B. Noszal. Acid-base profiling of imatinib (gleevec) and its fragments. J Med Chem. 48:249-255 (2005).
17. J.C. Waterval, J.C. Bloks, R.W. Sparidans, J.H. Beijnen, I.M. Rodriguez-Campos, A. Bult, H. Lingeman, and W.J. Underberg. Degradation kinetics of aplidine, a new marine antitumoural cyclic peptide, in aqueous solution. J Chromatogr B Biomed Sci Appl. 754:161-168 (2001).
18. T. Kristmundsdottir, E. Jonsdottir, H.M. Ogmundsdottir, and K. Ingolfsdottir. Solubilization of poorly soluble lichen metabolites for biological testing on cell lines. Eur J Pharm Sci. 24:539-543 (2005).
19. A. Hazekampand R. Verpoorte. Structure elucidation of the tetrahydrocannabinol complex with randomly methylated beta-cyclodextrin. Eur J Pharm Sci. 29:340-347 (2006).

5. Formulation Design and Development

5.1 Introduction

The diverse properties of nanoparticulate drug delivery systems such as selective biodistribution, in vitro and in vivo drug stability, intracellular trafficking, controlled drug release, etc. aid in meeting the challenges associated with the drug delivery applications. However, the preparation of nanoparticulate drug delivery system is challenging with influence of several formulation parameters such as nature and proportion of drug, polymers, stabilizers etc. and processing variables such as phase volume ratio, phase pH, mixing time and intensity, evaporation rate etc. on the performance of the drug delivery system (1-7). The formulation parameters and process variables affect the various characteristics and properties of the nanoparticulate formulations and ultimately govern the therapeutic performance of the product.

Different nanoparticulate delivery systems for IM have been proposed using biodegradable and biocompatible polymers such as poly (lactide-*co*-glycolic acid) [PLGA] and poly (ε-caprolactone) [PCL] and poly (ethyl cyanoacrylate) [PECA] (8). The study was carried out for the selection and optimization of suitable method by identifying critical variables. The desired product characteristics such as - low average particle size, narrow particle size distribution, high drug loading and entrapment efficiency, controlled release characteristics with selective biodistribution were aimed.

5.2 Experimental

5.2.1 Materials

Imatinib mesylate was received as a gift sample from Cipla (Mumbai, India). Poly (lactic-*co*-glycolic acid) [PLGA] copolymer with a molecular weight of 10,000 and a *d,l*-lactide to glycolide ratio of 52:48; Poly (ε-aprolactone) [PCL] with a molecular weight of 40,000; Ethyl-2-cyanoacryalte [ECA] monomers were used of Sigma Aldrich Chemicals, USA. Stabilizers such as polyvinyl alcohol [PVA] with a molecular weight of 13,000-23,000 [98% hydrolyzed]; Poloxamer 188 (Pluronic® F-68) [PF-68]; Polysorbate 80 (Tween® 80) [PT-80]; Lecithin (egg phosphatidyl choline) [LCT] were procured from Sigma Aldrich Chemicals, USA. All other chemicals and solvents procured were of the highest purity available and used as received without any additional treatments. Purified water was prepared by filtering the freshly collected Milli-Q® water (Millipore®, France) through 0.22 μm membrane filter (Millipore®, France).

5.2.2 Apparatus / Equipment / Instruments

Magnetic stirrer with temperature control (Stirrer, Remi, India); temperature controlled centrifuge - (Compufuge, Remi, India); and ultracentrifuge (L5-65, Beckman Instruments Inc., USA) were used for nanoparticles separation. A microtip probe sonicator (Microson, Misonix, USA) was used for the preparation of emulsion and vacuum evaporator (Rotavapor, Büchi, Switzerland) was used for evaporation of organic solvents. A lyophilizer (Heto-Dry-Lyo, Heto-Holten, Denmark) was used for freeze-drying after freezing sample at −20°C in a refrigerator (Frost-free, Vest-Frost, India).

A photon correlation spectroscope [PCS] (Zetasizer 3000 HSA, Malvern Instruments, UK) available at Panacea Biotech, Lalru was used for particle size analysis. A transmission electron microscope [TEM] (Morgagni, Philips, USA) equipped with a CCD camera (Megaview-III, Soft Imaging Systems) available at the All India Institute of Medical Sciences, New Delhi was employed for acquisition of the images. An atomic force microscope [AFM] (Nanoscope-III, Digital Instruments, USA) at Central Electrical and Electronics Research Institute, Pilani was used for morphological (size and shape) analysis.

5.2.3 Preparation of nanoparticles

The choice of a particular method for the preparation nanoparticles is principally determined by the physicochemical properties of the drug. In the present study, nanoparticles were prepared using co-precipitation of preformed polymers (PLGA & PCL) and in situ polymerization of monomers (ECA).

For the preparation of PLGA and PCL nanoparticles, a double emulsion solvent evaporation process was used as it provides better loading of hydrophilic drugs in to nanoparticulate matrix along with physical protection for enhanced stability (9). The drug entrapment process by the double emulsion solvent evaporation technique involves two major steps, the formation of stable primary emulsion and the subsequent removal of solvent from the double emulsion.

In the preparation of PECA nanoparticles, the mechanism of particle formation was based on an anionic radical polymerization initiated by covalent bases present in the medium (10-14). In case of alkyl cyanoacrylates, even weak bases are capable of ionizing the monomers, which subsequently form carbanions. These anions in turn react with other monomers forming continuous polymeric chains. The polymerization can be easily terminated by neutralizing the medium with addition of suitable cations (NaOH, KOH etc.) (7, 8, 15).

nanoparticles were subjected to alternate centrifugation and redispersion cycles to remove excess surfactant. Finally, the PECA nanoparticles were coated with either with polysorbate 80 (Tween® 80) by dispersing in 1% of respective surfactant solution for 3 h. Similarly, placebo nanoparticulate formulations were prepared by same method but without addition of the drug in the internal aqueous phase. Specific formulation parameters and process variables for individual formulations of PECA nanoparticles are presented in Table 5.3a and 5.3b.

c) Freeze-drying and storage

The prepared nanoparticles separated by ultracentrifugation technique were immediately freeze-dried using mannitol as a cryoprotective agent. For this purpose, individual formulations were conveniently transferred in glass containers and were frozen to −20°C for at least 24 h. Freeze drying was carried out with vacuum (1 mbar, −110°C), until free flowing powder was obtained. Processed samples were stored at refrigerated conditions in sealed glass containers.

5.2.4 Effect of formulation parameters and processing variables

The effect of various formulation parameters on the various characteristics of IM loaded PLGA, PCL and PECA nanoparticles were investigated by preparing batches with varying different parameters. The effect of individual parameters studied were organic phase, polymer proportion, drug proportion, surfactant - type and concentrations, phase ratio, aqueous phase pH, emulsification energy (intensity & duration of ultrasonication), evaporation rate (vacuum conditions) by varying one selected variable at a time, keeping all other parameters constant. Specific formulation parameters and process variables for individual nanoparticulate formulations are presented in Table 5.1-5.3.

5.2.5 Characterization of nanoparticles

Considering the fact that the enhanced therapeutic efficacy is principally attributed to their nano-dimensions, the prepared formulations were extensively characterized as per following procedures.

a) Drug analysis

The drug analysis was performed to determine the drug entrapment and loading efficiency of the individual nanoparticulate formulations. Accurately weighed freeze-dried nanoparticles were transferred to a fresh calibrated flask. In order to release entrapped drug, the nanoparticles were digested by dissolving the polymeric matrix in a suitable organic solvent system with an ultra-sonication treatment (10 min, 25°C). The amount of

drug was determined using analytical method reported in Chapter 3. Each determination was performed in triplicate and values are represented as average with standard deviations.

The drug entrapment efficiency (EE) was expressed as the percentage of the amount of drug entrapped in the nanoparticulate formulation relative to the initial amount of the drug added to the formulation. The EE was calculated from the total amount of the drug entrapped by using the following formula (20).

$$\text{EE (\% } w/w) = \frac{\text{Amount of drug in the product (mg)}}{\text{Amount of drug added (mg)}} \times 100$$

The drug loading efficiency (LE) was expressed as the percentage of the amount of drug present in the unit weight of the final nanoparticulate formulations. The LE was calculated from the amount of the drug present per unit weight of the final product using following formula (20).

$$\text{LE (\% } w/w) = \frac{\text{Amount of drug in the product (mg)}}{\text{Amount of the product (mg)}} \times 100$$

b) Particle size and size distribution

The average particle size and size distribution of individual formulation were analysed using a photon correlation spectroscopy. Freeze-dried nanoparticulate formulations were suitably dispersed in Milli-Q® water, which was previously ultra-sonicated for 30 min and filtered through 0.22 µm membrane using Millipore® filtration system. Prepared samples were subjected to particle size analyzer fitted with a He-Ne laser beam (4 mW) at a wavelength of 632.8 nm and fixed scattering angle of 90°. For each measurement, sufficiently diluted nanoparticle dispersions (1 mg mL^{-1}) were assessed for average particle size and polydispersity index (PI). PI values range between 0 to 1 indicating narrow size distribution (mono-dispersed phase) at lower side. While, the PI values greater than 0.5 indicates broader size distribution (poly-dispersed phase). The PI values lesser than 0.25 were considered as ideal and safe ideal for injectable preparations (21).

c) Particle shape and morphology

The morphological characterization and direct visualization of the prepared nanoparticulate formulations were performed using a transmission electron microscopy (TEM) and atomic force microscopy (AFM). The prepared nanoparticulate formulations were dispersed in pure water, previously ultrasonicated for 30 min and filtered using Millipore® ultrafiltration system.

For TEM, a drop of nanoparticulate formulation containing 0.02% *w/v* of phosphotungstic acid was placed on a carbon coated copper grid of TEM and allowed to equilibrate for 2 min. Excess liquid was removed and the grid was dried at room temperature. The prepared samples were micro-graphed at 80 to 100 kV on a digital TEM station. For AFM, a drop of nanoparticulate formulation was loaded onto an AFM silicone stub by spin coat technique and immediately dried under vacuum. Processed samples were scanned at 20 Hz in non-contact mode using a digital multimode scanning probe microscope station.

d) In vitro drug release studies

The drug release from the prepared nanoparticulate formulations were performed in modified dissolution apparatus with dialyzing membrane (MWC 14,000 Da, Sigma, USA) as previously reported by several authors (22-24). The release studies were carried out in phosphate buffer (100 mM) at physiological pH (7.4) as IM is freely soluble in water. Preformulation studies indicated that IM is stable in the phosphate buffer solution (pH 7.4) at 37°C over a period of seven days and the selected medium was sufficient to maintain the sink conditions through out the study. In addition, flux conditions were ensured by continuous stirring of the medium at 100 rpm.

The appropriate amount of IM loaded freeze dried nanoparticulate formulations were accurately weighed and dispersed in a phosphate buffer solution (100 mM, pH 7.4). The nanoparticulate dispersion was introduced into a dialysis membrane bag and the sealed bag was immediately placed in the release media. Studies were carried out in 25 mL of the phosphate buffer solution (100 mM, pH 7.4) maintained at 37 ± 2°C and the medium was covered to prevent evaporation losses. At predetermined time intervals, 1 mL aliquots of the sample was withdrawn from the release medium and it was replaced with equal volume of fresh medium. All samples were suitably diluted in mobile phase and IM concentration was determined. The percent cumulative drug release was calculated and plotted as a function of time and release kinetics were analysed using various mathematical models (zero order, first order, Higuchi, Hixson-Crowell, Weibull function). The mean dissolution time (MDT) was calculated from the first moment curve and it was used as a model independent parameter. The mechanism of drug release from the prepared nanoparticles was determined using the semi-empirical and power equation described by Korsmeyer and Peppas by fitting data up to 60% of drug release. In order to account for burst effect modified Korsmeyer and Peppas model was used, where burst effect was calculated as amount released in first hour, presented as M_{1h}. The regression

analysis (R^2), residual analysis (SSR & MSSR) and Akaike information criterion (AIC) were employed for data modeling. The model providing relatively lower SSR and AIC values along with high regression coefficient (nearing 1) were considered suitable. The time required to release 50% of the drug calculated using the best fit model was expressed as $T_{50\%}$ (h).

5.2.6 Stability studies

The physical state of entrapped drug in the optimized nanoparticulate formulations were assessed by performing thermal studies using a differential scanning calorimeter. All measurements were carried out on a previously calibrated differential scanning calorimeter, as described earlier. The glass transition temperature (T_g) was recorded as the midpoint of the curve between pre- and post-transition baselines. The peak melting temperature (T_m) and heat of fusion were determined using the software and were used to determine the percentage crystallinity. Reported data of the heat of fusion for complete crystalline state of the polymers was compared with standard values reported in literature (25, 26). The thermograms of the optimized nanoparticulate formulations loaded with and without IM were compared against the pure drug, pure polymers and a physical mixture.

Stability of optimized nanoparticulate formulations in dispersed and freeze-dried state was investigated over a period of time by exposing individual formulation to ambient ($25 \pm 2°C$), refrigerated ($5 \pm 3°C$) and freeze ($-20 \pm 5°C$) temperature conditions. Stability of the formulations were studied after 15 day, 1, 3 and 6 months and analyzed for product characteristics such as drug analysis (EE & LE), in vitro drug release studies etc. along with particle size and size distribution analysis at the end of the study.

Effect of freeze-drying on the average particle size and particle size distribution was studied by assessing redispersability for optimized formulations. For this purpose, the freeze-dried formulations were reconstituted by dispersing it into ultrapure water and comparison was done against the respective fresh formulation and analyzed without freeze-drying treatment.

5.3 Results and Discussions

Both emulsion solvent evaporation and interfacial polymerization techniques were found to be suitable for the preparation of IM loaded polymeric nanoparticles of good quality. Nanoparticle characteristics such as average particle size, size distribution, particle morphology, drug entrapment and loading efficiency were found to depend on various formulation and process parameters. All optimized methods produced stable, small and uniform particles with good entrapment efficiency and were found to be reproducible. In

addition, these parameters also showed influence on the in vitro drug release profile of IM from PLGA, PCL and PECA nanoparticles.

5.3.1 Effect of formulation parameters and processing variables

a) Effect of nature of organic phase

For PLGA nanoparticles, use of ethyl acetate as an organic solvent produced least average particle size with maximum entrapment and loading efficiency. Increase in the polarity of organic solvents used (chloroform < methylene chloride < ethyl acetate) resulted in a significant decrease in average particle size and increase in the drug entrapment and loading efficiency.

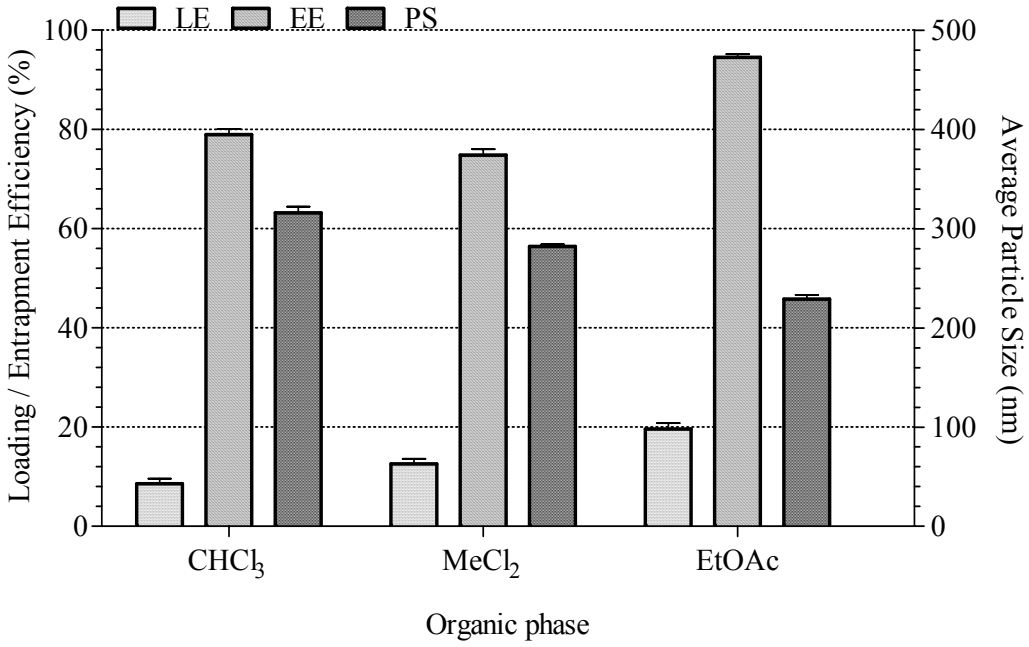

Fig. 5.2: Effect of the various organic phases on the characteristics of PLGA nanoparticles

Considering the fact that ethyl acetate has relatively higher aqueous solubility (≈ 8% *v/v*), quick solvent diffusion into external aqueous phase might have resulted in faster polymer precipitation forming smaller particles. Thus, the use of ethyl acetate provided nanoparticles with smaller average particle size, narrow size distribution and high drug entrapment efficiency as compared to other organic solvents studied. Moreover, particles were found to be of good spherical shape.

Similarly, PCL based nanoparticles prepared using chloroform found to have relatively higher average particle size and wider size distribution over the other solvents (Table 5.2). The drug entrapment and loading efficiency were found to be higher with use

of ethyl acetate (Fig. 5.3). However, the TEM studies revealed a few morphological deformations in nanoparticles prepared with ethyl acetate, however, formulations prepared with chloroform and methylene chloride showed good spherical shape with uniform size distribution (Table 5.2; Fig. 5.4). In literature, dissolution of PCL in organic solvent and subsequent phase separation of polymer molecules has been reported to govern the surface properties of the polymeric structures (27). PCL is more hydrophobic in comparison with other polyesters such as PLA, PLGA etc. and more soluble in chloroform and methylene chloride in comparison with ethyl acetate. Thus, the morphological inconsistency may be attributed to a relatively poor solubility of PCL in these solvents affecting the process of phase separation, as the polarity of the solvent is reported to control the polymer precipitation behavior principally (27).

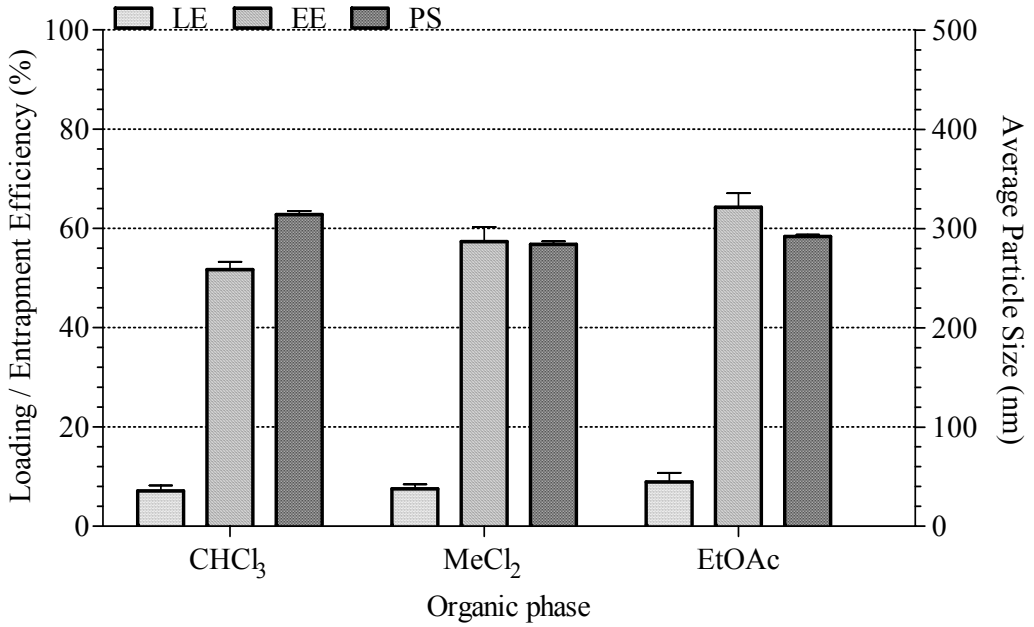

Fig. 5.3: Effect of the various organic phases on the characteristics of PCL nanoparticles

Similar polymeric structures of PCL exhibiting a filamentous morphology have also been reported in literature (28). Where, faster nucleation is reported to offer molecular restrictions on intra- and inter-molecular interactions resulting into formation of the filamentous structures. Considering the fact that PCL is more soluble in chloroform, higher solubility might have offered relatively high degree of freedom for proper intra-molecular assemblies of PCL molecules resulting in smooth surface structures. Frequently, the porous polymeric structures are formed by gradual precipitation process from polymeric solutions, in organic phase, induced by solvent extraction across a

semi-permeable polymeric membrane, which is formed in situ at the interface of the organic phase and the aqueous phase (28). Thus, the observed change in the characteristics of prepared nanoparticles for these formulations may be attributed to the differential solubility of polymer in the selected organic solvents.

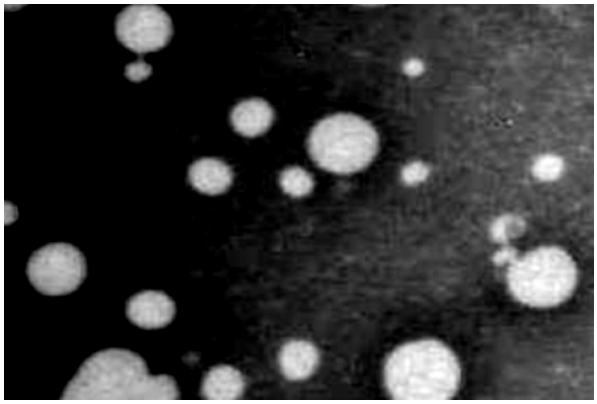

(a)

(b)

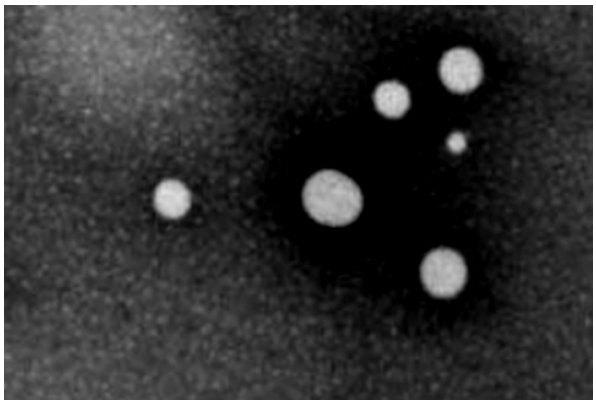

Fig. 5.4: TEM images of PCL nanoparticles prepared using different solvents (a) ethyl acetate and (b) chloroform

b) Effect of polymer proportion

The results indicated that the polymer proportion affects various properties and characters of prepared nanoparticles (Table 5.1-5.3; Fig. 5.5-5.7). In case of PLGA nanoparticles, the formulations prepared with 50 and 100 mg of PLGA provided relatively smaller particle size with absence of agglomerates. However, formulations prepared with 200 and 400 mg of PLGA have shown increased aggregation with high polydispersity index (Table 5.1a). Similar trend was also observed with PCL nanoparticles, as the average particle size of PCL nanoparticles was found to increase from 276 to 302 nm with increase in the polymer amount from 50 to 200 mg, maintaining its narrow size distribution. However, further increase to 400 mg led to increase in the average particle size to 369 nm with significant increase in the polydispersity index (Table 5.1a).

Moreover, a trend of increase in average particle size with increase in polymer proportion was observed for both, PLGA and PCL, polymers was in agreement with the previous reported work (4, 29-32). The increased polymer proportion leads to increased viscosity of polymeric phase offering high resistance against the shear forces during the ultrasonication treatment. This phenomenon subsequently leads to the formation of bigger droplets during emulsification due to poor dispersability of internal aqueous phase in the primary emulsion (*w/o*) and the primary emulsion (*w/o*) into the secondary aqueous phase leading to increased particle size (33, 34). Moreover, an increased probability of coalescence due to desolvated macromolecules in the concentrated polymeric solution contributes as an independent mechanism (35).

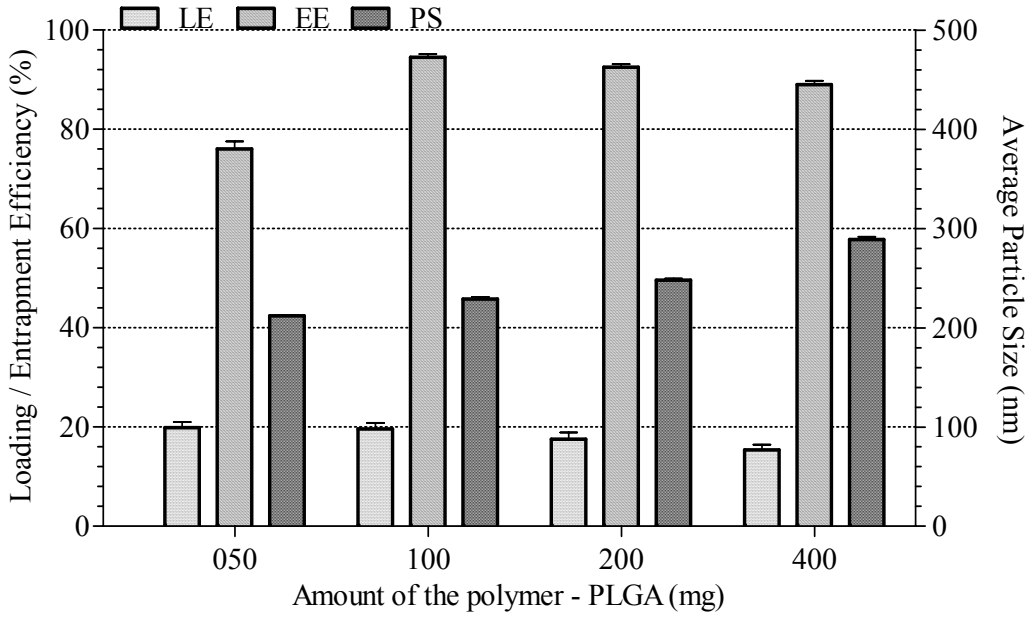

Fig. 5.5: Effect of the polymer amount on the characteristics of PLGA nanoparticles

PLGA nanoparticles have shown a significant gain in drug entrapment efficiency from 76.02 to 94.49% with increase in PLGA amount from 50 to 100 mg. However, no further increase in drug entrapment efficiency was observed with increase in PLGA amount up to 400 mg. In case of PCL nanoparticles, a trend of increase in drug entrapment efficiency was consistent with an increase in PCL amount (52.57 to 73.28%). Although less prominent, a similar trend was also observed in the drug entrapment efficiency with increase in polymer proportion. Increased viscosity of the polymeric phase with increase in polymer proportion may have contributed to stabilization of the primary emulsion subsequently preventing the drug diffusion into external aqueous phase (29, 30).

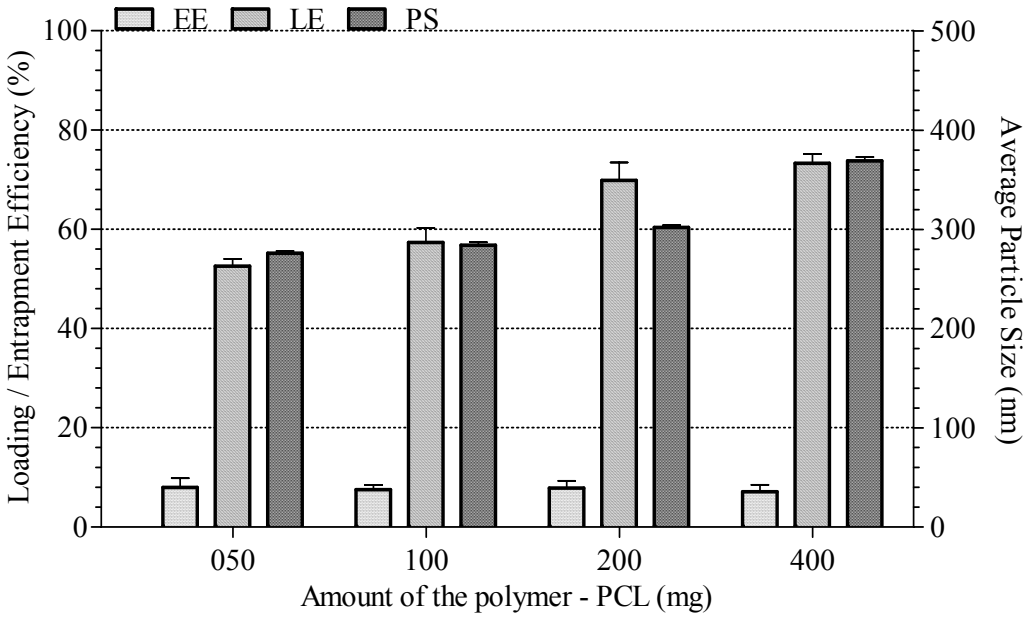

Fig. 5.6: Effect of the polymer amount on the characteristics of PCL nanoparticles

In case of PECA nanoparticles, an increase in the concentration of ethyl cyanoacrylate monomers has shown an increase in average particle size and size distribution. Similar increase was also observed in drug entrapment and loading efficiency (Fig. 5.7).

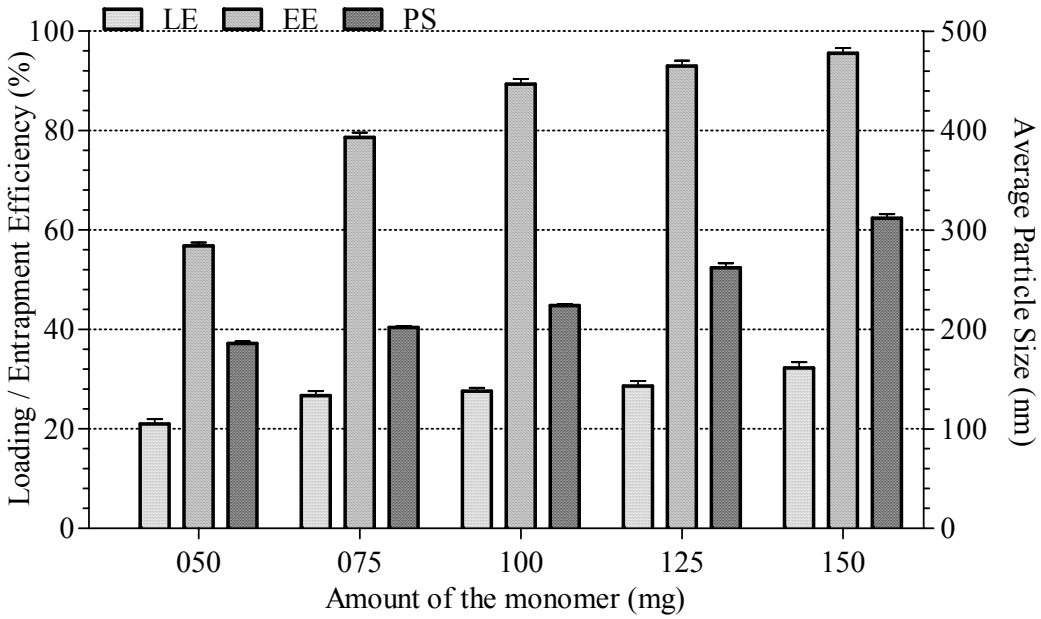

Fig. 5.7: Effect of monomer (ECA) amount on the characteristics of PECA nanoparticles

These findings are in agreement with the earlier reported work, wherein, the authors have observed increase in drug entrapment and loading efficiency with an increase in the concentration of alkyl cyanoacrylates monomers from 1 to 4% *w/v* (36-38).

c) Effect of stabilizer

In case of PLGA nanoparticles, the results indicated importance of concentration of surfactant in formation of the primary emulsion, as it was found to affect properties of the prepared nanoparticles (Fig. 5.8). Considerable reduction in the average particle size and size distribution was observed with the use of lecithin in the primary emulsion (*w/o*). An increasing sigmoidal trend indicated that the optimum concentration of lecithin is essential for the formation of the primary emulsion. However, lecithin above 0.3% did not result in appreciable reduction in average particle size, polydispersity index and increase in drug entrapment and loading efficiency (Table 5.1a).

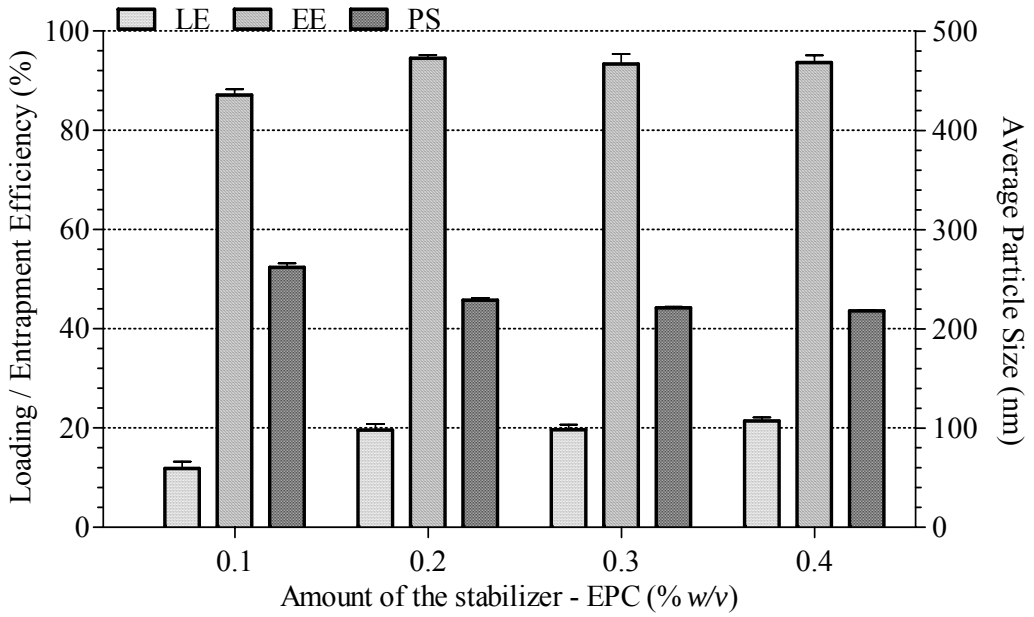

Fig. 5.8: Effect of stabilizer (LCT) amount on the characteristics of PLGA nanoparticles

Average particle size of the PLGA nanoparticles was found to decrease form 254 to 212 nm with an increase in PVA concentrations in the external aqueous phase from 0.5 to 2% *w/v*. Similarly, an increase in PF-68 concentration from 0.5 to 2% *w/v* led to a decrease in average particle size from 238 to 208 nm. Thus, both the stabilizers studied demonstrated a decrease in the average particle size with an increase in concentration of stabilizers.

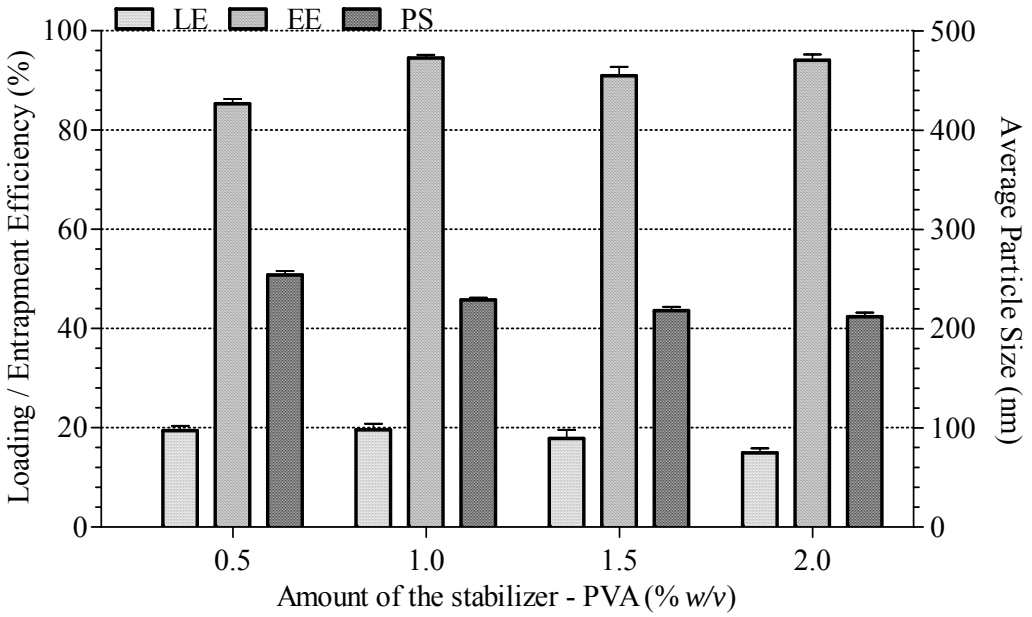

Fig. 5.9: Effect of stabilizer (PVA) amount on the characteristics of PLGA nanoparticles

Moreover, it was also observed that the particle size distribution becomes narrower with increasing stabilizer, which was in agreement with the previously reported results (39, 40).

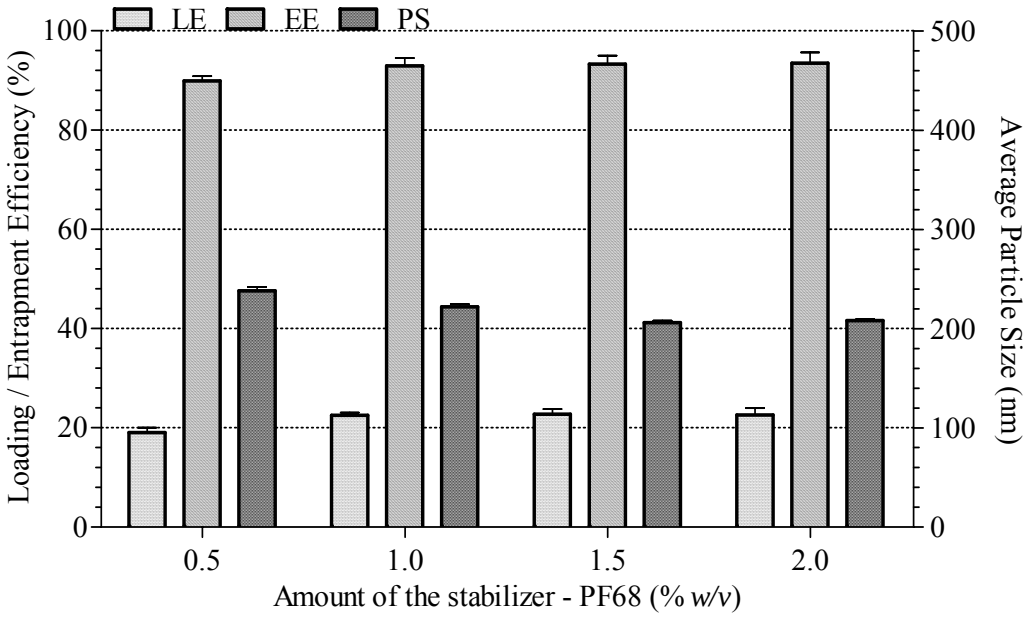

Fig. 5.10: Effect of stabilizer (PF-68) amount on the characteristics of PLGA nanoparticles

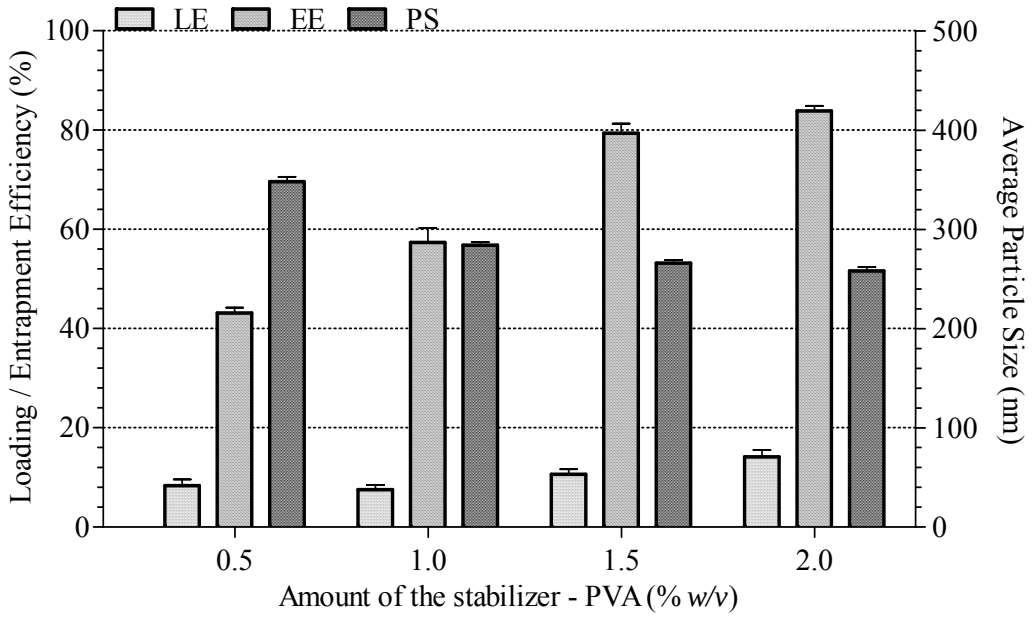

Fig. 5.11: Effect of stabilizer (PVA) amount on the characteristics of PCL nanoparticles

A similar trend was also observed in case of PCL nanoparticles as the average particle size and the polydispersity index were found to decrease with increasing concentrations of both the stabilizers - PVA and PF-68 (Fig. 5.11 & 5.12).

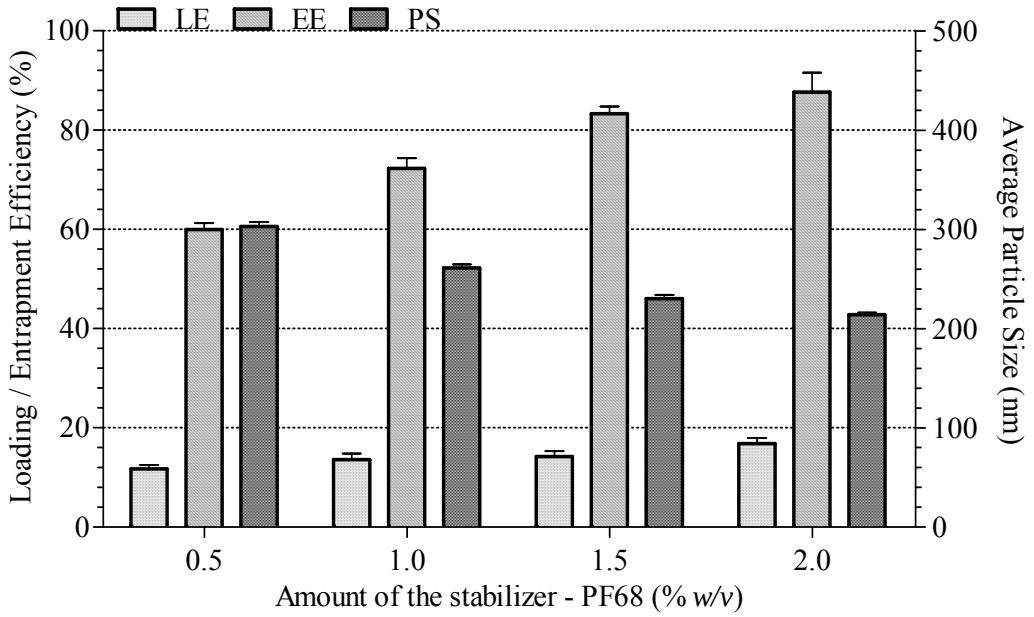

Fig. 5.12: Effect of stabilizer (PF-68) amount on the characteristics of PCL nanoparticles

At a high concentration of stabilizer, there is an increase in the number of surfactant molecules that orient at oil-water interface to reduce the interfacial tension. Subsequently,

it results in increased net shear stress leading to the formation of smaller droplets, at a constant emulsification energy (41-45). In case of PVA, the reduction in the surface tension would have overcome the effect of increasing viscosity (34, 40). Moreover, the physical adsorption of PVA molecules on to the newly formed nanoparticulate surface prevent agglomeration of particles, as the hydrated layer (OH^- groups) provide a steric hindrance (46, 45).

In case of PF-68, the stabilizer molecules orients to anchor the hydrophobic segments (PPO) on polymeric surface, while the hydrophilic segments (PEO) align towards aqueous phase reducing surface tension (Fig. 5.13) (47-50). Thus, it can be inferred that the high concentrations of stabilizers contribute to increased steric hindrance and reduced surface tension, preventing increase in the mean droplet size through coalescence. At all concentrations studied, use of PF-68 over PVA resulted in smaller particles with narrower size distribution. A relatively high viscosity of PVA solution over PF-68 solution may be an underlying cause, which contribute to increased particle size and wider size distribution.

A steady increase in drug entrapment efficiency of PLGA and PCL nanoparticles was observed with an increase in the PVA concentration. The present observation may be supported by the fact that a high concentration of PVA and PF-68 efficiently stabilizes the emulsion, subsequently prevents diffusional loss of drug. The stabilization mechanism is evident from the observation that a low concentration of PVA and PF-68 tends to form larger particles with a wider distribution. In addition, increased viscosity of the external aqueous phase at a high concentration of PVA may provide additional stability to the emulsion.

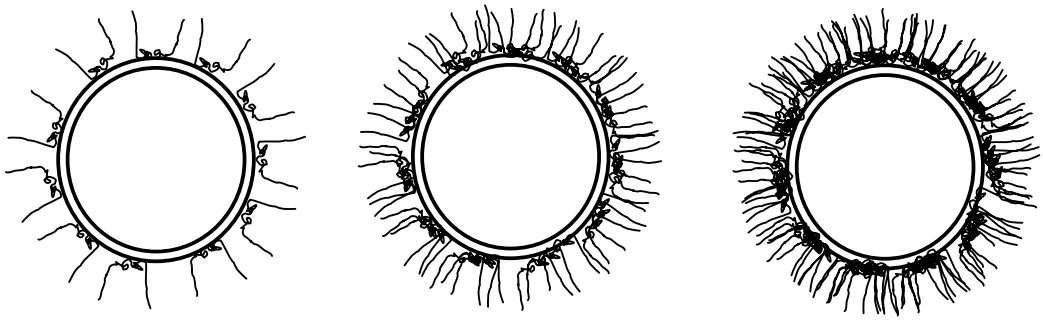

Fig. 5.13: Diagrammatic representation of association of PF-68 molecules onto nanoparticle surface with increasing concentration

In case of PLGA nanoparticles, there was a slight decrease in drug loading efficiency with increase in PVA concentrations. This observation may be attributed to increased

association of PVA molecules with polymeric matrix reducing relative amount of the drug. Interestingly, an opposite trend was observed with the use PF-68, which was found to be saturable above the 1% PVA concentration. However, PF-68 has shown a better drug entrapment and loading efficiency in comparison with PVA, at all respective concentration levels. In the literature, increased protein entrapment efficiency has been reported with the use of PVA over PF-68 (51). The authors suggested that the use of PVA in equal proportion with PLGA leads to small and uniform nanoparticles with good recovery.

In case of PECA nanoparticles, increased stabilizer concentration led to decreased average particle size and polydispersity index (Table 5.3a; Fig. 5.14). The role of a stabilizer was found to be crucial in the formation of PECA nanoparticles as in most of the cases poly-hydroxyl functional group favors the presence of OH^- ions in the medium. These OH^- ions act as initiators along with the stabilizing mechanism (36, 37, 52).

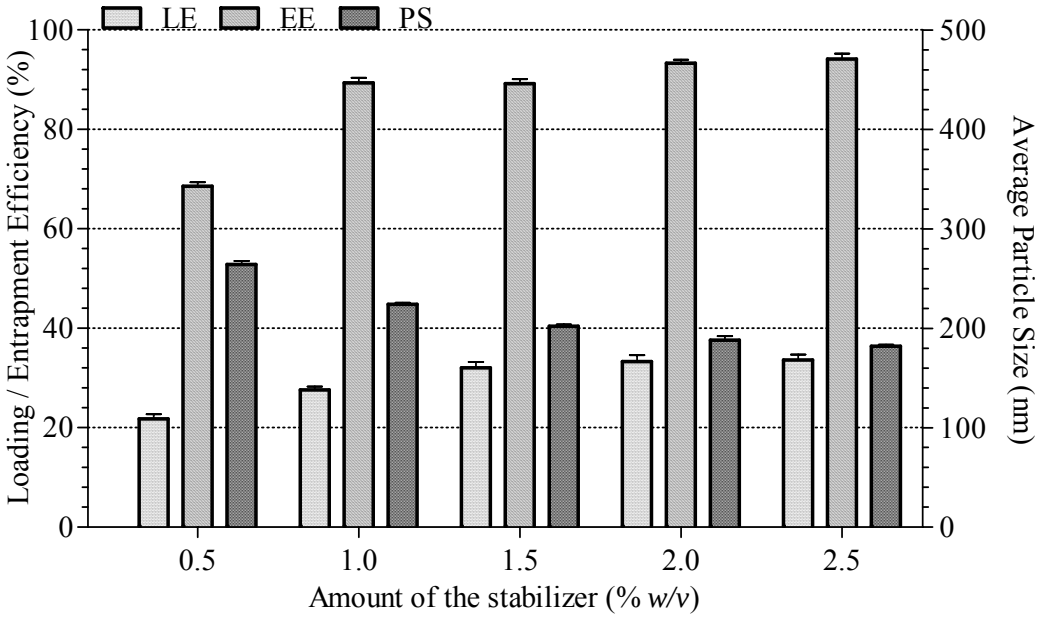

Fig. 5.14: Effect of stabilizer (LCT) amount on the characteristics of PECA nanoparticles

The particle size analysis results indicated that an increase in stabilizer concentration show saturable trend as beyond the optimum concentrations of stabilizer, there was no significant increase in the average particle size. In literature, few authors have reported smaller particle size with narrow size distribution with the use of PF-68 over dextran (53). Similarly, the some studies have also proved that polymerization of alkyl cyanoacrylates

in the presence of PF-68 did not show association with the growing polymer chains rather it was adsorbed on the surface of polymeric nanoparticles (14).

In the present study, the drug entrapment and loading efficiency results indicated a increasing saturable (exponential) trend with an increase in stabilizer concentration as beyond the optimum concentrations of stabilizer, there was no significant gain in drug entrapment and loading efficiency. Moreover, presence of the stabilizer was found to be essential for the formation of stable nanoparticles as nanoparticles prepared without stabilizer led to rapid aggregation with poor redispersability. Conversely, a very high concentration of stabilizer (> 2% *w/v*) was not found to improve the product quality. These results appear to be in contrast to some of the earlier reported work, wherein, the authors have observed no change in the drug loading or entrapment efficiency with increase in the concentration of dextran-70 as a stabilizer (37, 38, 52, 54).

d) Effect of drug proportion

Both the PLGA and PCL nanoparticles have shown no significant difference in the average particle size and size distribution between drug loaded and blank nanoparticles, suggesting that there was no influence of drug on the precipitation behavior of polymer (Fig. 5.15 & 5.16).

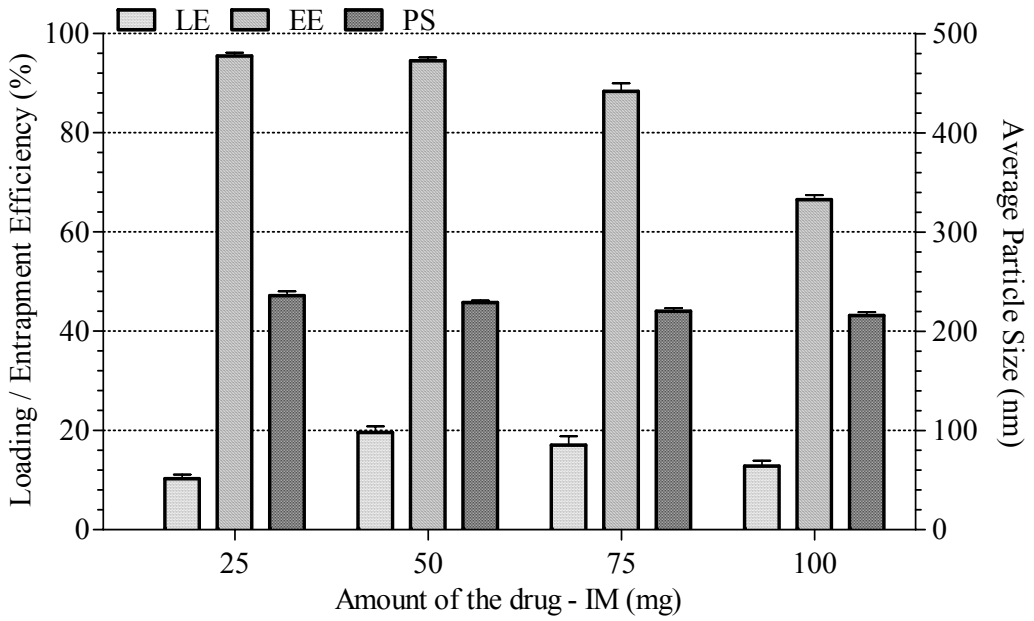

Fig. 5.15: Effect of the drug (IM) amount on the characteristics of PLGA nanoparticles

However, the results of PLGA nanoparticles indicated that optimum drug loading efficiency (≈ 20%) can be obtained between 50 to 75 mg of IM, the both extreme drug

proportions found to provide decreased drug loading efficiency 10.28% (25 mg) to 12.83% (100 mg). The drug entrapment efficiency results indicated a decreasing trend from 95.48 to 66.52% with increase in the drug amount from 25 to 100 mg, respectively.

The results of PCL nanoparticles have shown that the increasing drug proportion does not impact the average particle size and size distribution. Although an increase in drug amount led to well-defined increasing trend in drug loading efficiency, the drug entrapment efficiency was found to be relatively constant. In both the preformed polymers, increase in the free drug amount due to increase in drug proportion would have resulted in decreased drug entrapment and loading efficiency.

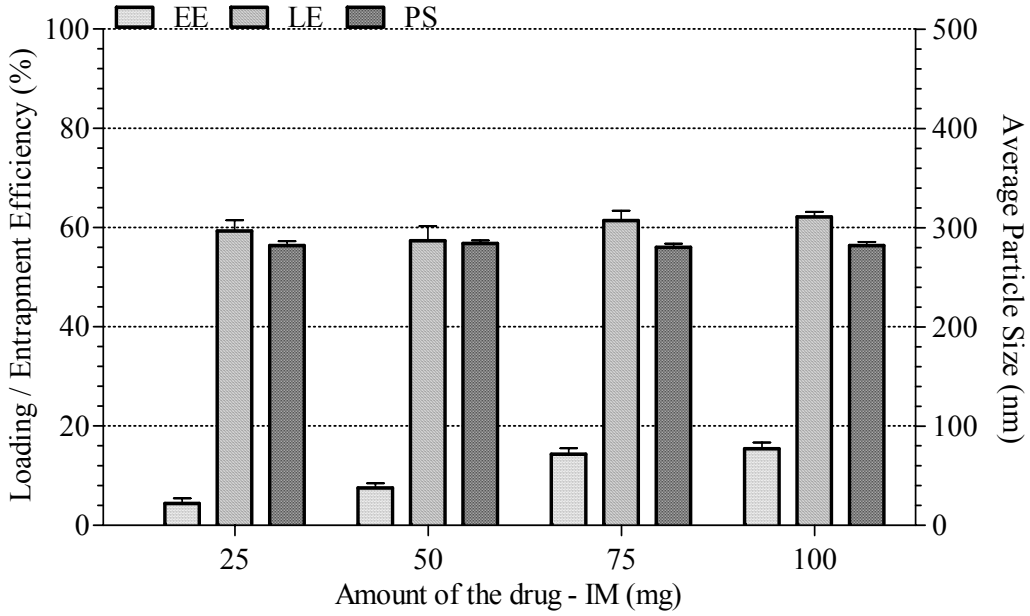

Fig. 5.16: Effect of the drug (IM) amount on the characteristics of PCL nanoparticles

In case of PECA nanoparticles, increase in the drug concentration has shown an increasing exponential trend in drug loading efficiency and decreasing trend in drug entrapment efficiency (Fig. 5.17). In literature, drug loading efficiency of poly (alkyl cyanoacrylate) particulate drug delivery systems have been shown to increase or decrease with increasing drug concentrations (55, 56, 13, 37, 38, 52, 54). However, there was no reason reported for these trends in the loading and entrapment efficiency of the PACA nanoparticles.

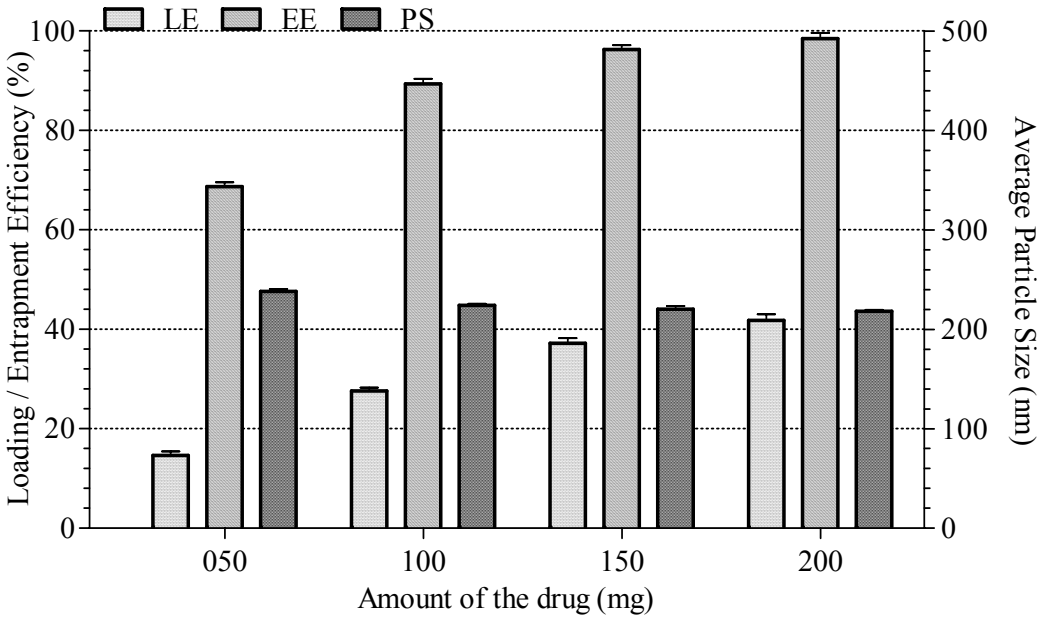

Fig. 5.17: Effect of the drug (IM) amount on the characteristics of PECA nanoparticles

e) Effect of phase volume ratio

A decrease in the internal phase volume of primary emulsion led to a decrease in the average particle size of PLGA nanoparticles from 244 to 218 nm with an increase in drug loading efficiency from 14.99 to 20.07%. An increase in the average particle size was attributed to reduction in the net shear exerted on the internal phase during the emulsification process. Similarly, a relative decrease in the internal phase volume resulted in decreased droplet size with subsequent formation of smaller size nanoparticles (Table 5.1b).

The observation may be explained by the fact that the relative increase in the external aqueous phase volume reduces the net shear stress at a constant energy level, leading to increase in the average particle size (57-59). However, it was observed that the drug entrapment efficiency remains unaffected at 15 and 20% phase volume ratio. Similarly, there was no substantial change in the drug loading efficiency for these formulations (Table 5.1b).

An increase in the external aqueous phase volume from 75 to 85% *v/v* led to a decrease in average particle size from 272 to 236 nm with increase in drug loading efficiency from 13.16 to 22.75% *w/w*. A slight decrease (≈ 7%) in drug entrapment efficiency was also observed with increase in the external phase volume. Moreover, there was no substantial

change in the drug entrapment and loading efficiency for the formulations prepared with 80 and 75% phase volume ratio.

In case of PECA nanoparticles, relative volume of oil to aqueous phase have shown an impact on product characteristics such as the formulations prepared with the increasing oil phase have shown an increase in average particle size (Table 5.3b). In addition, a decrease in drug entrapment and loading efficiency was observed with increased proportion of oil phase.

f) Effect of aqueous phase pH

Both the internal and external aqueous phase pH were found to affect characteristics of nanoparticles (Table 5.1 & 5.3). The internal aqueous phase pH of 7.4 coupled with the external aqueous phase pH 7.4 led to formation of nanoparticles with narrow size distribution. A decrease in internal aqueous phase pH resulted in increased average particle size and drug loading efficiency. Similarly, a decrease in external aqueous phase pH resulted in increased average particle size and decreased drug loading efficiency (Table 5.1b).

The observation was explained by the fact that the pH change affects the polymer precipitation behavior and controls the drug diffusion from internal to external aqueous phase. Increased solubility of IM at acidic pH of internal phase would have decreased diffusional losses into external aqueous phase resulting in increased drug entrapment and loading efficiency (Fig. 5.18). Similarly, decreased solubility of IM at basic pH of external phase would have decreased diffusional losses into external phase resulting in increased drug entrapment and loading efficiency.

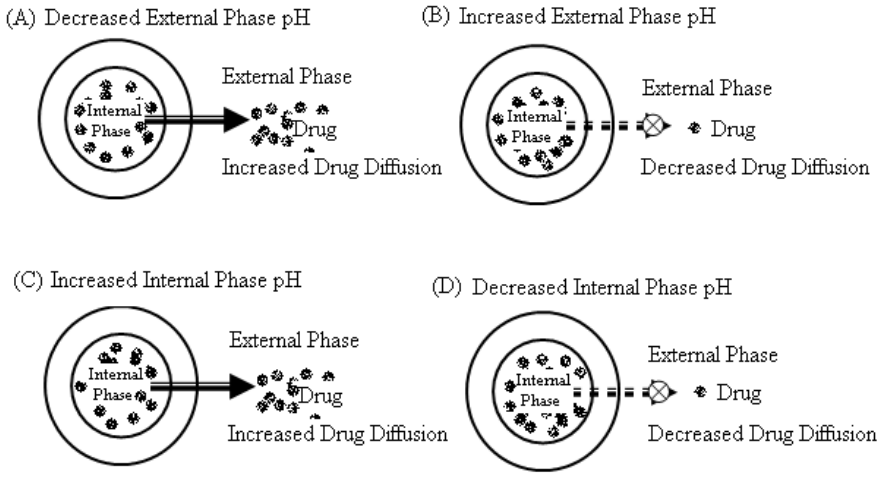

Fig. 5.18: Diagrammatic representation of pH dependent drug diffusion

Moreover, increased solubility of the polymer at basic pH of media would have resulted in slow precipitation at the interface forming bigger particles with wider size distribution.

In case of PECA nanoparticles, among all studied variables, the effect of medium pH on the various characteristics of PECA nanoparticles was most influential. There was a prominent trend of increased drug entrapment efficiency with increased pH (decreasing acidity) of the medium, within the studied levels (Table 5.3b; Fig. 5.19).

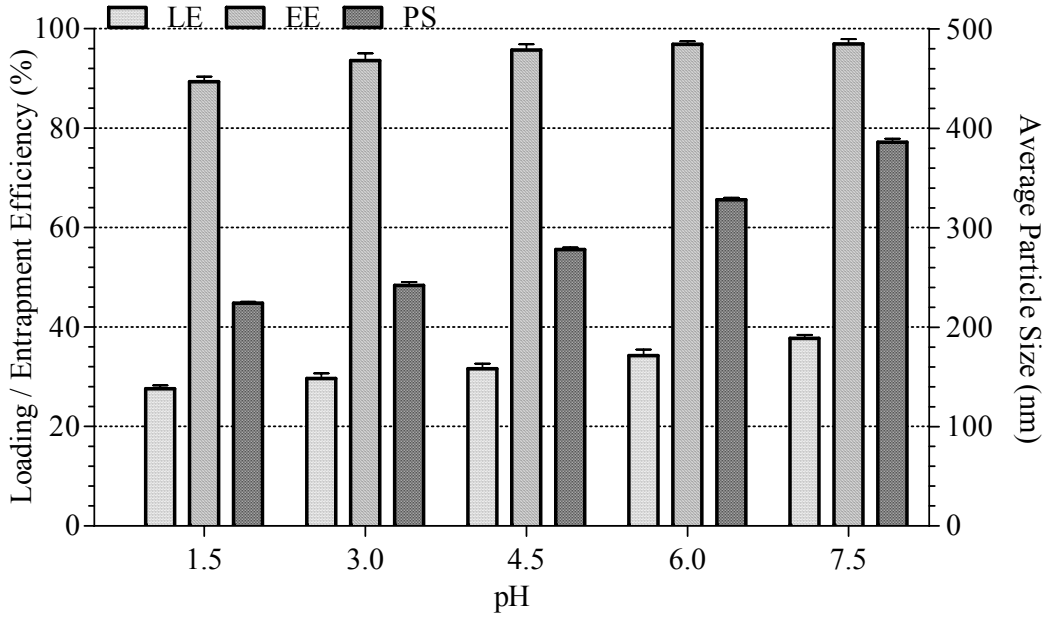

Fig. 5.19: Effect of the aqueous phase pH on the characters of PECA nanoparticles

These results are in agreement with the few reported studies and it was attributed to the accelerated polymerization process. The polymerization kinetics of an alkyl cyanoacrylate is controlled by the basicity of the medium (relative amounts of the OH^- ions from water dissociation) as it is initiated by covalent bases (15, 55, 22). The rate of polymerization indirectly affects the drug loading (entrapment, adsorption) process as accelerated conditions increase the loading efficiency by enhancing mechanically entrapment of drug (55, 60, 61, 8). Similar high loading efficacy was also reported for several other drugs such as Ciprofloxacin, 5-Flurouracil etc. (36, 55, 37, 38).

As IM fairly remains ionized at acidic pH, the drug loading mechanism is essentially governed by a mechanical entrapment of drug molecules in a polymeric network during formation of a nanoparticle (37, 38). Moreover, the pH partitioning studies have revealed that IM has more affinity towards the aqueous phase than the oil phase (Chapter 4). In an ionized state, it may be assumed that the drug fraction partitioned into oil phase will be

negligible. Thus, presence of electrostatic charge on IM molecules governs the drug entrapment process.

In case of non-ionic drugs, the low drug entrapment and loading efficiency was attributed principally to the diffusion of the drug from internal phase to external phase, which can be avoided simply by increasing polymerization rate. Thus, rapid polymerization leads to entrapment of drug inside polymeric network and reduces the time dependent loss of a drug in an external phase (38).

In addition, another independent mechanism of drug loading is adsorption of the drug on the surface of the polymeric nanoparticles. The extent of drug adsorption depends on the surface properties of nanoparticles and the physicochemical properties of drug (pKa, log P etc). Moreover, a decrease in the degree of ionization of the polymer with increased medium pH has reported to reduce electrostatic repulsion in polymeric chains (inter- and intra-chain) forming smaller particle size (62). In the present study, exactly opposite trend was observed as the average particle size was found to decrease with increased pH and it was attributed to increased rate of polymerization at alkaline conditions (36-38)

g) Effect of energy

A prominent trend was observed for average particle size and drug loading efficiency with change in the intensity and duration of ultrasonication treatment (Table 5.2). An increase in ultrasonication energy from 10 to 20 W resulted in a considerable decrease in average particle size of PLGA nanoparticles from 275 to 222 nm and drug loading efficiency from 19.39 to 16.77%. A similar trend was also observed with an increase in the duration of ultrasonication treatment from 5 to 15 min for average particle size (305 to 212 nm) and the drug loading efficiency (19.39 to 15.19%).

Thus, it can be inferred that the increased emulsification energy associated with either increased duration or intensity of the ultrasonication treatment aid in rapid dispersion of organic phase forming uniform nano-droplets, which subsequently provide smaller nanoparticles with narrow size distribution.

Although ultrasonication was performed in temperature controlled conditions, high energy associated with ultrasonication treatment may rise temperature in microenvironment of the probe facilitating drug diffusion process. Moreover, increased solubility of the drug at elevated temperature may be a contributing factor to a decrease in drug loading efficiency at high-energy conditions (intensity & duration).

In case of PCL nanoparticles, the formulations prepared with increasing duration of ultrasonication treatment has shown a decreasing trend in the average particle size (Table 5.2). A similar decreasing trend was also observed with increasing duration of ultrasonication treatment. However, there was a decrease in drug entrapment and loading efficiency beyond optimum duration of 5 min. Size distribution (polydispersity index) was also found to increase with increasing duration of ultrasonication treatment.

In case of PECA nanoparticles, a decrease in average particle size was observed with increase in the duration in a saturable manner. However, there was significant impact on the drug entrapment and loading efficiency (Table 5.3b).

h) Effect of evaporation

Selected three conditions of solvent evaporation were found to influence the various characteristics of prepared nanoparticles as the formulations prepared with reduced pressure showed smaller average particle size with monomodal size distribution (Table 5.1b). Similarly, formulations evaporated at the atmospheric pressure using a magnetic stirrer provided relatively higher average particle size and polydispersity index (Table 5.1b).

A decrease in average particle size at reduced pressure can be attributed to higher solvent removal rates (63, 57). In literature, studies have also indicated increased extent of droplet dispersion due to higher kinetic energy at the interface resulting from rapid evaporation of organic solvent (64). In addition, during the formation of the nanoparticle, there is a gradual decrease in the volume of dispersed phase resulting from solvent removal (evaporation and diffusion). This phenomenon leads to an increase in viscosity of the dispersed droplets affecting the droplet size equilibrium, which subsequently results in droplet coalescence and agglomeration during early stage of the solvent removal process (63). Thus, the results indicated that reduced pressure (≈ 200 mmHg) is essential for the formation of uniformly distributed low size nanoparticles. However, there were no additional benefits observed at the high vacuum (< 50 mmHg).

i) Effect of polymerization duration

In case of PECA nanoparticles, the effect of the polymerization duration on the product characteristics was less significant after 4 h as the product characteristics were fairly unaffected by extended duration of polymerization after 4 h. Thus, it can be inferred that the 4 h duration of polymerization is sufficient for complete polymerization of ethyl cyanoacrylate monomers (Table 5.3a).

j) Effect of freeze drying

In present study, formulation prepared using different concentrations of stabilizers - PVA and PF-68 indicated linear increase in the redispersability with increasing stabilizer concentration. Moreover, the study proved that PVA concentration below 1% *w/v* may not demonstrate adequate redispersability, even after ultrasonic treatment. Conversely, the lowest studied poloxamer concentration (0.5% *w/v*) showed adequate redispersability with uniform size distribution. The complete characterization of freeze-dried nanoparticles revealed that there was no significant impact of freeze drying process on the various characteristics of prepared nanoparticles. TEM studies were in agreement with these findings as the optimized formulations showed smaller spherical particles with narrow size distribution and complete absence of free drug crystals.

In literature, few authours have indicated variable concentration of PVA for adequate redispersability of the prepared PLGA nanoparticles (65-67). Feczkó et al have described the significance of relative mass ratio (PLGA:PVA) for explaining the differences in reported data (51). However, removal of the surface associated stabilizer may presents significant challenge during preparation of polymeric nanoparticles as excess of stabilizer may add up toxic effects. Considering this fact, lowest concentration of stabilizers providing optimum properties were selected.

The morphology of the optimized formulations of PLGA, PCL and PECA were studied using transmission electron microscopy (TEM) and atomic force microscopy (AFM) are shown in Fig. 5.20-5.31. TEM images of the drug loaded PLGA nanoparticles showed spherical shape of the particles (Fig. 5.20). Images revealed that the particles are uniformly distributed and particle surface is smooth in nature.

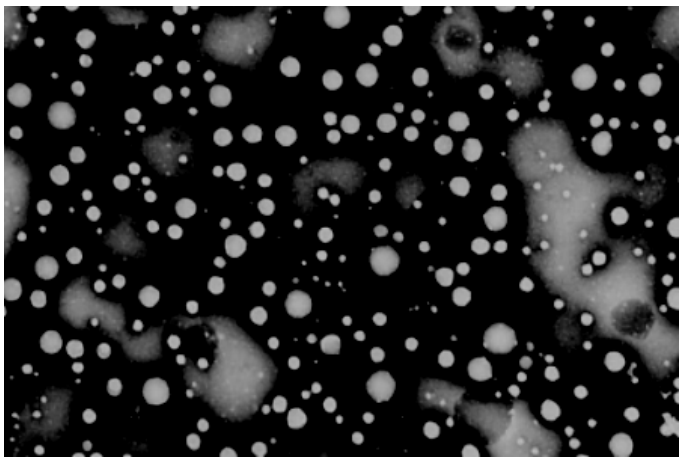

Fig. 5.20 : TEM image of PLGA nanoparticles (freeze dried with cryoprotectant)

Moreover, the average particle size and size distribution data was in agreement with the PCS analysis results. There was no significant impact of freeze drying process on the average particle size, size distribution and morphology of PLGA nanoparticle (Fig. 5.21). However, freeze drying without a cryoprotectant led to little aggregation, which is visible in following micrograph (Fig. 5.22).

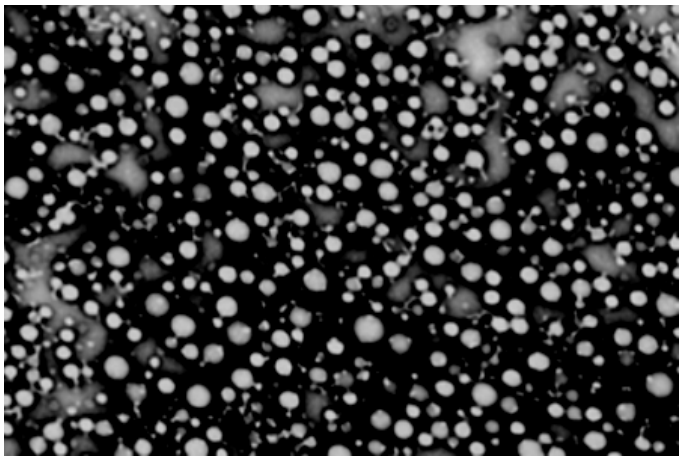

Fig. 5.21 : TEM image of PLGA nanoparticles (without freeze drying)

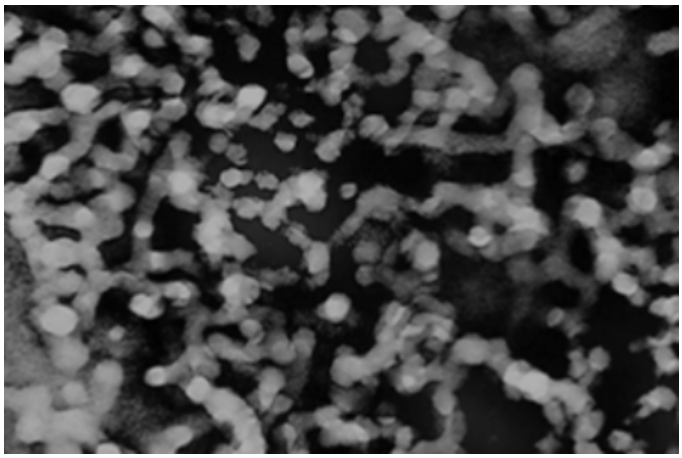

Fig. 5.22 : TEM image of PLGA nanoparticles (freeze dried without cryoprotectant)

TEM images of the drug loaded PCL nanoparticles also showed uniform spherical shape (Fig. 5.23). Moreover, analysis revealed uniform distribution and smooth surface morphology of the prepared nanoparticles. TEM results were also in agreement with the PCS analysis data. There was no significant impact of freeze drying process on the average particle size, size distribution and morphology of PCL nanoparticle (Fig. 5.24). Even at a high resolution, a single PCL nanoparticle showed uniform spherical shape (Fig. 5.25-5.26).

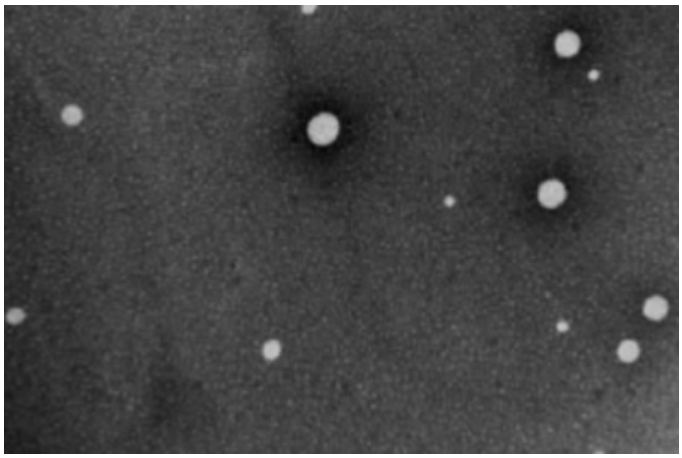

Fig. 5.23 : TEM image of PCL nanoparticles (freeze dried with cryoprotectant)

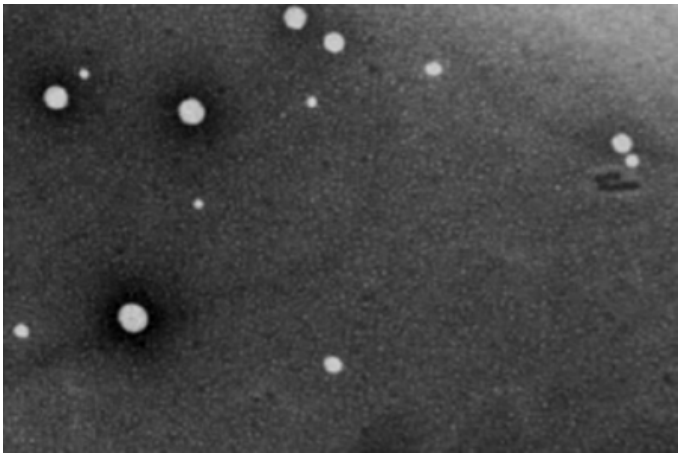

Fig. 5.24 : TEM image of PCL nanoparticles (without freeze drying)

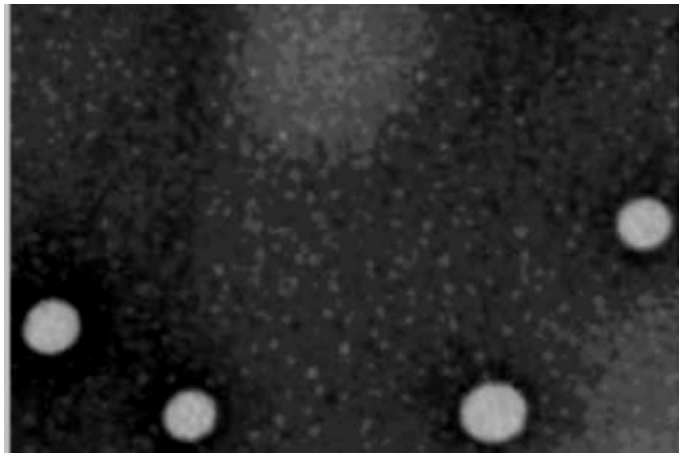

Fig. 5.25 : TEM image of PCL nanoparticles (freeze dried without cryoprotectant)

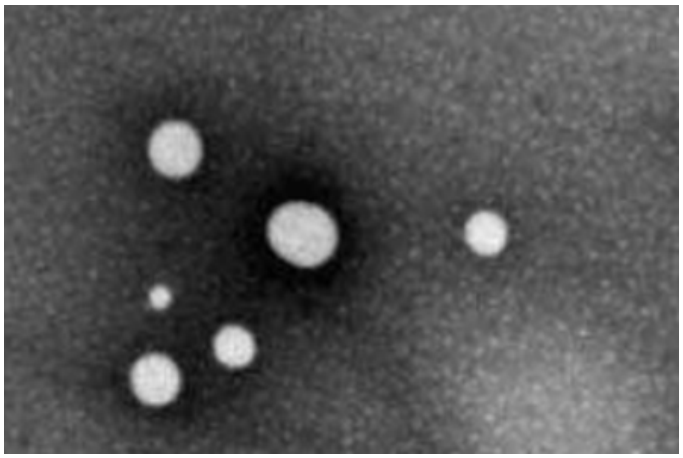

Fig. 5.26 : TEM image of PCL nanoparticles (Spherical particles)

PECA nanoparticles were also found to be in uniform spherical shape and smooth particle morphology (Fig. 5.27).

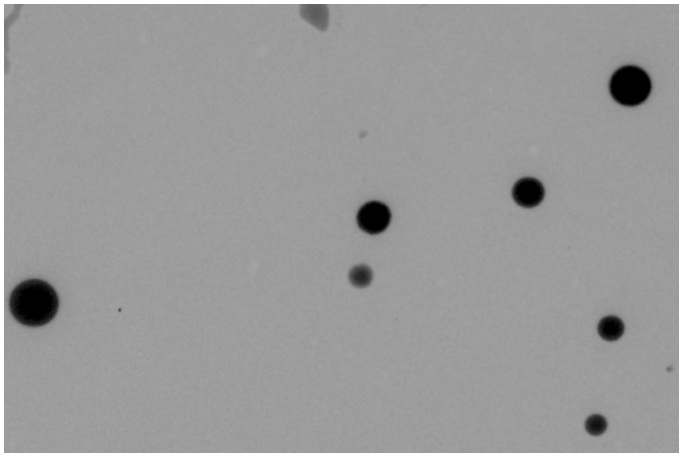

Fig. 5.27 : TEM image of PECA nanoparticles (without freeze drying)

IM loaded PECA nanoparticles were uniformly distributed and particle surface was smooth in nature. The various characteristics such as the average particle size, size distribution and morphology of PECA nanoparticle was found to be unaffected by freeze drying treatment, in presence of cryoprotectant (Fig. 5.28). Moreover, the average particle size and size distribution data was in agreement with the PCS analysis results. At high resolution, a single PECA nanoparticle showed uniform spherical shape (Fig. 5.29).

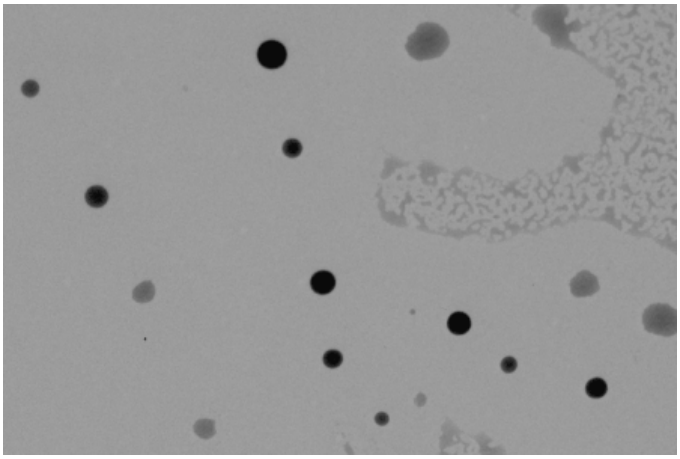

Fig. 5.28 : TEM image of PECA nanoparticles (freeze dried with cryoprotectant)

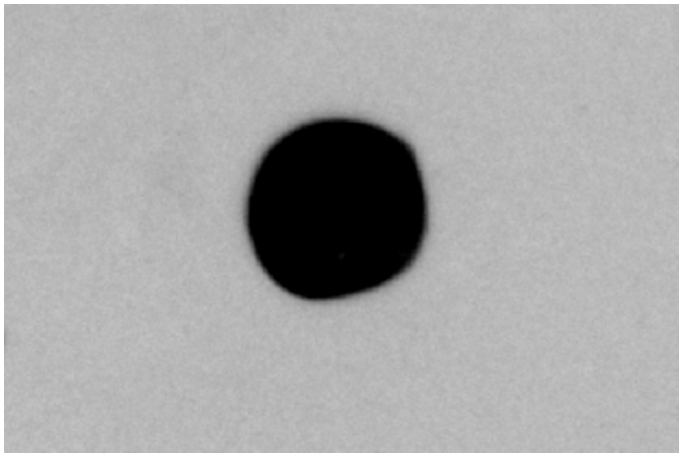

Fig. 5.29 : TEM image of PECA nanoparticles (single spherical particle)

Further, AFM analysis also confirmed the spherical shape of prepared nanoparticles (Fig. 5.30-5.31). Within the studied resolution of AFM, the surface morphology was found to be smooth without any noticeable deformations. AFM results were in perfect agreement of PCS and TEM analysis. Thus, the results of both TEM and AFM analysis confirmed that the prepared nanoparticles were in good spherical shape with smooth surface.

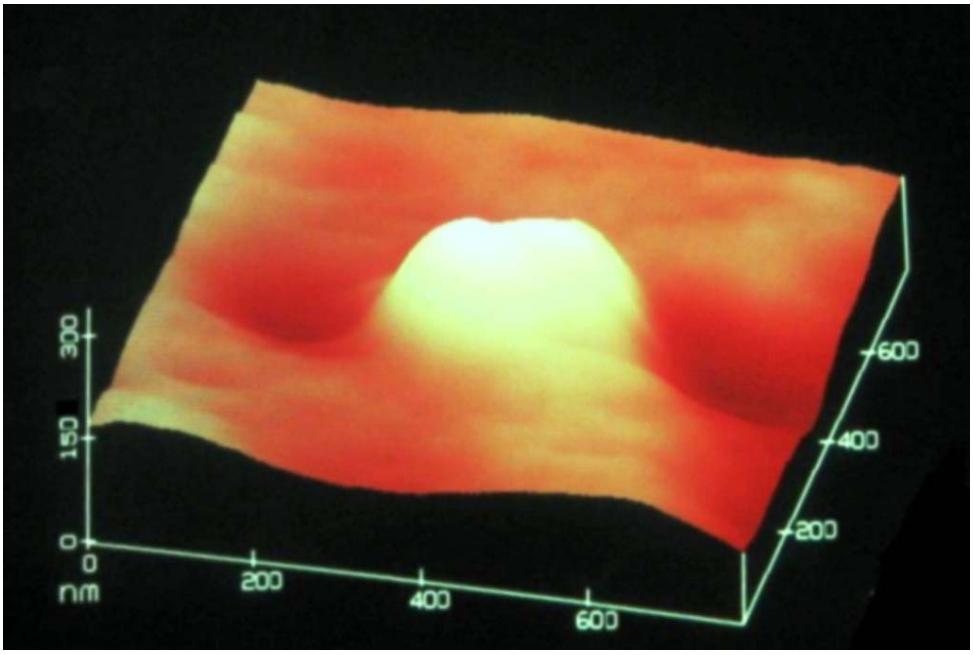

Fig. 5.30 : AFM image of PLGA nanoparticles (single spherical particle)

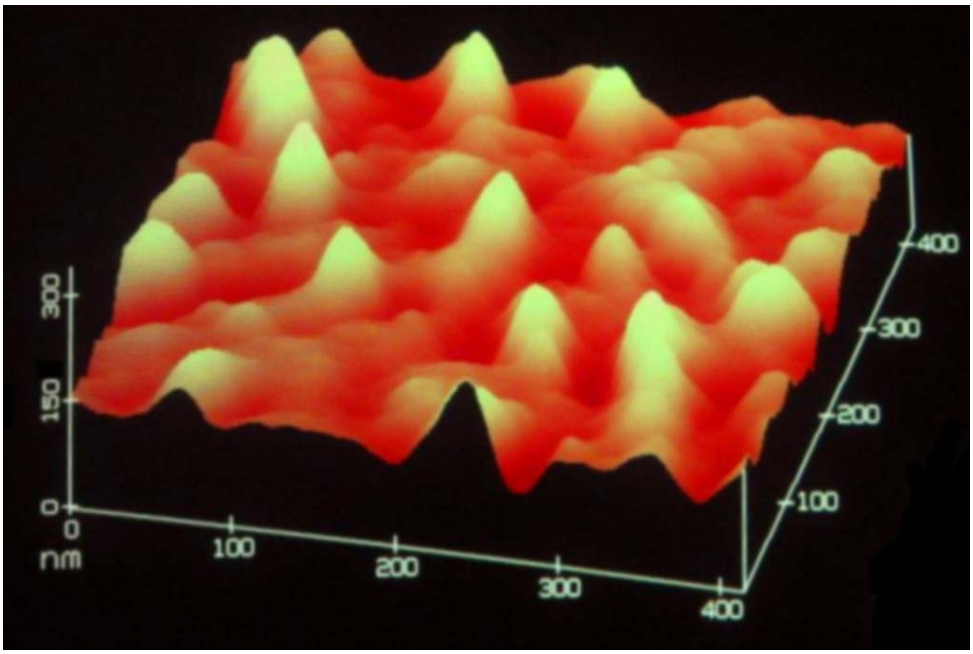

Fig. 5.31 : AFM image of PECA nanoparticles (spherical particles)

Thus, the various formulation and process parameters were found to have influence the characteristics of prepared PLGA, PCL and PECA nanoparticles.

5.3.2 In vitro drug release studies

The various formulations prepared to investigate the effect of formulation parameters have demonstrated considerable impact on the in vitro drug release profile (Fig. 5.34-5.46). Data fitting into various models indicated that the drug release data can be well described by first order kinetics. In addition, the modified Korsmeyer-Peppas model was found to be suitable for explaining drug release mechanism in all the formulations.

Almost all PLGA formulations demonstrated a bi-phasic controlled drug release with MDT ranging from 9.3 to 25.9 h (Fig. 5.34). While, the PCL formulations have shown characteristic tri-phasic release profiles with MDT ranging from 6.87 to 21.43 h (Fig. 5.35). The drug release profile of PECA nanoparticles was also found to be bi-phasic in nature (Fig. 5.36). A distinct first phase comprising rapid drug release was evident in most of the formulations (PLGA-NP, PCL-NP & PECA-NP).

This initial rapid release was principally attributed to direct dissolution of poorly entrapped and weakly bound drug to the large surface of the prepared nanoparticles (68). As described earlier, the surface properties of materials dominate over its bulk properties at the nano scale. A decrease in particle size results in increased surface to volume ratio subsequently providing a large surface area for interaction between release media, polymer and drug.

PCL nanoparticles have shown prominently high burst effect in comparison with PLGA nanoparticles, which was explained by the fact the PCL polymeric structures exists in amorphous form with high porosity. The high porosity offers high drug diffusion resulting in rapid mass transfer of the drug into the release medium.

Moreover, it also provides increased effective surface area for adsorption of the drug. In addition, high aqueous solubility of IM might have further contributed to high porosity and low crystallinity, releasing significant amount of IM during first few hours (3 h). The biphasic release profile of PECA nanoparticles indicated that the significant fraction of IM was adsorbed on the surface of the prepared nanoparticles as compared to the fraction of the drug entrapped into polymeric network.

In later phase, the entrapped drug into PLGA and PECA polymeric matrix was released slowly, which is controlled by the drug diffusion and polymer degradation processes. Similar findings are reported for different categories of drugs with varied physicochemical properties and suggest that it is a property of polymer rather than the loaded drugs (69-72). Previously, few authors reported that PLGA and PCL polymers

undergoes slow degradation process with selective bulk degradation over surface degradation (Fig. 5.32) (73). Moreover, studies have proved a little degradation of polymeric matrix during first several hours with negligible differences in the morphological characteristics of polymeric structures.

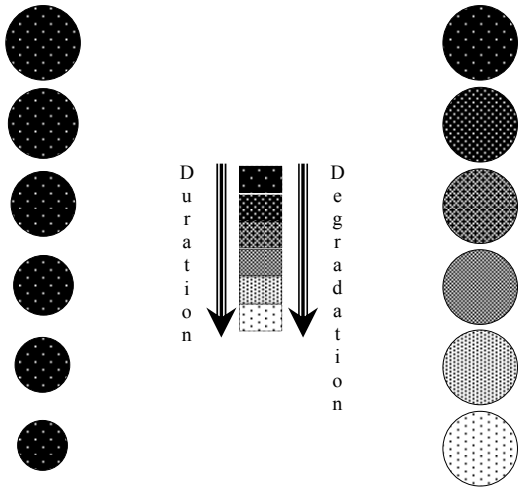

(Surface Erosion Mechanism) (Bulk Erosion Mechanism)

Fig. 5.32: Schematic representation polymer degradation mechanism in nanoparticles

In case of PCL nanoparticles, tri-phasic drug release profile was explained with the fact that the PCL polymer exists in amorphous and polymorphic forms and the variable ratio of amorphous to crystalline state of polymer may have controlled the release profile.

It is reported that the amorphous fraction of the polymeric matrix undergoes rapid degradation over crystalline fraction with release of the entrapped drug (Fig. 5.33) (74, 75).

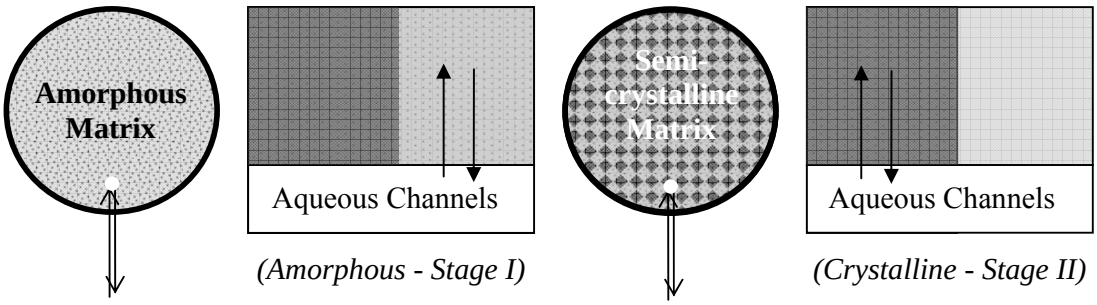

Fig. 5.33: Schematic model of two stages of polymeric matrix degradation and drug diffusion process

Therefore, the drug release in second phase may be due to diffusion of the drug incorporated in the polymeric matrix. Thus, the diffusion of drug and degradation of the polymer matrix may be a reason for the third phase providing the sustained release of the entrapped drug.

The PLGA formulations prepared with increasing relative drug proportions demonstrated an increasing burst effect (M_{1h}) from 10.3 to 28.6% with significant decrease in MDT from 21.2 to 9.3 h. The results from Peppas modified power law indicated the involvement of polymer relaxation (non-Fickian, anomalous drug transport) with exponent values being constant for increasing drug proportion ($n = 0.72 \pm 0.034$) (Table 5.4)

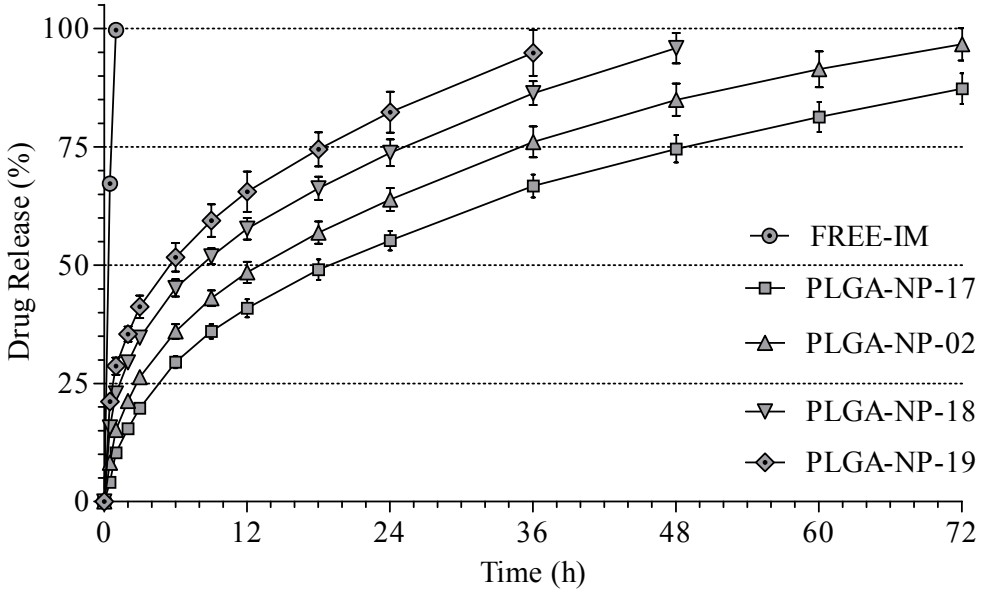

Fig. 5.34: In vitro drug release profile of PLGA nanoparticles prepared using different amount of the drug. (Each data represents the average of three independent determinations)

In case of PCL nanoparticles, an increase in the amount of the drug led to increase in the burst release (M_{1h}) from 13.4 to 45.7% and significant decrease in $T_{50\%}$ values from 13.4 to 8.3 h. The modified power law indicated that the both Fickian and non-Fickian transport processes were involved as the exponent value was constant with increase in the drug proportion ($n = 0.65 \pm 0.02$). The modified power law indicated anomalous drug diffusion mechanism with prevalence of the Fickian diffusion process, which was unaffected by increase in the drug proportion. However, it may suggested that one or

more secondary mechanisms including polymer erosion, polymer relaxation and even release of entrapped stabilizer might have contributed to a little extent (Table 5.5).

Table 5.4: Summary of in vitro drug release kinetics of PLGA nanoparticles

Batch No.	MDT (h)	First Order K_{fo} (R)	Modified Korsmeyer-Peppas $\alpha + K_{mkp} \times T^{n}$ (R)	$T_{50\%}$ (h)
PLGA-NP-02	19.6	0.044 (0.988)	$15.2 + 0.055 \times T^{0.68}$ (0.965)	15.8
PLGA-NP-04	12.5	0.066 (0.985)	$25.4 + 0.058 \times T^{0.68}$ (0.949)	10.5
PLGA-NP-05	21.2	0.040 (0.988)	$10.0 + 0.052 \times T^{0.70}$ (0.958)	17.3
PLGA-NP-06	22.3	0.040 (0.989)	$5.2 + 0.062 \times T^{0.67}$ (0.953)	17.3
PLGA-NP-10	12.8	0.053 (0.980	$27.3 + 0.077 \times T^{0.57}$ (0.929)	13.1
PLGA-NP-11	25.9	0.033 (0.982)	$9.1 + 0.042 \times T^{0.74}$ (0.979)	21.0
PLGA-NP-12	22.6	0.040 (0.983)	$8.1 + 0.032 \times T^{0.86}$ (0.979)	17.3
PLGA-NP-13	10.0	0.079 (0.991)	$22.3 + 0.043 \times T^{0.87}$ (0.950)	8.8
PLGA-NP-14	16.0	0.055 (0.993)	$13.0 + 0.037 \times T^{0.86}$ (0.974)	12.6
PLGA-NP-15	21.1	0.048 (0.982)	$4.0 + 0.034 \times T^{0.87}$ (0.959)	14.4
PLGA-NP-16	22.6	0.043 (0.979)	$6.1 + 0.024 \times T^{0.94}$ (0.975)	16.1
PLGA-NP-17	21.2	0.041 (0.990)	$10.3 + 0.051 \times T^{0.70}$ (0.960)	16.9
PLGA-NP-18	13.1	0.058 (0.982)	$22.9 + 0.054 \times T^{0.72}$ (0.969)	12.0
PLGA-NP-19	9.3	0.075 (0.973)	$28.6 + 0.054 \times T^{0.76}$ (0.967)	9.2
PLGA-NP-21	15.22	0.055 (0.981)	$20.8 + 0.058 \times T^{0.68}$ (0.965)	12.6
PLGA-NP-22	20.63	0.041 (0.990)	$12.1 + 0.058 \times T^{0.67}$ (0.968)	16.9
PLGA-NP-23	20.93	0.043 (0.987)	$9.0 + 0.065 \times T^{0.65}$ (0.969)	16.1
PLGA-NP-24	19.50	0.043 (0.986)	$14.8 + 0.055 \times T^{0.67}$ (0.966)	16.1
PLGA-NP-25	21.60	0.042 (0.989)	$5.6 + 0.062 \times T^{0.67}$ (0.965)	16.5
PLGA-NP-26	20.37	0.043 (0.988)	$10.4 + 0.057 \times T^{0.68}$ (0.964)	16.1
PLGA-NP-27	24.43	0.039 (0.988)	$5.0 + 0.044 \times T^{0.75}$ (0.967)	17.8
PLGA-NP-28	17.84	0.044 (0.984)	$23.0 + 0.050 \times T^{0.67}$ (0.965)	15.8

MDT is mean dissolution time; K_{fo} and K_{mkp} are the kinetic release rate constants respectively for first order kinetics and modified Korsmeyer-Peppas (mKP) model; α is burst release calculated as ($100 \times Mb/M_{\infty}$) by mKP model; T is time; n is diffusional exponent value for mKP model and R is correlation coefficient. Each data represents the average of three determinations.

Table 5.5: Summary of in vitro drug release kinetics of PCL nanoparticles

Batch No.	MDT (h)	First Order K_{fo} (R)	Modified Korsmeyer-Peppas $\alpha + K_{mkp} \times T^{n}$ (R)	$T_{50\%}$ (h)
PCL-NP-02	13.68	0.053 (0.979)	$20.4 + 0.065 \times T^{0.64}$ (0.932)	13.1
PCL-NP-04	8.80	0.085 (0.986)	$36.0 + 0.047 \times T^{0.74}$ (0.952)	8.2
PCL-NP-05	12.73	0.065 (0.994)	$13.5 + 0.062 \times T^{0.69}$ (0.882)	10.7
PCL-NP-06	12.04	0.066 (0.988)	$12.2 + 0.060 \times T^{0.71}$ (0.850)	10.5
PCL-NP-07	11.32	0.055 (0.963)	$30.5 + 0.071 \times T^{0.59}$ (0.918)	12.6
PCL-NP-08	12.31	0.071 (0.996)	$17.1 + 0.052 \times T^{0.78}$ (0.951)	9.8
PCL-NP-09	18.07	0.044 (0.985)	$12.6 + 0.055 \times T^{0.71}$ (0.928)	15.8
PCL-NP-10	14.72	0.040 (0.944)	$30.4 + 0.063 \times T^{0.57}$ (0.985)	17.3
PCL-NP-11	21.43	0.037 (0.992)	$14.4 + 0.038 \times T^{0.78}$ (0.966)	18.7
PCL-NP-12	12.50	0.064 (0.992)	$14.3 + 0.050 \times T^{0.82}$ (0.983)	10.8
PCL-NP-13	16.27	0.052 (0.994)	$11.1 + 0.040 \times T^{0.85}$ (0.951)	13.4
PCL-NP-14	14.55	0.052 (0.977)	$13.4 + 0.074 \times T^{0.63}$ (0.919)	13.4
PCL-NP-15	11.79	0.056 (0.975)	$30.2 + 0.059 \times T^{0.64}$ (0.928)	12.4
PCL-NP-16	6.87	0.084 (0.968)	$45.7 + 0.050 \times T^{0.68}$ (0.923)	8.3

MDT is mean dissolution time; K_{fo} and K_{mkp} are the kinetic release rate constants respectively for first order kinetics and modified Korsmeyer-Peppas (mKP) model; α is burst release calculated as $(100 \times Mb/M_{\infty})$ by mKP model; T is time; n is diffusional exponent value for mKP model and R is correlation coefficient. Each data represents the average of three determinations.

Table 5.6: Summary of in vitro drug release kinetics of PECA nanoparticles

Batch No.	MDT (h)	First Order K_{fo} (R)	Modified Korsmeyer-Peppas $\alpha + K_{mkp} \times T^{n}$ (R)	$T_{50\%}$ (h)
PECA-NP-01	1.00	0.994 (0.999)	$58.7 + 0.114 \times T^{1.11}$ (1.000)	0.7
PECA-NP-02	7.36	0.107 (0.991)	$23.8 + 0.110 \times T^{0.56}$ (0.898)	6.5
PECA-NP-03	2.32	0.353 (0.978)	$45.0 + 0.108 \times T^{0.76}$ (0.976)	2.0
PECA-NP-04	9.09	0.087 (0.982)	$14.5 + 0.115 \times T^{0.58}$ (0.889)	8.0
PECA-NP-05	8.95	0.094 (0.992)	$12.2 + 0.096 \times T^{0.64}$ (0.885)	7.4
PECA-NP-06	3.29	0.230 (0.980)	$40.3 + 0.130 \times T^{0.57}$ (0.954)	3.0
PECA-NP-07	7.66	0.100 (0.972)	$18.5 + 0.138 \times T^{0.54}$ (0.926)	6.9
PECA-NP-08	11.43	0.066 (0.975)	$22.0 + 0.075 \times T^{0.66}$ (0.928)	10.5
PECA-NP-09	13.15	0.059 (0.979)	$14.1 + 0.087 \times T^{0.63}$ (0.943)	11.7
PECA-NP-10	6.34	0.114 (0.974)	$28.4 + 0.111 \times T^{0.59}$ (0.884)	6.1
PECA-NP-11	3.54	0.221 (0.983)	$36.5 + 0.128 \times T^{0.60}$ (0.933)	3.1
PECA-NP-12	1.93	0.459 (0.983)	$47.9 + 0.148 \times T^{0.59}$ (0.958)	1.5
PECA-NP-14	7.92	0.100 (0.987)	$23.3 + 0.079 \times T^{0.71}$ (0.915)	6.9
PECA-NP-15	8.86	0.093 (0.994)	$21.7 + 0.061 \times T^{0.74}$ (0.937)	7.5
PECA-NP-16	4.23	0.168 (0.971)	$33.7 + 0.143 \times T^{0.53}$ (0.920)	4.1
PECA-NP-17	3.02	0.251 (0.979)	$39.3 + 0.164 \times T^{0.50}$ (0.924)	2.8
PECA-NP-18	5.40	0.133 (0.972)	$29.9 + 0.132 \times T^{0.53}$ (0.882)	5.2
PECA-NP-19	4.43	0.157 (0.969)	$32.4 + 0.139 \times T^{0.54}$ (0.908)	4.4
PECA-NP-20	6.05	0.130 (0.988)	$25.0 + 0.087 \times T^{0.73}$ (0.934)	5.3
PECA-NP-21	5.10	0.135 (0.960)	$32.4 + 0.148 \times T^{0.48}$ (0.905)	5.1
PECA-NP-22	4.24	0.188 (0.984)	$31.6 + 0.117 \times T^{0.65}$ (0.957)	3.7
PECA-NP-23	2.96	0.280 (0.989)	$37.2 + 0.116 \times T^{0.71}$ (0.959)	2.5
PECA-NP-24	2.17	0.114 (0.974)	$46.2 + 0.121 \times T^{0.70}$ (0.964)	6.1

MDT is mean dissolution time; K_{fo} and K_{mkp} are the kinetic release rate constants respectively for first order kinetics and modified Korsmeyer-Peppas (mKP) model; α is burst release calculated as ($100 \times Mb/M_{\infty}$) by mKP model; T is time; n is diffusional exponent value for mKP model and R is correlation coefficient. Each data represents the average of three determinations.

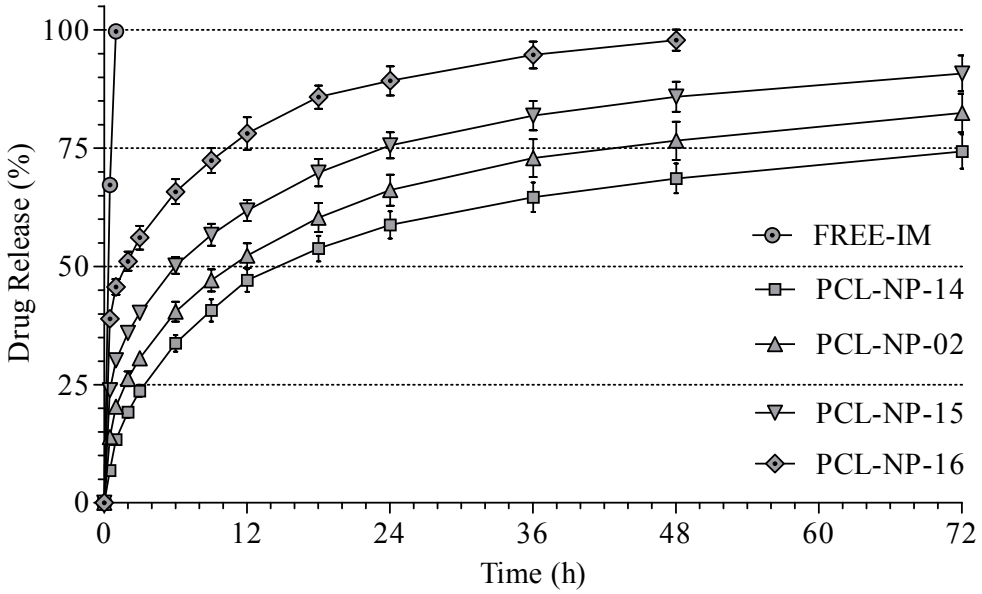

Fig. 5.35: In vitro drug release profile of PCL nanoparticles prepared using different amount of the drug. (Each data represents the average of three independent determinations)

In case of PECA nanoparticles, it was observed that the MDT was extended from 1.93 to 7.36 h with an increase in the amount of drug from 100 to 200 mg.

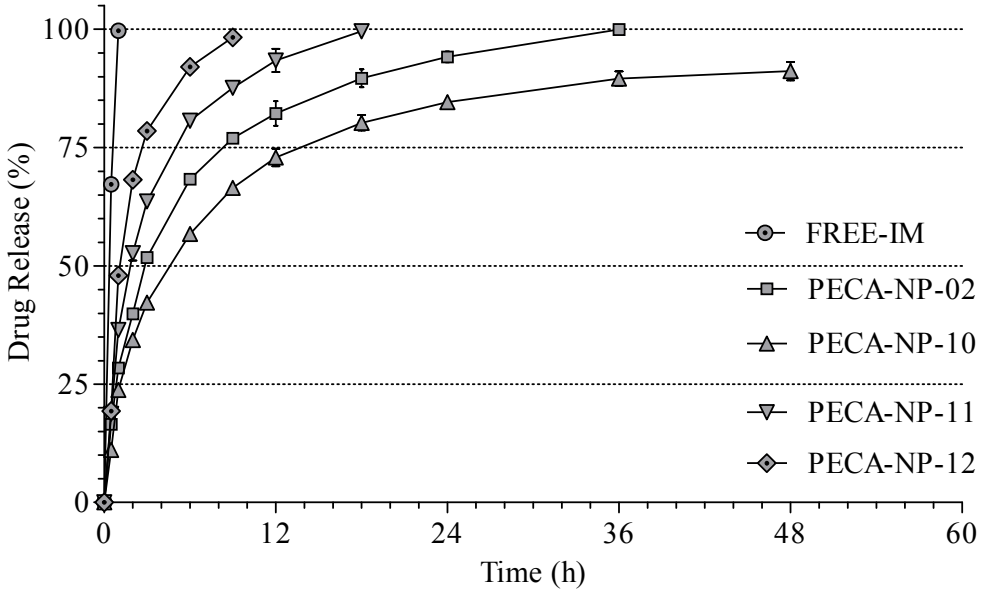

Fig. 5.36: In vitro drug release profile of PECA nanoparticles prepared using different amount of the drug. (Each data represents average of three independent determinations)

The exponent values calculated from the modified Peppas model were ranging between 0.56 and 0.60 implying the mechanism of drug release was anomalous (non-Fickian) type. Thus, it can be inferred that the increase in initial drug amount leads to increase in the fraction of surface bound drug in comparison with the fraction entrapped in the polymeric matrix. Further, it was supported by the fact that the formulations showed a trend of increasing burst release with increase in initial drug amount (Table 5.6).

PLGA formulations demonstrated significant decrease in the burst effect (M_{1h}) from 25.4 to 5.2% with an increase in the polymer proportion (Table 5.4). Similarly, MDT was found to increase from 12.5 to 22.3 h (Fig. 5.37). Interestingly, the mechanism of drug release was found to be unaffected as modified power law equation clearly indicated no change in exponent values ($n = 0.68 \pm 0.01$).

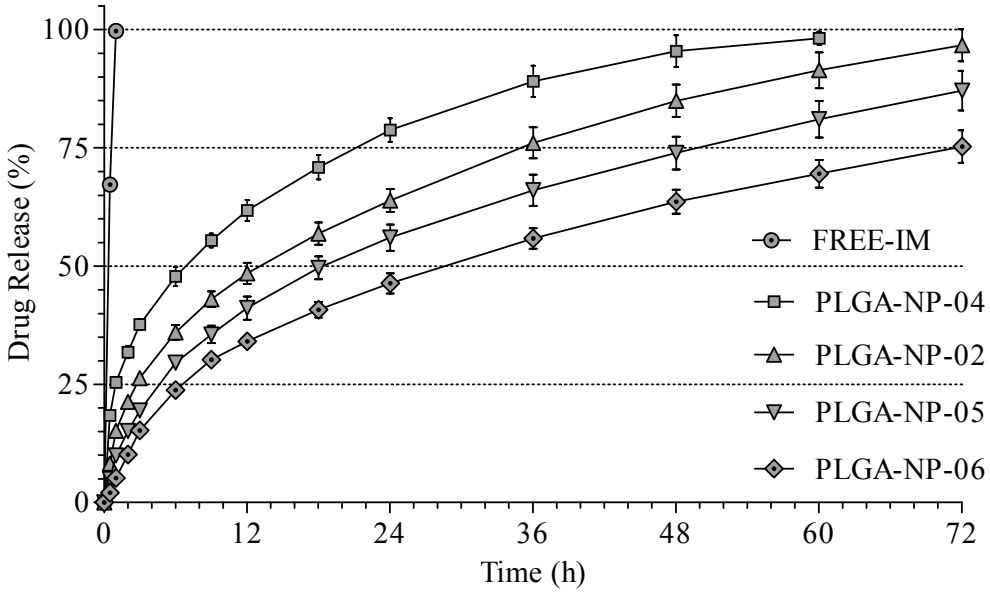

Fig. 5.37: In vitro drug release profile of PLGA nanoparticles prepared using different amount of the polymer. (Each data represents the average of three independent determinations)

A similar prominent decrease in burst effect (M_{1h}) from 36.0 to 12.2% was also observed with increase in the polymer proportion in PCL nanoparticles (Table 5.5; Fig. 5.38). Although the polymer amount from 50 to 100 mg has shown significant increase in MDT (≈ 55%), it was found to be unaffected (12.9 ± 0.8) by further increase in the amount of polymer up to 400 mg. Moreover, the MDT values were in agreement with recorded $T_{50\%}$ values of prepared formulations (Table 5.5).

Peppas modified power law model indicated that the release mechanism can be conveniently described by the anomalous diffusion process with the predominance of Fickian transport processes ($n = 0.70 \pm 0.04$) for high polymer proportion. However, at low polymer proportion (50 mg), the drug transport was purely Fickian diffusion type. Smaller particle size obtained with low polymer amount of 50 mg may be a reason for lower diffusional path length providing rapid drug release.

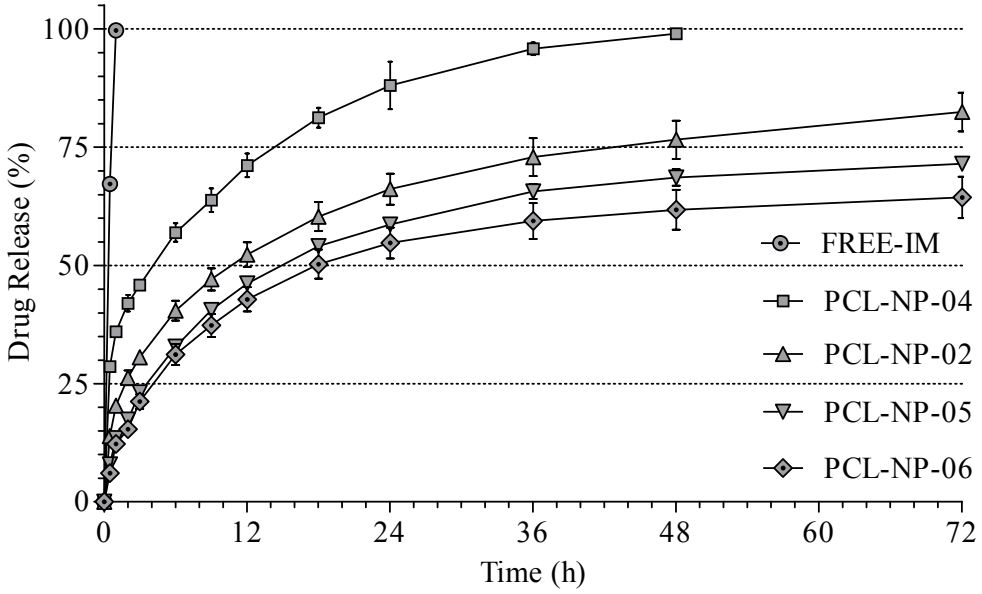

Fig. 5.38: In vitro drug release profile of PCL nanoparticles prepared using different amount of the polymer. (Each data represents the average of three independent determinations)

Moreover, the high drug release rate would have depleted significant fraction of the entrapped drug leaving only a small fraction of it in the polymeric matrix, which was latter released by non-Fickian transport mechanism.

On the other hand, formulations prepared with increasing amount of the polymer from 100 to 400 mg demonstrated increasing exponent value ($n = 0.64$ to 0.71) indicating significance of non-Fickian transport mechanism due to association of drug in the polymeric network. Further, increase in the average particle size with increasing polymer proportion led to increased diffusional path length that might have contributed to the decrease in release rate.

In case of PECA formulations, increase in amount of the monomer from 50 to 150 mg was found to extend the drug release with increase in MDT from 1 to 9 h

(Table 5.6; Fig. 5.39) The exponent values calculated from modified Peppas model were ranging between 0.64 and 1.11 implying the mechanism of drug release to be non-Fickian anomalous type.

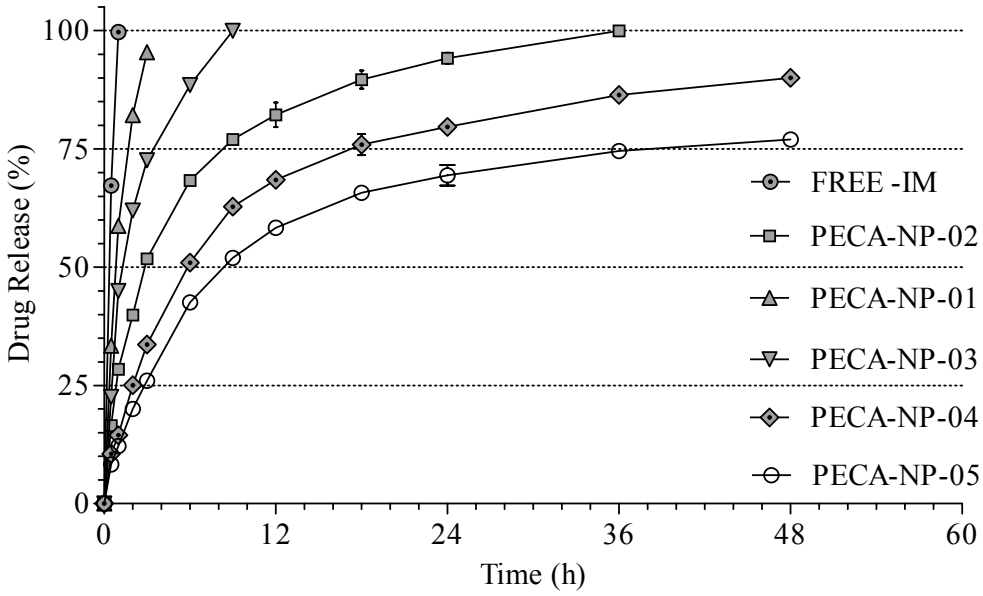

Fig. 5.39: In vitro drug release profile of PECA nanoparticles prepared using different amount of ECA monomer. (Each data represents the average of three independent determinations)

A higher drug release rate observed in the formulations with low monomer amount (50 mg) was due to relatively higher proportion of drug within the polymeric matrix. Thus, explaining the release mechanism as super case II.

The drug release from PLGA nanoparticles showed a decrease in the burst release with increase in the stabilizer concentration (Fig. 5.40 & 5.41). However, the extent of decrease in burst effect was significantly different for PVA and PF-68. Thus, it may be inferred that both the stabilizers aid in entrapment of the drug within polymeric matrix thereby reducing the surface adsorption of IM leading to decreased burst effect. Moreover, the entrapped drug might have been distributed evenly within the polymeric matrix as it resulted in nearly zero order drug release at higher concentrations of stabilizer.

In case of PCL nanoparticles prepared with PVA and PF-68 stabilizer resulted in a decreased burst effect with increasing stabilizer concentration. Moreover, both the stabilizers showed increase in MDT. However, the trend and magnitude of change was different (Table 5.5; Fig. 5.42 & 5.43). PVA showed a linear decrease in burst effect with

increasing stabilizer amount up to 2% *w/v*; while PF-68 demonstrated sudden decrease in burst effect with increase from 0.5 to 1% *w/v*, which was constant up to 2% *w/v*. Similarly, this trend was complemented by the observed values of MDT and $T_{50\%}$ for both the stabilizers.

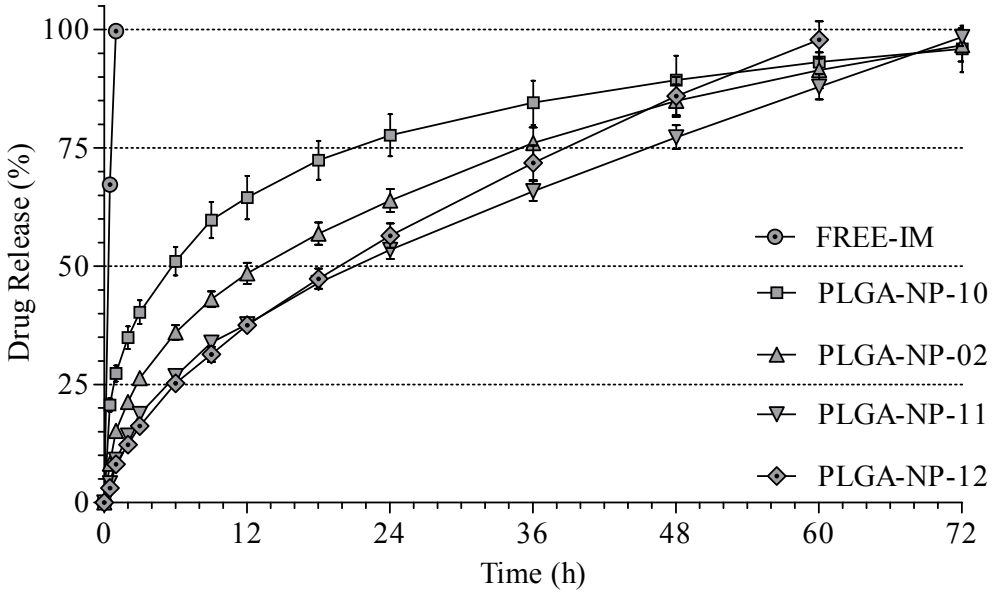

Fig. 5.40: In vitro drug release profile of PLGA nanoparticles prepared using different amount of PVA. (Each data represents the average of three independent determinations)

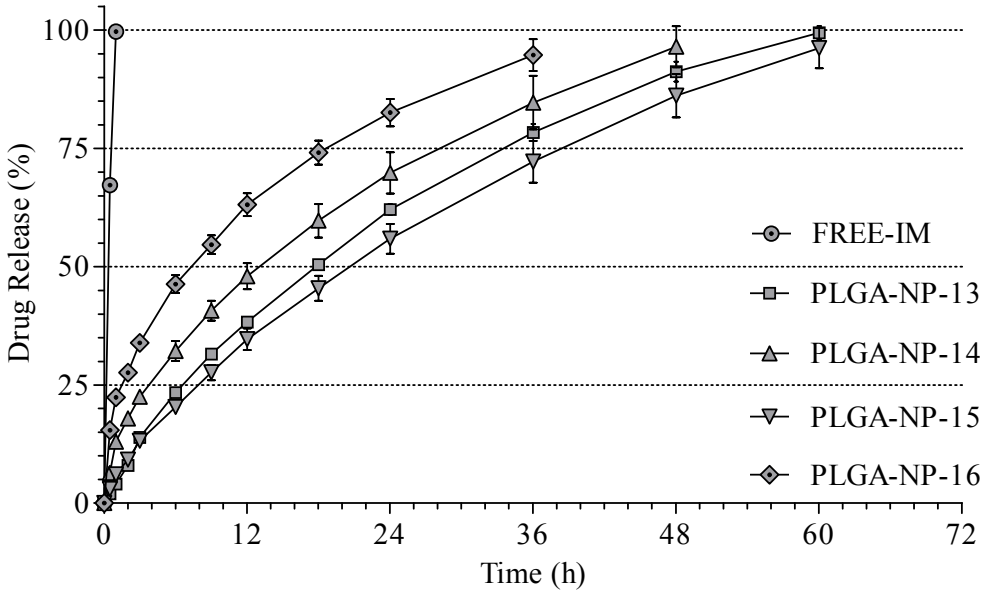

Fig. 5.41: In vitro drug release profile of PLGA nanoparticles prepared using different amount of PF-68. (Each data represents the average of three independent determinations)

The mechanism of the drug release from formulations prepared with PVA was found to be a combination of Fickian and non-Fickian transport processes. Considering a prominently increase in the obtained exponent value (n) from 0.59 to 0.78 with increasing stabilizer concentrations from 0.5 to 1.5% *w/v*, it can be suggested that the stabilizer contributed in the uniform dispersion of drug within the polymeric matrix. Moreover, non-Fickian drug transport processes play a significant role in latter cases where the drug is properly entrapped or associated within the polymeric network. Similar observations were also recorded with increasing concentrations of PF-68 (Table 5.5).

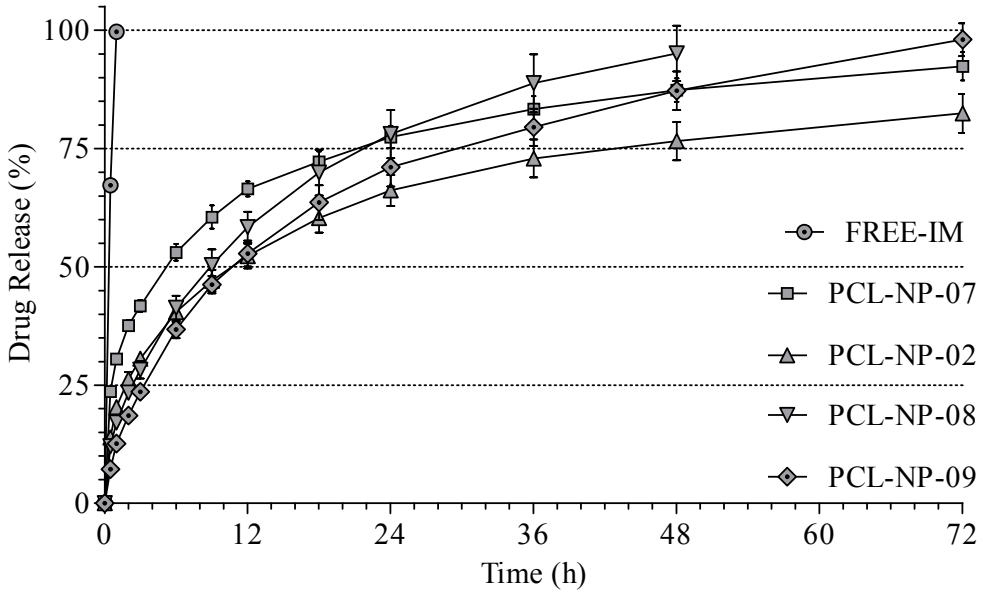

Fig. 5.42: In vitro drug release profile of PCL nanoparticles prepared using different amount of PVA. (Each data represents the average of three independent determinations)

However, a low release rate was observed with the use of PVA as a stabilizer in comparison with PF-68 (Fig. 5.42 & 5.43). This can be justified on the basis of previously reported findings that indicate the concurrent release of PVA with drug in micro-aqueous channel contributes to increased viscosity within these micro-channels that decreases drug diffusion (76). However, this phenomenon is absent in case of PF-68 as it led to relatively faster drug release from nanoparticles.

As described previously, a low particle size and increased porosity of polymeric system usually results in increased burst effect due to increased surface area and low diffusional path length. Conversely, in the present study, decrease in the average particle size with increasing stabilizer concentration did not result significant increase in burst release. The observation may be supported with the fact that the polymer degradation may initiate the

release of co-entrapped PF-68 molecules subsequently blocking the interconnected release pathways by converting into liquid crystalline state (47, 48). Similar findings are also reported in literature indicates altered drug release kinetics with the use of PF-68 in polymeric drug delivery systems (47, 48, 77-80). In the case of PVA, the release of PVA molecules may result in increased viscosity within the channels. Thus, the diffusional barrier within the polymeric matrices due to blockade of formed channels control the drug release with almost complete elimination of burst effect (76).

In general, poloxamers may increase or decrease the drug release by affecting the properties of drug delivery system such as miscibility, morphology, erosion, hydration etc. Few studies have also indicated that the co-encapsulation of various poloxamers into polymeric matrix systems result in the morphological transformations (47, 48, 77, 78). Poloxamer copolymers are reported to induce morphological transitions in the polymeric systems as increasing proportion of poloxamers in PLGA systems produce highly porous and capsular structures (78).

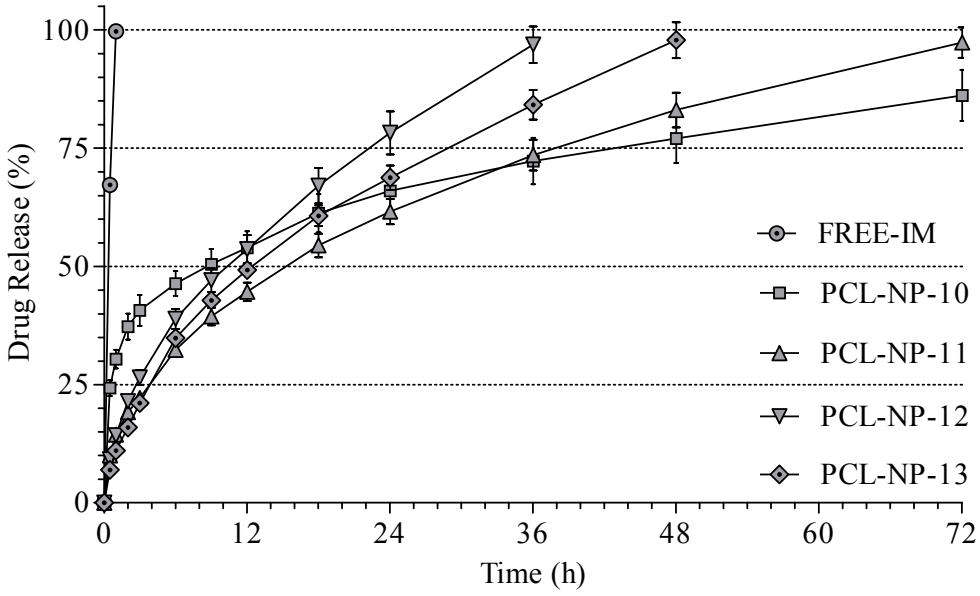

Fig. 5.43: In vitro drug release profile of PCL nanoparticles prepared using different amount of PF-68. (Each data represents the average of three independent determinations)

In case of PECA nanoparticles, an increase in amount of stabilizer resulted in proportionate increase in MDT from 3.3 to 13.2 h and the exponent values ranged between 0.57 and 0.66 (Table 5.6). The drug release mechanism was relatively unaffected by addition of stabilizer (Fig. 5.44).

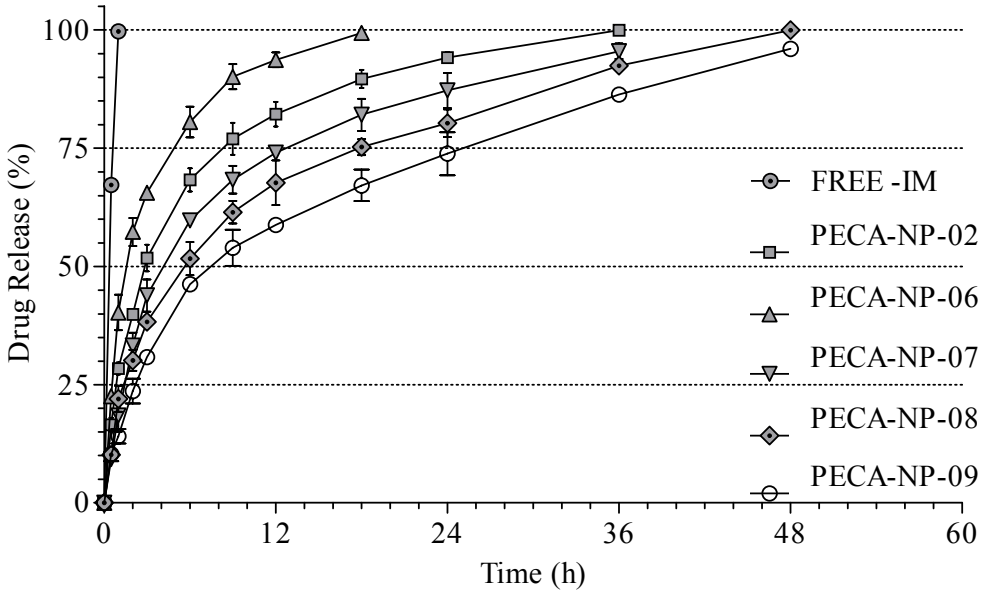

Fig. 5.44: In vitro drug release profile of PECA nanoparticles prepared using different amount of the stabilizer. (Each data represents the average of three independent determinations)

In case of PLGA nanoparticles, the aqueous phase pH has shown a considerable impact in the burst effect of PLGA nanoparticles as internal phase pH of 2.5 demonstrated less burst effect, which was found to increase with the increasing pH (Table 5.4). Similarly, the external phase pH of 6.5 showed negligible burst effect (M_{1h} < 5%), which was increased up to 23% with change in pH to 8.5 (Fig. 5.45). However, the exponent values of modified power law were found to be constant ($n = 0.69 \pm 0.03$) suggesting the combination of Fickian and non-Fickian drug transports as a release mechanism (Table 5.4). The effect of oil-water ratio of the primary and secondary emulsification was also found to be insignificant as the drug release profile remained unaffected by slight change in the aqueous phase ratio (Fig. 5.46). The exponent value from modified power law indicated that the drug release mechanism remains relatively unchanged ($n = 0.67 \pm 0.01$).

In case of PECA nanoparticles, the drug release profile was almost unaffected with change in pH of aqueous phase and duration of polymerization indicating complete polymerization in 4 h (Table 5.6; Fig. 5.47 & 5.48).

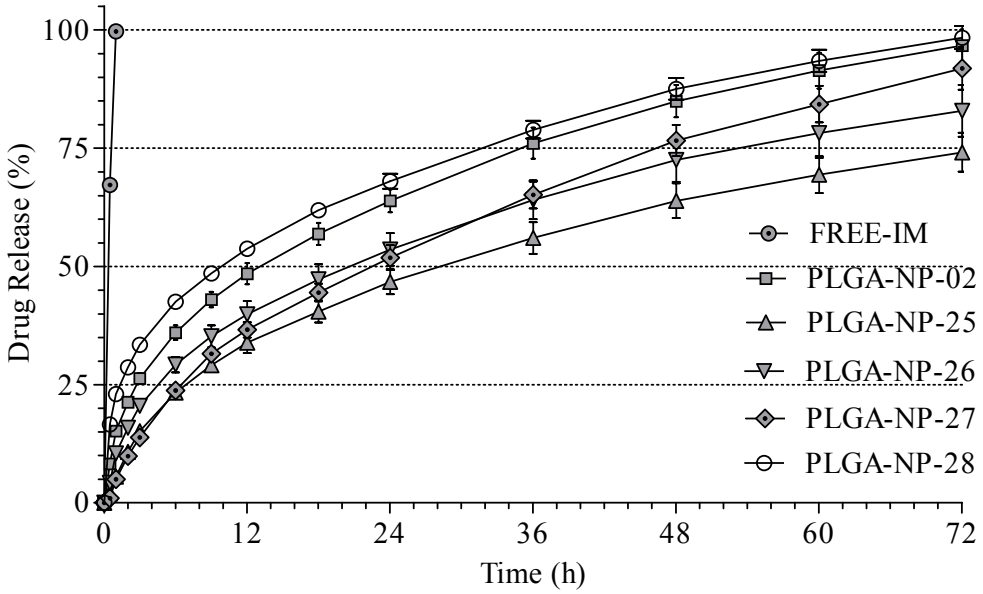

Fig. 5.45: In vitro drug release profile of PLGA nanoparticles prepared by changing the pH of aqueous phase. (Each data represents the average of three independent determinations)

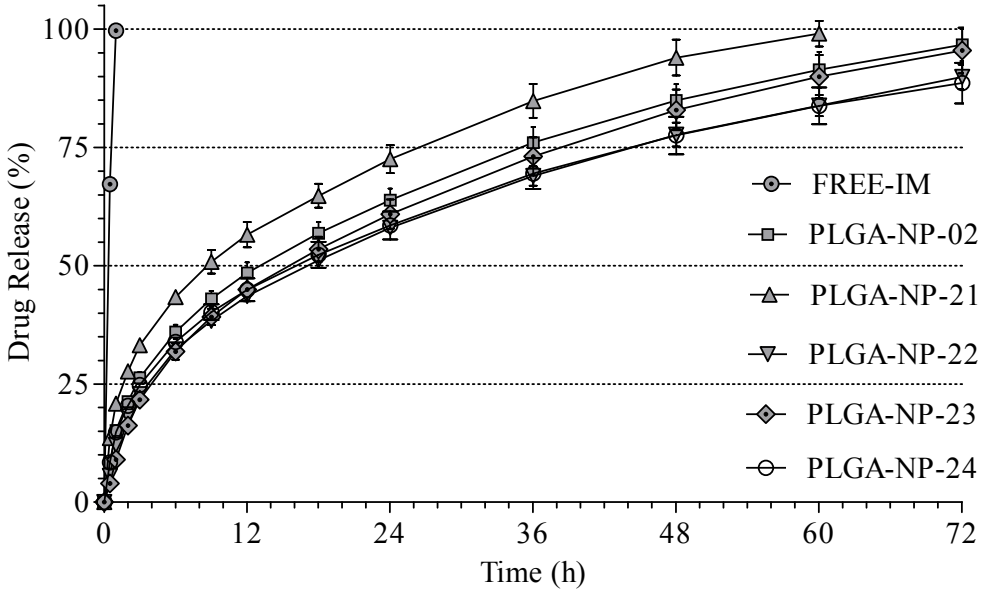

Fig. 5.46: In vitro drug release profile of PLGA nanoparticles prepared by changing the phase volume ratio. (Each data represents the average of three independent determinations)

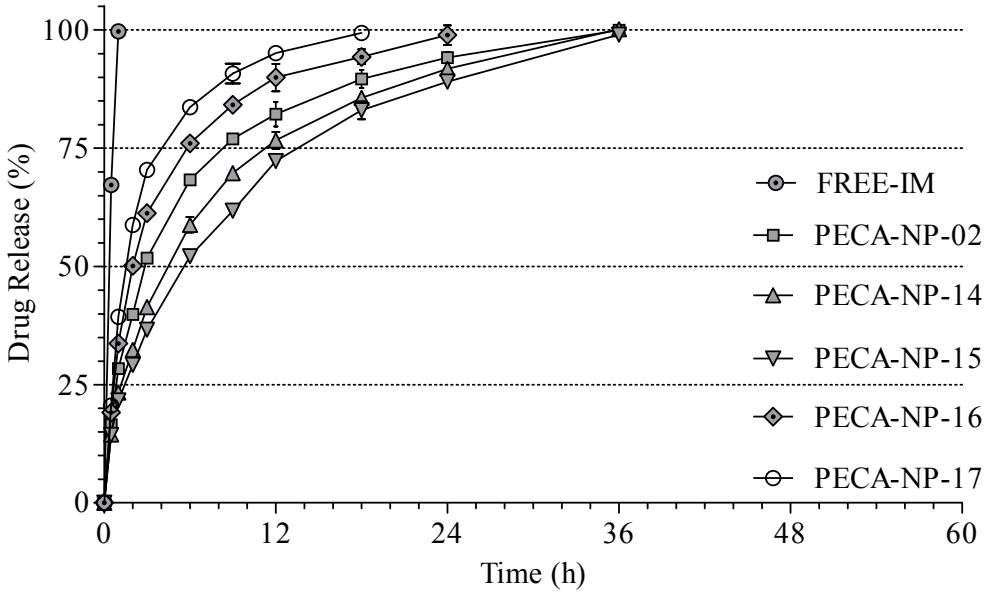

Fig. 5.47: In vitro drug release profile of PECA nanoparticles prepared by changing the pH of aqueous phase. (Each data represents the average of three independent determinations)

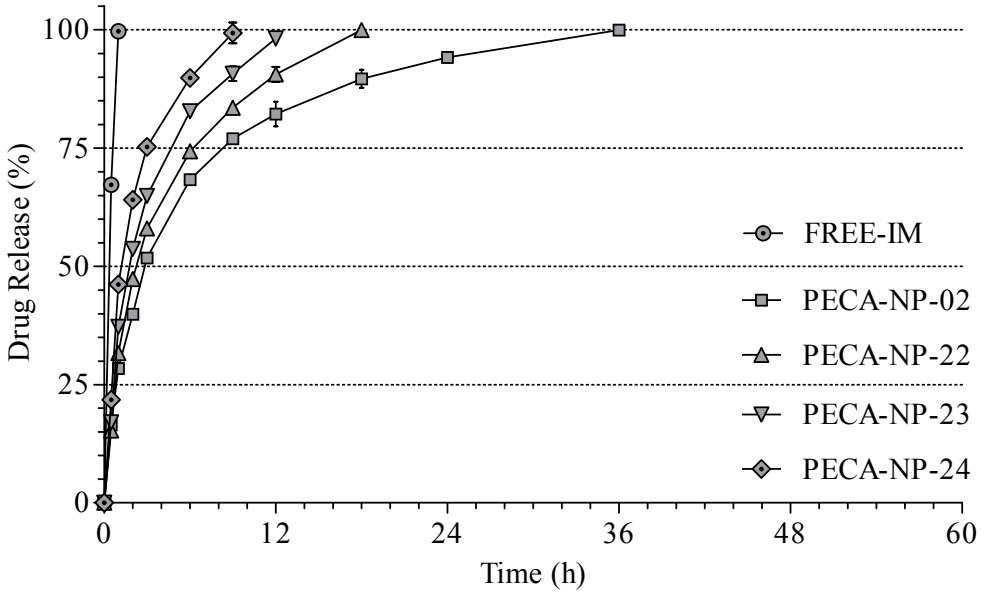

Fig. 5.48: In vitro drug release profile of PECA nanoparticles prepared by changing polymerization duration. (Each data represents the average of three independent determinations)

Thus, the emulsion solvent evaporation and interfacial polymerization techniques were found suitable for the preparation of IM loaded nanoparticles. The studied formulation and process parameters were found to influence the in vitro drug release characteristics of IM loaded PLGA, PCL and PECA nanoparticles.

5.3.3 Thermal analysis

DSC thermograms of PLGA nanoparticles have shown a glass transition temperature at 44.5°C with complete absence of melting endotherm up to 300°C. The thermograms of PCL and PECA nanoparticles showed a melting endotherm at 59.8 and 197°C, corresponding to the pure polymer. As described earlier, the DSC thermogram of the pure drug demonstrated a sharp endothermic peak ranged from 211.5ºC to 220.8ºC with average melting temperature (T_m) of 217°C ($\Delta H = -127.4\ J\ g^{-1}$). DSC thermograms of drug loaded formulations of PLGA, PCL and PECA have shown to preserve the pure drug endotherm peak between 211.5 and 220.8°C with slight decrease in enthalpy. Previously, several authours have observed similar findings, which were attributed to loss of crystallinity resulting from molecular level dispersion of the drug within the polymeric matrix. The DSC thermograms of physical mixtures further supported this fact as the melting endotherm and enthalpy values were found to be unaffected. Similar observations were also made in case of PECA nanoparticles, as the thermal analysis of physical mixture of polymer and IM was in good agreement with the drug loaded PECA nanoparticles suggesting molecular level dispersion of drug within the polymeric matrix. The thermograms indicated the association of stabilizer molecules PVA and PF-68 in the polymer matrix with the corresponding sharp melting peaks.

Further, the drug present in the physical mixture has shown sharp melting endotherm which was diminished in the formulations suggesting loss in crystallinity. Thermal analysis results indicated that the physical state of drug remains unchanged with the treatments given during manufacturing process and there is less possibility of physical interactions between the drug and polymers or other excipients.

5.3.4 Stability studies

PLGA formulations showed good dispersion state stability up to ten days at room temperature. Conversely, most of the PCL formulations have shown detectable aggregation within a week at room temperature. PECA nanoparticles have shown highest dispersion state stability at room temperature for 15 days. The observed aggregation in case of PLGA and PECA nanoparticles could be easily re-dispersed with mild ultrasonication treatment (1 min, at 15 W). PLGA nanoparticles showed good drug

stability for 15 days with better drug loading and entrapment efficiency. However, within 15 days PECA nanoparticles have shown highest drug loss with poor drug loading and entrapment efficiency (Table 5.7 & 5.8).

PLGA and PECA formulations stored at refrigerated temperature (5 ± 3°C) for three months in dispersed state have shown negligible aggregation with slight increase in average particle size and size distribution. PCL nanoparticles were found to be aggregated at the end of two months with significant increase in average particle size and size distribution. Moreover, the drug entrapment and loading efficiency were also found to affected. PLGA, PCL and PECA formulations stored at freeze temperature (−20 ± 3°C) did not show considerable change in initial properties up to three months.

Freeze dried formulations stored at refrigerated and freeze temperature were found to be stable for 6 months with acceptable change in various product characteristics such as size and size distribution, drug entrapment and loading efficiency. At room temperature, PCL nanoparticles showed poor redispersability even with ultrasonication treatment after three months. However, there was no significant change in the drug entrapment and loading efficiency. All freeze dried formulations showed better redispersability even after 1 year of storage at −20°C.

5.3.5 Redispersibility studies

For successful administration of prepared nanoparticles should be readily re-dispersed in media to provide uniform dispersion without aggregation. Redispersibility was studied after freeze drying of the formulations and the particle size and size distribution was compared with fresh dispersions. All freeze-dried samples PLGA and PECA nanoparticulate formulations showed acceptable re-dispersability in TDW with and without stabilizers. PCL nanoparticles showed slight increase in average particle size and polydispersity index. Excellent re-dispersability was recorded with PLGA formulations. The effect on particle size and size distribution of freeze dying was studied using particle size analysis and TEM is shown below.

Table 5.7: Stability of nanoparticles stored at various temperature conditions (1 month).

	Batch No.	Initial		AT (25 ± 1°C)		RT (5 ± 3°C)		FT (-20 ± 3°C)	
		PS	Assay (LE‡)	PS	Assay (LE‡)	PS	Assay (LE‡)	PS	Assay (LE‡)
Dispersions	PLGA-NP-02	229 ± 2.07	19.63 ± 1.18	254 ± 3.15	14.77 ± 0.84	242 ± 2.66	17.43 ± 1.13	236 ± 3.56	19.24 ± 1.49
	PLGA-NP-14	212 ± 2.61	22.54 ± 0.55	240 ± 1.89	16.74 ± 1.23	234 ± 4.72	19.94 ± 1.04	220 ± 4.21	22.23 ± 0.74
	PCL-NP-02	284 ± 3.20	7.54 ± 0.93	354 ± 2.34	5.84 ± 1.05	342 ± 2.98	6.01 ± 0.93	328 ± 4.87	7.12 ± 0.87
	PCL-NP-11	261 ± 3.63	13.61 ± 1.18	312 ± 5.98	10.69 ± 1.12	298 ± 3.77	12.13 ± 1.34	292 ± 2.95	13.14 ± 1.34
	PECA-NP-02	226 ± 1.91	25.58 ± 0.89	220 ± 2.09	16.81 ± 0.98	228 ± 4.52	23.18 ± 1.36	234 ± 3.44	25.09 ± 1.22
	PECA-NP-25	232 ± 1.69	24.58 ± 0.74	226 ± 3.11	14.97 ± 1.31	232 ± 3.92	22.09 ± 1.51	238 ± 4.07	24.49 ± 1.07

PS - average particle size (nm); LE - drug loading efficiency (% *w/w*) presented as assay. ‡Each data represents the average and standard deviation of three independent determinations.

Table 5.8: Stability of nanoparticles stored at various temperature conditions (6 months).

	Batch No.	Initial		AT (25 ± 1°C)		RT (5 ± 3°C)		FT (-20 ± 3°C)	
		PS	Assay (LE‡)	PS	Assay (LE‡)	PS	Assay (LE‡)	PS	Assay (LE‡)
Freeze dried	PLGA-NP-02	233 ± 1.93	19.63 ± 1.18	242 ± 2.03	18.77 ± 0.66	239 ± 3.13	19.12 ± 1.32	233 ± 3.99	19.14 ± 0.99
	PLGA-NP-14	222 ± 1.78	22.54 ± 0.55	231 ± 2.55	21.74 ± 0.72	228 ± 4.34	21.94 ± 1.35	222 ± 5.01	22.24 ± 0.34
	PCL-NP-02	324 ± 1.55	7.54 ± 0.93	336 ± 3.94	6.84 ± 0.39	332 ± 2.73	6.94 ± 0.78	324 ± 5.22	7.04 ± 0.42
	PCL-NP-11	288 ± 2.32	13.61 ± 1.18	311 ± 5.05	12.69 ± 0.98	298 ± 3.98	13.13 ± 1.01	288 ± 3.31	13.23 ± 0.78
	PECA-NP-02	228 ± 1.76	25.58 ± 0.89	248 ± 4.43	24.81 ± 1.12	238 ± 3.98	24.29 ± 0.76	230 ± 4.87	25.11 ± 0.93
	PECA-NP-25	235 ± 1.13	24.58 ± 0.74	251 ± 4.35	23.97 ± 0.33	243 ± 3.88	23.74 ± 0.93	235 ± 4.09	24.57 ± 0.33

PS - average particle size (nm); LE - drug loading efficiency (% *w/w*) presented as assay. ‡Each data represents the average and standard deviation of three independent determinations.

5.4 Conclusions

PLGA and PCL nanoparticles were prepared successfully using double emulsion - solvent evaporation technique, whereas the interfacial in situ polymerization technique was used successfully for the preparation of PECA nanoparticles. The various formulation parameters such as polymer, surfactant and drug proportion along with other processing conditions were found to affect critical properties of nanoparticles including particle size, size distribution, entrapment and loading efficiency, in vitro drug release profile. Further, the studied correlations helped in designing formulations of intended characteristics such as high drug entrapment efficiency, smaller particle size and size distribution by optimization of critical parameters.

The developed formulations have shown high drug entrapment within the polymeric matrix with excellent particle morphology. PLGA and PCL formulations prepared using PF-68 and PVA found to have small particle size with narrow size distribution. Similarly, interfacial in situ polymerization method has shown to provide small PECA nanoparticles with uniform size distribution. The drug release characteristics were achieved found to be influenced by the proportion of polymer, drug and stabilizer. The in vitro drug release studies revealed that the developed formulations extended the drug release over 48-72 h, which could be useful for controlled drug delivery properties.

Thus, the nanoparticles prepared using biodegradable polymers were found to be suitable for the drug delivery application of hydrophilic drug with high drug entrapment and better loading efficiency. Moreover, the thermal studies have confirmed uniform distribution of the drug, at molecular level, within the polymeric matrix without showing any chemical and physical interactions between the drug and polymer or excipients. The optimized freeze-dried formulations have shown better stability at freeze temperature as the formulations have shown acceptable redispersability with no significant change in average particle size, size distribution and entrapment efficiency. Consequently, the developed methods were found to be simple and suitable for the preparation of stable polymeric nanoparticles with acceptable reproducibility. However, increasing drug loading efficiency remains a significant challenge for hydrophilic drugs. The obtained results also justify the rationale for conducting preclinical investigations including in vivo pharmacokinetic and biodistribution studies to assess the suitability of the controlled and/or targeted drug delivery application of IM.

Considering the advantages such as smaller particle size, narrow size distribution (monodispersed), biodegradability and biocompatibility properties, the prepared

nanoparticles would suitable for oral and intra-venous administration. In addition, the extended drug release characteristics would be advantageous for the long term intracellular drug delivery. Thus, it may aid in enhancing the therapeutic efficacy of drug along with improved safety and increased patient compliance. The proposed method of preparation of polymeric nanoparticles can extended to other hydrophilic drugs including protein and peptide drugs to improve stability and/or enhance tissue specific bioavailability.

References

1. G.M. Barratt. Therapeutic applications of colloidal drug carriers. Pharm Sci Technolo Today 3:163-171 (2000).
2. K. Westesen, H. Bunjes, G. Hammer, and B. Siekmann. Novel colloidal drug delivery systems. PDA J Pharm Sci Technol. 55:240-247 (2001).
3. I. Brigger, C. Dubernet, and P. Couvreur. Nanoparticles in cancer therapy and diagnosis. Adv Drug Deliv Rev. 54:631-651 (2002).
4. M. Chorny, I. Fishbein, H.D. Danenberg, and G. Golomb. Lipophilic drug loaded nanospheres prepared by nanoprecipitation: effect of formulation variables on size, drug recovery and release kinetics. J Control Release. 83:389-400 (2002).
5. C. Duclairoir, A.M. Orecchioni, P. Depraetere, and E. Nakache. Alpha-tocopherol encapsulation and in vitro release from wheat gliadin nanoparticles. J Microencapsul. 19:53-60 (2002).
6. C. Duclairoir, A.M. Orecchioni, P. Depraetere, F. Osterstock, and E. Nakache. Evaluation of gliadins nanoparticles as drug delivery systems: a study of three different drugs. Int J Pharm. 253:133-144 (2003).
7. C. Vauthier, D. Labarre, and G. Ponchel. Design aspects of poly(alkylcyanoacrylate) nanoparticles for drug delivery. J Drug Target. 15:641-663 (2007).
8. C. Vauthier, C. Dubernet, E. Fattal, H. Pinto-Alphandary, and P. Couvreur. Poly(alkylcyanoacrylates) as biodegradable materials for biomedical applications. Adv Drug Deliv Rev. 55:519-548 (2003).
9. Y. Tabata, S. Gutta, and R. Langer. Controlled delivery systems for proteins using polyanhydride microspheres. Pharm Res. 10:487-496 (1993).
10. J. Kreuter and H.R. Hartmann. Comparative study on the cytostatic effects and the tissue distribution of 5-fluorouracil in a free form and bound to polybutylcyanoacrylate nanoparticles in sarcoma 180-bearing mice. Oncology. 40:363-366 (1983).

11. M.R. Gasco and M. Trotta. Nanoparticles from microemulsions. Int J Pharm. 29:267–268 (1986).
12. A.E. Gulyaev, S.E. Gelperina, I.N. Skidan, A.S. Antropov, G.Y. Kivman, and J. Kreuter. Significant transport of doxorubicin into the brain with polysorbate 80-coated nanoparticles. Pharm Res. 16:1564-1569 (1999).
13. J.L. Arias, V. Gallardo, S.A. Gomez-Lopera, R.C. Plaza, and A.V. Delgado. Synthesis and characterization of poly(ethyl-2-cyanoacrylate) nanoparticles with a magnetic core. J Control Release. 77:309-321 (2001).
14. A. Bootz, V. Vogel, D. Schubert, and J. Kreuter. Comparison of scanning electron microscopy, dynamic light scattering and analytical ultracentrifugation for the sizing of poly(butyl cyanoacrylate) nanoparticles. Eur J Pharm Biopharm. 57:369-375 (2004).
15. E. Fattal, B. Roques, F. Puisieux, M.J. Blanco-Prieto, and P. Couvreur. Multiple emulsion technology for the design of microspheres containing peptides and oligopeptides. Adv Drug Deliv Rev. 28:85-96 (1997).
16. S. Watnasirichaikul, N.M. Davies, T. Rades, and I.G. Tucker. Preparation of biodegradable insulin nanocapsules from biocompatible microemulsions. Pharm Res. 17:684-689 (2000).
17. S. Watnasirichaikul, T. Rades, I.G. Tucker, and N.M. Davies. In-vitro release and oral bioactivity of insulin in diabetic rats using nanocapsules dispersed in biocompatible microemulsion. J Pharm Pharmacol. 54:473-480 (2002).
18. S. Watnasirichaikul, T. Rades, I.G. Tucker, and N.M. Davies. Effects of formulation variables on characteristics of poly (ethylcyanoacrylate) nanocapsules prepared from w/o microemulsions. Int J Pharm. 235:237-246 (2002).
19. N. Behan, C. Birkinshaw, and N. Clarke. Poly n-butyl cyanoacrylate nanoparticles: a mechanistic study of polymerisation and particle formation. Biomaterials. 22:1335-1344 (2001).
20. T. Govender, S. Stolnik, M.C. Garnett, L. Illum, and S.S. Davis. PLGA nanoparticles prepared by nanoprecipitation: drug loading and release studies of a water soluble drug. J Control Release. 57:171-185 (1999).
21. M. Muller, B. Kessler, and S. Richter. Preparation of monomodal polyelectrolyte complex nanoparticles of PDADMAC/poly(maleic acid-alt-alpha-methylstyrene) by consecutive centrifugation. Langmuir. 21:7044-7051 (2005).

22. M.T. Peracchia, C. Vauthier, F. Puisieux, and P. Couvreur. Development of sterically stabilized poly(isobutyl 2-cyanoacrylate) nanoparticles by chemical coupling of poly(ethylene glycol). J Biomed Mater Res. 34:317-326 (1997).
23. J.W. Nah, Y.W. Paek, Y.I. Jeong, D.W. Kim, C.S. Cho, S.H. Kim, and M.Y. Kim. Clonazepam release from poly(DL-lactide-co-glycolide) nanoparticles prepared by dialysis method. Arch Pharm Res. 21:418-422 (1998).
24. S. Movva. Studies on preparation, characterization and pharmacokinetics of etoposide loaded nanoparticles, Ph. D. Thesis, Birla Institute Technology and Science, Pilani, Rajasthan, 2006.
25. C.G. Pitt, M.M. Gratzl, G.L. Kimmel, J. Surles, and A. Schindler. Aliphatic polyesters II. The degradation of poly (DL-lactide), poly (epsilon-caprolactone), and their copolymers in vivo. Biomaterials. 2:215-220 (1981).
26. A.G. Coombes, S.C. Rizzi, M. Williamson, J.E. Barralet, S. Downes, and W.A. Wallace. Precipitation casting of polycaprolactone for applications in tissue engineering and drug delivery. Biomaterials. 25:315-325 (2004).
27. I. Engelberg and J. Kohn. Physico-mechanical properties of degradable polymers used in medical applications: a comparative study. Biomaterials. 12:292-304 (1991).
28. Z.G. Tang, R.A. Black, J.M. Curran, J.A. Hunt, N.P. Rhodes, and D.F. Williams. Surface properties and biocompatibility of solvent-cast poly[-caprolactone] films. Biomaterials. 25:4741-4748 (2004).
29. Y. Ogawa, M. Yamamoto, H. Okada, T. Yashiki, and T. Shimamoto. A new technique to efficiently entrap leuprolide acetate into microcapsules of polylactic acid or copoly(lactic/glycolic) acid. Chem Pharm Bull (Tokyo). 36:1095-1103 (1988).
30. A. Lamprecht, N. Ubrich, M. Hombreiro Perez, C. Lehr, M. Hoffman, and P. Maincent. Biodegradable monodispersed nanoparticles prepared by pressure homogenization-emulsification. Int J Pharm. 184:97-105 (1999).
31. H. Murakami, M. Kobayashi, H. Takeuchi, and Y. Kawashima. Preparation of poly(DL-lactide-co-glycolide) nanoparticles by modified spontaneous emulsification solvent diffusion method. Int J Pharm. 187:143-152 (1999).
32. H.Y. Kwon, J.Y. Lee, S.W. Choi, Y. Jang, and J.H. Kim. Preparation of PLGA nanoparticles containing estrogen by emulsification-diffusion method. Colloid Surf A Physicochem Eng Asp 182:123-130 (2001).

33. H. Jeffery, S.S. Davis, and D.T. O'Hagan. The preparation and characterization of poly(lactide-co-glycolide) microparticles. II. The entrapment of a model protein using a (water-in-oil)-in-water emulsion solvent evaporation technique. Pharm Res. 10:362-368 (1993).
34. A. Budhian, S.J. Siegel, and K.I. Winey. Haloperidol-loaded PLGA nanoparticles: systematic study of particle size and drug content. Int J Pharm. 336:367-375 (2007).
35. D. Quintanar-Guerrero, H. Fessi, E. Allemann, and E. Doelker. Influence of stabilizing agents and preparatives variables on the formation of poly(d,l-lactic acid) nanoparticles by an emulsification-diffusion technique. Int J Pharm. 143:133–141 (1996).
36. M.I. Llovet, M.A. Egea, J. Valero, M.A. Alsina, M.L. García, and A. Chauvet. Methotrexateloaded nanoparticles: Analysis of drug content and study of the matrix structure. Drug Dev Ind Pharm. 21:1761-1771 (1995).
37. J.L. Arias, V. Gallardo, S.A. Gómez-Lopera, and A.V. Delgado. Loading of 5-Fluorouracil to poly (ethyl-2-cyanoacrylate) nanoparticles with a magnetic core. J Biomed Nanotechnol. 1:214-223 (2005).
38. J.L. Arias, V. Gallardo, M.A. Ruiz, and A.V. Delgado. Ftorafur loading and controlled release from poly(ethyl-2-cyanoacrylate) and poly(butylcyanoacrylate) nanospheres. Int J Pharm. 337:282-290 (2007).
39. S.K. Sahoo, J. Panyam, S. Prabha, and V. Labhasetwar. Residual polyvinyl alcohol associated with poly (D,L-lactide-co-glycolide) nanoparticles affects their physical properties and cellular uptake. J Control Release 82:105-114 (2002).
40. X. Song, Y. Zhao, W. Wu, Y. Bi, Z. Cai, Q. Chen, Y. Li, and S. Hou. PLGA nanoparticles simultaneously loaded with vincristine sulfate and verapamil hydrochloride: Systematic study of particle size and drug entrapment efficiency. Int J Pharm *In press* (2007).
41. S. Tesch, B. Freudig, and H. Schubert. Production of Emulsions in High-Pressure Homogenizers Part I: Disruption and Stabilization of Droplets. Ultrasound. 7:8.
42. B. Freudig, S. Tesch, and H. Schubert. Production of emulsions in high-pressure homogenizers-Part 2: Significance of cavitation for size reduction droplets. Chemie Ingenieur Technik. 74:880-880 (2002).
43. S. Tesch, B. Freudig, and H. Schubert. Production of emulsions in high-pressure homogenizers-Part 1: Size reduction and stabilization of droplets. Chemie Ingenieur Technik. 74:875-879 (2002).

44. J. Floury, J. Legrand, and A. Desrumaux. Analysis of a new type of high pressure homogeniser. Part B. study of droplet break-up and recoalescence phenomena. Chemical Engineering Science. 59:1285-1294 (2004).
45. S. Galindo-Rodriguez, E. Allemann, H. Fessi, and E. Doelker. Physicochemical parameters associated with nanoparticle formation in the salting-out, emulsification-diffusion, and nanoprecipitation methods. Pharm Res. 21:1428-1439 (2004).
46. F. Boury, H. Marchais, J.P. Benoit, and J.E. Proust. Surface characterization of poly(alpha-hydroxy acid) microspheres prepared by a solvent evaporation/extraction process. Biomaterials. 18:125-136 (1997).
47. T.G. Park, S. Cohen, and R. Langer. Controlled protein release from polyethyleneimine-coated poly(L-lactic acid)/pluronic blend matrices. Pharm Res. 9:37-39 (1992).
48. T.G. Park and A.S. Hoffman. Estimation of temperature-dependent pore size in poly(N-isopropylacrylamide) hydrogel beads. Biotechnol Prog. 10:82-86 (1994).
49. M. Tobio, J. Nolley, Y. Guo, J. McIver, and M.J. Alonso. A novel system based on a poloxamer/PLGA blend as a tetanus toxoid delivery vehicle. Pharm Res. 16:682-688 (1999).
50. M.N. Ravi Kumar. Nano and microparticles as controlled drug delivery devices. J Pharm Pharm Sci. 3:234-258 (2000).
51. T. Feczkó, J. Tóth, and J. Gyenis. Comparison of the preparation of PLGA-BSA nano- and microparticles by PVA, Poloxamer and PVP. Colloid Surf A Physicochem Eng Asp In Press:doi:10.1016/j.colsurfa.2007.1007.1011 (2007).
52. J.L. Arias, M.A. Ruiz, V. Gallardo, and A.V. Delgado. Tegafur loading and release properties of magnetite/poly(alkylcyanoacrylate) (core/shell) nanoparticles. J Control Release *In press* (2007).
53. B. Petri, A. Bootz, A. Khalansky, T. Hekmatara, R. Muller, R. Uhl, J. Kreuter, and S. Gelperina. Chemotherapy of brain tumour using doxorubicin bound to surfactant-coated poly(butyl cyanoacrylate) nanoparticles: revisiting the role of surfactants. J Control Release. 117:51-58 (2007).
54. J.L. Arias, M.A. Ruiz, M. Lopez-Viota, and A.V. Delgado. Poly(alkylcyanoacrylate) colloidal particles as vehicles for antitumour drug delivery: A comparative study. Colloids Surf B Biointerfaces *In press* (2007).

55. F. Fawaz, M. Guyot, A.M. Lagueny, and J.P. Devissaguet. Ciproflexacin-loaded polyisobutylcyanoacrylate nanoparticles: Preparation and characterization. Int J Pharm. 154:191-203 (1997).
56. G. Fontana, G. Pitarresi, V. Tomarchio, B. Carlisi, and P.L. San Biagio. Preparation, characterization and in vitro antimicrobial activity of ampicillin-loaded polyethylcyanoacrylate nanoparticles. Biomaterials. 19:1009-1017 (1998).
57. R.M. Mainardes and R.C. Evangelista. PLGA nanoparticles containing praziquantel: effect of formulation variables on size distribution. Int J Pharm. 290:137-144 (2005).
58. R.M. Mainardes and R.C. Evangelista. Praziquantel-loaded PLGA nanoparticles: preparation and characterization. J Microencapsul. 22:13-24 (2005).
59. R.M. Mainardes, M.V. Chaud, M.P. Gremiao, and R.C. Evangelista. Development of praziquantel-loaded PLGA nanoparticles and evaluation of intestinal permeation by the everted gut sac model. J Nanosci Nanotechnol. 6:3057-3061 (2006).
60. M.T. Peracchia, C. Vauthier, C. Passirani, P. Couvreur, and D. Labarre. Complement consumption by poly(ethylene glycol) in different conformations chemically coupled to poly(isobutyl 2-cyanoacrylate) nanoparticles. Life Sci. 61:749-761 (1997).
61. C. Vauthier, C. Dubernet, C. Chauvierre, I. Brigger, and P. Couvreur. Drug delivery to resistant tumors: the potential of poly(alkyl cyanoacrylate) nanoparticles. J Control Release 93:151-160 (2003).
62. S.J. Douglas, L. Illum, S.S. Davis, and J. Kreuter. Particle size and size distribution of poly (butyl-2-cyanoacrylate) nanoparticles. I: Influence of physicochemical factors. J Colloid Interface Sci. 101:149-158 (1984).
63. A. Lamprecht, N. Ubrich, H. Yamamoto, U. Schafer, H. Takeuchi, C.M. Lehr, P. Maincent, and Y. Kawashima. Design of rolipram-loaded nanoparticles: comparison of two preparation methods. J Control Release 71:297-306 (2001).
64. T. Jung, W. Kamm, A. Breitenbach, E. Kaiserling, J.X. Xiao, and T. Kissel. Biodegradable nanoparticles for oral delivery of peptides: is there a role for polymers to affect mucosal uptake? Eur J Pharm Biopharm. 50:147-160 (2000).
65. D. Lemoine, C. Francois, F. Kedzierewicz, V. Preat, M. Hoffman, and P. Maincent. Stability study of nanoparticles of poly(epsilon-caprolactone), poly(D,L-lactide) and poly(D,L-lactide-co-glycolide). Biomaterials 17:2191-2197 (1996).
66. D. Lemoine and V. Preat. Polymeric nanoparticles as delivery system for influenza virus glycoproteins. J Control Release 54:15-27 (1998).

67. J. Panyam, M.M. Dali, S.K. Sahoo, W. Ma, S.S. Chakravarthi, G.L. Amidon, R.J. Levy, and V. Labhasetwar. Polymer degradation and in vitro release of a model protein from poly(D,L-lactide-co-glycolide) nano- and microparticles. J Control Release 92:173-187 (2003).
68. N. Brasseur, D. Brault, and P. Couvreur. Adsorption of hematoporphyrin onto polyalkylcyanoacrylate nanoparticles: carrier capacity and drug release. Int J Pharm. 70:129-135 (1991).
69. M.A. Radwan. In vitro evaluation of polyisobutylcyanoacrylate nanoparticles as a controlled drug delivery system of theophylline. Drug Dev Ind Pharm. 21:2371-2375 (1995).
70. F. Némati, C. Dubernet, H. Fessi, A.C. de Verdière, M.F. Poupon, F. Puisieux, and P. Couvreur. Reversion of multidrug resistance using nanoparticles in vitro: influence of the nature of the polymer. Int J Pharm. 138:237-246 (1996).
71. G. Gonzalez-Martin, I. Merino, M.N. Rodriguez-Cabezas, M. Torres, R. Nunez, and A. Osuna. Characterization and trypanocidal activity of nifurtimox-containing and empty nanoparticles of polyethylcyanoacrylates. J Pharm Pharmacol. 50:29-35 (1998).
72. C.E. Soma, C. Dubernet, D. Bentolila, S. Benita, and P. Couvreur. Reversion of multidrug resistance by co-encapsulation of doxorubicin and cyclosporin A in polyalkylcyanoacrylate nanoparticles. Biomaterials 21:1-7 (2000).
73. F. Burkersroda, L. Schedl, and A. Göpferich. Why degradable polymers undergo surface erosion or bulk erosion. Biomaterials. 23:4221-4231 (2002).
74. M. Miyajima, A. Koshika, J. Okada, A. Kusai, and M. Ikeda. Factors influencing the diffusion-controlled release of papaverine from poly (L-lactic acid) matrix. J Control Release 56:85-94 (1998).
75. M. Miyajima, A. Koshika, J. Okada, and M. Ikeda. Effect of polymer/basic drug interactions on the two-stage diffusion-controlled release from a poly(L-lactic acid) matrix. J Control Release 61:295-304 (1999).
76. J.R. DesNoyer and A.J. McHugh. The effect of Pluronic on the protein release kinetics of an injectable drug delivery system. J Control Release 86:15-24 (2003).
77. H. Huatan, J.H. Collett, and D. Attwood. The microencapsulation of protein using a novel ternary blend based on poly (epsilon-caprolactone). Journal of Microencapsulation 12:557-567 (1995).

78. M.D. Blanco and M.J. Alonso. Development and characterization of protein-loaded poly (lactide-co-glycolide) nanospheres. European Journal of Pharmaceutics and Biopharmaceutics 43:287-294 (1997).
79. M. Tobío, R. Gref, A. Sánchez, R. Langer, and M.J. Alonso. Stealth PLA-PEG Nanoparticles as Protein Carriers for Nasal Administration. Pharmaceutical Research 15:270-275 (1998).
80. K.G. Carrasquillo, A.M. Stanley, J.C. Aponte-Carro, P. De Jesus, H.R. Costantino, C.J. Bosques, and K. Griebenow. Non-aqueous encapsulation of excipient-stabilized spray-freeze dried BSA into poly(lactide-co-glycolide) microspheres results in release of native protein. J Control Release 76:199-208 (2001).

6. Pharmacokinetic Studies

6.1 Introduction

The fundamental objective of any drug delivery system is to provide effective therapeutic concentration at the site of action for intended duration to produce the desirable pharmacological effects with minimal or no undesirable or toxicological effects. Although the therapeutic advantage of the drug regimen is principally attributed to its intrinsic activity, the concentration levels and duration for which it is maintained at the site of action are critical for successful therapy. After administration of the dosage form, the conventional delivery systems (CDDS) undergoes processes such as release of the free drug from dosage form, absorption of the free drug into systemic circulation through various biological membranes, distribution to several body tissues including the site of action, subsequently providing the therapeutic effect. Further, the free drug also undergoes metabolism and excretion from the body. Thus, the main drawback of conventional delivery system is a non-selective distribution of drug in the body leading to wastage of drug resulting from the distribution to undesired sites. Moreover, it leads to the untoward and toxic effects to normal host cells.

On the contrary, the nanoparticulate drug delivery system (Nano-DDS) is capable of selectively crossing some of the biological barriers to reach targeted organs of the body depending upon their characteristics. In addition, it also offers extended protection to drug from enzymatic and chemical degradation on its transit towards the site of action from the site of administration. The spatial distribution of a drug inside the body is also altered by the physicochemical properties of the polymeric material. Thus, the Nano-DDS may exhibit significantly different biodistribution compared to CDDS in the sequence of events that transfer a drug to the site of action and maintain its concentration throughout the treatment (1, 2). Thus, the increased rate and extent of drug delivery to the site of action along with the controlled distribution of drug inside the body would eventually improve the efficiency of drug delivery system leading to quicker onset of action, better therapeutic efficacy with minimal untoward effects and better patient compliance (3, 4).

From a regulatory point of view, an important consideration for the development of any drug delivery system (DDS) is the quantity of evidence needed under particular circumstances to substantiate the proof of therapeutic effectiveness. The concept of improved therapeutic efficacy by using Nano-DDS is based on the assumption that nanoparticles, with the specific properties, are capable of selectively crossing cellular barriers and delivering drug to the site of action at a controlled rate (5-7). Considering the fact that the in vivo fate of drug in a Nano-DDS is significantly different compared to

CDDS, detailed in vivo investigations to determine the biological fate of prepared Nano-DDS is essential (8). Moreover, as the formulations based on Nano-DDS have capability to modulate in vivo absorption, distribution, metabolism and elimination behavior of drug, the pharmacokinetic profile of Nano-DDS and CDDS may not be identical (9). Further, the drug release from Nano-DDS can be extended because of polymer presence. Thus, it is important to have complete understanding of the relationship between drug concentration and therapeutic effect or response, in the preclinical animal models before exploring its final clinical benefits. Thus, the effectiveness of a developed Nano-DDS as a new drug product can not be demonstrated without complete pharmacokinetic studies (10, 11).

Although FDA has not released specialized guidelines for nanotechnology based formulations, the pharmacokinetic requirements for NDDS covered under federal register are extended to these formulations (21 CFR Part 314, 1998) (12). As of now, these regulations indicate that pharmacokinetic data obtained from the plasma concentration time profile of a drug under investigation is sufficient for its regulatory approval as Nano-DDS. Although the purpose of a pharmacokinetic study is to verify the safety and efficacy of the candidate drug, the application of pharmacokinetic principles in the design and development of the Nano-DDS provide the rational for designing effective and better drug delivery system (13-15). Moreover, the study aid in understanding the complex relationship of these unit biological processes to modulate the intensity and time duration of therapeutic and adverse effects of drug.

6.2 Experimental

6.2.1 Materials and Instruments

Drug and all chemicals were obtained from sources as mentioned in Chapter 5. A peristaltic pump (Heidolph, Germany) fitted with silastic cannula (1/16" *i.d.* × 3/16" *o.d.*) was used for pulse free movement of perfusion and drug solution. Urethane procured from Sigma Aldrich Chemicals, USA was used as an anesthetic agent. A tissue tearer - Sorvall® (DuPont Instruments, USA) and ultrasonic cell disruptor - Microson™ (Misonix, USA) were used for tissue homogenization. All surgical instruments such as scissors, forceps, glass syringes, silk suture etc. were used after sterilization.

a) Animals

Healthy male Wistar rats were selected for pharmacokinetics and biodistribution studies of pure drug IM and two IM loaded nanoparticulate formulations in serum, brain and lungs. Rats with average weight of 225 ± 25 g (12-15 weeks old) were procured from

Central Animal Facility (CAF), BITS, Pilani. Selected animals were housed in a group of three in standard plastic cages. Animals were maintained at controlled environmental conditions (temperature 20 ± 2°C & relative humidity 50 ± 10%) and artificial light-dark cycle (12 h). Rats were acclimatized to the study environment for at least five days prior to commencement of work. Animals were fed with standard laboratory pellet food (Hindustan Unilever Ltd., India) with water *ad libitum*. All experimental protocols were approved by the Institutional Animal Ethics Committee (IAEC) prior to the commencement of work and all experimental procedures including euthanasia and disposal of carcass were in accordance with the guidelines set by the Institute, IAEC and the Committee for the Purpose of Control and Supervision of Experiments on Animals (CPCSEA), India. All animals were kept under observation during the entire study for any unusual signs, general conditions, potential clinical signs, toxicity or mortality.

b) Blank biological matrix

Few untreated healthy rats (225 ± 25 g) were selected for generation of drug-free bio-matrix pool of serum, brain and lungs.

6.2.2 In situ rat intestinal absorption studies

In order to study the role of efflux proteins on the absorption kinetics of IM, the in situ rat intestinal absorption studies were carried out with the pure drug IM (IM-PD) and the effect of 1% *w/v* Polysorbate-80 (IM + PT-80) and 1% *w/v* Poloxamer 188 (IM + PF-68) on the absorption kinetics of IM was compared with the known efflux transport inhibitor - 2% *w/v* Cyclosporine A (IM + CS-A). Moreover, selected nanoparticulate formulations (PLGA-NP, PCL-NP & PECA-NP) were also investigated. The principle objective was to investigate the permeability and absorption kinetics of IM, the role of efflux proteins on the permeability and absorption kinetics of the drug and the effect of efflux mechanism on the selected IM loaded nanoparticulate formulations. Although nanoparticulate inherently bypass efflux transporters, the free drug released from nanoparticles inside the cell remains a good substrate for efflux proteins (Fig. 1.3). Incorporation of efflux protein inhibitors in nanoparticles may provide additional mechanism that inhibits the efflux transport and thereby increase the intracellular residence time of the free drug. Previously, several authors have used rat as an experimental model for investigating the intestinal transport kinetics of various drugs (16-22). Moreover, it has also been extensively used to explore the role of particular efflux protein by selectively inhibiting one or more efflux proteins (19, 23-26).

a) Preparation of solutions and buffers

Sorensen's buffer was prepared fresh by mixing 19.2 mL of 0.067 M KH_2PO_4 and 80.8 mL of 0.067 M Na_2HPO_4 solutions and pH was adjusted to 7.4 using orthophosphoric acid. Similarly, perfusion solution was prepared fresh by dissolving 8.48 g of NaCl, 0.34 g of KCl, 0.14 g of $CaCl_2$ and 0.78 g of NaH_2PO_4 in a liter of pure water.

Urethane solution was prepared fresh by dissolving 10 g of urethane in 10 mL of pure water and it was administered at a dose of 1 g per Kg of the body weight.

b) Formulation and sample preparation

Aqueous solutions of IM prepared by dissolving the pure drug in Sorensen's buffer (pH 7.4) at 37 ± 2°C at three concentration levels (10, 100 & 1000 µg mL^{-1}) were used for pure drug in situ absorption studies. Aqueous dispersions of nanoparticulate formulations prepared by dispersing the amount equivalent to 1 mg of IM in 10 mL of Sorensen's buffer (pH 7.4) were used for in situ absorption studies of nanoparticulate formulations. Aliquot of the freshly reconstituted formulations and drug solutions were analyzed for the drug content by using chromatographic method as described in Chapter 3. All the solutions were prepared fresh and used immediately without any additional treatments.

c) Preliminary studies

Before initiating the rat intestinal absorption studies, solubility of IM in Sorensen's buffer (pH 7.4) at 37 ± 2°C was determined as per the procedure described in Chapter 4. Stability of the drug in Sorensen's buffer was also carried out at 37 ± 2°C for six hours at three concentration levels (10, 100 & 1000 µg mL^{-1}). The peristaltic pump was calibrated for accurate and stable delivery of drug solution at a flow rate of 0.9 mL min^{-1}.

Finally, the adsorption of the drug on silastic cannula was studied at three concentration levels to confirm the suitability of the recirculation model. For this purpose, 10 mL of the drug solution in Sorensen's buffer was placed in reservoir and re-circulated through the silastic cannula for 120 min. Samples were withdrawn at predetermined intervals from the drug solution reservoir and the percentage of the drug adsorbed onto silastic cannula was calculated.

d) Surgical procedure, sample collection and processing

Selected rats were fasted overnight (15-18 h) before initiating the study with water *ad libitum*. Lapractomy was performed on individual animal after intra-peritoneal

administration of 1% *w/v* urethane solution (1 g Kg^{-1}). The abdomen region of rat was depilated and approximately 1 cm mid-ventral abdominal incision was made under anesthesia. Small intestine was exposed gently and ligament of trietz was identified. A small incision was made on the intestine at 5 cm distal to the ligament of trietz (pyloric end).

One end of silastic cannula was secured tight in jejunum (pyloric end) and other end was dipped inside perfusion reservoir passing though the cassette of peristaltic pump. Another small incision was made at 15 cm distal to the first incision and intestine was flushed by passing perfusion solution (37 ± 2°C). One end of second cannula was secured tight at the lower end, which was marked at 15 cm distal to first incision and the free end was placed inside perfusion reservoir forming a closed-loop recirculation model. Surgical procedure was performed carefully such that none of the major blood vessels were blocked and the exposed part of the intestine was gently placed inside the abdominal cavity (Fig. 6.1).

Initially, perfusion solution was removed by passing air and pre-weighed reservoir containing drug solution in Sorenson buffer was attached to the peristaltic pump. Immediately, the drug solution was passed through intestine at a flow rate of 0.9 mL min^{-1} and the experimental setup was maintained at 37 ± 2°C.

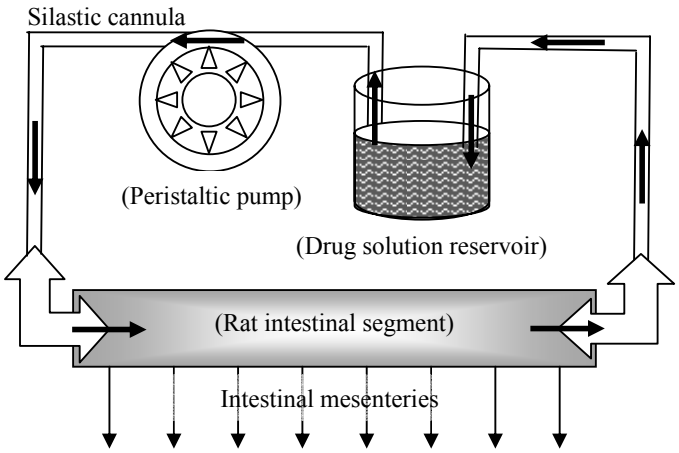

Fig. 6.1: Schematic representation of the closed-loop recirculation model of in situ intestinal absorption studies.

At predetermined time intervals, aliquot of 100 µL samples were collected from the reservoir during the experiment. After 2 h, the drug solution was collected in the reservoir by passing the air and the final volume was recorded. All studies were performed in triplicate and samples were suitably diluted, centrifuged (10,000 rpm, 5 min & 15°C) and

analyzed by the chromatographic method. Correction factor was employed to account the losses due to water absorption during the experimental duration.

In addition, the luminal excretion studies were also carried out in a similar manner as that of the in situ rat intestinal absorption studies. For this purpose, drug was administered at a dose of 25 mg per Kg of the body weight though intra-venous route and blank Sorensen's buffer was circulated in the lumen. At predetermined time intervals, aliquot of 100 µL samples were collected from the reservoir and excretion of the drug in lumen was monitored by the chromatographic method.

e) Data analysis

The log percentage of the drug remaining to be absorbed was plotted as function of time and the least square linear regression analysis was performed. The slope of curve (m) was used to calculate the apparent absorption rate constant and the absorption half-life using following formulae.

$$\text{The apparent absorption rate constant } (K_a) = \text{slope of the curve (m)} \times -2.303$$

$$\text{The apparent absorption half-life } (HL_a) = 0.693 / K_a$$

Statistical significance of the individual treatment on the apparent absorption rate constant and the absorption half-life of IM was determined using Student's t-test at 5% level of significance.

6.2.3 In vivo pharmacokinetic and biodistribution studies

Single dose intravenous and oral pharmacokinetic studies were carried out for pure drug IM (IM-PD) and selected nanoparticulate formulations (PECA-NP & PLGA-NP). The drug concentration levels in serum, brain and lungs were determined in healthy rat model for determining biodistribution profile, pharmacokinetic parameters and expected therapeutic efficacy. The principle objective was to investigate the overall systemic and tissue specific bioavailability and understand the difference between the in vivo biodistribution behavior of pure drug and drug loaded nanoparticles after oral and intra-venous administration.

a) Formulation and sample preparation

The pure drug was administered in the form of aqueous solution, which was prepared fresh by diluting IM with phosphate buffer saline (pH 7.4). Similarly, the nanoparticulate formulations were administered in a form of aqueous dispersions, which were prepared fresh in phosphate buffer saline (pH 7.4) by vortex mixing. Aliquot of the freshly reconstituted formulations and drug solutions were analyzed for the drug content by the

validated chromatographic method as described in Chapter 3. The prepared solutions were used immediately for pharmacokinetic and biodistribution studies of IM without any additional treatments.

b) Administration of free drug and nanoparticles

For each study, the selected animals (36 rats) were divided randomly in a group of three and all studies were carried out in triplicate. Rats were fasted overnight (15-18 h) before starting the study, however, adequate water was provided. Before drug treatment, all rats were marked according to the standard labeling scheme and animal weights were recorded. The in vivo pharmacokinetic and biodistribution studies were performed for oral and intra-venous administration of pure drug and drug loaded formulations as per standard protocol.

For intra venous administration, the dose equivalent to 25 mg of IM per kg of the body weight was administrated through the caudal vein using a 1 mL syringe (25 G × ½" needle) under light ether anesthesia, after dilating the vein with xylene. For oral administration, the dose equivalent to 50 mg of IM per Kg of the body weight of individual animal was delivered by intra-gastric administration using an oral feeding catheter.

c) Serum and tissue sample collection and processing

From each animal, one blood sample was collected per animal from heart using a cardiac puncture technique at predetermined time intervals (at 0.5, 1, 1.5, 3, 6, 9, 12, 18, 24, 36, 48 & 72 h of the post-dosing). At each time point, approximately 0.6 mL of blood sample was withdrawn using a 2 mL syringe (21 G × 1" needle) under ether anesthesia. Collected samples were transferred immediately to a labeled glass tubes and it was allowed to clot naturally for 60 min at room temperature. Serum samples were harvested by centrifugation (3000 rpm, 15 min & 4°C). Separated serum samples were labeled and stored at – 80°C in a sealed cryovials, until analysis.

Immediately after blood sampling, the whole blood was drained from the *inferior vena cava* using a 10 mL syringe (21 G × 1" needle) and lungs and brain were collected by surgical process. For this purpose, under ether anesthesia the abdominal incision was made with a clean scissor to expose all organs and whole blood was drained. Lungs were perfused with phosphate buffer saline to remove residual blood inside organs and they were carefully excised. Separated lungs sample was transferred to an ice-cold Petri dish containing phosphate buffer saline and temperature was maintained. All tissues were cleaned with 2 to 5 mL of phosphate buffer saline and blotted dried with Whatman filter

paper. Further, rat was laid on its ventral aspect in the dissection tray and the skin over the head was removed in order to completely expose the skull surface. A midline incision was made over the skull with a surgical knife and the entire brain was dissected out.

Each tissue sample was weighed accurately and chopped using a tissue tearer. Immediately, it was transferred to a clean and dried tissue homogenizer and equal volume of phosphate buffer saline was added. Before drug extraction, individual tissues were homogenized (2.5 min, 30 s/cycle & 10 W) to get fine suspension using a tissue homogenizer - ultrasonic cell disruptor in an ice-cold bath. Fine tissue homogenates were properly labeled and stored in a clean sealed glass vial at –80°C, until analysis. All samples were processed and analyzed by the validated chromatographic method, within 15 days time period from the sample collection.

d) Analysis of biological samples

The serum and tissue samples obtained from each animal at respective time point were processed independently. Concentration of the drug in biological matrices was determined by the bioanalytical method described in Chapter 3.

e) Pharmacometric data analysis

The drug concentration in various tissues such as serum, brain and lungs at different time intervals were analyzed by the non-compartmental analysis method using WinNonlin® *ver.* 2.1 (Pharsight Corporation, USA) software. The maximum drug concentration (C_{max}) and time to reach maximum concentration (T_{max}) were determined by model independent method. While, various pharmacokinetic parameters such as the area under the curve (AUC), the area under the moment curve (AUMC), the mean residence time (MRT) etc. were obtained from WinNonlin®. In addition, the mean absorption time (MAT) was calculated from the obtained MRT values of respective formulations after the oral and intra-venous administration. Finally, the results of the in vivo pharmacokinetic and biodistribution studies were assessed using suitable statistical tests with $P < 0.05$ level of significance.

6.3 Results and Discussion

6.3.1 In situ rat intestinal absorption studies

a) Preliminary studies

The drug was found to be freely soluble in Sorensen's buffer (pH 7.4) with approximate solubility of 1.15 ± 0.09 mg mL^{-1} at 37 ± 2°C. IM showed no significant degradation in the buffer at 37 ± 2°C for six hours at three selected concentration levels (10, 100 &

1000 µg mL^{-1}). At 20 rpm, the peristaltic pump accurately delivered 0.9 mL min^{-1} of drug solution for 2 h. Adsorption studies confirmed that IM does not adsorb on silastic cannula significantly and the maximum percentage loss in drug concentration recorded over 2 h was less than 0.2 ± 0.081% at 100 µg mL^{-1}. Thus, the preliminary studies confirmed that the experimental setup is suitable for in situ rat intestinal absorption studies as the drug was stable in Sorensen's buffer. Moreover, there was no significant loss observed due to adsorption of IM on the walls of silastic cannula under the experimental conditions.

b) Intestinal absorption and efflux studies

In situ rat intestinal absorption studies of pure drug indicated excellent intestinal permeability of free IM with a rapid decrease in concentration of IM from the system. Statistical analysis indicated the absorption kinetics can be well described by the first order process. Although insignificant, a slight increase in the apparent absorption rate constant was recorded with increase in the drug concentration levels from 10 to 100 µg mL^{-1} (Table 6.1). But there was no further increase observed with increase in the drug concentration level to 1000 µg mL^{-1}. This phenomenon indicated the saturating behavior of luminal efflux transporters with increasing drug concentration.

Table 6.1: Summary of the in situ absorption parameters

Treatments	Apparent Absorption Rate Constant (h^{-1})	Apparent Absorption Half-life (h)	Flux (µg h^{-1} cm^2)
IM (10 µg mL^{-1})	0.35 ± 0.09	2.09 ± 0.58	0.29 ± 0.07
IM (100 µg mL^{-1})	0.58 ± 0.06	1.20 ± 0.12	0.58 ± 0.06
IM (1000 µg mL^{-1})	0.61 ± 0.55	1.13 ± 0.11	0.56 ± 0.07
CS-A (2% *w/v*) + IM (100 µg mL^{-1})	0.81 ± 0.04	0.86 ± 0.04	0.69 ± 0.06
PT-80 (1% *w/v*) + IM (100 µg mL^{-1})	0.73 ± 0.04	0.95 ± 0.05	0.68 ± 0.04
PF-68 (1% *w/v*) + IM (100 µg mL^{-1})	0.74 ± 0.06	0.94 ± 0.08	0.63 ± 0.08
PLGA-NP (100 µg mL^{-1})	0.51 ± 0.09	1.38 ± 0.25	0.42 ± 0.06
PCL-NP (100 µg mL^{-1})	0.29 ± 0.06	2.48 ± 0.53	0.26 ± 0.07
PECA-NP (100 µg mL^{-1})	0.54 ± 0.05	1.29 ± 0.11	0.43 ± 0.05

The high apparent absorption rate constant of 0.58 ± 0.06 h^{-1} was recorded for free drug (100 µg mL^{-1}) and the apparent absorption half-life was approximately 1 20 ± 0.12 h. The luminal excretion studies indicated that almost 2.56 ± 0.45% of the dose is eliminated in the small intestine with the 2 h of study duration, which may have been principally eliminated by drug efflux transporters.

When co-administered with P-gp inhibitor – CS-A, the drug showed enhanced permeation with increased flux and decreased absorption half-life. Thus, it may be confirmed that IM is a good substrate for efflux proteins like P-gp. Intestinal drug efflux mechanism has been reported as the major rate limiting step in the absorption of several anticancer drugs and it is a single largest factor known to contribute towards the acquired pharmacokinetic resistance. It can be concluded that like all other anti-cancer drugs, IM has potential to develop acquired pharmacokinetic resistance which may be overcome by co-administering a P-gp inhibitor.

Moreover, studies revealed that PF-68 and PT-80 used in the preparation of nanoparticles have potential in inhibiting the efflux mechanisms effectively. Nanoparticles prepared using these stabilizers would release it constantly along with the drug preventing efflux transport of the free drug. Thus, the application of nanoparticles would eliminate the chances of acquired resistance.

In situ rat intestinal absorption studies of prepared nanoparticles revealed that the PLGA and PECA nanoparticles are absorbed rapidly with the apparent absorption rate constant of 0.51 and 0.54 h^{-1}, respectively. Both, the PLGA and PECA nanoparticles showed similar absorption behavior with the apparent half-life of 1.38 and 1.29 h, respectively. PCL nanoparticles showed slow absorption behavior among all studied nanoparticles with the apparent absorption rate constant of 0.29 h^{-1} and the apparent half-life of 2.48 h.

6.3.2 In vivo pharmacokinetic and biodistribution studies

a) Serum pharmacokinetic studies

i) Intra-venous administration

The drug concentration in serum versus time curve following single intra-venous dose of the pure drug, PECA nanoparticles and PLGA nanoparticles are shown in Fig. 6.2. The various pharmacokinetic parameters calculated using a data modeling software are listed in Table 6.2. Pharmacokinetic profile of intra-venous administration of IM showed a rapid distribution of IM into tissues with fall in the concentration of drug in the systemic circulation followed by a slow elimination of the drug suggesting two-compartment distribution profile. Even at 72 h of the post dosing, the detectable amount of the drug (0.056 mg L^{-1}) was found in serum.

The non-compartmental data analysis indicated AUC_{∞} of 102.72 mg h L^{-1} and $AUMC_{\infty}$ of 1010.31 mg h^2 L^{-1}. MRT was found to be 9.83 h and apparent volume of distribution at steady-state (V_{ss}) was recorded as 2.40 L kg^{-1}. The total systemic clearance (Cl) was

found to be 0.24 L kg^{-1} h^{-1} and the elimination half-life in serum was approximately 6.81 h.

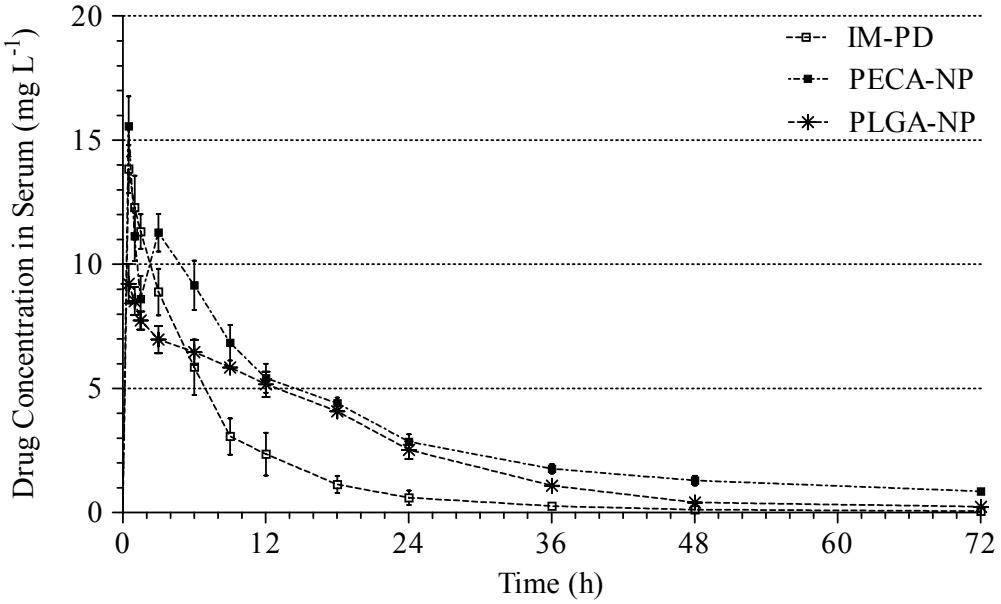

Fig. 6.2: IM concentration in serum versus time profile following intra-venous administration of the pure drug, PECA nanoparticles and PLGA nanoparticles in rats (Each value represents the mean ± standard deviation of three independent determinations)

Intra-venous administration of PECA nanoparticles indicated significant increase in AUC_{∞} to 262.29 mg h L^{-1}. MRT was found to increase to 31.15 h with reduced systemic clearance (Cl) to 0.10 L kg^{-1} h^{-1}. The apparent volume of distribution at steady-state (V_{ss}) was found to be 3.91 L kg^{-1} with increase in elimination half-life in the serum (21.59 h).

Intra-venous administration of PLGA nanoparticles also resulted in increased retention of the drug in the body with increased AUC_{∞} to 166.85 mg h L^{-1}. The MRT was found to increase to 17.98 h with reduced total systemic clearance (Cl) to 0.15 L kg^{-1} h^{-1}. The apparent volume of distribution at steady-state (V_{ss}) was found to be 3.07 L kg^{-1} with increased elimination half-life in serum (12.46 h).

Thus, both the PLGA and PECA nanoparticles were effectively increased serum drug concentration for longer duration of time with approximate two and three fold increase in drug residence time in the body, respectively. The increased AUC and serum concentration levels may be attributed to change in overall distribution profile. In

addition, increased retention of drug in the serum with reduced elimination would have contributed further.

Table 6.2: Summary of the pharmacokinetic parameters in serum after intra-venous administration of IM and IM loaded nanoparticles.

Parameters	Pure Drug Imatinib Mesylate	PECA Nanoparticles	PLGA Nanoparticles
AUC_{∞} (mg h L^{-1})	102.72	262.28	166.85
V_{ss} (L kg^{-1})	2.40	3.91	3.07
Cl (L h^{-1} kg^{-1})	0.24	0.10	0.15
Half-life (h)	6.81	21.59	12.47
MRT (h)	9.83	31.15	17.99

ii) Oral administration

The drug concentration in serum versus time curve following single oral dose of the pure drug, PECA nanoparticles and PLGA nanoparticles are shown in Fig. 6.3. The various pharmacokinetic parameters calculated are listed in Table 6.3. The oral pharmacokinetic studies of the pure drug indicated a rapid absorption of IM into systemic circulation with the maximum drug concentration (C_{max}) of 15.45 mg L^{-1} in serum at 3 h (T_{max}) of the post dosing. Results were in agreement with the in situ rat intestinal absorption studies, wherein, the rate of pure drug disappearance was significantly high and the apparent absorption half-life. Immediately after oral administration of the pure drug, a quantifiable amount of the drug (6.89 mg L^{-1}) was found in serum at 0.5 h.

In non-compartmental data analysis, the zero and first moment of serum concentration versus time curve foe pure drug resulted in the AUC_{∞} of 178.79 mg h L^{-1} and $AUMC_{\infty}$ of 2011.20 mg h^2 L^{-1}. The mean residence time (MRT) was found to be 11.25 h and apparent volume of distribution (V_d/F) was recorded as 3.14 L kg^{-1}. The apparent clearance (Cl/F) was found to be 0.28 L kg^{-1} h^{-1} and the elimination half-life in serum calculated based on MRT was about 7.80 h.

Oral pharmacokinetic studies of PECA formulations revealed that the nanoparticles has relatively slower rate of absorption but increased extent of absorption in comparison with the pure drug. The maximum drug concentration (C_{max}) of 14.08 mg L^{-1} was found in serum at 9 h (T_{max}) of the post dosing. These findings were in agreement with the in situ rat intestinal absorption studies, wherein, the rate of the drug disappearance from rat

intestinal compartment was relatively slow in comparison with the pure drug. After drug administration, a quantifiable amount of drug was found in serum (1.58 mg L^{-1}) at 0.5 h.

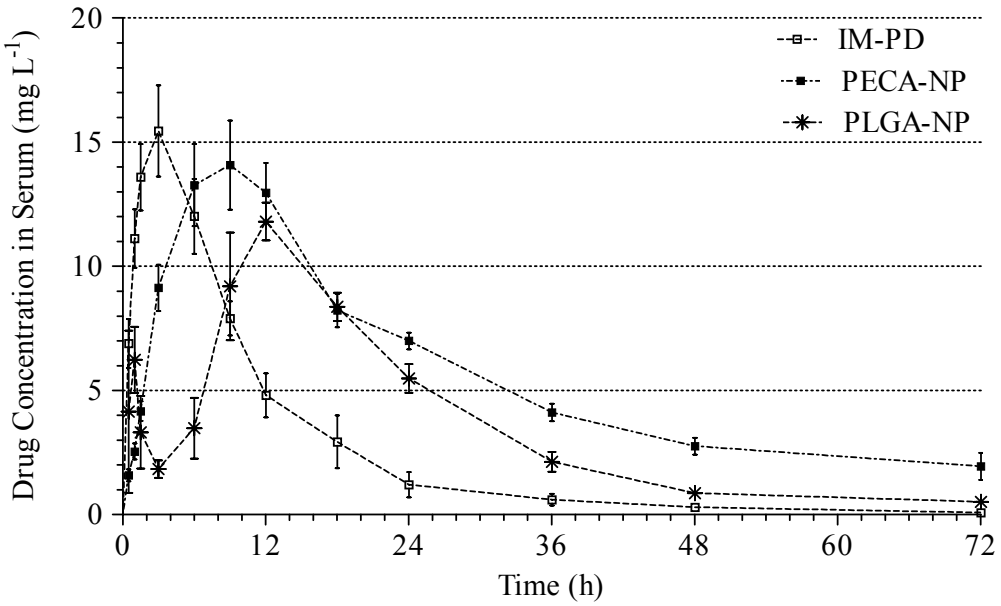

Fig. 6.3: IM concentration in serum versus time profile following oral administration of the pure drug, PECA nanoparticles and PLGA nanoparticles in rats (Each value represents the mean ± standard deviation of three independent determinations)

Interestingly, the non-compartmental data analysis indicated significant increase in the AUC_{∞} of 465.58 mg h L^{-1}, more than two fold. The drug has shown increase in the amount in serum and increase in residence in the body with approximate two fold increase in the elimination half-life in serum (25.62 h) and significant decrease in the apparent clearance (Cl/F) to 0.10 L kg^{-1} h^{-1}. Moreover, MRT of IM loaded PECA nanoparticles was significantly increased in comparison to pure drug (11.81 to 36.97 h). The changed apparent volume of distribution (V_d/F) of 4.15 L kg^{-1} and increased serum concentration levels indicated altered distribution profile of IM.

Similar to PECA nanoparticles, the PLGA nanoparticles also showed relatively slower absorption rate but increased extent of absorption in comparison with the pure drug. The maximum drug concentration (C_{max}) of 11.80 mg L^{-1} in serum was observed at 12 h (T_{max}) of the post dosing.

After oral administration of PLGA nanoparticles, a quantifiable amount of drug (4.15 mg L^{-1}) was found in serum at 0.5 h. The non-compartmental data analysis indicated considerable increase in the AUC_{∞} to 253.36 mg h L^{-1}.

Table 6.3: Summary of the pharmacokinetic parameters in serum after oral administration of IM and IM loaded nanoparticles.

Parameters	Pure Drug Imatinib Mesylate	PECA Nanoparticles	PLGA Nanoparticles
T_{max} (h)	3.00	9.00	12.00
C_{max} (mg L^{-1})	15.45	14.08	11.80
AUC_{∞} (mg h L^{-1})	178.79	465.58	253.36
V_d/F (L kg^{-1})	3.14	4.15	4.09
Cl/F (L h^{-1} kg^{-1})	0.28	0.11	0.20
Half-life (h)	7.80	25.62	16.30
MRT (h)	11.25	36.97	23.52
MAT† (h)	1.42	5.82	5.53
F†	0.87	0.88	0.76

†comparative in vivo data between the oral and intra-venous administrations

PLGA nanoparticles have shown significant increase in drug serum concentrations and serum residence time with approximate two fold increase in MRT (23.52 h). Moreover, the changed apparent volume of distribution (V_d/F) of 4.09 L kg^{-1} indicated altered distribution of IM.

For individual formulation, the bioavailability (F) was calculated against the respective intravenous pharmacokinetic data. As there was no significant change observed in F values suggesting the increase in AUC is probably only due to change in distribution profile of the drug.

b) Brain biodistribution studies

i) Intra-venous administration

The drug concentration in the rat brain following single intra-venous dose of the pure drug, PECA nanoparticles or PLGA nanoparticles was determined and plotted as a function of time (Fig. 6.4). The various pharmacokinetic parameters calculated are listed in Table 6.4. Brain biodistribution studies after intra-venous administration of the pure drug indicated a slow and poor permeation of free drug to the brain. The maximum drug concentration (C_{max}) observed in brain was 0.6 μg g^{-1} at 3 h (T_{max}) of the post dosing.

Intra-venous administration of PECA nanoparticles also indicated increase in the maximum drug concentration (C_{max}) to 1 μg g^{-1} in brain at 3 h (T_{max}) of the post dosing. Against the pure drug, a significant increase in the permeation and retention of the drug was observed with increase in the AUC_{∞} to 26.24 μg h g^{-1}.

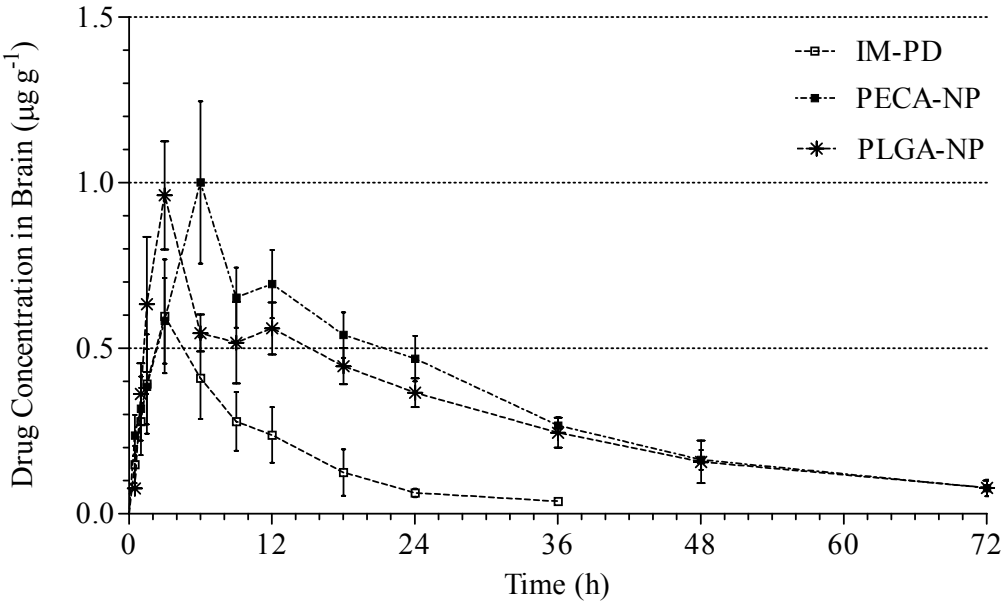

Fig. 6.4: IM concentration in brain versus time profile following intra-venous administration of the pure drug, PECA nanoparticles and PLGA nanoparticles in rats (Each value represents the mean ± standard deviation of three independent determinations)

Table 6.4: Summary of the pharmacokinetic parameters in brain after intra-venous administration of IM and IM loaded nanoparticles.

Parameters	Pure Drug Imatinib Mesylate	PECA Nanoparticles	PLGA Nanoparticles
T_{max} (h)	3.00	6.00	3.00
C_{max} (μg g^{-1})	0.60	1.00	0.96
AUC_{∞} (μg h g^{-1})	7.43	26.24	23.54
Cl (g h^{-1} kg^{-1})	3.36	0.95	1.06
Half-life (h)	11.41	20.14	22.11
MRT (h)	16.47	29.06	31.91

Moreover, approximately two fold increase in MRT was observed for PECA nanoparticles against the pure drug (16.47 to 29.06 h). Similarly, intra-venous administration of PLGA nanoparticles also indicated increased retention of the drug with increased AUC_{∞} to 23.54 μg g^{-1}. MRT was found to increase to 31.91 h with increased elimination half-life in brain to 22.11 h. Increased AUC and MRT indicated more permeation of the drug to brain in Nano-DDS with extended release.

ii) Oral administration

For the brain biodistribution studies, the drug concentration in rat brain following single oral dose of the pure drug, PECA nanoparticles and PLGA nanoparticles were determined and plotted as a function of time (Fig. 6.5). The various pharmacokinetic parameters calculated using a data modeling software are listed in Table 6.5.

Brain biodistribution studies of the pure drug after oral administration confirmed a slow and poor distribution of free drug to brain with the maximum drug concentration (C_{max}) of 0.82 μg g^{-1} at 3 h (T_{max}) the post dosing. Although the drug concentration levels in brain tissues were extremely poor with AUC_{∞} of 11.93 μg h g^{-1}, a quantifiable amount of IM observed at 0.5 h was 0.054 μg g^{-1}. Biodistribution profile obtained after oral administration and intra-venous administration of the pure drug were in agreement and indicated a slow onset and poor permeability.

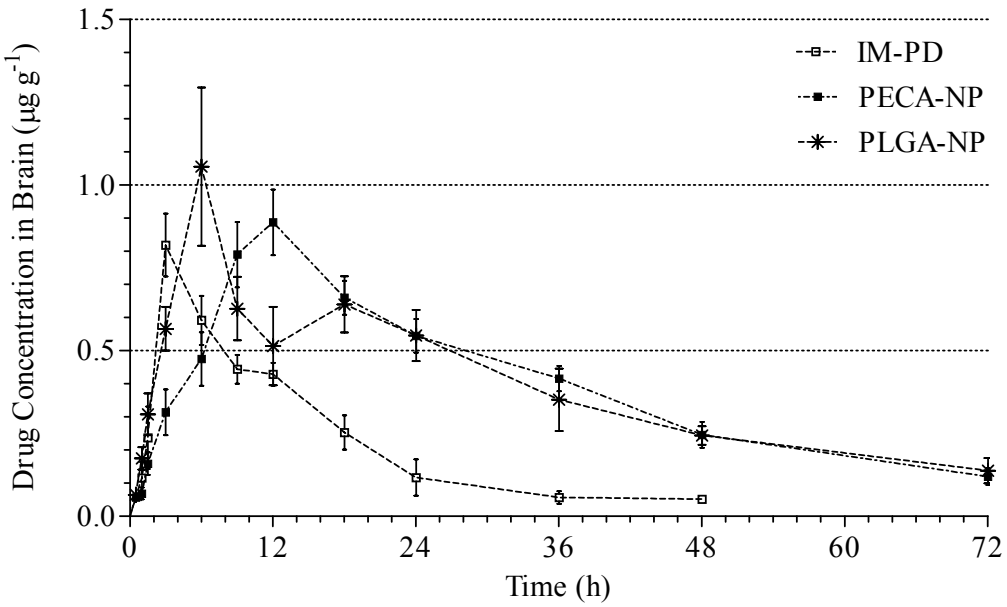

Fig. 6.5: IM concentration in brain versus time profile following oral administration of the pure drug, PECA nanoparticles and PLGA nanoparticles in rats (Each value represents the mean ± standard deviation of three independent determinations)

Moreover, a secondary peak observed after intra-venous administration of the pure drug was found to be preserved at 12 h of oral dosing. Both, oral and intra-venous, routes of administration resulted in poor drug concentration levels in brain tissue in comparison with serum drug concentration levels.

Oral administration of PECA nanoparticulate formulations revealed that the nanoparticles show relatively slower absorption rate but increased extent of absorption with the maximum drug concentration (C_{max}) of 0.89 μg g^{-1} in brain at 12 h (T_{max}) of the post dosing. Immediately after oral administration of PECA nanoparticles, a quantifiable amount of the drug (0.057 μg g^{-1}) was found in brain at 0.5 h. The non-compartmental data analysis indicated significant increase in the AUC_{∞} to 31.78 μg h g^{-1} suggesting enhanced distribution to the brain. PECA nanoparticles have shown increased residence time of the drug in the brain with significant increase in the elimination half-life in the brain (25.06 h). Moreover, MRT of IM from the drug loaded PECA nanoparticles increased considerably in comparison with the pure drug (20.7 to 36.16 h).

Table 6.5: Summary of the pharmacokinetic parameters in brain after oral administration of IM and IM loaded nanoparticles.

Parameters	Pure Drug Imatinib Mesylate	PECA Nanoparticles	PLGA Nanoparticles
T_{max} (h)	3.00	12.00	6.00
C_{max} (μg g^{-1})	0.82	0.89	1.06
AUC_{∞} (μg h g^{-1})	11.93	31.78	32.44
Cl/F (g h^{-1} kg^{-1})	4.19	1.57	1.54
Half-life (h)	14.35	25.06	26.61
MRT (h)	20.70	36.16	38.40

Studies with PLGA formulations also indicated increased drug absorption with the maximum drug concentration (C_{max}) of 1.06 μg g^{-1} in the brain at 6 h (T_{max}) of the post dosing with significant increased AUC_{∞} to 32.44 μg h g^{-1}. A quantifiable amount of drug (0.065 μg g^{-1}) was found in the brain at 0.5 h after oral administration. The non-compartmental data analysis indicated significant increase in the AUC_{∞} to 32.44 μg h g^{-1} due to enhanced permeation to the brain. PLGA nanoparticles have shown increase in the elimination half-life in the brain (26.61 h) indicating increased residence time of IM. MRT of IM loaded PLGA nanoparticles was increased in comparison to the pure drug (20.70 to 38.40 h).

Thus, it can be concluded that both the IM loaded nanoparticulate formulations increased the extent of drug permeation to the brain with nearly 100% increase in MRT and three-fold increase in AUC_{∞} against the pure drug.

c) Lungs biodistribution studies

i) Intra-venous administration

The drug concentration in rat lungs following single intra-venous dose of the pure drug, PECA nanoparticles or PLGA nanoparticles was determined and plotted as a function of time (Fig. 6.6). The various pharmacokinetic parameters are listed in Table 6.6.

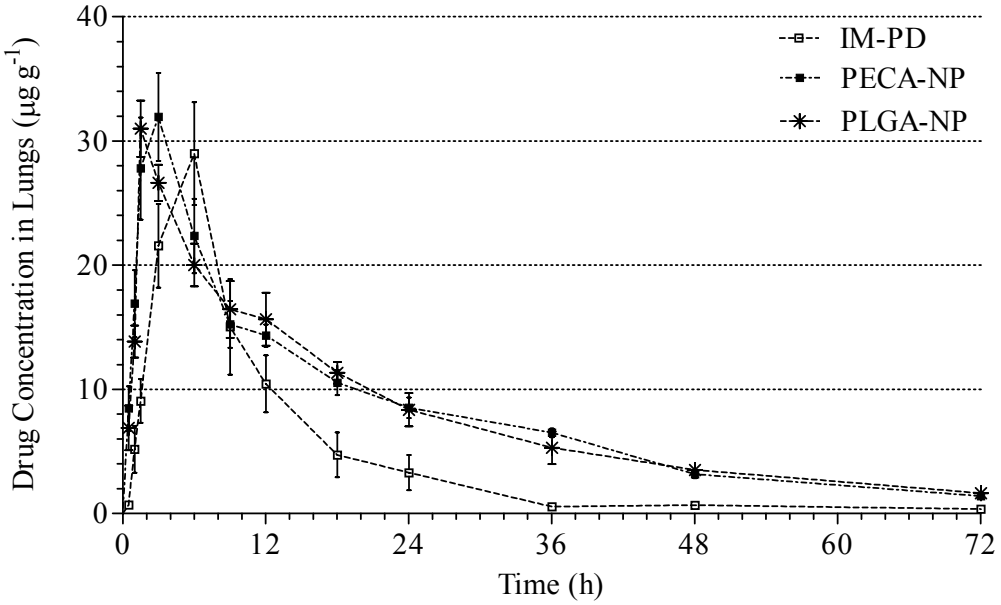

Fig. 6.6: IM concentration in lungs versus time profile following intra-venous administration of the pure drug, PECA nanoparticles and PLGA nanoparticles in rats (Each value represents the mean ± standard deviation of three independent determinations)

Intra-venous administration of the pure drug resulted in the maximum drug concentration (C_{max}) of 28.99 μg g^{-1} in lungs at 6 h (T_{max}) of the post dosing. Administration of the pure drug resulted in AUC_{∞} of 316.9 μg h g^{-1}. MRT of the pure drug was found to be 14.6 h and elimination half-life in lungs was 10.11 h. Moreover, the drug biodistribution profile to lungs has also shown a biphasic nature with initial rapid distribution to lungs followed by a fast elimination up to 12 h and then a very slow elimination with a secondary shoulder peak at 12 h of the post dosing.

Biodistribution studies of intra-venous administration of PECA nanoparticles revealed that the maximum drug concentration (C_{max}) was 31.94 μg g^{-1} in lungs at 3 h (T_{max}) of the post dosing. Moreover, in the case of PECA nanoparticles AUC_{∞} was increased to

608.01 μg h g^{-1} against the AUC_{∞} 316.9 μg h g^{-1} for the pure drug. MRT was also found to increase to 24.73 h with increased elimination half-life in the lungs (17.14 h).

Similarly, intra-venous administration of PLGA nanoparticles also indicated increased distribution of the drug with increased AUC_{∞} to 611.36 μg h g^{-1} in the lungs. Administration of PLGA nanoparticles resulted in the maximum drug concentration (C_{max}) of 30.99 μg g^{-1} in the lungs at (T_{max}) 1.5 h of the post dosing. The MRT was found to increase to 27.1 h with increased elimination half-life in the lungs (18.78 h).

Table 6.6: Summary of the pharmacokinetic parameters in lungs after intra-venous administration of IM and IM loaded nanoparticles.

Parameters	Pure Drug Imatinib Mesylate	PECA Nanoparticles	PLGA Nanoparticles
T_{max} (h)	6.00	3.00	1.50
C_{max} (μg g^{-1})	28.99	31.94	30.99
AUC_{∞} (μg h g^{-1})	316.90	608.01	611.36
Cl (g h^{-1} kg^{-1})	0.08	0.04	0.04
Half-life (h)	11.12	17.14	18.78
MRT (h)	14.60	24.73	27.10

ii) Oral administration

For the biodistribution studies in lungs for oral administration, the drug concentration in rat lungs following single oral dose of the pure drug, PECA nanoparticles or PLGA nanoparticles was determined and plotted as a function of time (Fig. 6.7). The various pharmacokinetic parameters calculated are listed in Table 6.7.

Oral administration of the pure drug also indicated a rapid distribution of IM into lungs with the maximum drug concentration (C_{max}) of 51.44 μg g^{-1} at 6 h (T_{max}) of the post dosing. The drug concentration levels in lung tissue were significantly higher than the drug concentration in serum suggesting the rapid onset and good lung permeability of the pure drug. The biphasic nature of biodistribution profile in the lungs was in agreement with intra-venous administration with the secondary shoulder peak of the concentration 10.44 ± 2.29 μg g^{-1} was found to be preserved at 12 h of the post dosing. Thus, both the routes of administration revealed initial rapid distribution of IM to lungs followed by a fast elimination up to 12 h and subsequent very slow elimination. Thus, the results obtained from both, intra-venous and oral, routes of administration were in agreement.

Moreover, a comparison between serum pharmacokinetic and lungs biodistribution profile indicated high drug concentration of IM in the lungs tissue over serum.

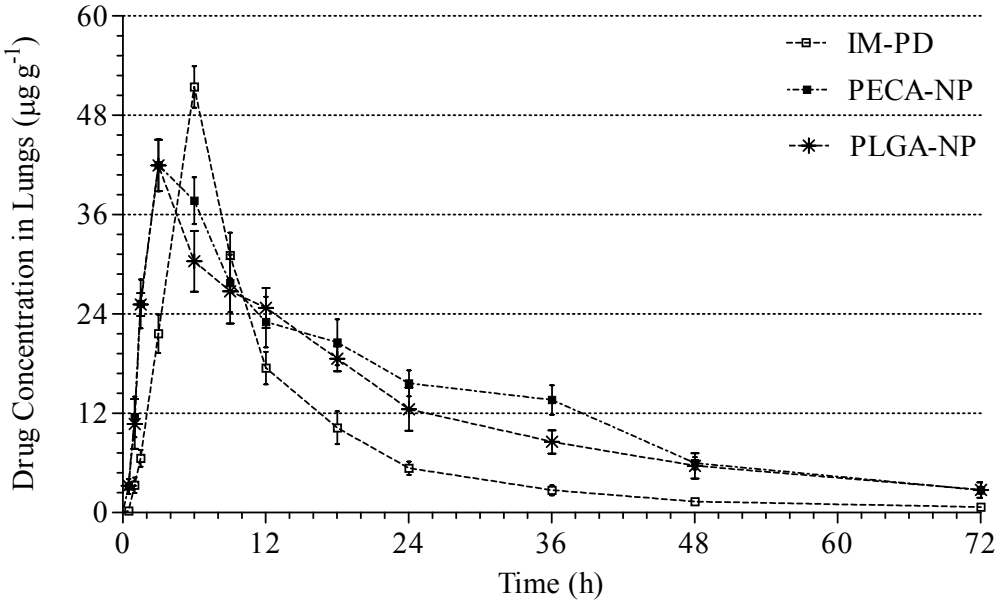

Fig. 6.7: IM concentration in lungs versus time profile following oral administration of the pure drug, PECA nanoparticles and PLGA nanoparticles in rats (Each value represents the mean ± standard deviation of three independent determinations)

In the case of PECA formulations, the nanoparticles showed relatively faster permeation with the maximum drug concentration (C_{max}) of 41.96 μg g^{-1} in lungs at 3 h (T_{max}) of the post dosing. Immediately after oral administration, a quantifiable amount of the drug (3.19 μg g^{-1}) was found in the lungs at 0.5 h. The non-compartmental data analysis indicated considerable increase in the AUC_{∞} to 1048.97 μg h g^{-1}. MRT of IM loaded PECA nanoparticles was also significantly increased in comparison with the pure drug (16.76 to 27.33 h).

Biodistribution studies with PLGA formulations also revealed that the PLGA nanoparticles show relatively faster distribution in comparison with the pure drug. Although the maximum drug concentration (C_{max}) of 41.96 μg g^{-1} observed in lungs was almost similar to that of the pure drug in the lungs, the non-compartmental data analysis indicated considerable increase in the AUC_{∞} to 945.49 μg h g^{-1}. Immediately after 0.5 of oral administration, a quantifiable amount of the drug (3.25 μg g^{-1}) was found in lungs. MRT of IM loaded PLGA nanoparticles was also significantly increased in comparison with the pure drug (16.76 to 29.13 h).

Table 6.7: Summary of the pharmacokinetic parameters in lungs after oral administration of IM and IM loaded nanoparticles.

Parameters	Pure Drug Imatinib Mesylate	PECA Nanoparticles	PLGA Nanoparticles
T_{max} (h)	6.00	3.00	3.00
C_{max} (μg g^{-1})	51.44	41.96	41.96
AUC_{∞} (μg h g^{-1})	559.47	1048.97	945.49
Cl/F (g h^{-1} kg^{-1})	0.09	0.05	0.05
Half-life (h)	11.55	18.94	20.19
MRT (h)	16.76	27.33	29.13

Although the drug biodistribution profile is governed by several physicochemical properties and physiological factors, the most significant determinants of free drug biodistribution are reported to be plasma protein binding, drug solubility and partition coefficient, perfusion and extraction efficiency of each tissue and inherent tissue affinity for the drug. As described previously, the significant fraction of Imatinib is present in the bound state with approximate total free fraction of 10% (27). This suggests that insufficient free drug levels are available for biodistribution though lipid membranes in various lipophilic tissues such as brain. One additional reason for these observations can be high water solubility and poor lipid solubility of IM.

6.4 Conclusions

In the in situ absorption studies, IM found to undergo the first order absorption in the intestine. The drug was also found to be a good substrate of efflux transport proteins. The known efflux transport inhibitor - CS-A and surfactants - PT-80 and PF-68 found to increase intestinal permeability. PLGA and PECA nanoparticles showed a rapid and good absorption similar to the pure drug. However, PCL nanoparticles demonstrated slower absorption.

The oral pharmacokinetic studies revealed that IM is rapidly absorbed in serum after oral administration with the drug concentration levels sufficient for therapeutic activity. Studies also indicated an initial rapid biodistribution followed by a slower elimination suggesting two compartment distribution. Results were in agreement with the serum pharmacokinetic studies carried out with intra-venous administration.

The biodistribution studies confirmed that IM is rapidly distributed in higher extent into the lungs. However, the brain concentration levels were very poor in comparison with

serum concentration levels during the entire course of study. Oral administration of both, PLGA and PECA, nanoparticles showed a slower absorption rate. However, the extent of availability was increased significantly with increased residence time of the drug in systemic circulation and elimination half life. Moreover, the area under the drug concentration time curve and mean residence time in serum was found to be increased with both, oral and intra-venous, routes of administration. Interestingly, the distribution of IM to the brain was significantly enhanced with PECA and PLGA nanoparticulate formulations as found with increased AUC and MRT. Oral and intra-venous administration of IM loaded nanoparticles have also shown better distribution to brain. Enhanced serum concentration levels indicated change in distribution profile of IM.

Thus, pharmacokinetic and biodistribution studies confirmed that the biodistribution of the drug can be modulated with the aid of nanoparticulate drug delivery systems efficiently. The drug specific problems such as P-gp efflux and tissue specific bioavailability could be addressed. The optimized drug delivery system may show enhanced therapeutic efficacy due to these advantages. Moreover, the enhanced permeation and retention (EPR) effect would further demonstrate added benefits in cancer subjects resulting in targeting the considerable amount of the drug to solid tumors.

References

1. O.C. Farokhzadand R. Langer. Nanomedicine: developing smarter therapeutic and diagnostic modalities. Adv Drug Deliv Rev. 58:1456-1459 (2006).
2. I. Brigger, C. Dubernet, and P. Couvreur. Nanoparticles in cancer therapy and diagnosis. Adv Drug Deliv Rev. 54:631-651 (2002).
3. K.S. Soppimath, T.M. Aminabhavi, A.R. Kulkarni, and W.E. Rudzinski. Biodegradable polymeric nanoparticles as drug delivery devices. J Control Release 70:1-20 (2001).
4. O. Salata. Applications of nanoparticles in biology and medicine. J Nanobiotechnology 2:3 (2004).
5. J.K. Vasirand V. Labhasetwar. Biodegradable nanoparticles for cytosolic delivery of therapeutics. Adv Drug Deliv Rev. 59:718-728 (2007).
6. P. Blasi, S. Giovagnoli, A. Schoubben, M. Ricci, and C. Rossi. Solid lipid nanoparticles for targeted brain drug delivery. Adv Drug Deliv Rev. 59:454-477 (2007).
7. S. Azarmi, W.H. Roa, and R. Lobenberg. Targeted delivery of nanoparticles for the treatment of lung diseases. Adv Drug Deliv Rev. *In press* (2008).

8. J. Wong, A. Brugger, A. Khare, M. Chaubal, P. Papadopoulos, B. Rabinow, J. Kipp, and J. Ning. Suspensions for intravenous (IV) injection: A review of development, preclinical and clinical aspects. Adv Drug Deliv Rev. *In press* (2008).
9. F. Kesisoglou, S. Panmai, and Y. Wu. Nanosizing - oral formulation development and biopharmaceutical evaluation. Adv Drug Deliv Rev. 59:631-644 (2007).
10. F. Delie. Evaluation of nano- and microparticle uptake by the gastrointestinal tract. Adv Drug Deliv Rev. 34:221-233 (1998).
11. S.M. Moghimiand T. Kissel. Particulate nanomedicines. Adv Drug Deliv Rev. 58:1451-1455 (2006).
12. Federal Register. 21 CFR Part 314 - Applications for FDA approval to market a new drug. National Archives and Records Administration, USA (1998).
13. Y.J. Son, J.S. Jang, Y.W. Cho, H. Chung, R.W. Park, I.C. Kwon, I.S. Kim, J.Y. Park, S.B. Seo, C.R. Park, and S.Y. Jeong. Biodistribution and anti-tumor efficacy of doxorubicin loaded glycol-chitosan nanoaggregates by EPR effect. J Control Release 91:135-145 (2003).
14. T. Okuda, S. Kawakami, T. Maeie, T. Niidome, F. Yamashita, and M. Hashida. Biodistribution characteristics of amino acid dendrimers and their PEGylated derivatives after intravenous administration. J Control Release 114:69-77 (2006).
15. P. Singh, D. Prasuhn, R.M. Yeh, G. Destito, C.S. Rae, K. Osborn, M.G. Finn, and M. Manchester. Bio-distribution, toxicity and pathology of cowpea mosaic virus nanoparticles in vivo. J Control Release 120:41-50 (2007).
16. J.T. Doluisio, N.F. Billups, L.W. Dittert, E.T. Sugita, and J.V. Swintosky. Drug absorption. I. An in situ rat gut technique yielding realistic absorption rates. J Pharm Sci. 58:1196-1200 (1969).
17. Y.A. Xu, G. Fan, S. Gao, and Z. Hong. Assessment of intestinal absorption of vitexin-2"-o-rhamnoside in hawthorn leaves flavonoids in rat using in situ and in vitro absorption models. Drug Dev Ind Pharm. 34:164-170 (2008).
18. K.S. Pang, V. Yuen, S. Fayz, J.M. te Koppele, and G.J. Mulder. Absorption and metabolism of acetaminophen by the in situ perfused rat small intestine preparation. Drug Metab Dispos. 14:102-111 (1986).
19. S. Berggren, J. Hoogstraate, U. Fagerholm, and H. Lennernas. Characterization of jejunal absorption and apical efflux of ropivacaine, lidocaine and bupivacaine in the rat using in situ and in vitro absorption models. Eur J Pharm Sci. 21:553-560 (2004).

20. P. Sharma, M.V. Varma, H.P. Chawla, and R. Panchagnula. In situ and in vivo efficacy of peroral absorption enhancers in rats and correlation to in vitro mechanistic studies. Farmaco 60:874-883 (2005).
21. Y.V. Rama Prasad, T. Minamimoto, Y. Yoshikawa, N. Shibata, S. Mori, A. Matsuura, and K. Takada. In situ intestinal absorption studies on low molecular weight heparin in rats using labrasol as absorption enhancer. Int J Pharm. 271:225-232 (2004).
22. J.D. Rogers, N.F. Ho, and W. Morozowich. Physical model approach to gastrointestinal absorption of prostaglandins III: In situ rat intestinal absorption of dinoprostone. J Pharm Sci. 73:1594-1599 (1984).
23. F. Cao, H. Zhang, J. Guo, and Q. Ping. Mrp2-related efflux of scutellarin in the intestinal absorption in rats. Pharmazie 63:75-80 (2008).
24. T.T. Mariappanand S. Singh. Evidence of efflux-mediated and saturable absorption of rifampicin in rat intestine using the ligated loop and everted gut sac techniques. Mol Pharm. 1:363-367 (2004).
25. B.M. Johnson, W. Chen, R.T. Borchardt, W.N. Charman, and C.J. Porter. A kinetic evaluation of the absorption, efflux, and metabolism of verapamil in the autoperfused rat jejunum. J Pharmacol Exp Ther. 305:151-158 (2003).
26. A.V. Kamath, R.A. Morrison, T.W. Harper, S.J. Lan, A.M. Marino, and S. Chong. Multiple pathways are involved in the oral absorption of BMS-262084, a tryptase inhibitor, in rats: role of paracellular transport, binding to trypsin, and P-glycoprotein efflux. J Pharm Sci. 94:1115-1123 (2005).
27. O. Kretz, H.M. Weiss, M.M. Schumacher, and G. Gross. In vitro blood distribution and plasma protein binding of the tyrosine kinase inhibitor imatinib and its active metabolite, CGP74588, in rat, mouse, dog, monkey, healthy humans and patients with acute lymphatic leukaemia. Br J Clin Pharmacol. 58:212-216 (2004).

7. Conclusions

7 Conclusions

Over the last few years, nanotechnology has emerged as a novel drug delivery system for enhancing the therapeutic efficacy and patient compliance. In the current research, studies were carried out to design and characterize nanoparticulate delivery systems to enhance the therapeutic efficacy of IM by effective delivery into the brain, a primary metastatic site.

As analysis is an integral part of pharmaceutical product development, new analytical methods were developed and validated for various studies. The developed spectroscopic and liquid chromatographic methods were found to be selective in the determination of IM in bulk and formulations. These validated analytical methods were successfully used for various preformulation and formulation development studies. The developed bioanalytical methods were also found to be selective and sensitive for the determination of IM in biological samples such as rat serum, brain and lungs. These validated bioanalytical methods were successfully employed for in vivo pharmacokinetic and biodistribution studies of the pure drug and nanoparticulate formulations in rats. The developed methods were found to have various advantages over the reported methods.

Preformulation studies indicated that the drug demonstrates a charge dependent solubility profile with increasing solubility towards acidic pH. IM was found to have four ionization constants (pKa - 1.47, 3.92, 7.61 & 9.25). The pH partition studies showed that ionization of the drug molecules controls the fraction distributed to oil phase. In liquid state, IM was found to be most stable at pH 7.4 and it was sensitive towards extreme acidic and alkaline conditions. The drug was most susceptible for oxidative stress condition and it was stable under photolytic stress conditions. Results of the drug-excipient compatibility studies demonstrated no significant interaction with various excipients used in the formulations.

Emulsion solvent evaporation and interfacial polymerization techniques were found to be suitable for the preparation of IM loaded nanoparticles using the preformed polymers (PLGA and PCL) and monomers (ECA), respectively. Nanoparticle characteristics such as average particle size and size distribution, particle morphology, drug entrapment and loading efficiency were found to be dependent on various formulation and process parameters. In addition, these parameters were found to influence the in vitro drug release characteristics of IM loaded PLGA, PCL and PECA nanoparticles.

The optimized experimental conditions provided good quality nanoparticles with reproducible characteristics. The particle size analysis and microscopic imaging revealed that the optimized nanoparticulate formulations were of the small and uniform particle

size with spherical shape. In vitro drug release from the prepared nanoparticles was controlled over 48 h and it could be well explained by the first order release kinetics. The various parameters such as polymer amount, the drug amount, stabilizer concentration found to have impact on the characteristics and properties of the prepared formulations. Increasing polymer proportion and stabilizer concentrations were found to sustain the drug release.

All optimized formulations of PLGA and PECA nanoparticles demonstrated adequate redispersability after freeze-drying. The prepared formulations showed good stability in dispersed state as the critical properties of nanoparticles including average particle size, size distribution, drug entrapment and loading efficiency were unaffected during 3 months storage period at −20°C. Freeze-dried formulations of the prepared nanoparticles demonstrated better stability for more than 6 months with no considerable change in the initial properties. Moreover, the drug release profile and redispersability of nanoparticles were relatively unaffected during the storage.

In situ absorption studies confirmed that IM is a good substrate for efflux transport proteins. The stabilizers such as poloxamer and polysorbate 80 used in the preparation of nanoparticles were found to increase intestinal permeability by inhibiting intestinal efflux transporters. Increased permeability and inhibition of efflux transport proteins would together enhance intracellular concentration of the drug. Moreover, it may even reduce the chances of inter-subject variability resulting from the differential expression of efflux transport proteins.

In vivo pharmacokinetic and biodistribution studies in rat indicated that PLGA and PECA nanoparticles are potential carriers for effective delivery of IM with promising enhanced brain uptake and sustaining the drug release under in vivo conditions. The biodistribution profile of the drug was found to be altered when delivered in nanoparticles. A multi fold increase was observed in the area under the drug concentration curve in serum with IM loaded PLGA and PECA nanoparticles. Similarly, an increase in elimination half life indicated increase in drug residence time in the systemic circulation. Brain biodistribution studies revealed increased drug availability and residence time in the brain tissues. The increase in distribution of IM to the brain may provide sufficient concentration levels to eliminate metastasized tumor cells reducing chances of resistance and relapse. Studies also indicated good compatibility of developed formulations in rats without any immediate undesirable effects.

Thus, delivery of IM using nanoparticles would be advantageous over the available conventional formulations with specific delivery to the site of action over extended duration. In cancer subjects, nanoparticulate drug delivery system would be preferentially localized in tumors cells through the extended retention and permeation (EPR) effects providing multifold increase in drug concentration at the site of action. Moreover, it may offer benefit of reduced dose or dosing frequency leading to decreased untoward effects, improved patient compliance and increased therapeutic efficacy. Collectively, these results indicate that IM loaded PECA and PLGA nanoparticles have great potential as targeted delivery systems for cancer treatment such as CML and GIST.

In order to establish the benefit to risk ratio, further studies need to be carried out for the developed formulations in the diseased subjects. Current therapy of IM demands chronic administration of the drug which would up-regulate the certain efflux transport proteins. Multiple and chronic dosing pharmacokinetic studies would address the effectiveness of nanoparticulate drug delivery systems in such cases. Additionally, in vitro cell uptake studies may be carried out to investigate the intracellular concentration levels of the drug.

Appendix

Publications

Girish Bende, Sivacharan Kollipara, Vasanthakumar Sekar and Ranendra Saha "Validation of UV-spectrophotometric method for determination of Imatinib mesylate and its application in solubility studies", Die Pharmazie, Accepted (P-8094).

Girish Bende, Sivacharan Kollipara, Snehalatha Movva and Ranendra Saha "Validation of an HPLC Method for determination of Imatinib mesylate in rat serum and its application in a pharmacokinetic study", Journal of Chromatographic Science, Accepted (JCS-07-266.R2).

Girish Bende, Sivacharan Kollipara, Venugopal Kolachina, and Ranendra Saha "Development and validation of a stability-indicating RP-LC method for determination of Imatinib mesylate" Chromatographia 66(11) 2007 859-866.

Paper Presentations in Conferences

Girish Bende, Sivacharan Kollipara and Ranendra Saha "Preparation and optimization of Paclitaxel-PLGA nanoparticles using rotatable circumscribed central composite design" 7th International Symposium - Advances in Technology and Business Potential of New Drug Delivery Systems, Controlled Release Society, Mumbai (February 13-14, 2007).

Girish Bende, Sivacharan Kollipara and Ranendra Saha "Preparation and characterization PLGA nanoparticles for effective brain delivery of anticancer drug - Imatinib mesylate" 9th Annual Meeting of the Canadian Society for Pharmaceutical Sciences, CSPS, Ottawa, Canada (May 24-27, 2006).

Girish Bende, Snehalatha Movva, Sivacharan Kollipara and Ranendra Saha "Preparation and characterization of PLGA nanoparticles for anticancer Drug - Imatinib mesylate" NIPER-NANO-2006, National Institute of Pharmaceutical Education and Research (NIPER), SAS Nagar, Punjab (February 17-18, 2006).

Girish Bende, Snehalatha Movva, Shrikant Charde and Ranendra Saha "A new, sensitive, and stability indicating method for determination of Imatinib mesylate by high performance liquid chromatography" Annual Meeting and Exposition – 2005, American Association of Pharmaceutical Scientists, Tennessee, USA (November 6-10, 2005).

Girish Bende, Snehalatha Movva and Ranendra Saha "Preparation and characterization of nanoparticles containing Imatinib mesylate" 32nd Annual Meeting and Exposition - Controlled Release Society, Miami, Florida, USA (Jun 18 - 22, 2005).

Biography of Girish Bende

Mr. Girish Bende has completed his bachelor degree in Pharmacy (B. Pharm) from Poona college of Pharmacy under University of Pune. He has completed his post graduation from Birla Institute of Technology and Science, Pilani in the year 2002. He has been working as a research scholar at BITS, Pilani. He has published research articles in renowned journals and presented papers in national and international conferences in India and abroad.

Biography of Prof. Ranendra N. Saha

Dr. Ranendra N. Saha is Professor of Pharmacy and Dean, Faculty Division III and Educational Development Division, BITS, Pilani. He completed his Bachelor of Pharmacy and Master of Pharmacy (Pharmaceutics) degrees from Jadavpur University, Kolkata and obtained his Doctor of Philosophy degree from BITS, Pilani. He has more than 28 years of teaching and research experience and guided several doctoral, postgraduates and undergraduate students. He has published research articles in renowned international and national journals and presented papers in conferences India and abroad. Dr. Saha has successfully completed several government and industry sponsored projects. He has also developed commercial products and transferred technologies to production analytical departments. He is expert member of various committees including UGC and others. He is a member of CSIR selection committee, several universities, colleges etc. He is also a member of Board of studies of several universities and colleges and acting as a visiting Professor to few universities.